EXPERIMENTAL INVESTIGATION OF ACTIVE
PNEUMATIC SUSPENSIONS

by

LONG-CHAIN CHEN

B.S.M.E.,Tatung Institute of Technology
Taipei, Taiwan, ROC
(1973)

SUBMITTED TO THE DEPARTMENT OF
MECHANICAL ENGINEERING IN PARTIAL
FULFILLMENT OF THE REQUIREMENTS
FOR THE DEGREEE OF

MASTER OF SCIENCE IN
MECHANICAL ENGINEERING

at the

MASSACHUSETTS INSTITUTE OF TECHNOLOGY

May 1984

© Massachusetts Institute of Technology 1984

Signature of Author _____
Department of Mechanical Engineering
May, 1984

Certified by _____
J.Karl Hedrick
Thesis Supervisor

Accepted by _____
Warren M. Rohsenow
Chairman, Departmental Graduate Committee

EXPERIMENTAL INVESTIGATION OF ACTIVE PNEUMATIC SUSPENSIONS

by

LONG-CHAN CHEN

Submitted to the Department of Mechanical Engineering on
May 10, 1984, in partial fulfillment of the requirements
for the degree of Master of Science in Mechanical
Engineering.

ABSTRACT

The secondary lateral suspension system of the passenger rail vehicle
is the plant to be controlled whereas a pneumatic active suspension system
(the LASC controller) is the controller to be implemented with the above
plant for better ride quality control. Results of field measurements of
the plant are used to determine the size and mounting position of the
controller proposed. A 5th order state equation, the transfer functions
of interest, and the transformed phase-variable representation of the
argumented system are derived. The performance requirements and design of
the LASC Controller are investigated.

Using Dynamic Similitude Methods, a laboratory apparatus (the LASC
tester) is designed to perform testings of the controller. Components of
the testing facility are analyzed and calibrated. Two control circuits,
the PWM and the BbLC, are investigated to drive the solenoid valve.
Experimental results of various actuators, valves, and control circuits
are compared with that of computer simulations to select adequate
components based on their capabilities vs. power consumption.

Significant improvements of ride quality control are found by
experiment and simulation. Using a PARKER HMA 14, a 4" bore cylinder, the
FESTO valve set, and the ꓶBLC circuit, a 22% reduction in the r.m.s.
lateral suspension stroke and a 49% reduction in the r.m.s. carbody
lateral acceleration is achieved at power consumption of 9.3 to 13.7 H.P.
per car.

The performances of the simple, economical and reliable LASC
controller are demonstrated. Similarly, the LASC tester does perform as a
good testing facility. Both the LASC controller and the LASC tester
can also be applied to other vehicles to improve the ride quality
control.

Thesis Supervisor: Dr. J. Karl Hedrick.
Title: Professor of Mechanical Engineering

ACKNOWLEDGEMENT

My mother, Lu Shen-Nie Chen 陳盧賢女 , father Guan Chen 陳管 , brothers 陳宏基 陳宏文 , sisters 陳秋香, 陳春櫻, 陳麗屏, my wife Win-chain Chiang 江文琴, and my daughter Xanadu X. Chen 陳珊妲.

And finally, but most importantly, my late grandfather Bi Cheng. 雪比

I am so lucky to be able to study at MIT through so many persons' assistance. I like Boston, the Charles, and MIT very much and would like to express my gratitude to those who work, teach, study at this institute. Thank all of you who made this place wonderful for me to stay, to study, to work, to teach, to relax and to live happily.

Let's work together again to make this world more beautiful.
共創美好的世界

TABLE OF CONTENTS

LIST OF FIGURES

- 15 -

LIST OF TABLES

LIST OF TABLES

CHAPTER I

INTRODUCTION

1.1 Background

The boom period of the rail transportation industry began in the middle of the nineteenth century with the industrial revolution and ran until the end of the Second World War. The railroads suffered about a quarter of a century of neglect, leaving a nation-wide network of aging rolling stocks, tracks, and terminals. Because of concern over environmental protection, pollution, resource reallocation, and because of worsening traffic congestion, there has been a renewed interest in the railroad. Since a large capital investment has already existed in the current equipment, tracks, and facilities, a relatively small additional investment is needed in order to meet the high performance demands of the current highly competitive transportation field. This is really a major advantage of railroad transportation over other innovative alternative transit systems.

Since 1970 with the passage of the Rail Passenger Act, the National Railroad Passenger Corporation (AMTRAK) was created to improve rail service. In the intercity transit systems such as the BART of San Francisco and (T) of Boston, and in the shorter routes such as from Boston to New York and from Los Angeles to San Diego, where trip time is more comparable with airline transportation, a comfortable train ride will make the rail transportation more competitive. A comfortable train ride includes two parts: one is good service characteristics such as convenience, cost and trip time; and another one is good ride quality which includes compartment seat accommodation, air conditioning,

reduction of noise, and carbody accelerations. The linear and angular accelerations of the carbody, which are heavily determined by the carbody suspension design, are an important dynamic characteristic of the rail vehicle.

In order to make railroad transportation viable as a transportation mode, much research has been done in rail vehicle dynamics in recent years [1,2,3]. Different research can be classified into four categories, which have some overlapping, as follows:

(1) Wheel-rail interactions [4,5]

(2) Curving mechanics [6,7]

(3) System performance [8,9]

(4) Suspension design [10,11,12]

To AMTRAK, it is more economically feasible to use an innovative design of the suspension system of the rolling stock to increase the performance without increasing current level of track maintenance [1]. Unfortunately, there is a secondary suspension/ride quality tradeoff existing in the current suspension design. If the suspension travel distance is increased, the acceleration environment of the passenger is decreased because the lateral stability is decreased when the guidance to negotiate a curve is increased by limiting the carbody strokes. This is the so-called trade-off phenomena which has been recognized as a serious limiting constraint for rail vehicles of passive suspension design [8].

This is one of the reasons why the active suspension systems were proposed, including those studied by Goodall et al. [14] and Klinger et

*[ ] numbers in brackets refer to reference at the end of the thesis.

al. [13]. The purpose of active suspension design is to use control theory techniques to reduce the above mentioned trade-off phenomena and improve the rolling stock performance without large increase of the current amount of track maintenance. The preliminary cost-effect studies, which compare the added cost of design implementation, maintenance, and operation of the active suspension to the upgrading of the vehicle performance, indicate a positive recommendation for adopting the active suspension system in [13] and [14].

1.2 Suspension Elements of Rail Vehicles

Figures 1-2-1 and 1-2-2 show a schematic diagram of the Budd Pioneer III truck that is currently used in AMCOACH lines of AMTRAK. The definition of directional terminology is illustrated in Figure 1-2-3. The objectives of a railroad suspension are to support the carbody weight, improve the truck ability to negotiate its desired path, and isolate the carbody from disturbances caused by aerodynamic impacts and track irregularities. Both passive and active elements can be used in meeting the suspension needs. Passive elements, which can only store (spring type) or dissipate (damper type) energy, include friction wedges, swing hangers, rubber bushings, chevrons, hydraulic shock absorbers, doughnuts, coilsprings and air springs. Active elements can be used to put energy into the control system by connecting them to an external energy source. Actuators of various kinds, such as electro-magnetic, hydraulic, electro-mechanical, and pneumatic types are used as active elements in vehicle suspension systems.

Carbody

Anchor Rod,
Bushings and
Longitudinal
Stiffness of
Coil Spring

Stabilizer Rod,
Rubber Spacers,
and
Lateral Shear
Stiffness of
Coil Spring

Primary
Stiffness

Yaw
Damper *

Lateral
Damper
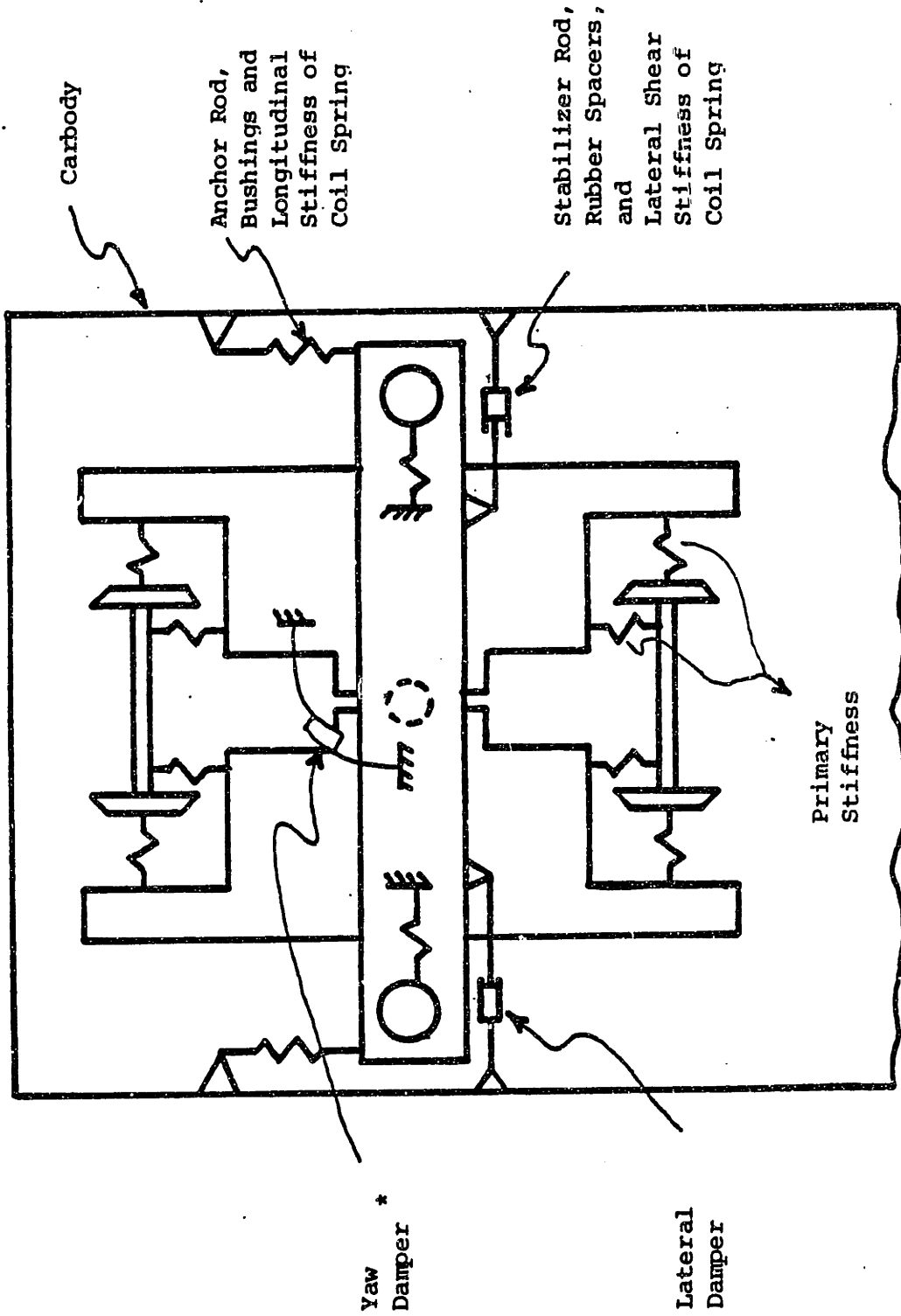
* Yaw damper represents dry friction at centerplate and side bearings

Figure 1-2-1   Top View of Pioneer III Truck
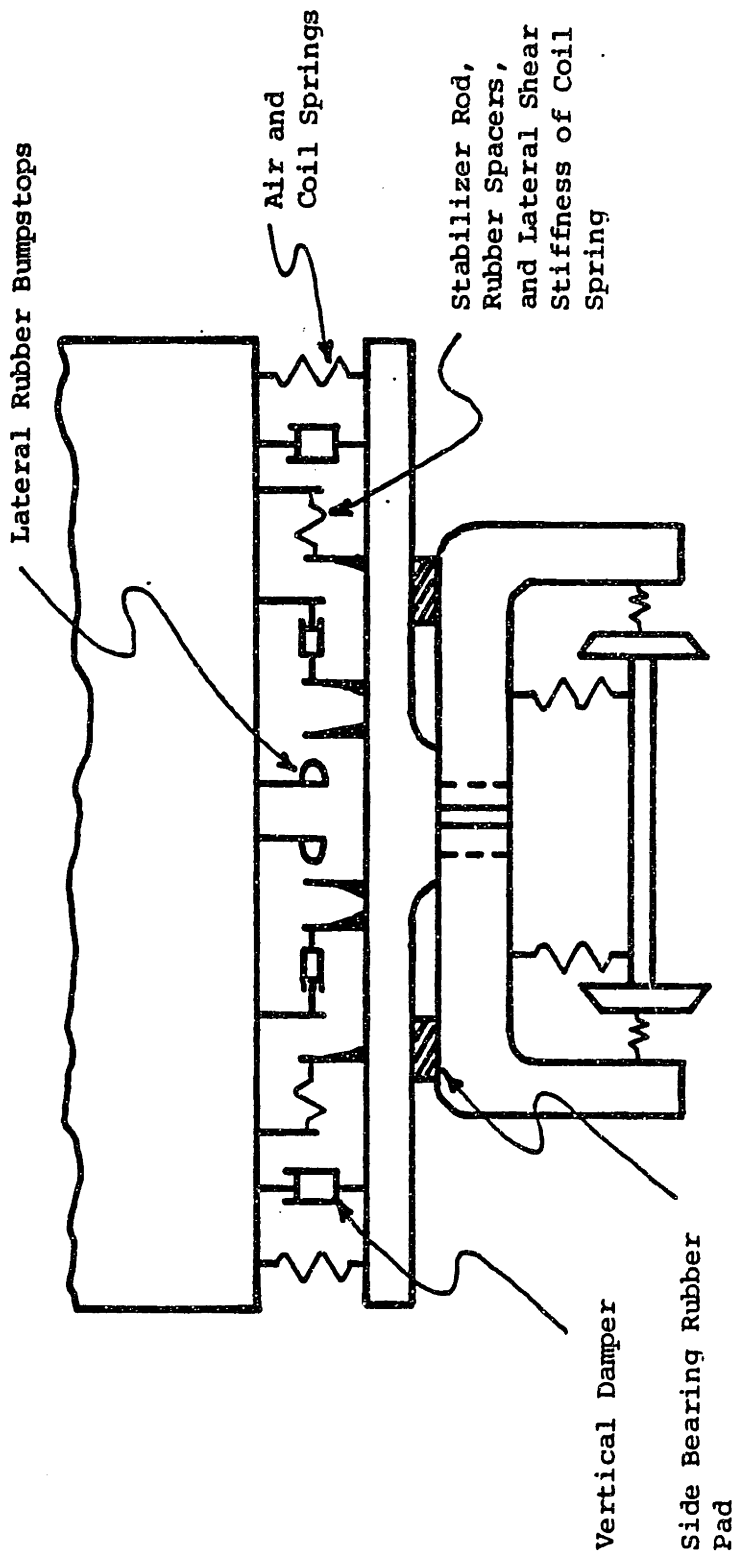
Figure 1-2-2   Rear View of Pioneer   III

The rail vehicles suspension can be further separated into the primary suspension and the secondary suspension according to the location where the suspension element is applied as shown in Figure 1-2-3. The primary suspension, which connects the truck frame with the wheelsets, consists of rubber springs between the side frames and the axles, and side bearers between the side frame and the bolster. The secondary suspension, which separates the carbody from the truck frame, includes dampers, springs, airsprings, and the bolster assembly. The bolster assembly is a unique secondary suspension design which is a hollow, slender, horizontal steel structure to straddle the truck on its center, and to carry the carbody load from two side spring sets (coil steel spring plus air bag) to the center plate and side pads of the truck frame.

The lateral secondary suspension of the Pioneer III, which is the plant to be controlled in this research, is further explained as follows:

1. General lateral stiffness - this results from the shearing of the coil springs, and from the lateral stabilizer rods with rubber bushings at ends.

2. Special lateral stiffness - this is added from the hard rubber bumpstops which are struck after 1.5 inches of relative motion between carbody and truck.

3. Lateral damping - this is provided by two rotary shock absorbers as shown in Figure 1-2-2 [15].
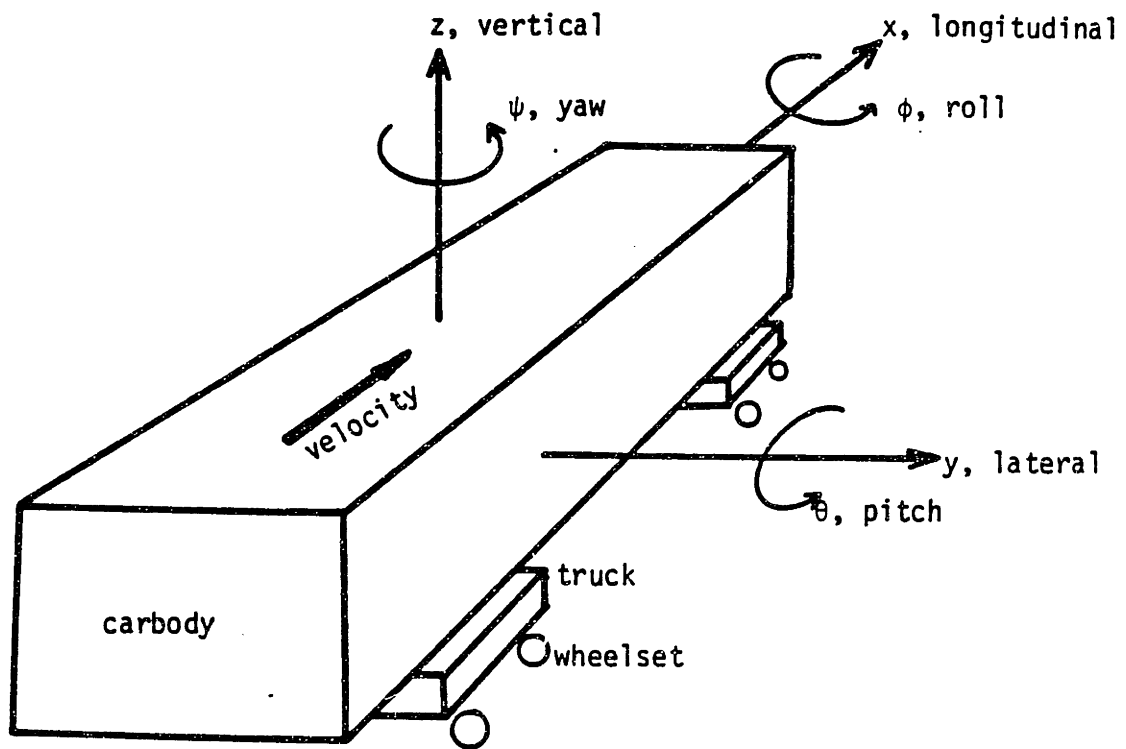
a) definition of directional terminology

Figure 1-2-3   Definitions of Directional Terminology
(translational and rotational)
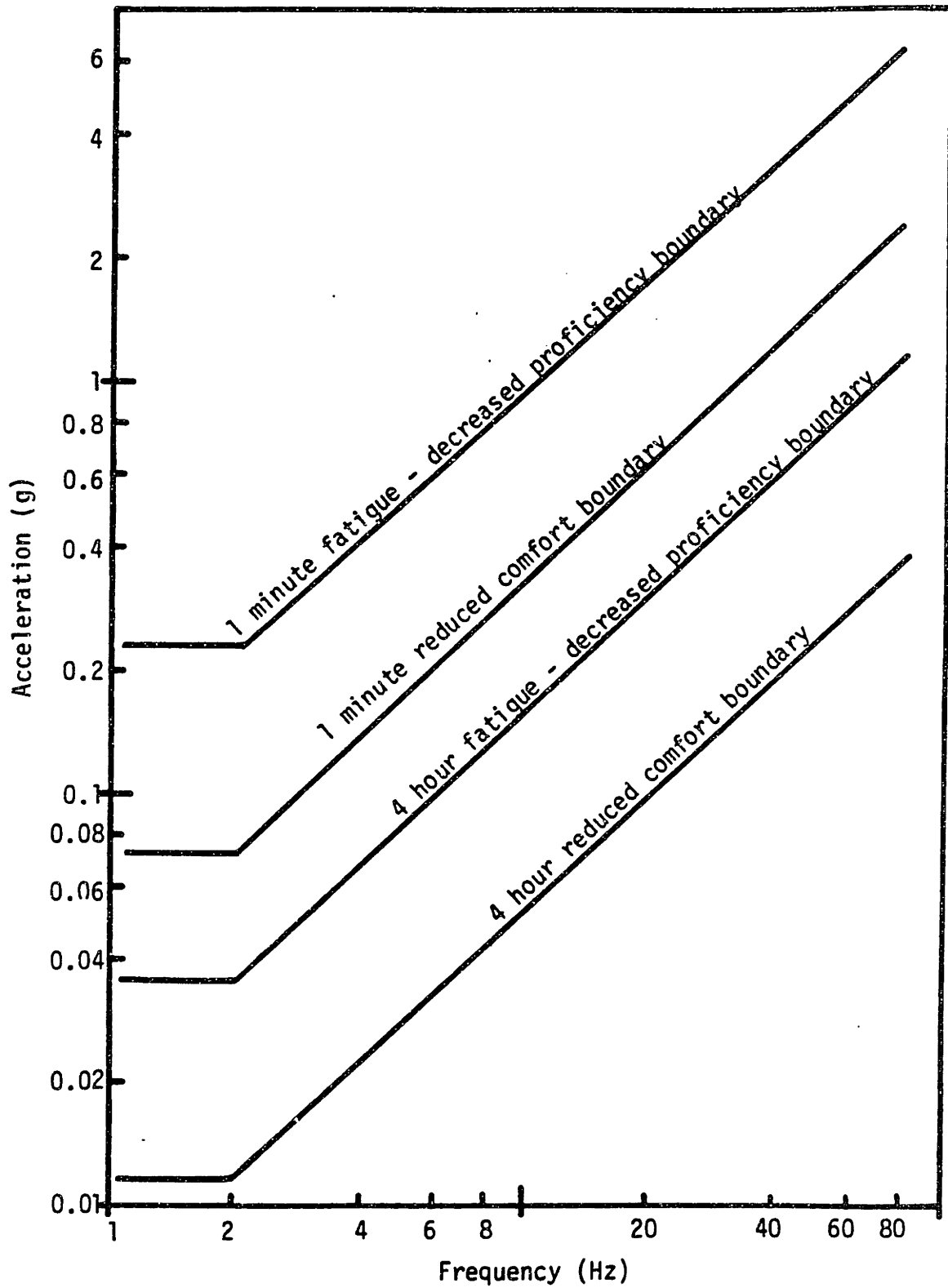
Figure 1-2-4   Transverse Acceleration Limits as a Function
of Frequency and Exposure Time

Passengers are exposed to the carbody accelerations, and the

exposure limits to the whole-body vibration had been studied in [16, 17,

18]. The International Organization for Standardization, I.S.O., 2631's

"reduced comfort boundary" is adopted as guidelines in this research.

The human body exposure limit is influenced by the frequency, direction,

and duration of vibration. Figure 1-2-4 related lines of the reduced

comfort boundary to the lines of the fatigue-decreased proficiency

boundary for the transverse direction based on different frequencies and

durations. In addition, the transverse exposure limit is much lower

than that in the vertical direction.

1.3 Previous Work:

The Vehicle Dynamics Laboratory at MIT has been doing research to

improve the vibration isolation without damaging the stability

characteristics of the conventional secondary passive suspension system.

Partridge [19] investigated various methods of modifying the current

lateral secondary suspension by passive approach. Her conclusion was

that by employing a smoothly hardening spring, only moderate improve-

ments could be achieved.

Using a 15 DOF frequency domain study, Celniker [20] demonstrated

that the lateral acceleration vibrations are typically one Hz. distur-

bance at the present operating speed range (80 mph -10 mph). These

vibrations are mostly transmitted through the secondary suspensions,

since the frequency of the secondary suspension is in the 1 Hz.

neighborhood. In parallel with the conventional passive secondary

suspension, he developed an active feedback control scheme to control

the carbody's lateral, roll, and yaw vibration modes, and the truck-

wheelset hunting mode. The "local" ride controller proposed by him generates relative forces proportional to the carbody accelerations and velocities measured on each truck. Celniker [21] also showed that a 67% reduction in r.m.s.* secondary lateral acceleration, and a 17% r.m.s. in secondary lateral suspension stroke can be achieved with a r.m.s. force of 900 lb_f at an operating speed of 100 mph.

Field measurements on an AMTRAK passenger coach travelling on the Northeast Corridor were completed by Hedrick, et al. [22] to measure the lateral acceleration and determine the magnitude and frequency of the acceleration. Subsequently, Buzan [23] modelled Celnicker's local ride controller as a first-order lag force generating element which has a limited bandwidth. He also modelled 1/2 of a vehicle (1/2 plant) as a one DOF system with FIRESTONE® #25 224 airsprings as the actuator for the local ride controller. A 40% r.m.s. reduction in secondary lateral acceleration, and 12% r.m.s. reduction in secondary lateral suspension stroke were achieved at a power consumption of 27-38 HP/car.

This power refinement is too high and beyond the availability of the existing air compressor on board. An alternate approach needs to be investigated in order to have the active suspension controller applied on the passenger rail vehicle without replacing the existing air compressors on board.

----

*root mean square

1.4 Active Control

With the conventional passive lateral secondary suspension elements

unchanged, Celniker [20] applied two parallel actuators to overcome the

trade-off phenomena of passive suspension. He used a 15 DOF model to run

the computer simulation on his "local ride controller" and showed the

following improvements could be made. At an travelling speed of 100 mph,

the local side controller can reduce the r.m.s[*] lateral acceleration

by 67%, and the r.m.s. secondary suspension displacement by 17% with a

r.m.s. of 900 lb_f.

(1) Figure 1-4-1 shows the schematic diagram of the local ride

controller, and the control law is stated as follows:

$$F_{AD} = C_v \, \dot{y}_{cl} + C_A \, \ddot{y}_{cl} \qquad (1)$$

where F_{AD} = the total lateral force desired

$\dot{y}_{cl}$ = velocity of the local accelerometer, i.e., the carbody

velocity

$\ddot{y}_{cl}$ = acceleration of the local accelerometer, i.e, the carbody

acceleration

C_v = feedback gain for $\dot{y}_{cl}$

C_a = feedback gain for $\ddot{y}_{cl}$

The local ride controller responds to the absolute carbody velocity

and the absolute carbody acceleration through an ideal infinite bandwidth

actuator as assumed by Celniker.

Since an active suspension controller can add energy through an

external power source to the control system, the above mentioned improve-

ments in the acceleration, and stroke displacement over the passive

suspension, were plausible.
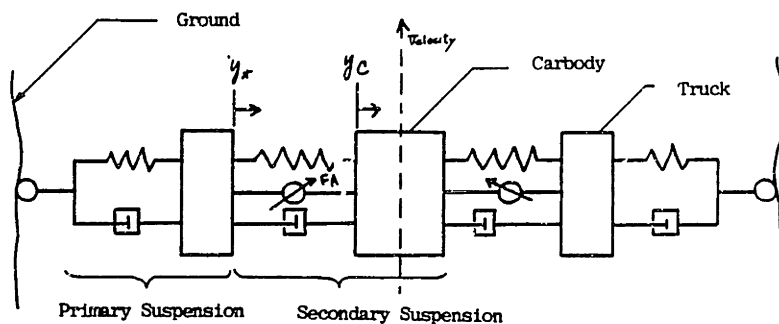
(a) The Lateral Suspension of a Passenger Rail Vehicle
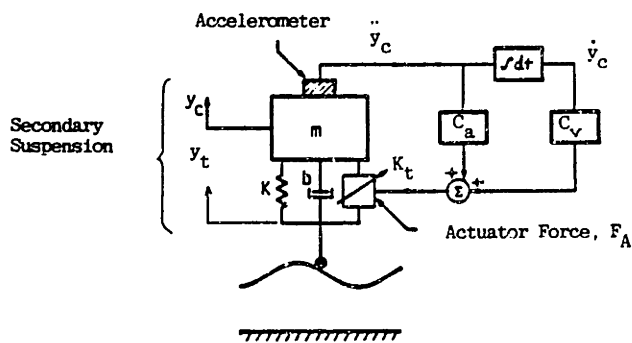
(b) The Schematic Diagram of a Local Ride Controller

Figure 1-4-1   The Schematic Diagram of the Secondary Lateral
Suspension with a Local Ride Controller
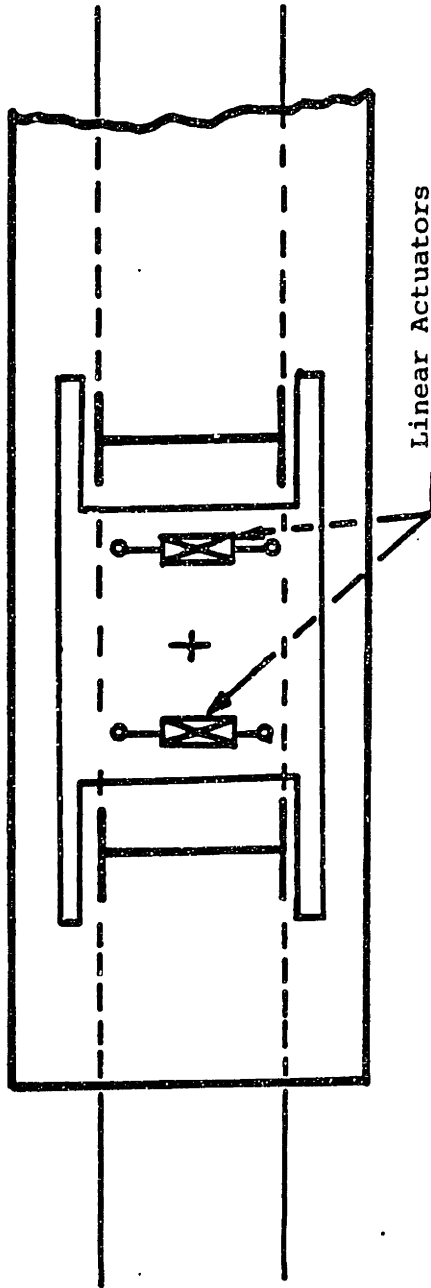
Figure 1-4-2   Actuator Positions on Truck for Torque and Force
Actuation
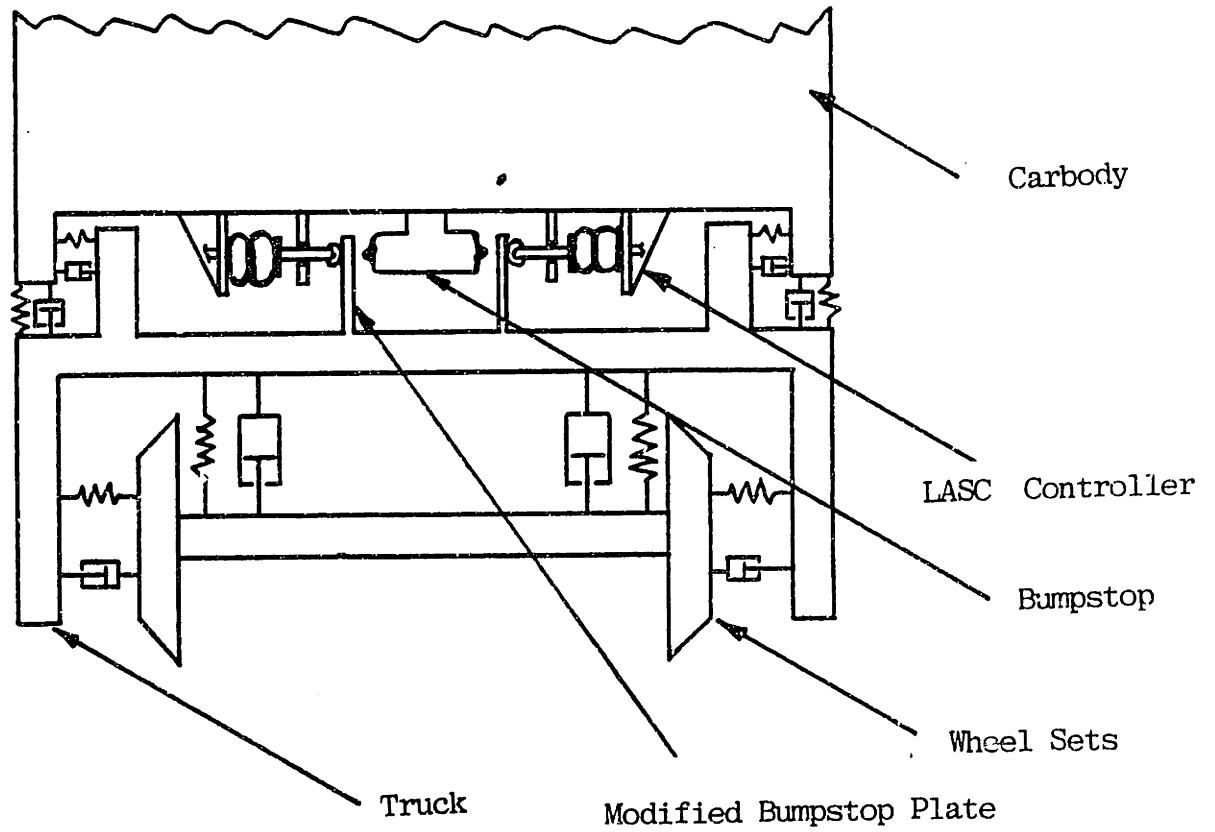
Figure 1-4-3   The Relationships Among the Truck, Carbody
and the LASC Controller

(2) At higher speeds, a kinematic yaw controller, which would apply

yaw torque between the truck and the carbody was proposed by Celniker.

At 185 mph travelling speed, he showed that 53% reduction of r.m.s.

acceleration, and 35% reduction of the r.m.s. stroke displacement with a

r.m.s. force of 5.500 lbf could be implemented. The control law was

stated, referenced to Figure 1-2-3, as follows:

$$\tau_{yaw} = -c_1 \dot{y}_t - c_2 \dot{\psi}_t \tag{2}$$

where τ_{yaw} = the yaw torque

$\dot{y}_t$ = rate of the truck lateral motion

$\dot{\psi}_t$ = rate of the truck yaw motion

$- c_1, -c_2$ = feedback gains

In addition to the lateral actuator for linear secondary vibration

control, a kinematic yaw torque controller was required while the train

is operating at higher speeds. Both lateral and yaw operations could be

provided by a pair of actuators on each truck as shown in Figure 1-4-2.

Since a kinematic yaw torque controller required too much effort, and was

needed only at higher travelling speeds, it was not studied in this

research. Under this consideration, the two actuators on each truck to

provide both the lateral and yaw operation were replaced by only one

lateral active suspension controller, i.e. the LASC controller, on each

truck as shown in Figure 1-4-3.

1.5 Design of an Lateral Active Suspension Controller

A real actuator had a finite response time, τ, whereas the ideal

actuator, proposed by Celniker, had an infinite bandwidth. After

studying the dynamic effect of the actuator on the local ride

controller, a model for the real actuator to relate the input command
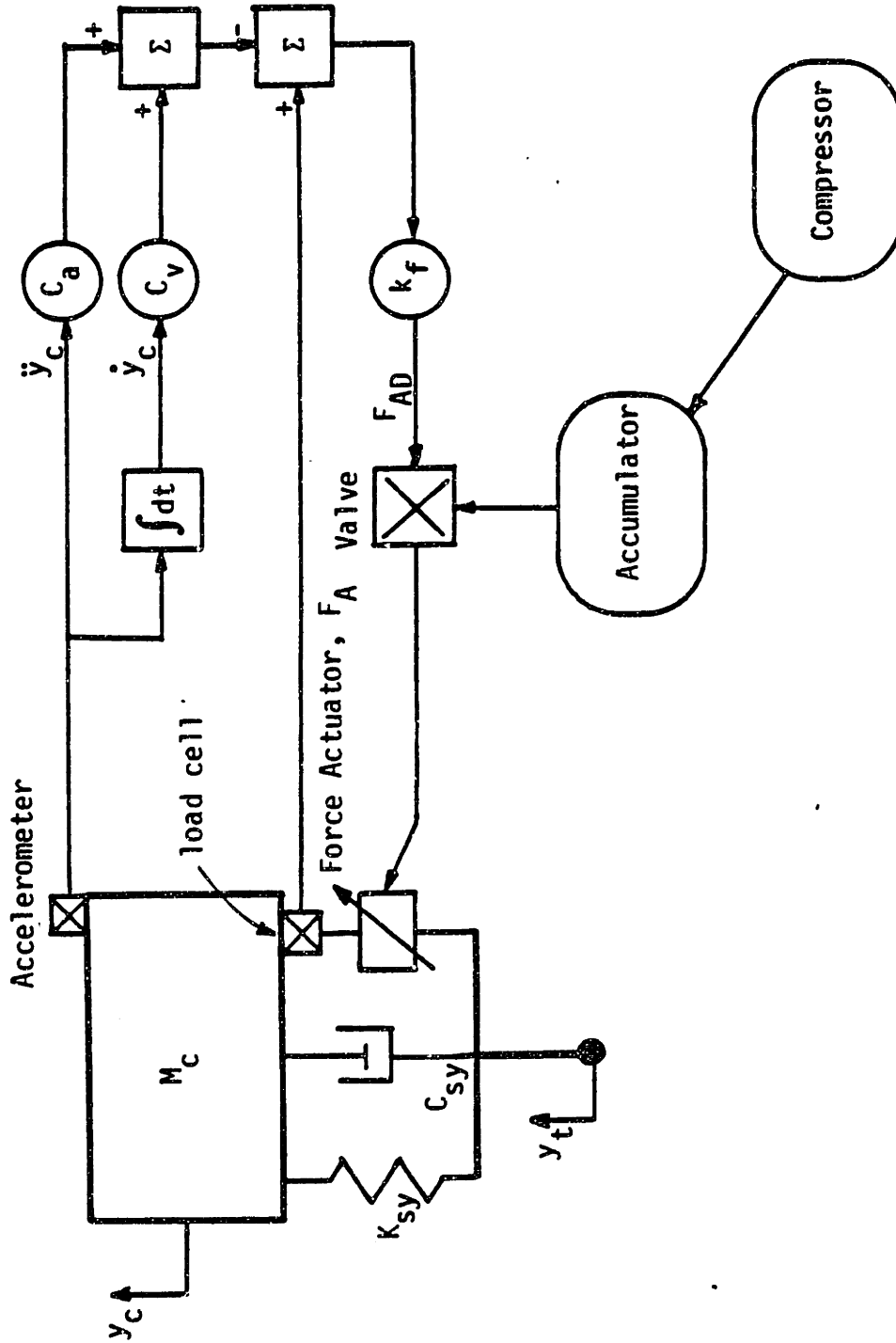
Figure 1-5-1   The Schematic Diagram of a ½ Vehicle Model Implemented with a Local Ride Controller

and the output response could be established. Buzan [23] modelled the

actuator as a first-order lag force actuating element as decribed below:

$$\tau \dot{F}_A + F_A = F_{AD} \qquad (3)$$

where F_{AD} = the desired force

F_A = the actual actuator output force

$\frac{1}{\tau}$ = the bandwidth of the actuator

A schematic model with the local ride controller is sketched in

Figure 1-5-1. A force feedback gain, K_f, was added to multiply the error

signal between the desired force, F_{AD}, and the actuator force, F_A. Buzan

used the field data of the lateral acceleration, which is of an AMTRAK

passenger vehicle travelling on the Northeast Corridor to determine the

frequency and magnitude of the random vibration. Based on the field data

processed at M.I.T., Buzan used a 1 DOF model to represent 1/2 of a

passenger vehicle (i.e., 1/2 the carbody mass and 1/2 the secondary

lateral suspension elements). A FIRESTONE® #225 airspring (with a

proportional control valve) was considered to be the actuator of the

controller, which had a peak force of 3.000 lb_f with 3-5 Hz bandwidth

according to the computer simulation made by Buzan. The following

feedback gains were used in the computer simulation:

k_a = acceleration feedback gain = 400 lb_f/ft/sec^2

k_v = velocity feedback gain = 9.000 lb_f/ft/sec^2

k_f = force error signal feedback gain = 0.0003 in^2/lb$_f$

The computer simulation showed that 40% reduction of the r.m.s.

acceleration and 12% reduction of the r.m.s. lateral displacement could

be achieved. However, the simulated pneumatic power consumption was

calculated as high as 27 to 38 HP per car, i.e., 270 to 380 HP is needed for a train which has ten passenger cars.

Due to the high horsepower requirement, alternate approaches to controller design and components were under study and supervised by Professor Hedrick. At the same time, the first laboratory apparatus for testing general controllers was designed and fabricated. Subsequent research included the following major areas:

1. power consumption studies, (including air compressor studies)

2. different valves, including

    a) the proportional valve

    b) the FESTO 8161 MC - 4/5 - 1/2 valve

    c) the FESTO MC valve set

3. different actuators:

    a) the FIRESTONE #25® airspring

    b) the PARKER single-rod cylindrical actuator

    c) the ANA double-rod cylinder

4. different control circuits:

    a) the pulse width modulation circuit, i.e., the PWM circuit

    b) the Bang-Bang with lead compensation circuit, i.e., the BBLC circuit.

1-6 Scope and Objectives

One means of overcoming the ride quality/suspension stroke trade-off

problem of the passive suspension control for passenger rail vehicles is

to use active control instead of passive control. The active control can

not only store (or dissipate) energy but also input (increase) energy

into the system actively from external energy sources. Based on the

system states, active control laws can be implemented beyond the limits

of the constitutive relations of the passive suspension elements. The

background of, motivation for, and introduction to, the pneumatic

controller for the secondary lateral active suspension control system are

discussed in Chapter I.

In Chapter II, physical considerations of the Passenger Rail

Vehicle, i.e. the Budd Pioneer III truck, were made to study the

feasibility of implementing an active controller. The Lateral Active

Suspension Controller (LASC) was designed to meet these considerations,

and its characteristics are discussed in detail. The system elements

such as the air compressor, the valve, and the actuator were modelled and

analyzed resulting in adequate constitutive equations for controler

elements. A fifth order state-variable equation was derived to represent

the pneumatic secondary lateral active suspension system. Transfer

functions were derived from the state variable representation to

determine the system characteristics. Phase-variable representation of

the same system was also presented to result in other forms of transfer

functions of interest.

The design and fabrication of the testing facility for the Lateral

Active Suspension Controller, i.e. the LASC tester, are the major topics

discussed in Chapter III. The Dynamic Similitude method was used to

calculate the parameter values for the scale model from the full size system. Based on the parameter values calculated for the scale model, the system elements were analyzed separately. The mechanical assembly, flexibility of the LASC tester to perform different testings for various kinds of actuators, valves, control system of higher orders, control systems of higher DOF's, and multiple system inputs are also discussed.

In Chapter 4 the experimental results of testings are obtained and compared with the theoretical values of the digital computer simulation. This chapter includes: (1) dynamic tests and static tests of two kinds of actuators - the airspring and the actuator; (2) two types of control circuits - the pwm control circuit and the BBLC control circuit; (3) and two sets of valves - the FESTO 4861MC-5/4-1/2 valve and the 4-FESTO-MX-2-1/4. Selections of adequate control system elements were made according to theoretical and experimental results.

In Chapter 5 conclusions of this project, recommendations for further research, and guidelines to continue this project are presented.

- 37 -

CHAPTER 2

THE ANALYSIS OF THE LATERAL ACTIVE SUSPENSION SYSTEM

2.1 Introduction

The objective of this project is to experimentally evaluate the peformance of the pneumatic lateral active suspension controller. An active suspension can input energy to a control system and optimize the dynamics of the system in a preferred manner which a passive suspension can not achieve. Evaluation was made based on the controller capability of performing stability, accuracy, and speed of response vs. the economic cost which is expressed by the compressor power consumption.

In this chapter, the physical consideration of the plant to be controlled (the Budd Pioneer III truck) is investigated in the beginning. The Lateral Active Suspension Controller (the LASC Controller) is designed and proposed to meet the performance required and also to fit into the limited space available on the plant.

The characteristics of the LASC Controller are further studied and advantages of its design are presented in detail. Analytical Evaluation of LASC's major components is made and constitutive relations of the controller components are derived separately to understand dynamics of each of the components.

A 5th order state variable equation is then derived by using the constitutive laws of the components. This representation is important in doing the analytical evaluation and computer simulation. Transfer functions of interest are derived and transformation to the phase-variable representation of the LASC controller is also completed from the transfer function derived previously.

Figure 2-2-1   Truck Arrangement

Coil Spring

Air Spring

Bolster

Bump Stop Plates

Truck

Wheels and Axles
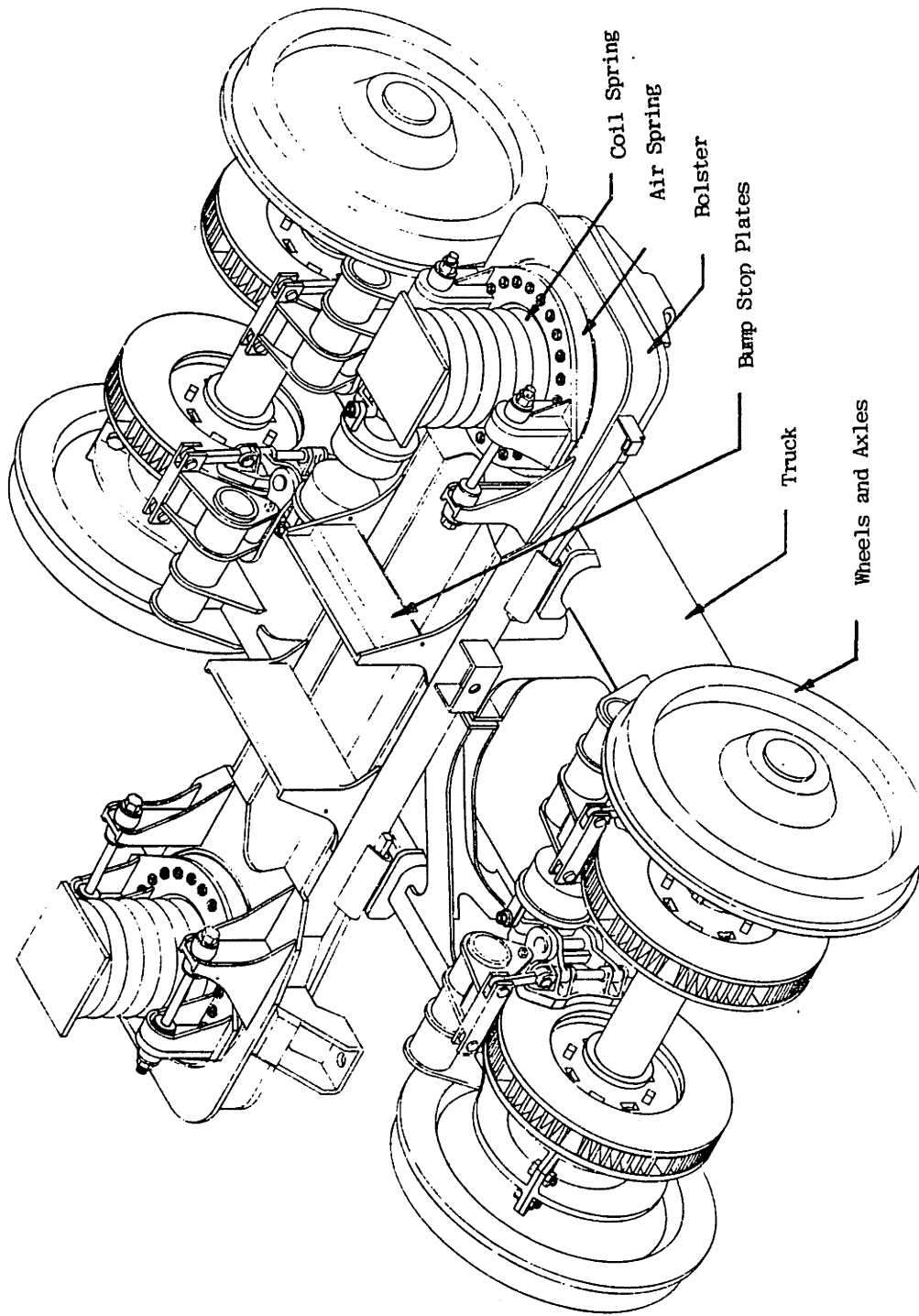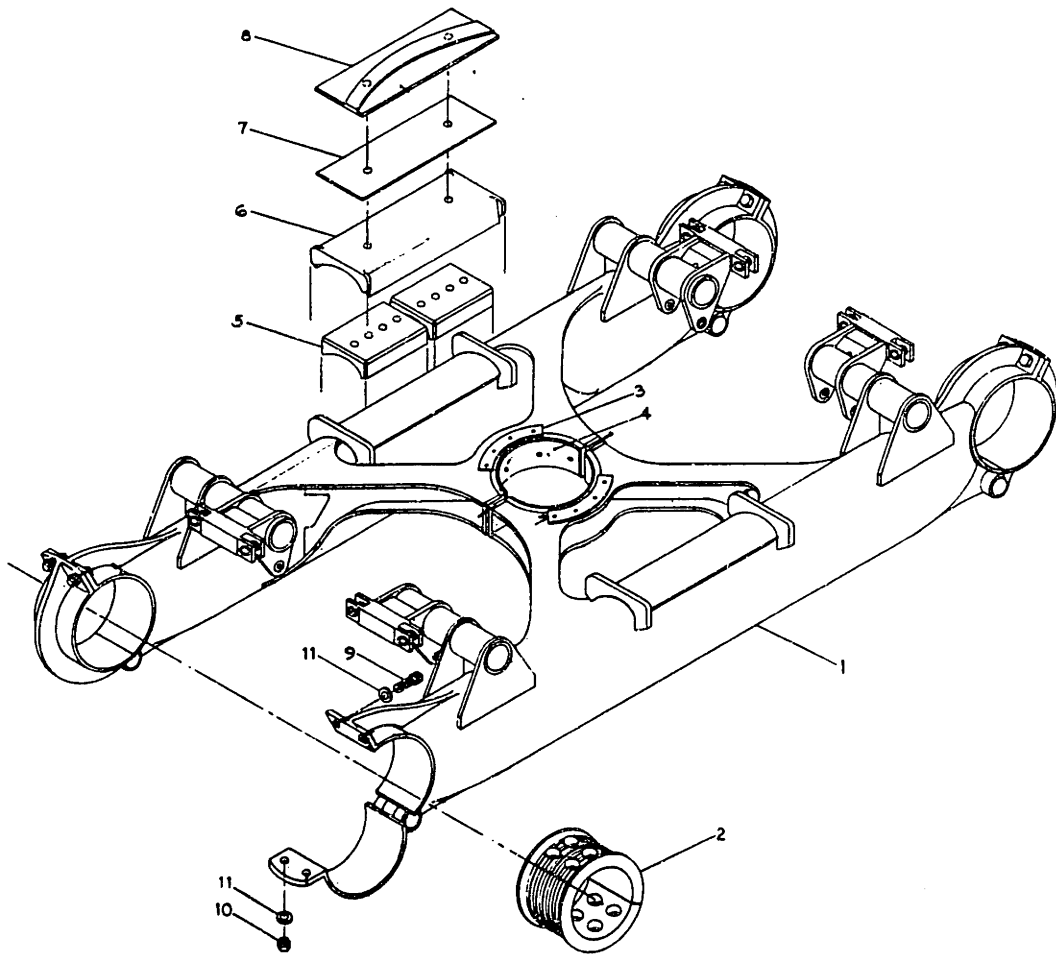
Figure 2-2-2   Truck Frame Arrangement
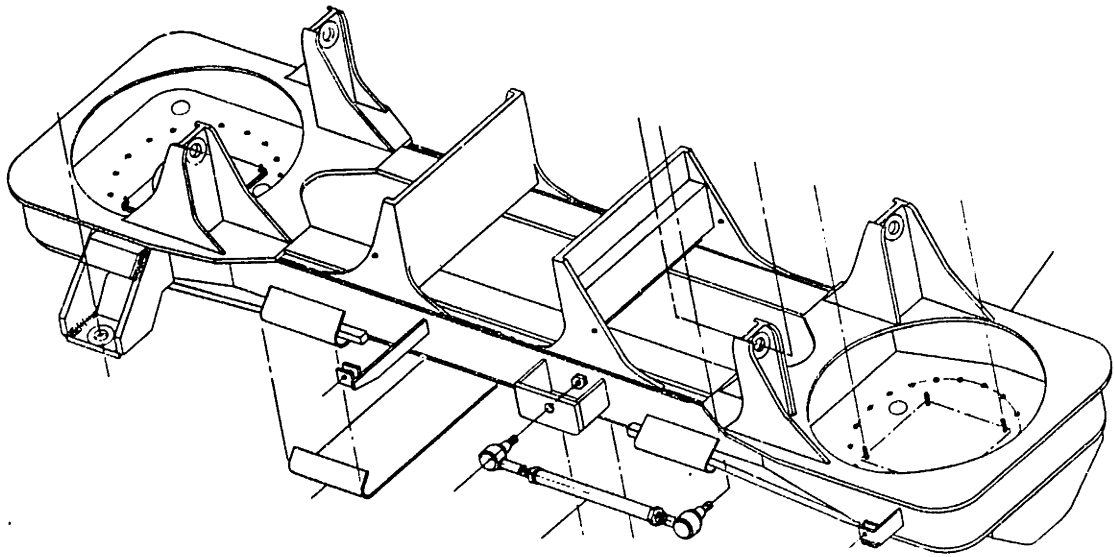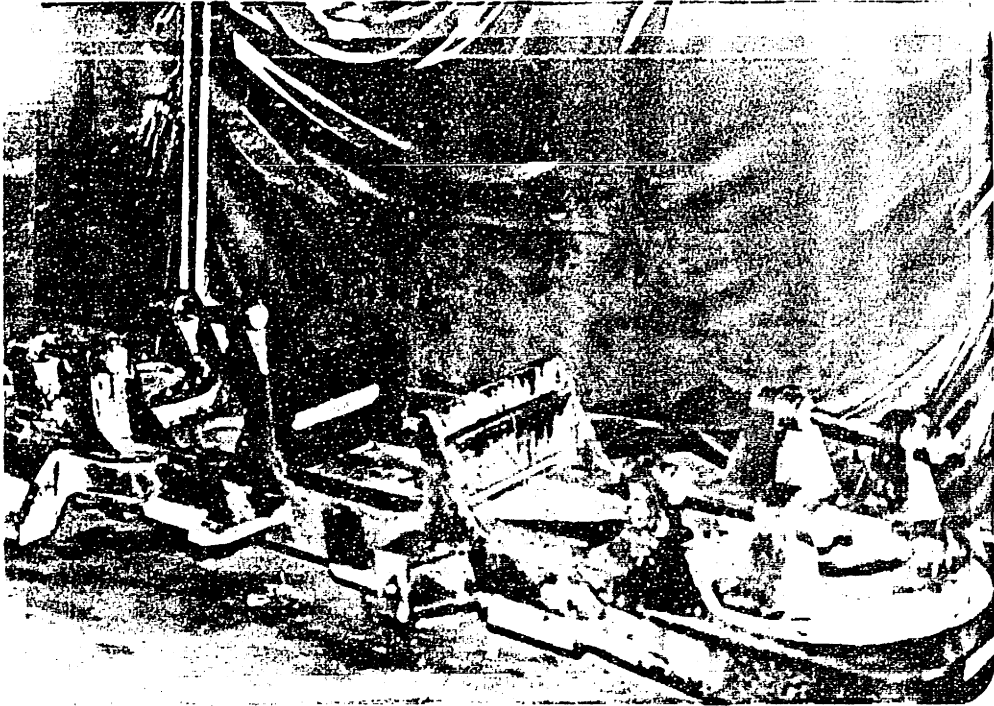
Figure 2-2-3   Bolster Assembly

2.2 Physical Consideration of the Passenger Rail Vehicle

2.2.1 Introduction

The Budd Pioneer IV truck is designed for lightweight use and includes the following major components: wheels and axles, journal bearings, speed sensors, truck brake equipment, ground straps, a spring suspension, a leveling valve, a center plate and pivot, side bearings, a lateral bumper, a shock absorber, and a bolster radius rod. The bolster center pivot fits into the center of the truck and is locked into position on the side frames by the center plate flange assembly. The carbody suspension consists of a coil spring mounted on top of an air spring. The bottom part of the air spring is mounted to the bolster with a bead ring. This assembly is placed at each end of the bolster to support the carbody. Forces are transmited from the truck to the car body by the bolster. The bumpstop plates are mounted vertically on the bolster structure to limit the relative lateral displacement between the carbody and the truck. The weight of the car body is supported by the bolster and transmitted to the truck frame. The details of the car body, bolster, and truck frame are shown in the preceding Figures:

(1) Figure 2-2-1: Truck Arrangment

(2) Figure 2-2-2: Truck Frame Arrangement

(3) Figure 2-2-3: Bolster Assembly

Several field trips were made to South Station, Boston to measure the available spaces for the active suspension controller. Detailed dimensions of the proposed spaces, as measured by Chen [13], which are currently occupied by pipe lines and electrical lines, are shown in the following Figures.

(1) Figure 2-2-4: The Relationship between the Carbody and

the Bolster of the Budd Pioneer III Truck

(2) Figure 2-2-5: The Location of the Controller when the

carbody is at its neutral position

(3) Table 2-2-1: The Parts List of Figures 2-2-4 and 2-2-5

The active suspension controller exerts the relative force between the

carbody and the truck, and will be mounted in parallel with the

lateral axis passing through the center of mass of the truck

arrangement.

2.2.2 Limited Space Available for Mounting the Lateral Active Controller

The lateral active suspension controller is shown in Figure 2-2-6

2-2-7 and is composed of the following major components: the pneumatic

actuator, the connecting rod with roller, the connecting rod bearing,

the air supply fixture, the controller mount, and the connection rod

guide. Two sets of controllers work together to exert relative forces

between the carbody and bolster. In order to have the roller move on

the bumpstop plate, the current bumpstop plate must be made flat. Due

to the possible relative lateral movement between the bolster and the

carbody, the available space to mount the active suspension controller

was carefully studied at various extreme relative positions. The

location of the controller is still within the limited available space

even if the car body is displaced 1.5 inches to the right (or left) as

shown in Fig. 2.2.6.

The vertical distance between the carbody and the bolster is not a

constant; it varies with the carbody weight, the relative force of the

Scale: 1/8
Unit = inch
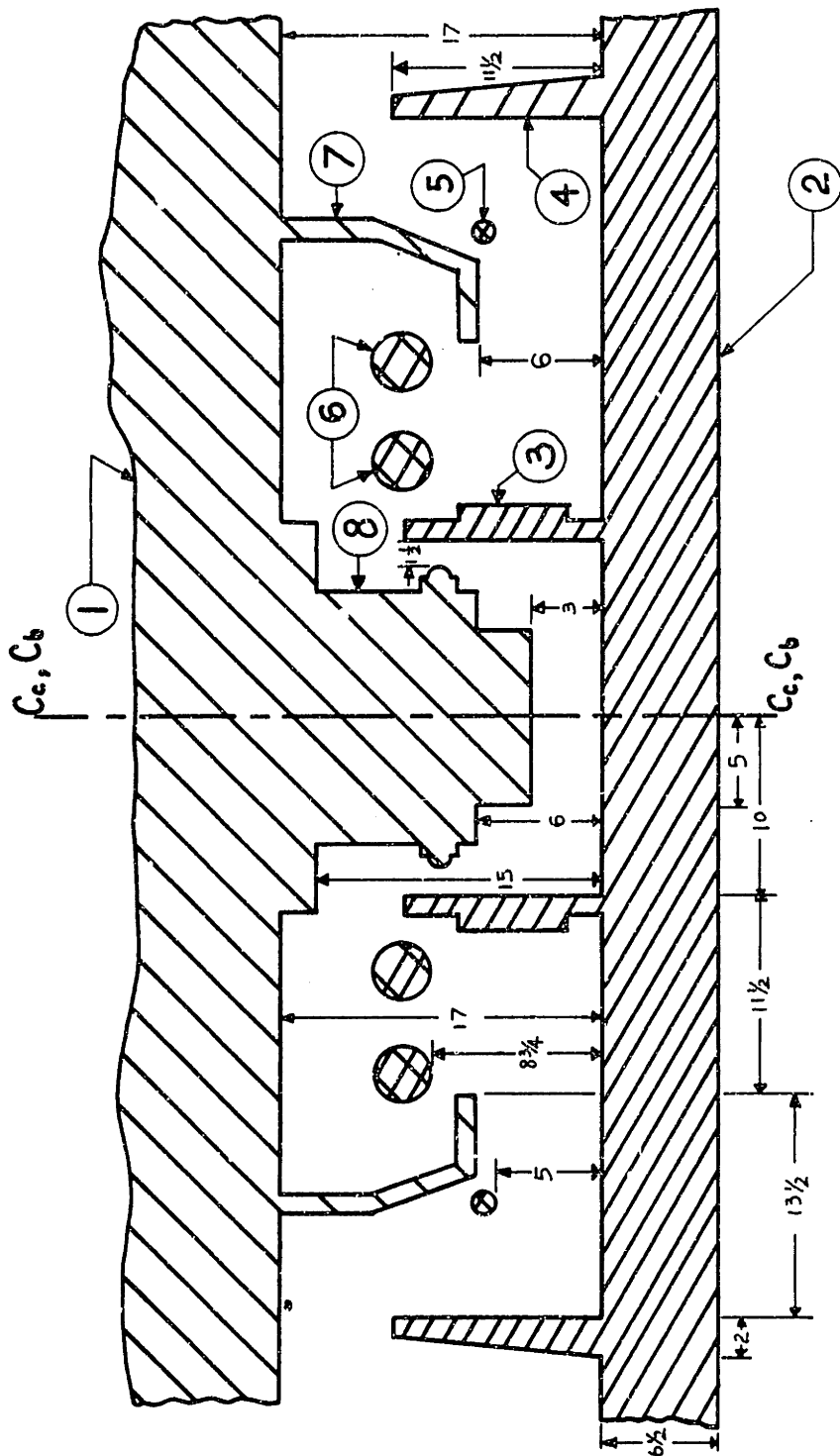
Figure 2-2-4 The Relationship Between the Carbody and the Bolster of the Budd Pioneer III Truck

Scale: 1/8
Unit = inch

Figure 2-2-5: The Location of the Controller when the Carbody
is at its Neutral Position

PART NO.	QTY.	DISCRIPTION
28	1	DRIVE ROD
27	1	AIR SUPPLY FIXTURE
26	1	MODIFIED BUMPSTOP PLATE
25	1	ROLLER
24	1	DRIVE ROD BEARING
23	1	ACTUATOR ROD GUIDE
22	1	PNEUMATIC ACTUATOR
21	1	ACTUATOR MOUNT
8	1	BUMPER
7	1	BEAM
6	2	PIPES
5	1	PIPES
4	1	VERTICAL SUSPENSION MOUNT
3	1	BUMPSTOP PLATE
2	1	BOLSTER
1	1	CARBODY

THE ACTIVE CONTROLLER

| SCALE | 1/8 | DATE | May'82 |

Table 2-2-1   Parts List of the LASC Controller   (Figure 2-2-4 and Figure 2-2-5)

coil spring, and the relative force of the air spring of the vertical
secondary suspension system. The maximum vertical displacement of the
carbody relative to the bolster is 3 inches. Therefore, the active
suspension controller must allow 3 inches of vertical displacement (as
shown in Fig. 2.2.6). The schematic diagram of the controller is shown
in Fig. 2.2.7. A roller is attached at the end of the drive rod and is
able to roll vertically on the modified bumpstop plate. The current
shape of the bumpstop plate must be remodelled to be flat in order to
have the roller move on it.

Two sets of the lateral active suspension controller work together
to exert relative force between the car body and the bolster. This type
of controller for passenger rail vehicle is called an LASC controller
and was designed by Chen [24]. Each LASC controller is composed of the
following major components: the actuator mount, the valve, the control
circuit, the actuator, the load cell, the string pot, the fluid tubing,
the drive rod, the roller, the dust shade, the drive rod bearing, and
the drive rod guide.

2.2.3 The Design of the Lateral Active Suspension Controller

The dust shade prevents the adherence and accumulation of dust or
other impurities on the roller and the bumpstop plate. The bumpstop
plate is lubricated by the controller to decrease the friction of the
roller movement. The main advantage of the LASC controller is that it
assures perfect axial alignment and also permits flexibility in using
different kinds of actuators such as airsprings or cylinders.

Scale: 1/8

Unit = inch
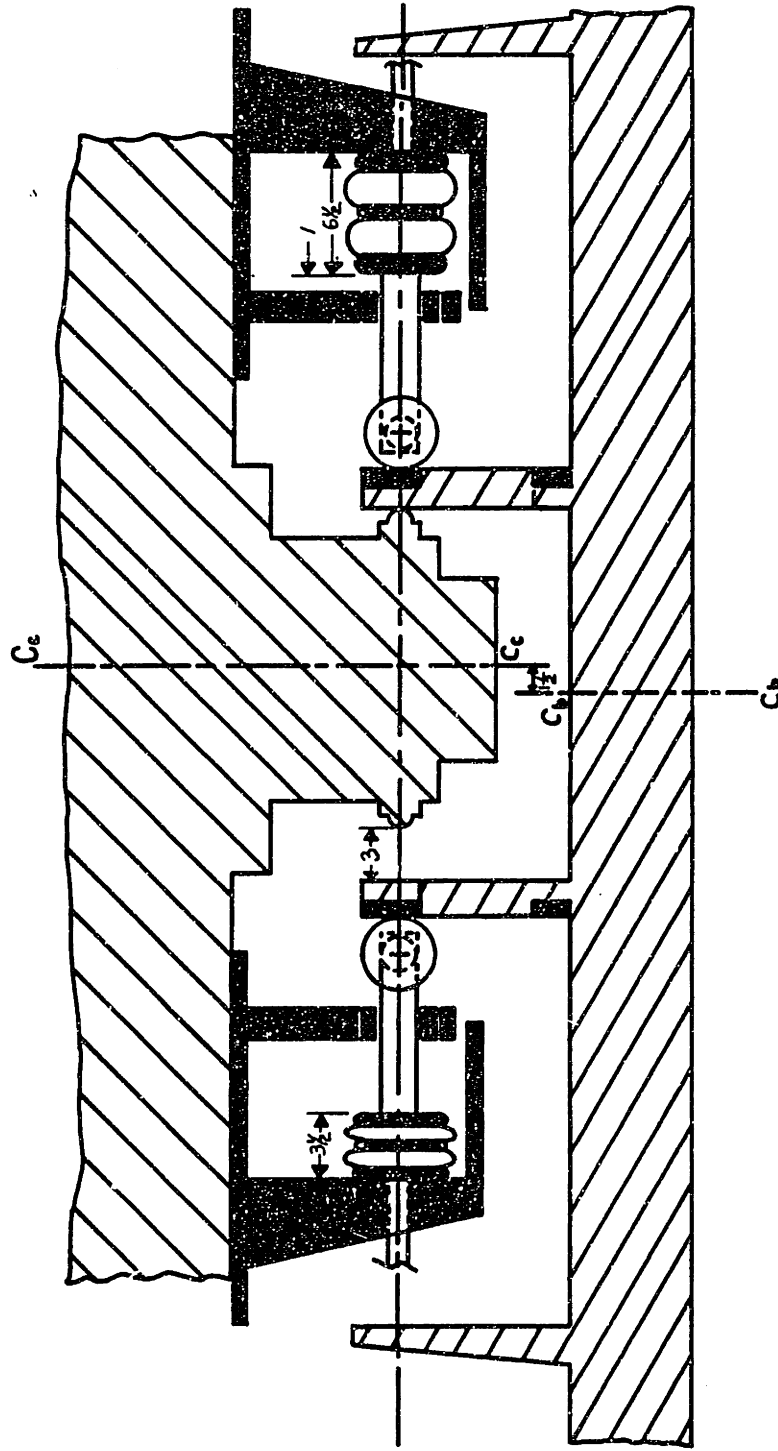
Figure 2-2-6   The Location of the Controller when the Carbody
is Displaced 1½ inches to the right

TABLE 2-2-2 BASELINE VEHICLE PARAMETERS

WHEEL RAIL PARAMETERS

a_{11}	wheelset roll coefficient	0.025
δ_o	centered contact angle	0.025
Δ	contact angle difference	0.000
f_{11}	lateral creep force coefficient	1.0×10^6 lb
f_{12}	lateral/spin creep coefficient	8500 ft-lb
f_{22}	spin creep coefficient	80 ft^2-lb
f_{33}	longitudinal creep force coefficient	8.0×10^6 lb

WHEEL PARAMETERS

a	half of track gauge	2.35 ft
N	load per wheelset	26100 lbs
λ	wheel conicity	0.025
Mw	wheelset mass	106.8 slugs
I_{wx}	wheelset roll moment of inertia	500 slugs-ft^2
I_{wy}	wheelset pitch moment of inertia	100 slugs-ft^2
I_{wz}	wheelset yaw moment of inertia	500 slugs-ft^2
Ro	centered wheel rolling radius	1.5 ft

TRUCK PARAMETERS

dp	1/2 of primary springs lateral spacing	1.9 ft
b	1/2 of wheelbase	4.25 ft
h_{tp}	vertical distance from truck c.g. to primary lateral springs	0.35 ft
h_{ts}	vertical distance from truck c.g. to secondary lateral springs	1.33 ft

TRUCK PARAMETERS

I_{tz}	truck frame yaw moment of inertia	2108 slug-ft^2
M_t	truck frame mass	212 slugs

CARBODY PARAMETERS

d_s	1/2 of secondary spring lateral spacing	3.75 ft
h_{cs}	vertical distance from carbody c.g. to secondary lateral springs	3.1 ft
ℓ_s	1/2 of truck center pin spacing	30 ft
w	weight of carbody	77433 lbs
I_{cz}	carbody yaw moment of inertia	1.483×10^6 slugs-ft^2
I_{cx}	carbody roll moment of inertia	64193 slugs-ft^2
M_c	carbody mass	2405 slugs

PRIMARY SUSPENSION PARAMETERS

k_{py}	primary lateral stiffness (4 per truck)	480,000 lb/ft
k_{px}	primary longitudinal stiffness (4 per truck)	960,000 lb/ft
c_{py}	primary lateral damping ($k_{py}/250$)	2020 $\frac{lb}{ft/sec}$
c_{px}	primary longitudinal damping ($k_{px}/250$)	2850 $\frac{lb}{ft/sec}$

SECONDARY SUSPENSION PARAMETERS

k_{sy}	secondary lateral stiffness (2 per truck)	24000 lb/ft
k_z	secondary vertical stiffness (2 per truck)	22200 lb/ft
k_{spsi}	secondary yaw stiffness (1 per truck)	1×10^6 ft-lb/rad

<u>SECONDARY SUSPENSION PARAMETERS</u>

c_{sy} secondary lateral damping
(2 per truck) $1200 \frac{lb}{ft/sec}$

c_{sz} secondary vertical damping
(2 per truck) $2000 \frac{lb}{ft/sec}$

c_{spsi} secondary yaw damping
(1 per truck) $4000 \frac{lb}{ft/sec}$

<u>PASSENGER LOCATIONS FOR RIDE QUALITY</u>

Front distance from carbody c.g. $x = 30$ ft $z = -1.7$ ft

Rear $x = -30$ ft $z = -1.7$ ft

<u>PERFORMANCE CAPABILITIES OF BASELINE VEHICLE</u>

Critical Speed   310 mph
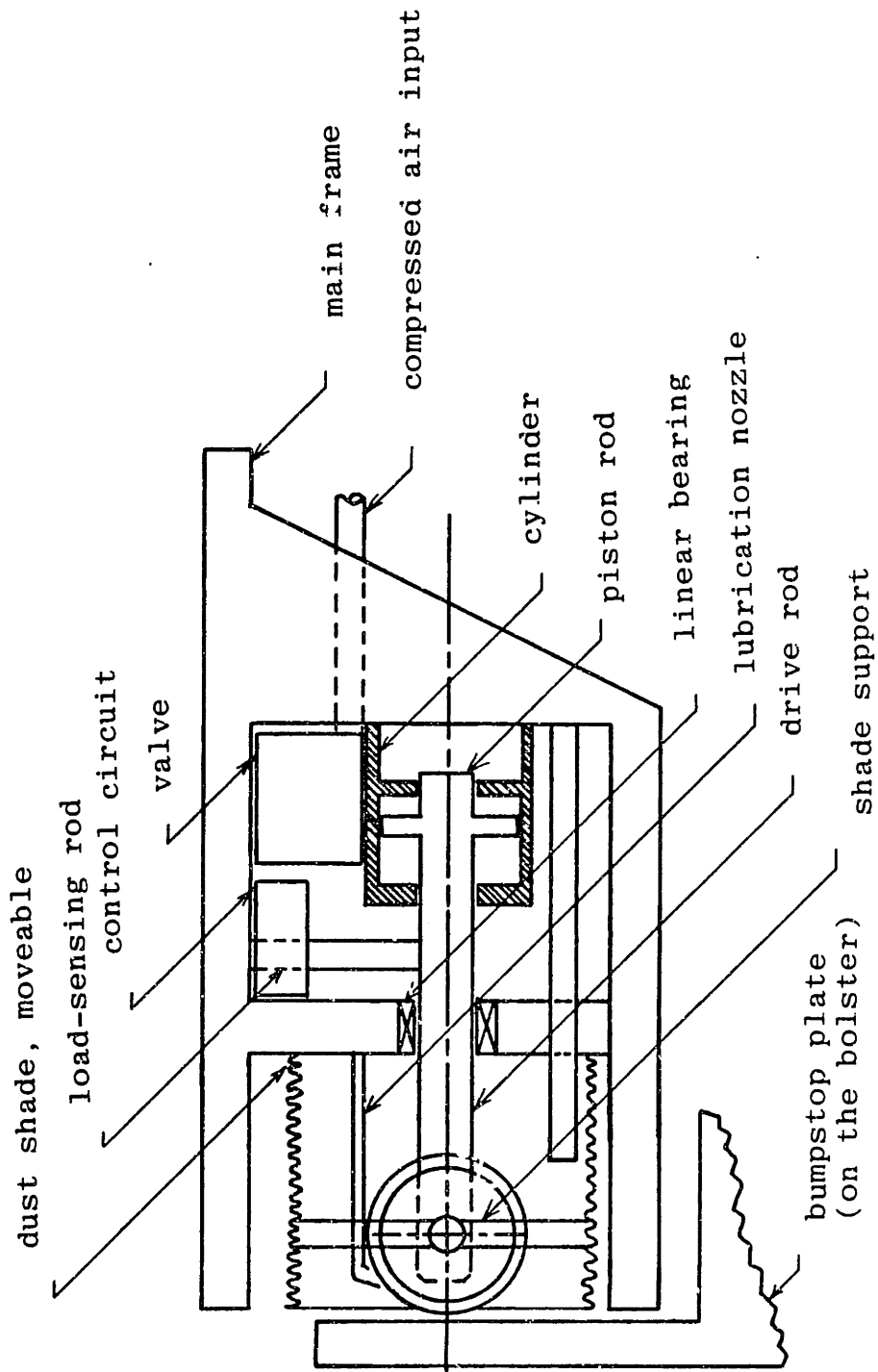
Figure 2-2-7   The Schematic Diagram of the Lateral Active Suspension
Controller

2.2.4 The Advantages of the Design of the LASC Controller

The LASC controller is a complete unit in itself because it can function automatically without external dependence when compressed air and electricity are furnished. The unnecessary interactions between the controller and other parts of the vehicle can be minimized by the "unification concept" of design which is adopted by the LASC controller. More advantages of the LASC controller are discussed below:

(1) The LASC controller is operated in a closed-loop by sensing, processing, and actuation automatically. It also allows the option of manual override.

(2) The LASC controller can be mounted and dismounted without much difficulty. The length of the drive rod between the end roller and the actuator can be adjusted to fit for different vehicles.

(3) The LASC controller is equipped with its own protection mount which is important when traveling on hazardous surfaces such as heavy snow areas.

(4) Every part of the LASC controller can be disassembled from the unit for replacement or maintenance without unloading the entire controller. The parts, such as the actuator, the drive rod, etc. can be made interchangeable for easy repair.

(5) The linear bearing which is placed between the drive rod and the drive rod guider has an efficiency of up to 99.8% [25]. Non-axial forces are eliminated by the linear bearing, i.e. the LASC controller can be operated unidirectionally.

(6) The manufacturing cost of the LASC controller can be decreased substantially after the standardization of parts is completed.

(7) Through an adequate arrangement, a 3-dimensional active suspension controller can be implemented to control an object in space. This idea is further illustrated in Section 3.13

2.3 Analytical Evaluation of Controller's Major Components

2.3.1 Introduction

In this section, the modelling, analysis, and evaluation of various controller components are studied to form the basis of component selection. These components include compressors, valves, actuators, and control circuits.

2.3.2 Air Compressors

An air compressor was used to compress the ambient air to the accumulated high pressure. The specific compressor work, w, can be calculated for the steady state, steady flow process as follows:

$$w = \int_{inlet}^{outlet} \frac{1}{\rho} \, dp \tag{1}$$

where   inlet = the ambient air at 70°F, 14.7 psia

outlet = the compressed air at 130° psig

Two different operating conditions, i.e., the isothermal process and the isentropic process, are assumed to calculate the compressor work as shown by Buzan [23].

1. Assuming isothermal process,

$$w = RT_{inlet} \, \ell n \, (\frac{P_{outlet}}{P_{inlet}}).$$ (2)

$$= 118 \text{ HP-sec/lb}_m$$

(2) Assuming isentropic process, i.e., the process is reversible and adiabatic

$$w = \frac{K}{K-1} R \, T_{inlet}[(\frac{P_{outlet}}{P_{inlet}})^{\frac{k-1}{k}} - 1]$$ (3)

$$= 166 \text{ HP-sec/lb}_m$$

where k = the specific heat ratio of air, 1.4

   R = the universal gas constant for air

2.3.3 Valves

For a compressible working medium such as air, the flow through a valve is a function of the upstream stagnation pressure, p_u, the downstream pressure, p_d, the upstram sagnation temperature, T_u, the discharge coefficient, C_d, and the orifice area A_o. The empirical relations describing compressible air flow through a single orifice area were calculated by Ezekiel in [26] and was used by Buzan in [23].

The equation of weight flow rate is divided into two cases, according to the critical value of the ratio of the downstream pressure over the upstream stagnation pressure, p_d/p_u, as follows:

Case (1) $p_d/p_u \geq 0.528$

$$\dot{\omega} \; C_1 C_d A_o \; \frac{p_u}{\sqrt{T_u}} \; (\frac{p_d}{p_u})[1 - (\frac{p_d}{p_u})^{\frac{k-1}{k}}] \qquad (4)$$

Case (2) $p_d/p_u < 0.528$

$$\dot{\omega} = C_2 C_d \; A_o \; \frac{p_u}{\sqrt{T_u}} \qquad (5)$$

where $\dot{\omega}$ = weight flow rate, lb_m/sec.

C_d = discharge coefficient of the orifice

A_o = orifice area, in^2

p_u = upstream stagnation pressure, psia

p_d = downstream pressure, psia

T_u = upstream stagnation temperature, $^\circ$R

k = 1.4

R = 2.48×10^5, $in^2/sec^2 \; ^\circ$R

$$C_1 = g \sqrt{\frac{2K}{R(K-1)}} = 2.06 \sqrt{\frac{^\circ R}{sec}}$$

$$C_2 = g \sqrt{\frac{K}{R(\frac{K+1}{2})^{(K+1)/(K-1)}}} = 0.532 \sqrt{\frac{^\circ R}{sec}}$$

2.3.4 Actuators

The lateral active suspension controller needs actuators to implement the control law and perform its active suspension function. An actuator is operated between two energy domains which may be the same or different according to the nature of the actuator employed. When using Bond Graph Modelling Methods, an actuator is always referred to as a transformer. A level arm with a pivot is a simple actuator which transfer power to and from the same mechanical energy domain. On the contrary, an electrical magnet, or a hydraulic cylinder, transfers power to and from different energy domains. Most industrial automatic controllers use pressurized fluid (such as oil or air) or electricity as power source. Automatic controllers are classified into different categories according to the working medium employed. There are hydraulic actuators, electro-magnetic actuators, electro-mechanical actuators, and pneumatic actuators, etc.

The LASC controller allows possibilities of using various kinds of actuators to achieve its active control goal. The hydraulic actuators are noted for their ability to exert large forces, to provide high bandwidth, and to give large displacement output. The AMTRAK's experience of using hydraulic controllers was unfortunately not very encouraging. The operating conditions of the AMTRAK, such as cost, availability, reliability, maintenance, and repair made the pneumatic actuator more adequate selection. Besides, AMTRAK's vehicles already had air compressors on board. A 75 horsepower electric compressor, and another 130 horsepower diesel compressor were mounted on the AEM-7 locomotive and the F-40 locomotive separately. The pneumatic power on board was used for braking the vehicle and supplying the water. In case

the hydraulic power was selected, then the introduction of a new power source would largely increase maintenance problems and the bulkiness of the system. The actuators under study at MIT are shown in Figure 2-3-1, and listed in Table 2-3-1. However, not all of the actuators listed in the above table will be discussed in the project.

Basically there are two kinds of actuators used in automatic controllers, one kind has a rigid side-wall (such as a cylinder), another kind has an elastic, flexible side-wall (such as an airspring). Cylinders can be further classified into single-rod cylinders or double-rod cylinders. For example, the PARKER cylinder, as shown on the left part in Figures 2-3-2 and 2-3-3, is a single-rod and the ANA cylinder is a double-rod.

In Chapter 3, the actuators used in generating external disturbance input to the control system will be discussed. The actuators studied in this section should not be confused with those investigated under another subject in Chapter 3.

2.3.5 Airsprings

A FIRESTONE #25® airspring was used in the design of the lateral active suspension controller for the railroad passenger vehicle. The following figures and tables explains the fundamental idea of the airspring.

(1) Figure 2-3-4: The Schematic Diagram of a Double Con-
volution airspring.

(2) Figure 2-3-5: The Schematic Diagram of the FIRESTON #25®
Airspring.

(3) Figure 2-3-6: The Characteristic Curves, Volume Curve, and
Recommended Operating Height of the FIRESTONE #25® airspring.
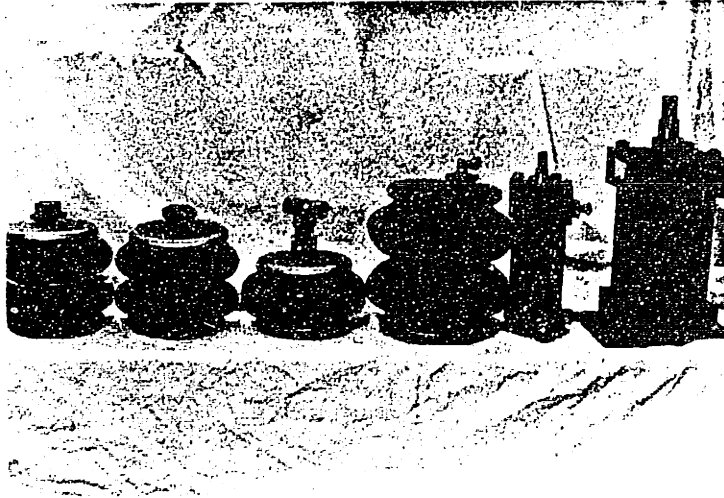
Figure 2-3-1   Different Actuators

No.	Type	Notes
		Different Actuators
1	Air Spring	FIRESTONE # 25
2	Air Spring	FIRESTONE # 25 with internal spacers
3	Air Spring	FIRESTONE #131 with internal spacers
4	Air Spring	FIRESTONE #224
5	Cylinder	PARKER Cylinder, 4" bore (Model HMA 14)
6	Cylinder	WABCO Cylinder 1½" bore (Model CMT2-PP-C)

Table 2-3-1   Different Actuators (from left to right in
Figure 2-3-1)
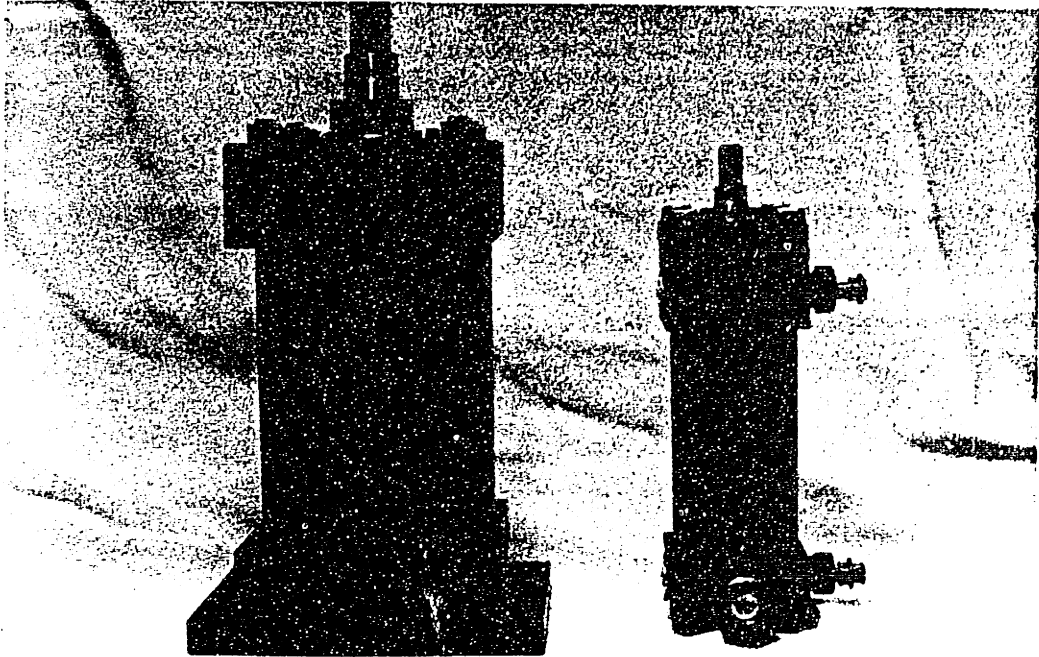
Figure 2-3-2   The PARKER Cylinder (in the left)
Model: HMA 14 , 4" bore

3 1/3

6 1/4

5 7/16

4 1/2

4 Holes, 7/16
These 4 Holes Need to be
Drilled for Mounting

Flange Mounts

5/8

7 5/8 + 3

6 1/4 + 3
(3" stroke)

1

1 1/8

Drive Rod, 3/4 - 16 Thread
Put Load Cell at this End

Unit: inch
Notes: 1. Critical alignment is needed
        2. Not to scale
        3. Model = HMA 14,4" bore cylinder
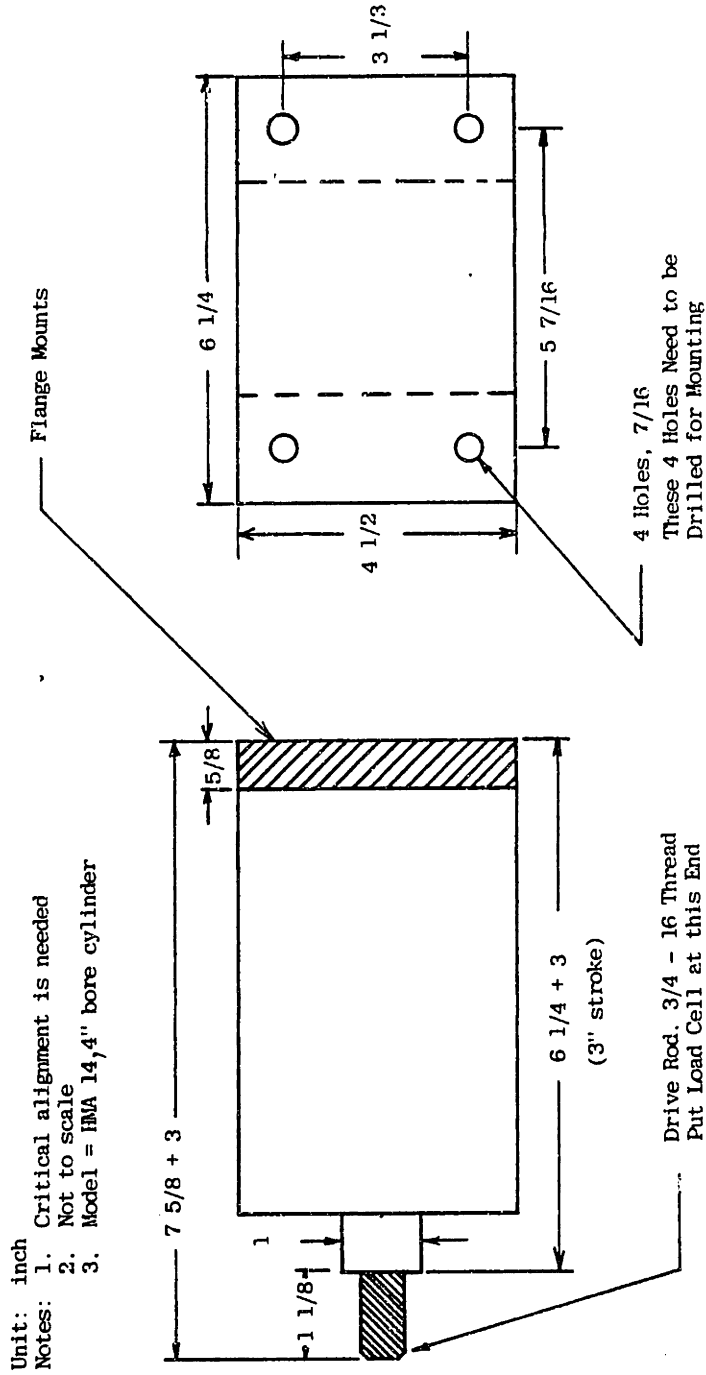
Figure 2-3-3   Dimensions of the PARKER Cylinder

Calculating the Application Area of Airspring

Taking 5.5 inches as the operating point, and linearizing the volume curve (Figure 2-3-4) at this operating point, the following equation can be derived

$$V_L(h) = V_o + A_p(h)$$

$$V_L(h) = 83.0 \text{ in}^3 + 18.8 \text{ in}^2(h) \tag{6}$$

where

V_o = the volume at the operating point, h_o, where h_o = 5.5 inches

A_p = the slope of the volume line

h = the displacement from the operating point

The cover bead area is calculated as 32.2 in^2, which is much larger than the application area A_p. The approximation error, e(h) is defined as the difference between $V_L(h)$ and V(h), (i.e., e(h) = $V_L(h)$-V(h)), where V(h) is the measured volume from the Figure 2-3-4. The values of V(h), $V_L(h)$, e(h), and e(h)/V(h) vs. the airspring height, h, are recorded in Table 2-3-4-2.

height h	$V_L(h)$	V(h)	e(h)	e(h)/V(h) %
h_1=4.0	54.8	58	-3.2	-5.5%
h_2=4.5	64.2	68	-3.8	-5.5%
h_o=5.5	83.0	83.0	0.0	0.0%
h_3=6.5	101.8	94.0	7.8	8.3%
h_4=7.0	111.2	98.0	13.2	1.30%

Table 2-3-2   The Linearization Error, unit = inches

2.3.6 Modelling the actuators

The actuators were modelled as capacitive elements. The constitutive relation of the actuators relating the rate of change of pressure, $\dot{p}$, and the mass flow rate $\dot{m}$, to the capacitance C is shown in the equation below:

$$\dot{p} = \frac{1}{C} \dot{m} \tag{7}$$

where $\dot{p}$ = rate of change of actuator pressure, $lb_f/in^2/sec$

  C = actuator capacitance, in^5/lb_f

  $\dot{m}$ = mass flow rate, lb_m/sec

Calculating the actuator capacitance

The actuator capacitance consists of fluid capacitance and mechanical capacitance which were experimentally calculated by Cho in [27]. Figure 2-3-7 shows the axial and radial expansions of the FIRESTONE #25 airspring which was fixed at 3" stroke and supplied with compression air of 130 psi.

(1) Since the side-wall of a cylinder is rigid, no expansion is allowed on the side-wall. The cylinder has only fluid capacitance, C_f, as expressed below:

$$\dot{p} = \frac{1}{C_f} \dot{W}$$

- 63 -
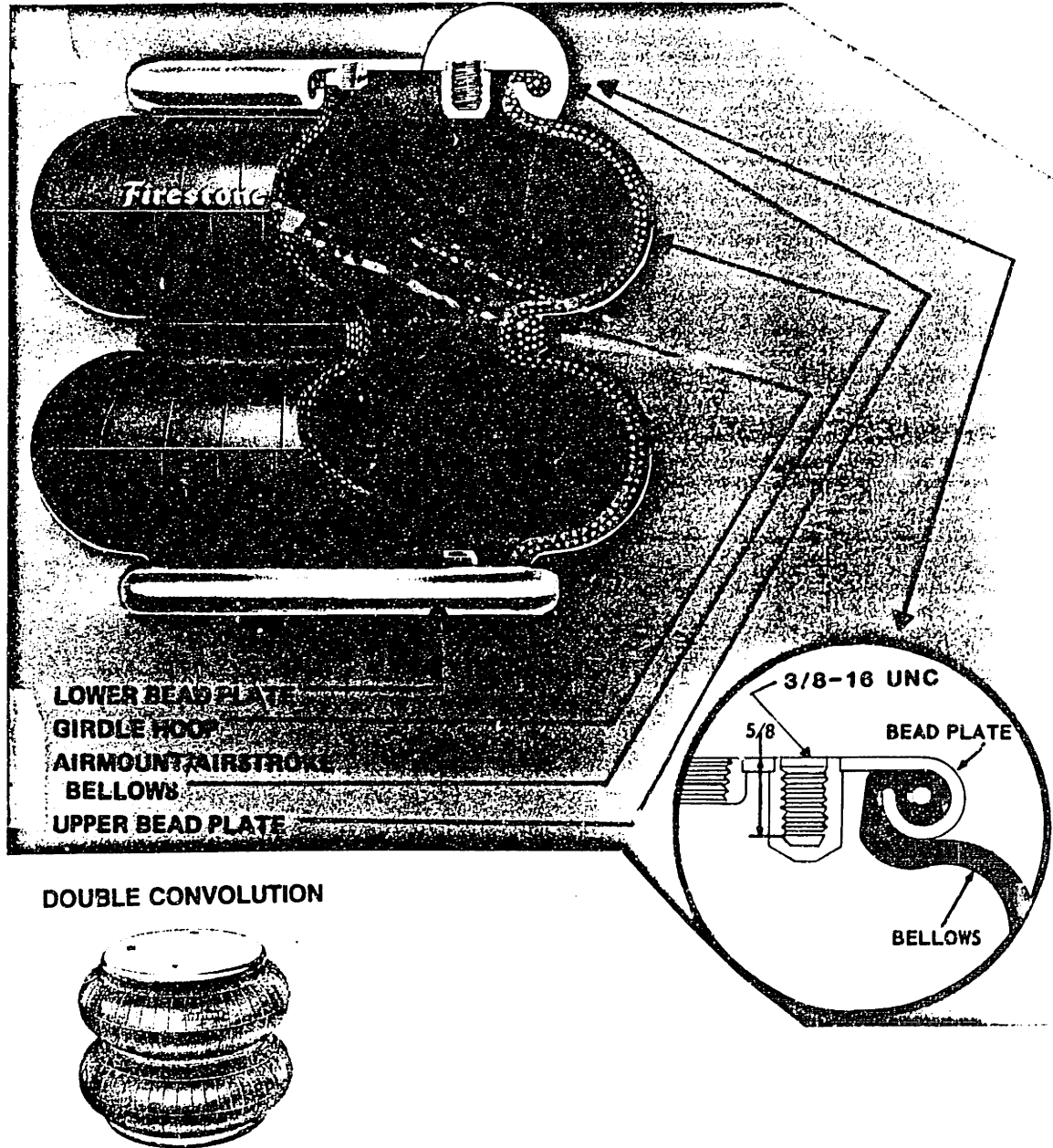
Figure 2-3-4   The Schematic Diagram of a Double-Convolution
              Air Spring [   ]

Figure 2-3-5   The Schematic Diagram of the
FIRESTONE #25 ® Air Spring
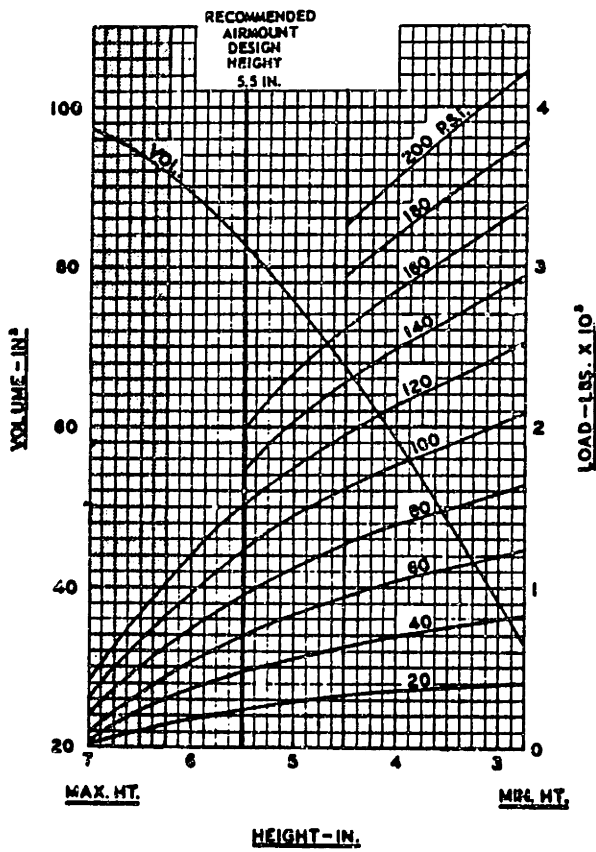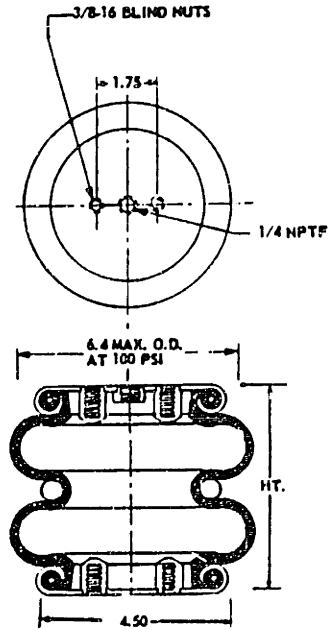
Figure 2-3-6 The
Characteristic Curves
of the FIRESTONE #25 ®
Air Spring
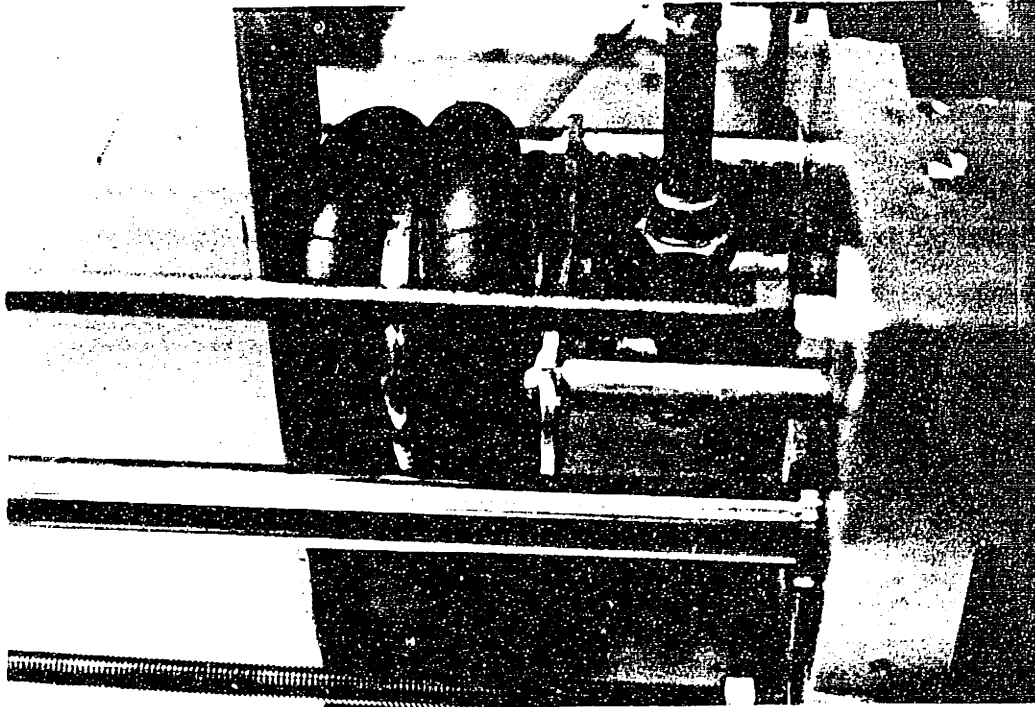
Figure 2-3-7   The Axial and Radial Expansion of the FIRESTONE® #25
                Airspring as it was Fixed at a 3" Stroke and Supplied
                with Compressed Air at 130 psi

Case 1: if an isothermal process is assumed,

$$\dot{m} = \frac{d}{dt}(\rho v)$$

$$\dot{\omega} = g\dot{m} = g\frac{d}{dt}(\ell v) = g\frac{d}{dt}\left(\frac{pV}{RT}\right)$$

$$\dot{\omega} = \frac{g}{RT}(\dot{pV})$$

$$\dot{p} = \frac{1}{c_f}\dot{\omega} = \frac{1}{\left(\frac{RT}{gv}\right)}\dot{\omega} \tag{8}$$

Case 2: if an isentropic process is assumed,

$$\dot{\omega} = \frac{gP_s^{(1-\frac{1}{k})}}{RT_s}\frac{d}{dt}(p^{\frac{1}{k}}V)$$

$$\dot{p} = \frac{1}{C_F}\dot{\omega} = \frac{1}{\frac{gV}{KRT_s}\left(\frac{P_s}{P}\right)^{1-\frac{1}{k}}}\dot{\omega} \tag{9}$$

where P_s = supply pressure

T_s = the temperature of the supplied fluid

(2) Since the side-wall of an airpring is elastic and flexible, the mechanical capacitance C_m, should be included as shown in the following equation.

$$\dot{p} = \frac{1}{C_f + C_m}\dot{\omega} \tag{10}$$

Case 1: If an isothermal expansion of the side-wall is assumed,

then

$$\dot{p} = \frac{1}{C_m} \dot{\omega} \frac{1}{\dfrac{gs[p + p_g) s - pdk_w x + pp_g ds]}{KRT_s K_w p}} \dot{\omega} \qquad (11)$$

Case 2: If an isentropic expansion of the side-wall is assumed,

then:

$$\dot{p} = \frac{1}{C_m} \dot{\omega} = \frac{1}{\dfrac{gs[(s + p_g)s - pdk_w x + p_g ds] p_s}{KRT_s K_w p}} \dot{\omega} \qquad (12)$$

where g = the gravity acceleration, 386 in/sec^2

   s = surface area of side wall, in^2

   p_g = gauge pressure, psig

   k_w = stiffness of side-wall lb$_f$/in

   x = expansion of side-wall, in^2

(3) If the volume, V, of the airspring changes, the rate of change

of volume must be taken into consideration when calculating the

total cpacitance. That is

$$\dot{p} = \frac{1}{C_f + C_m} \dot{\omega} + \frac{Kp}{V} \dot{V} \qquad (13)$$

where $\dot{V}$ = the rate of change of the airspring volume.

2.3.7 Control Circuits

2.3.7.1 Introduction

As stated in Chapter 1, the dynamics of a rail passenger vehicle were decoupled into vertical and lateral carbody motions. Since the yaw motion was neglected, the lateral dynamics of the carbody were then modelled to have only one degree-of-freedom. The LASC controller for the Lateral Active Suspension Control of the passenger rail vehicle was designed based on this one DOF model. In order to successfully apply the lateral active suspension controller to rail vehicles, it must be designed to be simple, reliable and economical. The local ride controller, which was proposed by Celniker [20] to overcome the ride quality/suspension stroke trade-off did require a proportional valve. Since air had been chosen as the working medium for the LASC controller, the proportional valve is needed to control the air flow. Due to the economic constraints and difficulty of maintenance of the pneumatic proportional valve, a solenoid (on/off) valve was chosen to replace the proportional valve. Solenoid valves are available commercially and inexpensively. However, they are more sluggish than the porportional valve and have air leakage problems (as discussed in Chapter 4).

The schematic diagram of the LASC controller was shown in Figure 1-5-1. Hedrick et al. [8] derived the following control law:

$$F_{AD} = C_V \dot{Y}_C + C_A \ddot{Y}_C \tag{1}$$

where F_{AD} is the force generated as a function of the state variables of the system such as $\dot{Y}_C$ and $\ddot{Y}_C$,

$\dot{y}c$ = the absolute velocity of the carbody

$\ddot{y}c$ = the absolute acceleration

C_A and C_V are constants

In order to avoid the theoretically infinite vibration amplitude of the carbody due to the failure of the LASC controller, the passive elements which are currently used in the secondary lateral suspension should not be removed. Equation (1) describes the desired actuator force in parallel with the passive components whose values are shown in Table 2-2-2.

The equation of motion for the passive model of the secondary lateral suspension was stated as follows:

$$M_c \, \dot{y}_c = \Sigma F = -K(y_c - y_t) - b(\dot{y}_c - \dot{y}_t) \tag{2}$$

After implementing the LASC controller, Equation (2) should be added to he term F_{AD} as follows:

$$M_c \, \ddot{Y}_c = \Sigma F = F_{AD} - K(y_c - y_t) - b(\dot{y}_c - \dot{y}_t) \tag{3}$$

The load cell of the controller gives the actual output force F_A as follows:

$$F_A = \text{the actual force generated by the actuator and} \tag{4}$$
$$\text{sensed by the load cell}$$

The error of the force was defined as

$$E_F = F_A - F_{AD} \tag{5}$$

A control unit should be implemented to control the solenoid (on/off) valve and route the air flow based on the input which is the force

error as shown in the following block diagram.
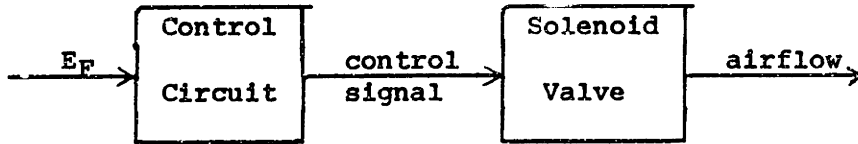
Figure 2-3-7-1

Two control circuits are discussed in this section. It was assumed that the control circuit could drive the solenoid valve fast enough to approximate a proportional valve. De Los Reyes [28] studied the Pulse Width Modulation circuit, the PWM control circuit, to drive the pneumatic solenoid valve. In parallel with this research, Barletta [29] studied the Bang-Bang with Lead Compensation Circuit, the BBLC circuit, the same idea presented above. Both of their works are discussed in the following sections.

2.3.7.2 The PWM Control Circuit

The Pulse Width Modulator (PWM) is an integrated circuit of Silicon General #SG 3526. Two PWM are needed to drive the control valve because one PWM can drive only one solenoid (valve) coil. The amplified error signal, ε, is formulated by amplifying the force error signal, E_F, with a force feedback gain, K_f.

$$\varepsilon = K_f \, E_F = K_f (F_{AD} - F_A) \qquad (6)$$

where F_{AD} is calculated from equation (1), ε has magnitude and sign.

The main function of the PWM circuit is to compare the input signal $|\varepsilon|$ with the sawtooth wave produced by the Pulse Width Modulator. The PWM control circuit outputs constant frequency pulses whose widths are porportional to the magnitude of the control signal according to the comparison between the error signal $|\varepsilon|$ and the sawtooth curve generated by the PWM.

- 71 -
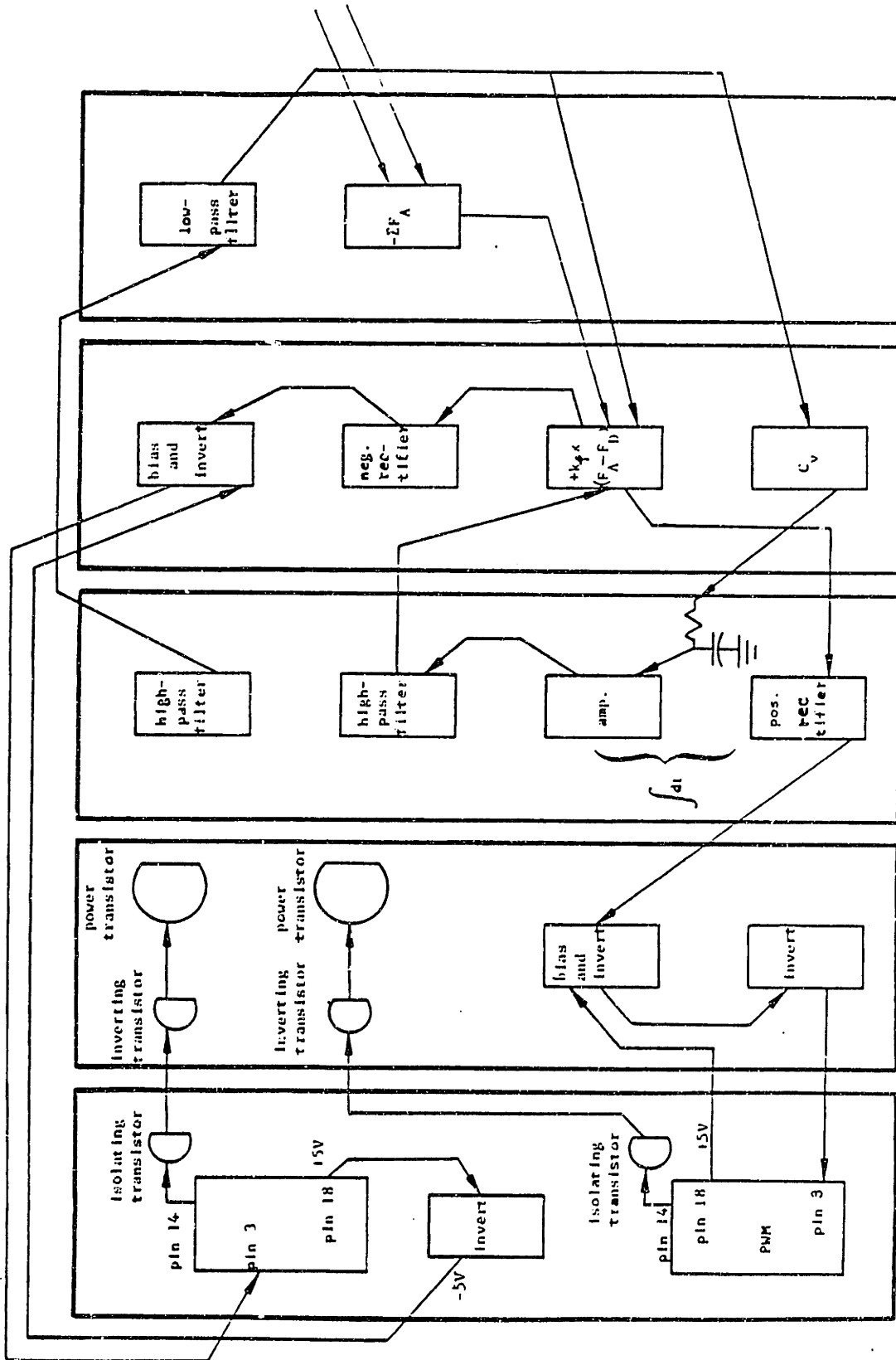
Figure 2.3.7.2 The PWM Control Circuit Hardware Layout (24)

The signals from the K_f amplifier, ε, are rectified (separated), and the negative ones are inverted because only positive input signals can be inputed to the 3rd pin of the PWM I.C.

The PWM electronic hardware layout is shown in Figure 2.3.7.2. Whenever the sawtooth curve is bigger than the input signal, $|\varepsilon|$, the pulse is defined as a "low" pulse because its magnitude is lower than the nominal peak voltage of +3.0 V of the modulator, otherwise the pulse is defined as a "high" pulse. Whenever there is a high pulse, the corresponding solenoid coil will be energized because a high pulse is produced only when the input signal exceeds the sawtooth curve of the modulator.

Due to the significant lag in turning on/off the solenoid valve, the bandwidth of the solenoid valve must be greater than 20 Hz to make the PWM control circuit successful. Such a valve can only be constructed at great cost which may make the proportional valve more favorable at the same price range.

2.3.7.3   The BBLC Control Circuit

The BBLC control circuit was developed by Barletta [29] in parallel with this research because the PWM control circuit cannot meet the requirements of driving a solenoid valve efficiently to control the air flow through the control valve and into or out of the actuators.

Figure 2.3.7.3 shows a schematic diagram of the BBLC circuit which can be flow charted as follows:

(1)   the desired force, F_{AD}, is generated by Equation (4).

(2)   the actual force, FA, is generated by Equation (4).
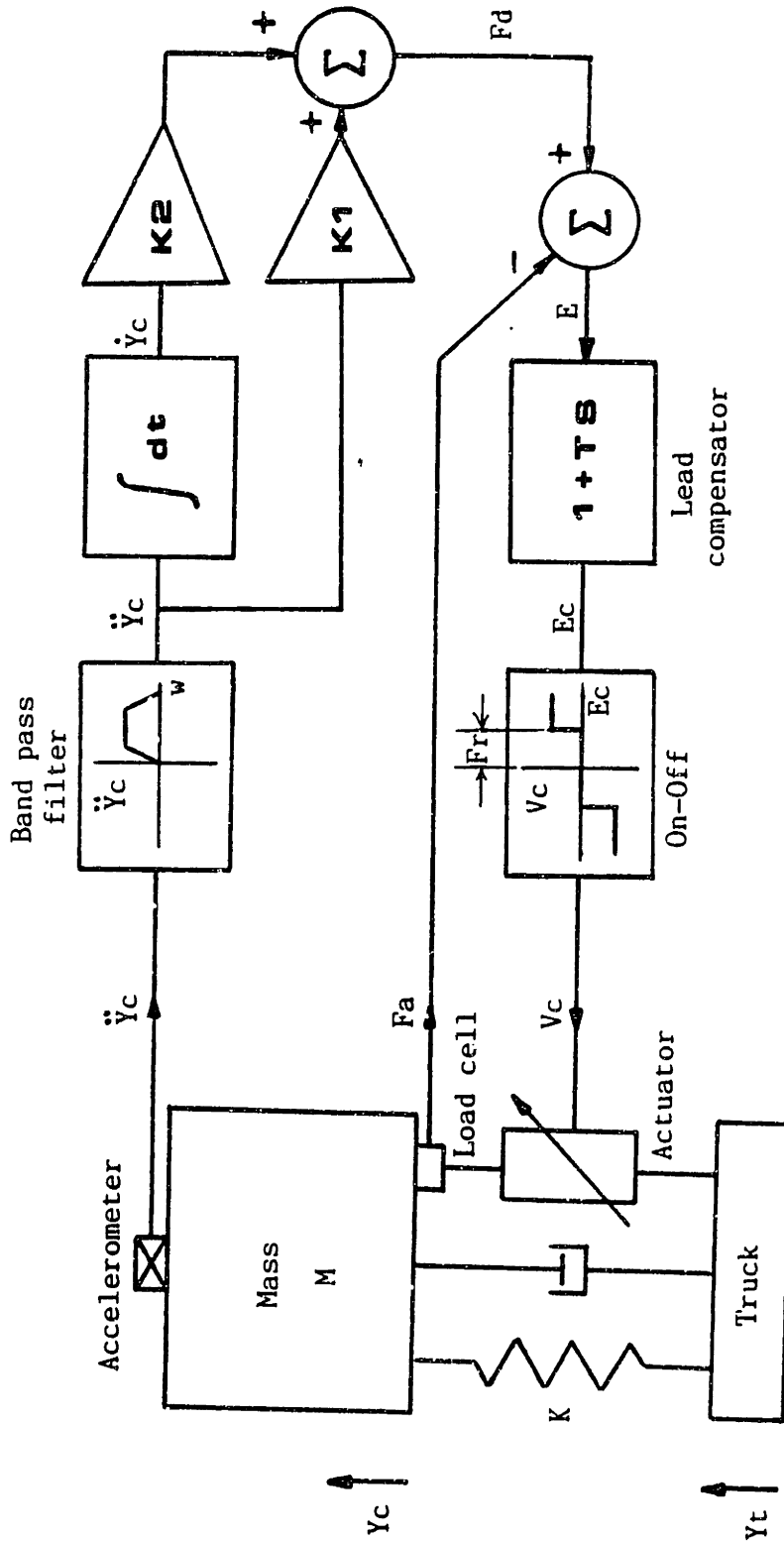
Figure 2.3.7.3. A Schematic Diagram of the BBLC Control Circuit (29)

(3) the error force, E'_F, is formulated by inverting E_F

$$E'_F = -E_F = F_{AD} - F_A \qquad\qquad (7)$$

(4) the compensated error, E_C, is formulated by passing the E'_F signal through a lead compensator $(1+\tau S)$ as shown in Figure 2.3.7.3.

(5) the dead zone of width which is equal to 2 times F_r, is then formulated in the BBLC control circuit to be compared with the input signal, (the compensated error force signal, E_C).

(6) the supply valve of the actuator is turned on when the compensated error, E_C, is bigger than the 1/2 dead zone width, F_r.

(7) the exhaust valve of the actuator is turned on when the compensated error, E_C, is less than the negative value of the 1/2 dead zone, $-F_r$.

(8) when the compensated error, E_C stays inside the dead zone, which ranges from $-F_r$ to $+F_r$, both the supply valve and exhaust valve remain closed and the actuator is in its hard spring mode.

Figure 2.3.7.4 shows a picture of the BBLC "4-FESTO MX-2-1/4 valve set". Two of the four valves are connected to one actuator while the remaining two valves are connected to another actuator.

The width of the dead zone is established to avoid too much oscillation in the neighborhood of the steady state. The value of F_r is evaluated based on the considerations of power consumption, system stability, and the valve's bandwidths.
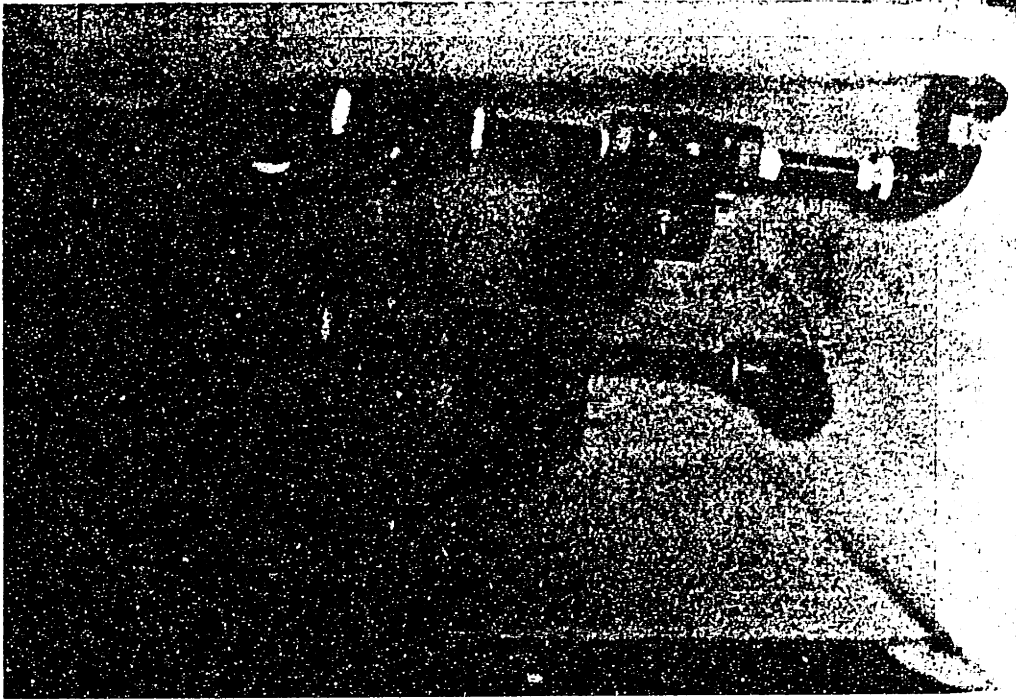
Figure 2.3.7.4   A Photograph of the 4-FESTO-
                 MX-2-$\frac{1}{4}$ Valve Set

2.4 The Derivation of Equation of Motion for Pneumatic Secondary Lateral Active Suspension System

2.4.1 Introduction

The schematic diagram of the lateral active suspension system is shown in Figure 2-4-1. Two opposing cylindrical actuators, either of which can exert force in only one direction, are placed in between the carbody and truck separately. The carbody responds dynamically to the distrubance inputs from the truck. This system is symmetric, and can be simplified into a dynamically equivalent diagram as shown in Figure 2-4-2.

The equivalent spring constant, k, is the sum of k_A and k_B because k_A and k_B are mounted at opposite sides of the carbody. These two springs seem to be in series but they are in parallel. Similarly, the equivalent damping coefficient, b, is the sum of $b_A + b_B$. The two opposing actuators are replaced by a single actuator, which can exert output force in either direction.

The valve is used to control both the direction and flow rate of the working fluid into and out of the actuator acording to the control signals from the control circuit. The actuator used is characterized by its double-ended rod to ensure that the same application area, A, is used on either side of the piston. The force generated by the actuator is determined by the pressure difference, Δp, between the two chambers A and B. Furthermore, the mass of the truck is neglected since the ratio of it to that of the carbody is about 1/300. At this stage, the secondary lateral active suspension control system of the railroad passenger vehicle is much further simplified (as shown in Figure 2-4-3). There is only one mass, the carbody, is considered. The truck mass is not included.
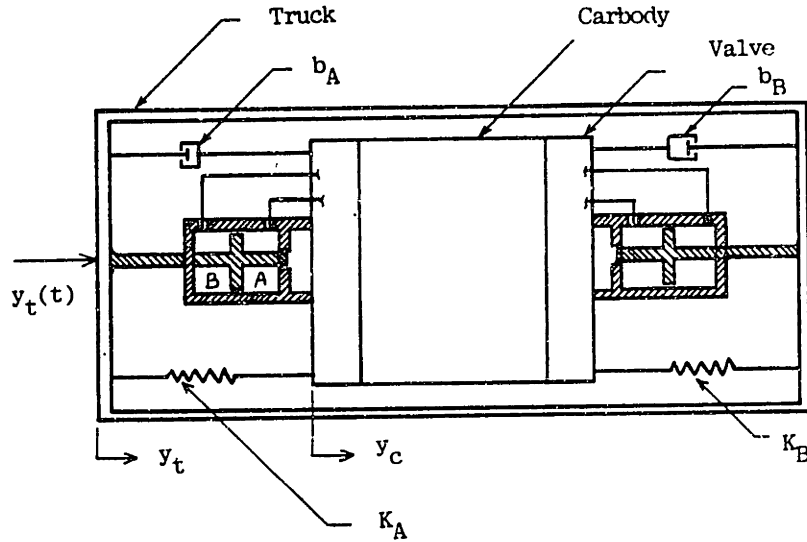
Figure 2-4-1   The Schematic Diagram of the Secondary Lateral Active
Suspension System

$$b = b_A + b_B$$
$$K = K_A + K_B$$
$$F_a = A\Delta p$$
$$A = A_{piston} - A_{drive\ rod}$$
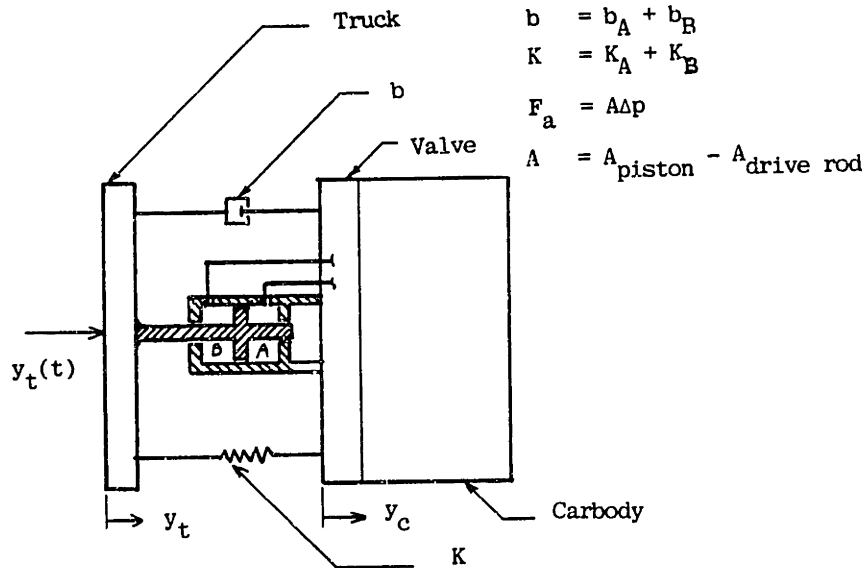
Figure 2-4-2   The Equivalent (and Simplified) Lateral Active
Suspension System
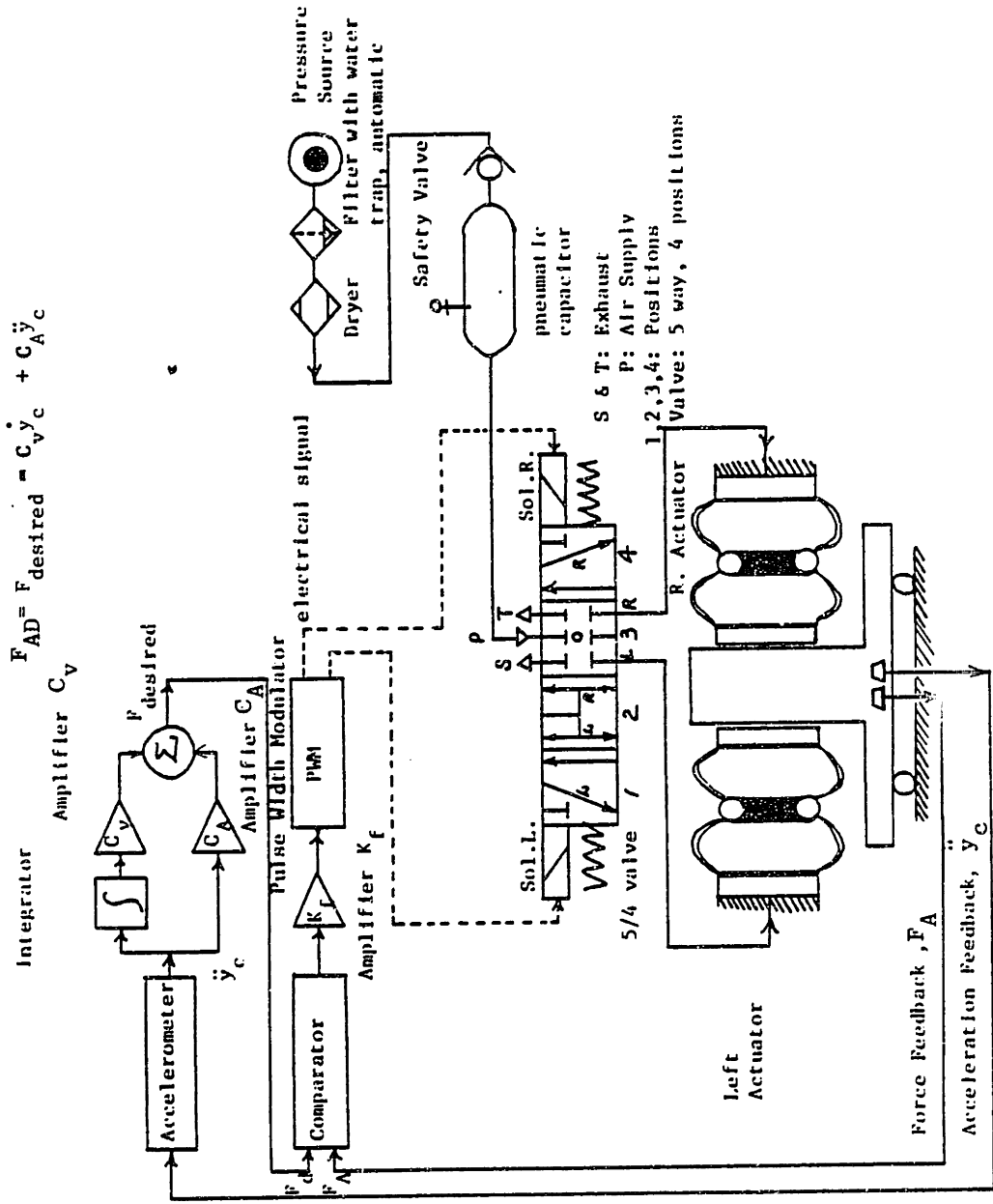
Figure 2-4-4 Schematic of Pneumatic Active Suspension
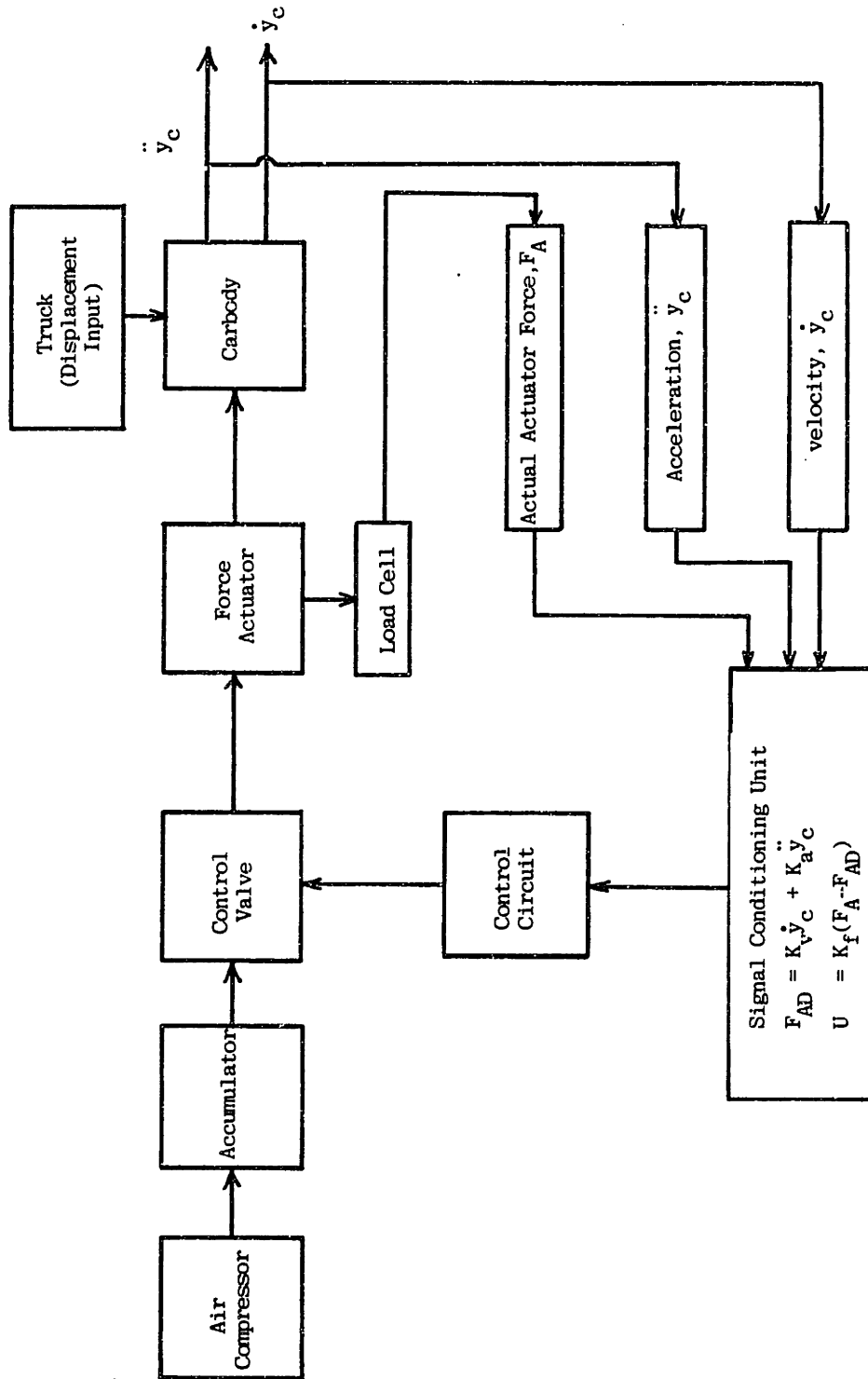
Figure 2-4-5 The Block Diagram of the Pneumatic Lateral Active Suspension Control System

Consider Figure 2-4-4. It represents the total control system where the penumatic power supply, the control circuit, the valve, the actuator, and the plant are all included. Figure 2-4-5 shows the corresponding block diagram. Because of the pressure difference created between the actuator's two chambers A, and B, a relative force is generated between the carbody and the truck. By using the control circuit to position the control valve, the actuated force can be regulated in both direction and magnitude. The time average of mass flow rate from the compressor to the actuator would be the same according to the mass conservation law. Since the analyses of system components were already made in previous sections, the equation of motion for the active control system will be derived in the following section.

2.4.2 The derivation of equation of motion for the control system

The schematic of the pneumatic secondary lateral active suspension control system (i.e. Figure 2-4-3) is again shown below. The carbody free-body-diagram is shown in Figure 2-4-6.

Carbody

Valve

$y_c(t)$

K   b

F_A

A

B

$y_t(t)$
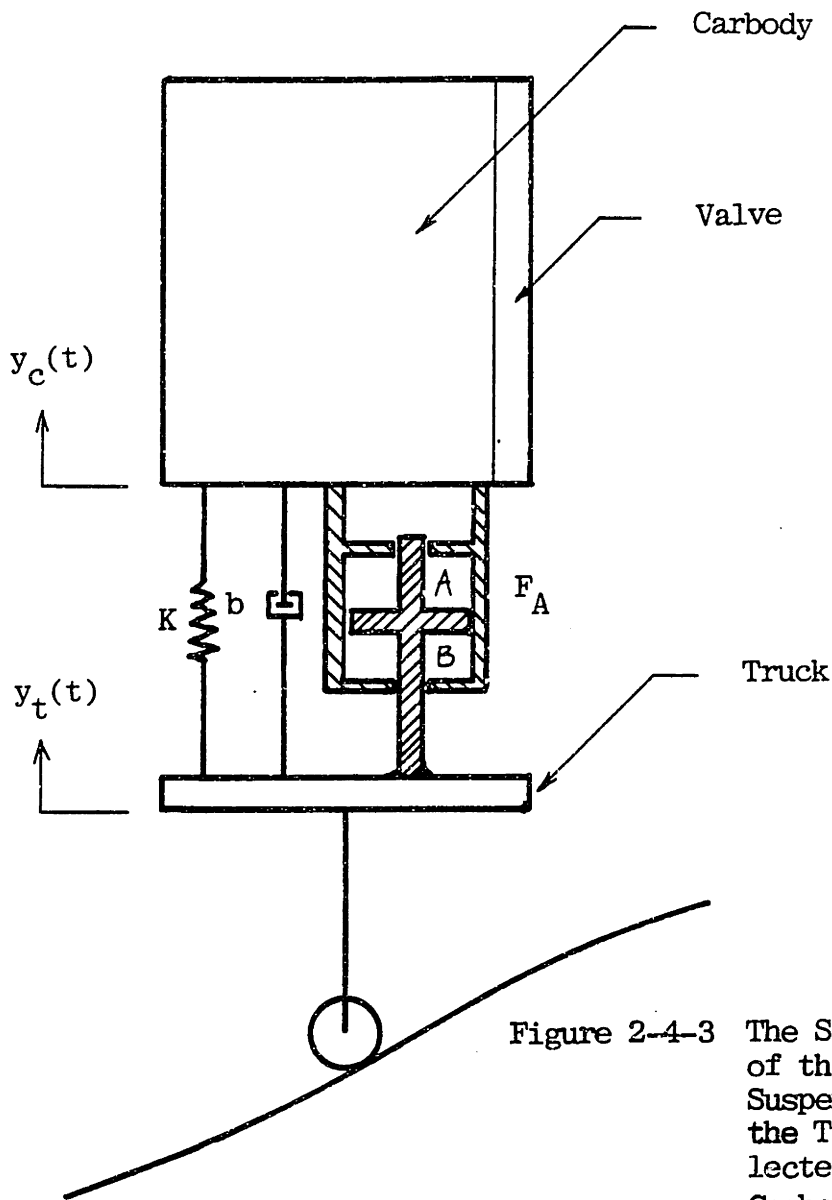
Truck

Figure 2-4-3 The Simplified Diagram
of the Lateral Active
Suspension System where
the Truck Mass is Neg-
lected and only the
Carbody Mass in Included.

$y_c(t)$ Carbody $\Sigma F_i = -F_s + F_A - F_b$

F_s F_b $-F_A$
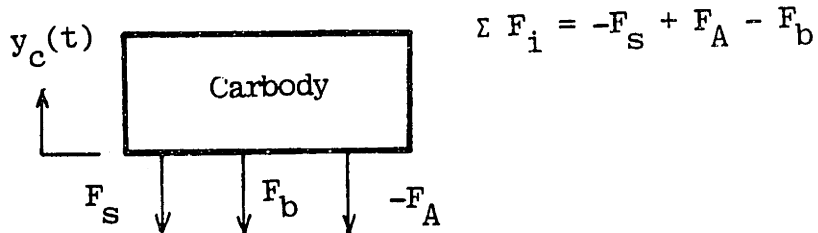
Figure 2-4-6*   The Free-Body-Diagram of the Carbody (for
deriving the equations of motion).

*The Figure number is not continuous here

By applying Newton's second law, the second-order differential equation of motion for the carbody can be derived as follows:

$$M_c \ddot{y}_c = \Sigma F$$

$$\Sigma F = F_S + F_A - F_b$$

$$F_S = K(y_c - y_t)$$

$$F_b = b(\dot{y}_c - \dot{y}_t)$$

$$M_c \ddot{y}_c = F_A - K(y_c - y_t) - b(\dot{y}_c - \dot{y}_t)$$

$$M_c \ddot{y}_c + K y_c + b\dot{y}_c = F_A + b\dot{y}_t + K y_t \qquad (1)$$

and $\qquad F_A = A(P_a - P_b) \qquad (2)$

where

M_c	=	carbody mass
F_S	=	spring force
F_b	=	damper force
K	=	spring constant
b	=	damping coefficient
y_c	=	displacement of the carbody
$\dot{y}_c$	=	volocity of the carbody
$\ddot{y}_c$	=	acceleration of the carbody
y_t	=	displacement of the truck
$\dot{y}_t$	=	velocity of the truck
F_A	=	real actuator force
P_a	=	pressure in chamber A
P_b	=	pressure in chamber B
$P_a - P_b$	=	relative pressure difference of the actuator (ΔP)
A	=	appøication area of the actuator

The mass flow rate into either chamber of the actuator, i.e., W_a or W_b, is influenced by the pressure change effect of the chamber, and the piston displacement effect as stated below:

$$W_a = C_p \dot{P}_a + C_y(\dot{y}_c - \dot{y}_t) \tag{3}$$

$$W_b = C_p \dot{P}_b - C_y(\dot{y}_c - \dot{y}_t) \tag{4}$$

where

W_a = mass flow rate of fluid into chamber A

$\dot{W}_b$ = mass flow rate of fluid into chamber B

$\dot{P}_a$ = rate of change of the pressure in chamber A

$\dot{P}_b$ = rate of change of the pressure in chamber B

$\dot{y}_c - \dot{y}_t$ = relative velocity change between the carbody and the truck

C_p = fluid capacitance due to the pressure change

c_y = fluid capacitance due to the relative velocity change

Using a 15 DOF vehicle model, Celniker [21] analyzed the dynamic performance of the passenger rail vehicle, and gives the following control law:

$$F_{AD} = C_a \ddot{y}_c + C_b \dot{y}_c$$

which can be regarded as control input to the system as follows:

$$U = - C_1 \ddot{y}_c - C_2 \dot{y}_c \tag{5}$$

where

U = the control input

$-C_1$ = the amplification coefficient which relates the control input to the carbody acceleration

$-C_2$ = the amplification coefficient which relates the control input to the carbody velocity.

The mass flow rate into an actuator chamber, which can also be expressed as a function of the control input and the chamber pressure

relative to the ambient pressure, P_o is expressed as follows:

$$W_a = K_{pa} (P_a - P_o) + K_u U \qquad (6)$$

$$W_b = K_{pa} (P_b - P_o) - K_u U \qquad (7)$$

where $\qquad P_o$ = the ambient pressure

$P_a - P_o$ = the relative pressure difference between the chamber A and the ambient

$P_b - P_o$ = the relative pressure difference between the chamber B and the ambient ·

K_u = the coefficient which relates the mass flow rate to the control input

K_{pa} = the coefficient relates mass flow rate to the relative pressure of chamber A

K_{pb} = the coefficient relates mass flow rate to the relative pressure of chamber B

2.4.3 Deriving the State-variable equation

Based on the above stated seven fundamental equations, the state equation, i.e., $\underline{\dot{X}} = \overline{A}\,\underline{X} + \overline{B_1}\,\underline{U} + \overline{B_2}\,\underline{\dot{U}}$, $\underline{Y} = \overline{C}\,\underline{X}$, can be derived as follows.

(1) Combining equations 3,4,6 and 7

for W_a: $\qquad C_p\dot{P}_a + C_y(\dot{y}_c - \dot{y}_t) = K_{pa} (P_a - P_o) + K_u U$

for W_b: $\qquad C_p\dot{P}_b - C_y(\dot{y}_c - \dot{y}_t) = K_{pb} (P_b - P_o) - K_u U$

(2) Substituting the control input equation of U, (i.e., the equation 5), into the two above equations:

$$C_p\dot{P}_a + C_y(\dot{y}_c - \dot{y}_t) = K_{pa} (P_a - P_o) + K_u (-C_1\ddot{y}_c - C_2\dot{y}_c) \qquad (8)$$

$$C_p\dot{P}_b - C_y(\dot{y}_c - \dot{y}_t) = K_{pb} (P_b - P_o) - K_u (-C_1\ddot{y}_c - C_2\dot{y}_c) \qquad (9)$$

(3) Substituting the real actuator force, F_A, of equation 2, into equation 1:

$$M_c \ddot{y}_c + K y_c + b \dot{y}_c = A(P_a - P_b) + b \dot{y}_t + K \dot{y}_t \tag{10}$$

(4) Combining equations 8,9 and 10 into state equation form,

$$\dot{\underline{X}} = \overline{\underline{A}}\,\underline{X} + \overline{\underline{B}}_1\,U + \overline{\underline{B}}_2\,\dot{U}$$

$$\underline{Y} = \overline{\underline{C}}\,\underline{X} \tag{11}$$

where $\underline{X}$, $\underline{U}$, and $\dot{\underline{U}}$ are defined as follows:

$$\underline{X} \overset{\Delta}{=} \begin{bmatrix} P_a \\ P_b \\ y_c \\ \dot{y}_c \end{bmatrix} \overset{\Delta}{=} \begin{bmatrix} \text{pressure in chamber A} \\ \text{pressure in chamber B} \\ \text{carbody displacement} \\ \text{carbody velocity} \end{bmatrix}$$

$$\underline{U} \overset{\Delta}{=} \begin{bmatrix} P_o \\ \\ y_t \end{bmatrix} \overset{\Delta}{=} \begin{bmatrix} \text{the ambient air pressure} \\ \\ \text{the truck displacement} \end{bmatrix}$$

$$\dot{\underline{U}} \overset{\Delta}{=} \begin{bmatrix} \dot{P}_o \\ \\ \dot{y}_t \end{bmatrix} \overset{\Delta}{=} \begin{bmatrix} \text{the ambient pressure change} \\ \\ \text{the truck velocity} \end{bmatrix}$$

(5) Rearranging equation 10,

$$\ddot{y}_c = \frac{1}{M_c} [- K y_c - b \dot{y}_c + A P_a - A P_b + b \dot{y}_t + K y_t]$$

$$\ddot{y}_c = \frac{-K}{M_c} y_c + \frac{-b}{M_c} \dot{y}_c + \frac{A}{M_c} P_a + \frac{-A}{M_c} P_b + \frac{b}{M_c} \dot{y}_t + \frac{K}{M_c} y_t$$

$$\tag{12}$$

(6) Forming the first derivative equations of the state variables as follows:

Rearranging equation 8, and substituting equation 12 into it:

$$\dot{P}_a = \frac{1}{C_p} [-C_y \dot{y}_c + C_y \dot{y}_t + K_{pa} P_a - K_{pa} P_o - K_u C_1 \ddot{y}_c - K_u C_2 \dot{y}_c]$$

$$= \frac{-C_y}{C_p} \dot{y}_c + \frac{C_y}{C_p} \dot{y}_t + \frac{K_{pa}}{C_p} P_a - \frac{K_{pa}}{C_p} P_o + \frac{K_u C_1 K}{C_p M_c} y_c + \frac{K_u C_1 b}{C_p M_c} \dot{y}_c$$

$$- \frac{K_u C_1 A}{C_p M_c} P_a + \frac{K_u C_1 A}{C_p M_c} P_b - \frac{K_u C_1 b}{C_p M_c} \dot{y}_t - \frac{K_u C_1 K}{C_p M_c} \dot{y}_t - \frac{K_u C_2}{C_p} \dot{y}_c$$

$$\dot{P}_a = (\frac{-K_u C_1 A}{C_p M_c} + \frac{K_{pa}}{C_p}) P_a + (\frac{K_u C_1 A}{C_p M_c}) P_b + (\frac{K_u C_1 K}{C_p M_c}) y_c$$

$$+ [\frac{-C_y}{C_p} + \frac{K_u}{C_p} (\frac{bC_1}{M_c} - C) - (2)] \dot{y}_c + (\frac{-K_{pa}}{C_p}) P_o + (\frac{-K_u C_1 K}{C_p M_c}) y_t$$

$$+ 0 \cdot \dot{P}_o + (\frac{C_y}{C_p} + \frac{-K_u C_1 b}{C_p M_c}) \dot{y}_t \qquad (13)$$

Rearranging equation 9, and substituing equation 12 into it:

$$\dot{P}_b = \frac{1}{C_p} [C_y \dot{y}_c - C_y \dot{y}_t + K_{pb} P_b - K_{pb} P_o + K_u C_1 \ddot{y}_c + K_u C_2 \dot{y}_c]$$

$$= \frac{C_y}{C_p} \dot{y}_c + \frac{-C_y}{C_p} \dot{y}_t + \frac{K_{pb}}{C_p} - \frac{K_{pb}}{C_p} P_o - \frac{K_u C_1 K}{C_p M_c} y_c + \frac{-K_u C_1 b}{C_p M_c} \dot{y}_c$$

$$+ \frac{K_u C_1 A}{C_p M_c} P_a - \frac{K_u C_1 A}{C_p M_c} P_b + \frac{K_u C_1 b}{C_p M_c} \dot{y}_t + \frac{K_u C_1 K}{C_p M_c} y_t + \frac{K_u C_2}{C_p} \dot{y}_c$$

$$\dot{P}_b = (\frac{K_u C_1 A}{C_p M_c}) P_a + (\frac{-K_u C_1 A}{C_p M_c} + \frac{K_{pb}}{C_p}) P_b + (\frac{-K_u C_1 K}{C_p M_c}) y_c$$

$$+[\frac{K_u}{C_p}(C_2 - \frac{C_1 b}{M_c})] \dot{y}_t + (\frac{-K_{pb}}{C_p}) P_o + (\frac{K_u C_1 K}{C_p M_c}) y_t + 0 \cdot \dot{P}_o$$

$$+(\frac{K_u C_1 b}{C_p M_c} - \frac{C_y}{C_p}) \dot{y}_t \qquad (14)$$

Rewriting $\dot{y}_c$ as:

$$\dot{y}_c = 0 \cdot P_a + 0 \cdot P_b + 0 \cdot y_c + 1 \cdot \dot{y}_c + 0 \cdot P_o + 0 \cdot y_t + 0 \cdot \dot{P}_o + 0 \cdot \dot{y}_t \qquad (15)$$

Rearranging equation 12 as:

$$\ddot{y}_c = (\frac{A}{M_c}) P_a + (\frac{-A}{M_c}) P_b (\frac{-K}{M_c}) y_c + (\frac{-b}{M_c}) \dot{y}_c + 0 \cdot P_o + (\frac{K}{M_c}) y_t$$

$$+ 0 \cdot \dot{P}_o + (\frac{b}{M_c}) \dot{y}_t \qquad (16)$$

(7) Combining equations 13, 14, 15 and 16 and rearranging into the state equation form as shown in equation 12, the matrices A, B_1, B_2, and C can be calculated as follows:

$$\underline{\dot{X}} = \overline{A} \underline{X} + \overline{B}_1 \underline{U} + \overline{B}_2 \underline{\dot{U}}$$

$$\underline{Y} = \overline{C} \underline{X}, \quad (\underline{Y} \overset{\Delta}{=} \underline{y}_c = [0,0,1,0] \underline{X})$$

where

$$
\overline{A} = \begin{bmatrix}
\dfrac{K_{pa}}{C_p} + \dfrac{-K_u C_1 A}{C_p M_c}, & \dfrac{K_u C_1 A}{C_p M_c}, & \dfrac{K_u C_1 A}{C_p M_c}, & \dfrac{K_u}{C_p}\left(\dfrac{bC_1}{M_c} - C_2\right) \\[2em]
\dfrac{K_u C_1 A}{C_p M_c}, & \dfrac{KP_b}{C_p} + \dfrac{-K_u C_1 A}{C_p M_c}, & \dfrac{-K_u C_1 K}{C_p M_c}, & \dfrac{K_u}{C_p}\left(C_2 - \dfrac{C_1 b}{M_c}\right) + \dfrac{C_y}{C_p} \\[2em]
0, & 0, & 0, & 1 \\[2em]
\dfrac{A}{M_c}, & \dfrac{-A}{M_c}, & \dfrac{-K}{M_c}, & \dfrac{-b}{M_c}
\end{bmatrix}
$$

$$
B_1 = \begin{bmatrix}
\dfrac{-K_{pa}}{C_p}, & \dfrac{-K_u C_1 K}{C_p M_c} \\[2em]
\dfrac{-Kp_b}{C_p}, & \dfrac{K_u C_1 K}{C_p M_c} \\[2em]
0, & 0 \\[2em]
0, & \dfrac{K}{M_c}
\end{bmatrix}, \text{ and } \quad
B_2 = \begin{bmatrix}
0, & \dfrac{C_y}{C_p} + \dfrac{-K_u C_1 b}{C_p M_c} \\[2em]
0, & \dfrac{K_u C_1 b}{C_p M_c} + \dfrac{-C_y}{C_p} \\[2em]
0, & 0 \\[2em]
0, & \dfrac{b}{M_c}
\end{bmatrix}
$$

2.4.4 Calculating transfer functions of interest:

In order to calculate transfer functions of interest, some assumptions and simplifications of notation are applied in the equations 1 through 7 as follows:

(1) Assuming $K_{pa} = K_{pb} = K_p$ and subtracting equations 4 from equation 3, we get:

$$W_a - W_b + K_p (P_a - P_b) + 2 K_u U \qquad (21)^*$$

(2) Letting $\Delta P = P_a - P_b$, and having ΔP substituted into equation 2, we get:

$$F_A = A(\Delta P) \qquad (22)$$

(3) Substracting equation 7 from equation 6, we get:

$$W_a - W_b = C_p (\dot{P}_a - \dot{P}_b) + 2C_y (\dot{y}_c - \dot{y}_t) \qquad (23)$$

Substituting equation 22 into equation 1, we get:

$$M_c \ddot{y}_c + K y_c + b \dot{y}_c = A(\Delta P) + b \dot{y}_t + k y_t$$

$$M_c \ddot{y}_c + K y_c + b \dot{y}_c - A(\Delta P) = b \dot{y}_t + K y_t \qquad (24)$$

(4) Equalizing equation 21 and equation 23 we get:

$$C_p \Delta \dot{P} + 2 C_y (\dot{y}_c - \dot{y}_t) = K_p \Delta P + 2K_u U$$

$$C_p \Delta \dot{P} + 2C_y \dot{y}_c - Kp \Delta P = 2K_u U + 2C_y \dot{y}_t \qquad (25)$$

----

* the equation number is not continuous here

(5) Assuming zero initial conditions and taking the Laplace transform of equation 25 and 24 we get:

$$C_p S \Delta P + 2C_y S y_c - K_p \Delta P = 2K_u U + 2C_y S y_t \qquad (26)$$

$$(M_c S^2 + bS + K) \, y_c - A(\Delta P) = (K + bS)y_t \qquad (27)$$

Similarly, taking the Laplace transform of equation 5, we get:

$$U = -C_1 \ddot{y}_c - C_2 \dot{y}_c$$

$$U(S) = (-C_1 S^2 - C_2 S)y_c \qquad (28)$$

(6) Substiting equation 28 into equation 26, we get:

$$(C_p S - K_p) \, \Delta P + 2C_y S y_c = 2Ku \, (-C_1 S^2 - C_2 S)y_c - 2C_y S y_t$$

$$(C_p S - K_p) \, \Delta P + 2[K_u C_1 S^2 + (K_u C_2 + C_y)S]y_c = 2C_y S y_t$$

$$\Delta P = \frac{2C_y S}{C_p S - K_p} \, y_t - \frac{2[K_u C_1 S^2 + (K_u C_2 + C_y)S]}{C_p S - K_p} \, y_c \qquad (29)$$

Substituting equation 29 into equation 27, we get:

$$(M_c S^2 + bS + K)y_c - A \left\{ \frac{2C_y S}{C_p S - K_p} \, y_t - \frac{2[K_u C_1 S^2 + (K_u C_2 + C_y)S]y_c}{C_p S - K_p} \right\}$$

$$= (K + bS) y_t$$

Rearranging the above equation we get:

$$\left[M_c S^2 + bS + K + \frac{2AK_u C_1 S^2 + 2A(K_U C_2 + C_y)S}{C_p S - K_p} \right] \ y_c$$

$$= \left[(k + bS) + \frac{2AC_y S}{C_p S - K_p}\right] \ y_t$$

$$y_c[(C_p S - K_p)(M_c S^2 + bS + K) + 2 AK_u C_1 S^2 + 2A(K_u C_2 + C_y)S]$$

$$= y_t[CK + bS)(C_p S - K_p) + 2AC_y S] \tag{30}$$

(7)   The transfer function is defined as the Laplace transfer form of output

over input, i.e., $T(S) = y_c(S)/y_t(s)$, where $y_c(s)$ and $y_t(S)$ are

the Laplace transforms of $y_c(t)$ and $y_t(t)$ separately.

$$T(S) = \frac{y_c(s)}{y_t(S)} = \frac{(C_p S - K_p)(K + bs) + 2AC_y S}{(C_p S - L_p)(M_c^2 + bS + K) + 2AK_u C_1 S^2 + 2A(K_u C_2 + C_y)s}$$

$$T(S) = \frac{C_p bS^2 + (-K_p B + KC_p + 2 AC_y)S - K_p K}{C_p M_c S^3 + (-K_p M_c + C_p b + 2 AK_u C_1)S^2 + [C_p K - K_p b + 2A(K_u C_2 + C_y)S - K_p K}$$

$$\tag{31}$$

$$T(S) = \frac{\dfrac{C_p b}{C_p M_c}[S^2 + \dfrac{KC_p + 2AC_y - K_p b}{C_p b} \ S + \dfrac{-K_p K}{C_p b}]}{S^3 + \dfrac{(C_p b + 2AK_u C_1 - K_p M_c)}{C_p M_c}S^2 + \dfrac{[C_p K - K_p b + 2A(K_u C_2 + C_y)}{C_p M_c}S - \dfrac{-K_p K}{C_p M_c}}$$

$$\tag{32}$$

We conclude that the lateral active suspension control system is a third-order system, its closed-loop transfer function is expressed explicitly in equation 32.

2.4.5 Transforming the transfer function into phase-variable representation

Since we are also interested in other phases of $y_c(t)$, it is necessary to transform the transfer function into phase variable form (as mentioned by Schultz and Melsa in [1W]).

(1) Writing the system representation in state-variable form:

$$\dot{\underline{X}} = \overline{\underline{A}}\,\underline{X} + \overline{\underline{B}}\,\underline{U}$$
$$\underline{Y} = \overline{\underline{C}}\,\underline{X}$$

$$\left. \right\} \qquad (40)^*$$

where equation 40 is different from equation 12 even though both of them are in state-variable forms which represent the control system.

(2) Define $\underline{X} \overset{\Delta}{=} \begin{pmatrix} x_1 \\ x_2 \\ x_3 \end{pmatrix} \overset{\Delta}{=} \begin{pmatrix} x_1 \\ \dot{x}_1 \\ \ddot{x}_1 \end{pmatrix} \overset{\Delta}{=} \begin{pmatrix} y_c \\ \dot{y}_c \\ \ddot{y}_c \end{pmatrix}$

---

* the equation numer is not continuous here

(3) $\overline{A}$, $\overline{B}$, and $\overline{C}$ are calculated by equation (2-5-10) of [1wsm] as follows:

$$\overline{A} = \begin{bmatrix} 0 & , & 1 & , & 0 \\ \\ \\ 0 & , & 0 & , & 1 \\ \\ \\ \dfrac{K_p K}{C_p M_c} & , & \dfrac{[C_p K - K_p b + 2A(K_u C_2 + C_y)]}{C_p M_c} & , & \dfrac{(C_p b + 2AK_u C_1 - K_P M_c)}{C_p M_c} \end{bmatrix}$$

$$\overline{B} = \begin{pmatrix} 0 \\ \\ 0 \\ \\ \\ \dfrac{b}{M_c} \end{pmatrix}, \text{ and } \overline{C} = [\dfrac{-K_p K}{C_p b} \quad , \quad \dfrac{K C_p + 2A C_y - K_p b}{C_p b} \quad , \quad 1 \;]$$

(4) Calculating the transfer function:

Define:

$$G(S) \overset{\Delta}{=} \begin{bmatrix} G_1(S) \\ \\ G_2(S) \\ \\ G_3(S) \end{bmatrix} \overset{\Delta}{=} \begin{bmatrix} y_c(S)/y_t(S) \\ \\ \dot{y}_c(S)/y_t(S) \\ \\ \ddot{y}(S)/y_t(S) \end{bmatrix}$$

and $\quad G(S) = \overline{C} \, (S\overline{I} - \overline{A})^{-1} \overline{B}$

By this approach, the transfer functions of $y_c(S)/y_t(S)$, $\dot{y}_c(S)/y_t(S)$ and $\ddot{y}_c(S)/y_t(S)$ can be calculated.

2.5 Conclusions

The physical consideration of the plant to be controlled in this project, the Budd pioneer III truck, was investigated in the beginning of this chapter. After careful calculation of the dimensions of the current truck, the limited space available for mounting a pneumatic active controller was studied and listed in Section 2.2.2. The Lateral Active Suspension Controller (The LASC controller) was then designed to meet the perfomance required by the passenger rail vehicle. The advantages of the design of the LASC controller were presented explicitly.

The second part of this chapter investigated the controller's major components such as air compressors, actuators, and valves. These components were selected, modelled, and analyzed to derive their constitutive laws respectively. Two control circuits, the PWM control circuit and the BBLC control circuit, were discussed and compared. Since the valve selected was a nonlinear on/off valve, the major function of the control circuit was to drive the solenoid valve as fast as possible to approximate a proportional Controller. It was found later, in Chapter 4, that the PWm control circuit could not perform dynamically at an acceptable level with the reularl pneumatic valve. Though the theory of th eBBLC control circuit was simple, it turned out to be a reliable, economical and efficient control circuit.

The equation of motion for the pneumatic secondary lateral active suspension system was derived from the previous results. A 5th order state equation was derived to represent the argumented system. Transfer functions were derived from the state variable representation. Transformation back to the phase-variable representation of the same system was completed in order to derive other transfer functions of interest.

CHAPTER III

THE DESIGN AND FABRICATION OF THE TESTING FACILITY FOR THE

LATERAL ACTIVE SUSPENSION CONTROLLER.

3.1 Introduction:

The secondary suspension system of the Budd's Pioneer IV passenger

rail vehicle was modelled and analyzed to result in the equations of

motion in the previous chapter. A Lateral Active Suspension Controller,

which was called the LASC controller, was designed to meet the

requirements of ride quality. In order to evaluate the components as

well as the whole system of the LASC controller, a laboratory apparatus

named the LASC tester was designed and fabricated at MIT. The

components of the LASC controller include actuators, valves, sensors,

control circuits, and signal conditioners. In this Chapter, the

physical implementation of the controller is briefly examined, and the

design and manufacture of the tester is thoroughly discussed. In

addition, the scaling technique and the flexibility of the LASC tester

are also topics of this Chapter. The results of laboratory testing will

be discussed in the following Chapter.

3.2 Dynamic Similitude Used in the Scaling techniques:

The objective of this Chapter is to develop experimental techniques

for studying the passenger rail vehicle dynamics as presented previously

through the use of a 1/484 scale model. Taking the specifica-

tions of this 1/484 scale model as the guideline, a testing machine for

the Lateral Active Suspension Controller was designed and constructed.

The scaling techniques are based on the consideration of dynamic

consideration of dynamic similitude (which was also adopted in other

research done by Jindzi, et al, in [30] and by Mauer in [31]). For

practical reasons, the mass of the scaled carbody is set to be 80lbs in

formulating the single degree-of-freedom, second-order system model. The

parameter values of the physical system are tabulated in Table 2-2-2 , in

Chapter 2, and are re-entered in the following Table 3-2-1.

(a)	M_c	carbody mass	2405 slugs
(b)	$1/2\,M_c$	carbody mass/track	1202.5 slugs
(c)	K_{sy}	secondary lateral stiffness/one unit	24,000 lb/ft
(d)	$2K_{sy}$	secondary lateral stiffness/truck	48,000 lb/ft
(e)	C_{sy}	secondary lateral damping coefficient/one unit	1,200 lb-sec/ft
(f)	$2C_{sy}$	secondary lateral damping coefficient/truck	2,400 lb-sec/ft
(g)	W_n	natural frequency	1.11 hz.
(h)	C_c	critical damping coefficient	86,22.6 lb-sec/ft
(i)	ξ	damping ratio	0.028
(j)	W_n	damped natural frequency	1.109 hz
(k)	τ	time constant of the envelop curves	32.2
(l)	$T_{settling}$	settling time for the transient response	128.8

Table 3-2-1   Parameter values of the full scale
lateral secondary suspension system of
the Pioneer III passenger rail vehicle

3.2.1 Parameter Values Calculations for the Full Scale System

The values of the natural frequency, W_n, the critical damping coefficient, C_c, the damped natural frequency, W_d, and the damping ratio, ξ, are calculated in the following:

$$1/2M_c = 1202.5 \text{ slugs} = 1202.5 \times 32.2 \text{ lbm} = 38,720.5 \text{ lbm}, \qquad (1a)$$

$$2K_{sy} = 48,000 \text{ lb}_f/\text{ft} \qquad (2a)$$

$$W_n = \sqrt{\frac{2K_{sy}}{1/2M_c}} = \sqrt{\frac{48,000}{38,720.5}} = \sqrt{1/24} = 1.11 \text{ Hz}, \qquad (3a)$$

$$C_c = 2 \ (1/2M_c 2K_{sy})^{1/2} = 2(38,720.5 \times 48,000)^{1/2}$$

$$= 86,222.6 \text{ lb-sec/ft}, \qquad (3b)$$

$$\xi = \frac{C_{sy}}{C_c} = \frac{2,400}{86,222.6} = 0.028, \qquad (5a)$$

$$W_d = W_n \sqrt{1-\xi^2} = 1.11 \times 0.9996 = 1.109 \qquad (6a)$$

$$\tau = \frac{1}{\xi W_n} = 32.2 \qquad (7a)$$

$$T_{settling} = 4\tau$$

$$= 128.8 \qquad (8a)$$

The secondary lateral suspension system of the half body of the Pioneer III passenger rail vehicle was modelled as a single degree-of-freedom, second-order system. The dominating parameters are shown above. The damping ratio, which is defined as the ratio of the actual damping coefficient in the system, $2C_{sy}$, to that damping coefficient

- 98 -

which would produce critical damping, Cc, is calculated as $\xi = 0.028$.
Since the value of ξ is less than unity, the object system is classified
as underdamped, and will have an oscillatory response. The governing
equation may be written as follows:

$$\frac{d^2 y}{dt^2} + \frac{2C_{sy}}{1/2M_c} \frac{dy}{dt} + \frac{2K_{sy}}{1/2M_c} y = \frac{2K_{sy}}{1/2M_c} x(t), \qquad (11^*)$$

where x(t) is the input, and the transfer function for this oscillatory
system may be written as follows

$$G(s) = \frac{y(s)}{x(s)} = \frac{W_n^2}{s^2 + 2\xi W_n S + W_n^2} \qquad (12)$$

The characteristic polynomial, cpoL is

$$cpoL = S^2 + 2\xi W_n S + W_n^2 \qquad (13)$$
$$= S^2 + 0.0\ 61716S + 1.2321$$

Letting the characteristic polynomial equal zero, roots of cpoL
equation can be calculated by the quadratic formula:

$$S_{1,2} = \frac{-0.061716 + \sqrt{0.061716 - 4 x.232}}{2} = 0.031 + j1.103$$

$$S_1 = 0.031 + j1.103 \qquad (14)$$

$$S_2 = 0.031 - j1.103 \qquad (15)$$
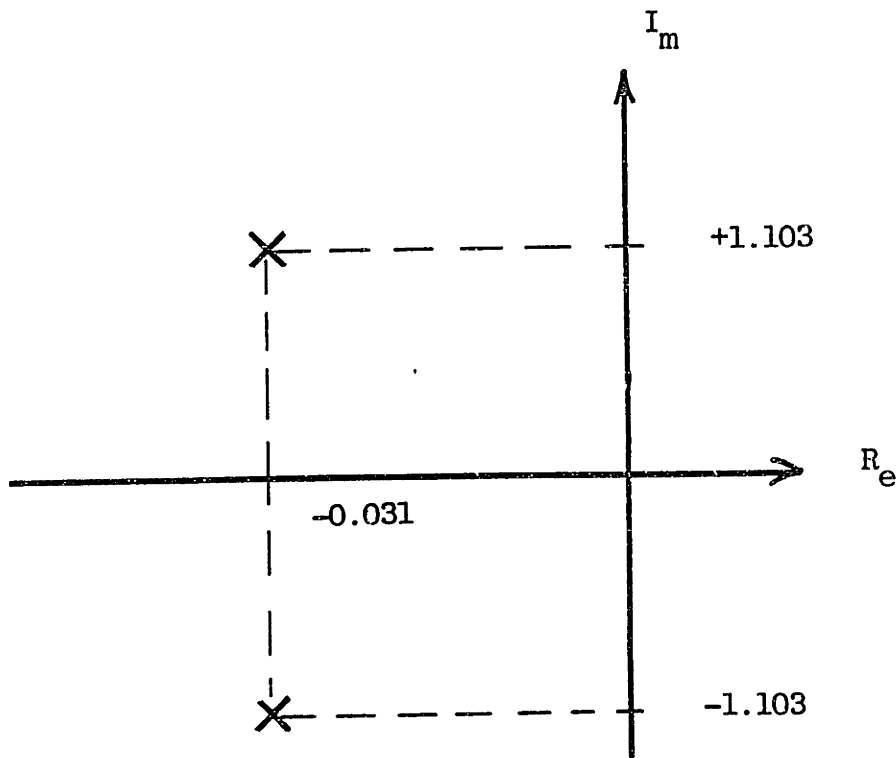
S-plane

Figure 3-2-1 Complex conjugate poles of the

Second-order underdamped system

S_1 and S_2 are also called the poles of the system and are plotted in the

S-plane to show that the system has two complex conjugate poles in the

left-hand side of the S-plane as shown in Figure 3-2-1, hence the system

is stable. The time constant, τ, for the envelope curves of the transient

response and the settling time, T settling for the system are also

calculated in the above.

3.2.2 Parameter Values Calculations for the Scaled Model System

The parameters of the scale model system are calculated based on the

dynamic similitude technique which requires that W_d and W_n of both

systems be identical. The calculation is carefully performed as

follows, and the results are tabulated in Table 3-2-2.

λ, scale factor = 1/484   (16)

W_n, scaled = W_n, full= 1.11   (3b*)

M_c, scaled = $1/2 M_c$ x λ = 1/484 x 38,7205 lbs

= 80 lbs   (1b)

k_{sy}, scaled/truck = $2K_{sy}$ x λ = 48,000 x 1/484 lbf/ft

= 99.2 lgf/ft   (2b)

C_c,scaled = $2(M_c,\text{scaled} \times k_{sy}, \text{scaled})^{1/2}$ = 178.1 lb_f - sec/ft   (4b)

ξ,scaled = $\dfrac{C_{sy},\text{scaled}}{C_c,\text{scaled}}$ = ξ_{full} = 0.028   (5b)

C_{sy},scaled = 0,028 x 178.1 = 4.952 lbf-sec/ft

W_d,scaled = W_n,scaled $\sqrt{1-\xi^2}$ = W_d,full   (6b)

τ,scaled = $\dfrac{1}{(\xi \cdot W_n)\text{scaled}}$ = 32.2   (7b)

T settling, scaled = 4τ, scaled = 128.8   (8b)

(a)	M_c, scaled,	carbody mass/truck	80 lbs
(b)	k_{sy}, scaled,	secondary lateral stiffness/truck	99.2 lbf/ft
(f)	C_{sy}, scaled	secondary lateral damping coefficient/truck	4.952 lbs-sec/ft
(g)	W_n, scaled	natural frequency	1.11 hz.
(h)	C_c, scaled,	critical damping coefficient	178.1 lb_f-sec/ft
(i)	ξ, scaled	damping ratio	0.028
(j)	W_d, scaled	damped natural frequency	1.109 hz.
(k)	τ, scaled	time constant of the envelop curves	32.2
(l)	T, settling, scaled	settling time for the transient response	128,8

Table 3-2-2   Parameter values of the scaled model of the lateral secondary suspension system of the Pioneer III passenger rail vehicle

* The equation number is not continuous here.

By the dynamic similitude technique, the two systems will have the same equations of motion, the same characteristic polynomial equation, and the same response curve corresponding to the same input. This is why it is named the similitude method. The LASC controller was designed to exert 1,500 lb for the full system. Since the carbody mass has been scaled down to 80 lbs at the scaling ratio of $\lambda = 1/484$, the actuator force should be also scaled by the same factor, λ, to generate the same dynamic performance.

$$F_{actuator, scaled} = 1.500 \times \frac{1}{484} = 3.1 \text{ lbf} \tag{17}$$

The distance from the bumpstop of the carbody to the bumpstop plate of the bolster is one and a half inches in each direction, (i.e., $d = \pm 1.5$ in). Due to the fact that the same acceleration is expected in both the full and scale system, this distance should not be altered by any factor, i.e.,

$$d_{scaled} = \pm 1.5 \text{ in.} \tag{18}$$

The parameter values calculated in this section will be used as the guideline for designing and fabricating the lateral active suspension controller's tester, i.e., the LASC tester, in the rest of the sections of this chapter.

3.3 Experimental Design

3.3.1 Introduction

The purpose of fabricating an active suspension testing facility is to compare the experimental results with the control law applied. The testing facility is shown in Fig. 3-3-1. It includes the following parts: the mechanical assembly, the instrumentation equipment, the control valve, the compressed air supply, the accelerometer, the vibration generator, the controller, the actuators, and the safety equipment. All of these are

illustrated in the following sections. In Figure 3-3-2 the whole set-up is explained by block diagrams.

3.3.2 The Mechanical Assembly

The mechanical assembly is composed of a base plate, two side supports, two horizontal shafts, four shaft support blocks, light ball bushing bearings, one C-mass, and one T-mass as shown in Table 1. It is assembled as follows: First, the two side supports are placed on the top of the base and then are tightly screwed together with the base. Second, two shaft support blocks are placed on the top of each side support, and screwed in place. These four shaft supporting blocks hold the two parallel, horizontal shafts, so that the distance between the two shafts is the same along the shafts. Third, well-manufactured C-mass and T-mass are placed in between the two side supports. The masses can slide on the two horizontal shafts by the use of linear ball bushing bearings. The C-mass and T-mass represent carbody and truck respectively.

Accurate alignment is very important because the two parallel shafts are used in precision application for this set-up. The two ball bushing bearings used on the C-mass are placed in tandem in order to keep the shaft aligned.

The parts list of the mechanical assembly is tabulated in Table 3-2-1.

Each of the two T-masses are placed in between the C-mass and the side supports. They are connected together by four threaded rods to form a rigid body. All of the masses can slide on the two parallel shafts with an efficiency rate of 99.998% by using the linear bearings [25]. The C-mass mass and the T-mass are connected by springs and dampers as shown in Figure 3-3-1, where the C-mass and the T-mass represent carbody and truck of the vehicle suspension separately.
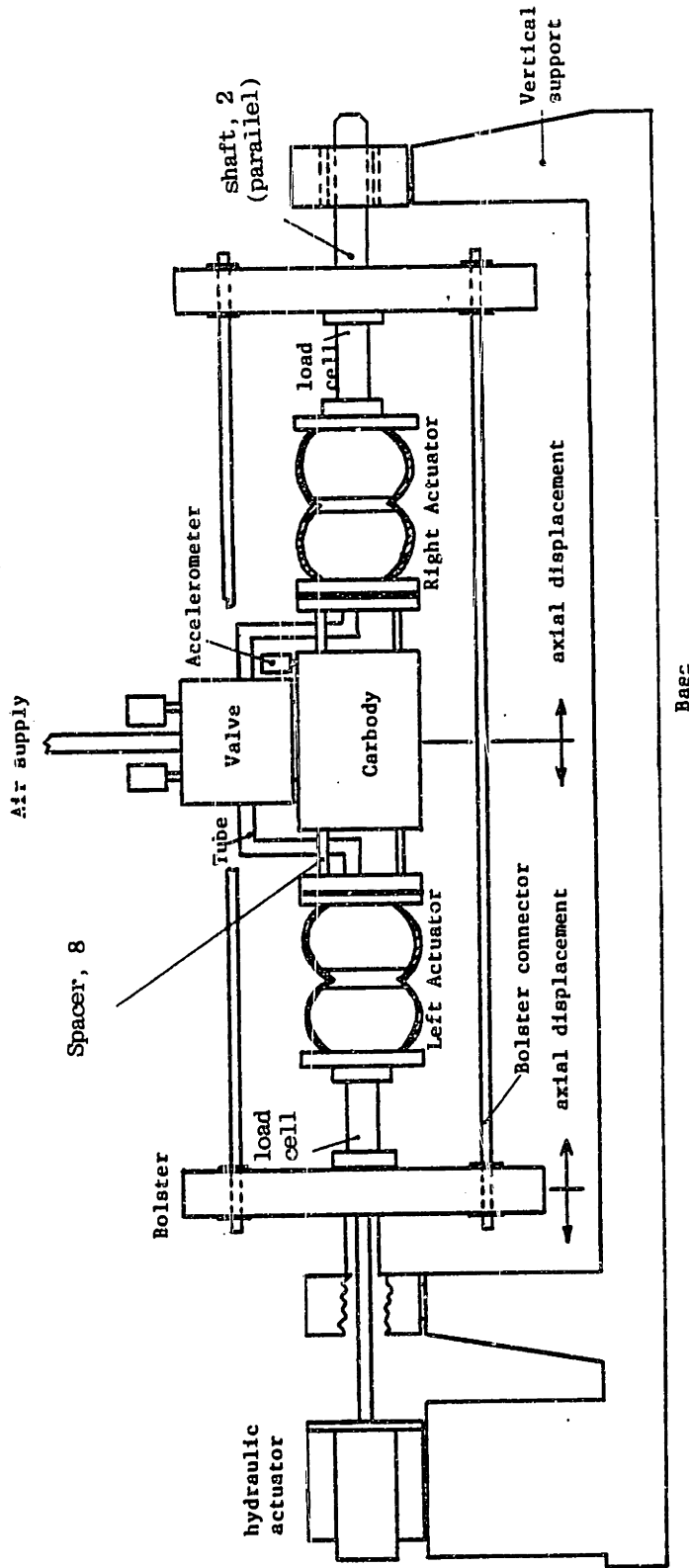
Figure 3-3-1 Laboratory Apparatus for the Lateral Active Suspension
Controller
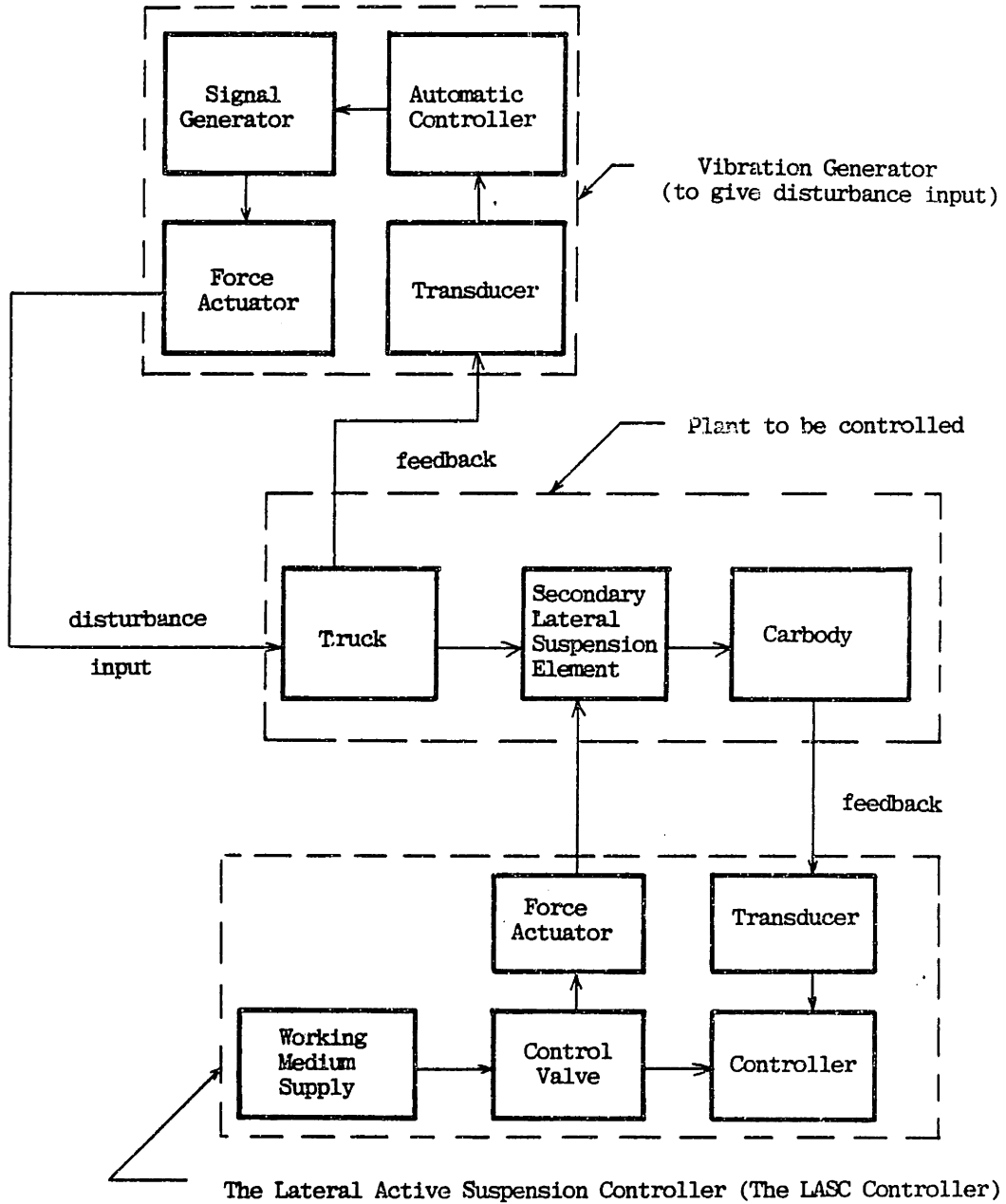
Figure 3-3-2   The Block Diagram Illustrating the Testing Facility for the Lateral Active Suspension Controller

The springs are mounted around the four threaded rods. The relative motion of one T-mass to another T-mass is not allowed. The system input is transmitted by an external actuator to the T-mass. The system output is the dynamic response of the C-mass.

Part No.	Part Name	Description	Quantity	Notes
1	base plate	1.5"x18.25"x46.25"	1	Aluminum
2	side support	6"x18.25"x3.5"	2	Aluminum I-beam,
3	shaft	diameter: 1" (0.995"/0.990") length: 48"	2	material: 1060 steel THOMSON class pD60 case shaft, weight 10 lbs.
4	shaft support block	nominal shaft diameter: 1"	4	material: Malleable iron, THOMSON part no.# SB-16
5	ball bushing bearing	working bore diameter: 1"	8	material: Stainless steel THOMSON part No. A-162536, max rolling load ratings: 350 lbs number of ball units:5
6	C-Mass	6"x9"x11"	1	aluminum, weight: 40 lbs
7	B-mass	0.5"x11"x7.5"	2	aluminum, weight: 6.1 lbs
8	spring		8	material: weight lbs k = , unit: linear ragne
9	damper		8	material: weight lbs b = unit linear range:

Table 3-3-1 Parts List of the Mechanical Assembly of the Testing Facility

3.4 The Load Cell

3.4.1 Introduction

The unknown value of the actuator force can be measured by applying a force to some elastic material and measuring the resulting deflection. This method is used in this project by mounting a strain-gage load cell at the end of the drive rod of the actuator as shown in Figure 3-2-1. The load sensing part is a maximum of 1 inch to prevent column buckling under the rated load of 4,000 lbs. force. The steel column is bounded by four Foil-type metal gages which are equally spaced around the column. The Foil-type metal gages are manufactured by the Micro-Measurements of Romulus, Michigan. This arrangement is insensitive to bending stress and temperature change since all four gages are placed symmetrically and isothermally. These cells all use 90-ohm gages and 10 V.D.C. volts bridge excitation. The wheatstone bridge is shown in Figure 3-4-1, the photograph of the load cell used in the LASC controller is shown in Figure 3-4-1-A and the resistances between different nodes are shown in Table 3-4-1. A signal conditioner made by the Gould Company of Cleveland, Ohio, is used with the load cell to provide the bridge excitation voltage and to process the output voltage from the wheatstone bridge of the load cell.

3.4.2 Calibrating the Load Cells

The load cell with the signal conditioned is then calibrated on an Instron testing machine according to the following process:

1. Placing the load cell at the ends of suitable mechanical fittings of the Instron testing machine,

2. Moving the crosshead to approach the load cell manually,

B

i_1 i_2 internal resistance is neglected

E_{ex}

A i_1+i_m i_1-i_m C   signal condi-tioner

D

i_m

Voltagemeter
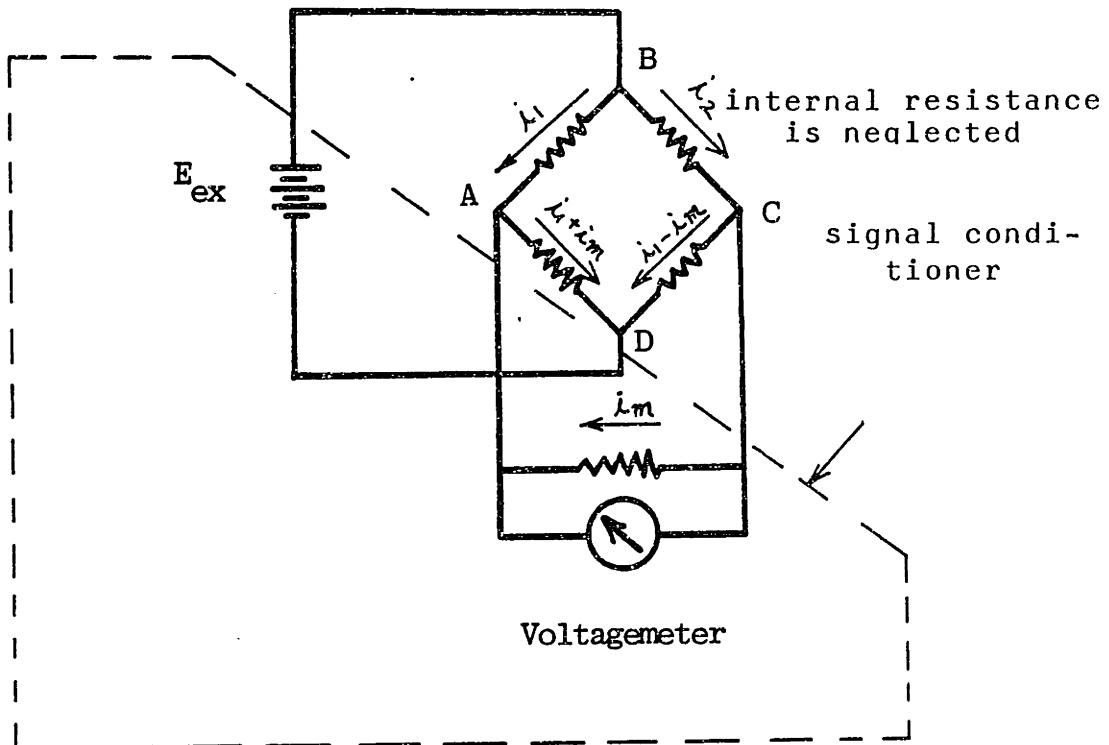
The Gould Signal Conditioner

Model = 11-4123-01

E_{ex} = 10 V.D.C. Voltage

Figure 3-4-1   The load cell Wheatstone Bride with the Gould signal conditioner

Nodes	Load Cell # 1, unit = Ω	Load Cell # 2 unit = Ω
A,B	89	91
A,D	89	91
C,B	90	91
C,D	89	91
A,C	119	121
B,D	119	121

Table 3-4-1   The resistance listing of the load cell Wheatstone bridge between different bridge nodes.
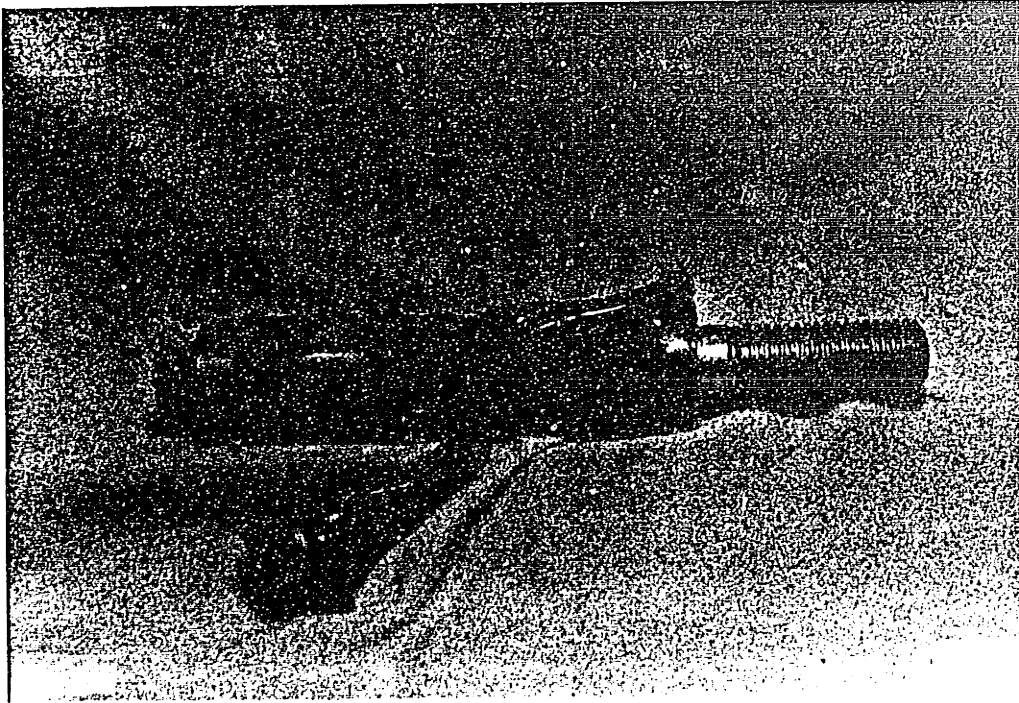
Figure 3.4.1.A   The Picture of the Load
                 Cell Used in the LASC
                 Controller

3. Adjusting the following knobs:

    a. the reading panels of loads and strains.

    b. the crosshead panel,

    c. the amplifier panel by zeroing the amplifier first, and then balancing the bridge and locking it up,

4. Calibrating the built-in signal amplifier on the Instron testing machine by simulating the design load,

    a. Calculating the design load (which is 4,000 lb_f.)0 for the actuator used in this research,

    b. Choosing 50 K Ω as the simulation load resistance from the table of the manual which is provided by the Instron Company, (i.e., adopting 50K Ω as the shunt resistance,)

    c. Shunting the resistance from the current value of 50K Ω; simultaneously the reading of the simulation load should be zero.

5. Applying various loads on the load cell and recording the result.

6. Adjusting the gain of the signal conditioner and locking up the the calibration knob of the Gould signal conditioner. The ratio of the gain is 1,000 lbs. force/volt, and the calibration knob setting is 2.11 for load cell #1 and 0.98 for the second load cell #2 as shown in Figure 3-4-2 and Figure 3-4-3.

3.5 The Pressure Transducers

3.5.1 Introduction

Most instruments used in measuring pressure operate by measuring force on a sensing element. Pressure can usually be transmitted to force by acting on a known area, hence the method of measuring force and
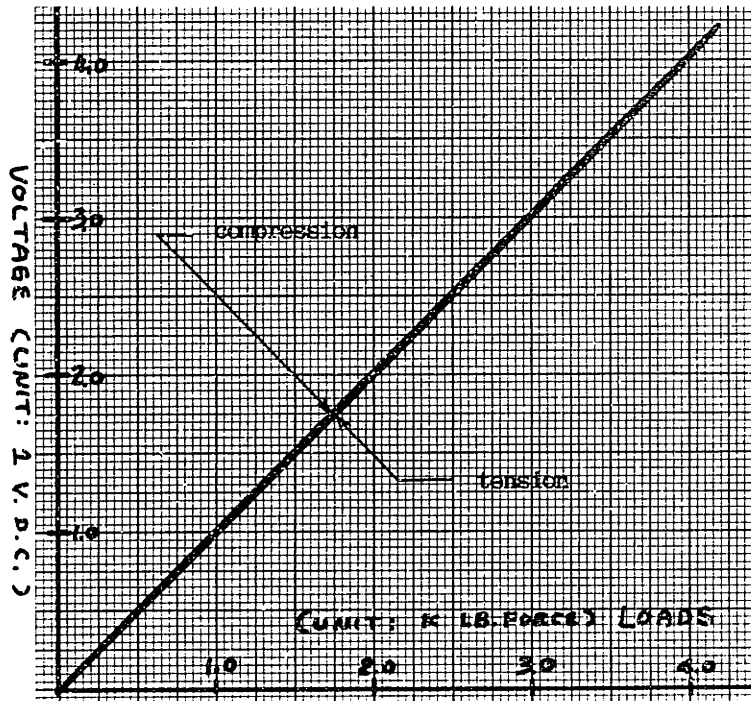
Loads (K.LB.F)	Voltage (1 V.D.V.)
4.0	4.0
3.5	3.49
3.0	3.0
2.49	2.48
2.0	1.99
1.5	1.5
1.0	1.0
0.5	0.49
0	0

Figure 3-4-2   The Characteristic Curves of the Load Cell #1
(Compression and Tension) with a Gould Signal
Conditioner
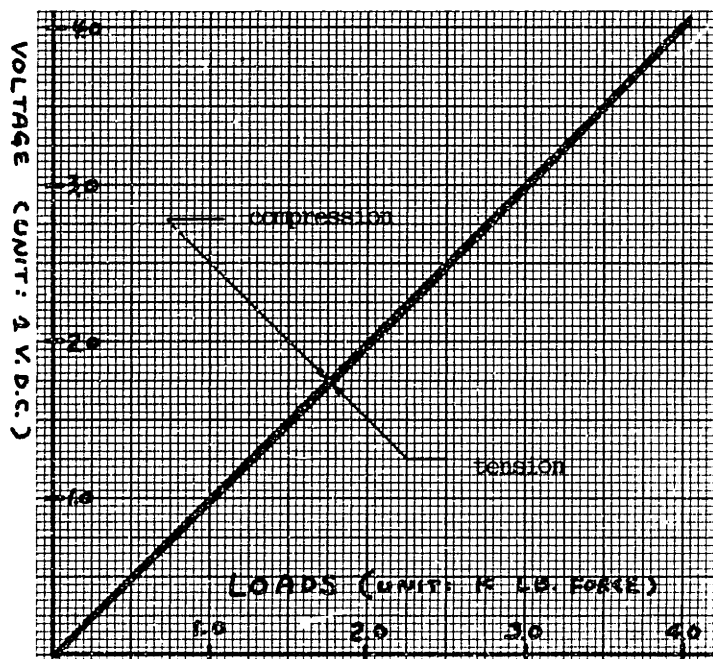
Loads (K.LB.F)	Voltage (1 V.D.C.)
4.0	4.0
3.5	3.5
3.0	2.99
2.49	2.49
2.0	1.99
1.6	1.5
1.0	1.0
0.5	0.5
0	0

Figure 3-4-3   The Characteristic Curves of the Load Cell #2
(Compression and Tension) with a Gould Signal
Conditioner

pressure are essentially the same. The pressure force is commonly balanced by gravity or by the stress in an elastic element. In the common dial type gage (the bourdon tube pressure gage) the pressure difference is balanced by the stresses in a curved tube. In the diaphragm pressure gage, the pressure force is balanced by the stresses in an elastic diaphragm the deflection of which is indicated mechanically or electrically. Two dial gages are, mounted right on the outlet of port A and port B of the control valve to measure the pressure of port A and port B separately. The readings on the dial are for reference only (rather than for processing) Pressure gages which produce an electric signal are called transducers. One pressure transducer made by the Statham Company is used to replace one of the dial gages in case the electrical signal of the pressure is needed. This Statham pressure transducer transforms the fluid pressure in the chamber into an electrical signal for further processing.

3.5.2 Calibrating the Pressure Transducer

In order to use a diaphragm-type strain-gage pressure transducer, an adequate diaphragm for the operating range (such as 200 psi) should be selected. There are 4 wires to be connected to make the transducer work. Two of the wires, red and green, will supply the bridge excitation voltage of 10 V. D.C. to the Wheatstone Bridge used in the transducer. The electrical signal coming from the rest of the wires, white and black, then connects to a signal conditioner for amplification. The Gould signal conditioner which was used with the load cells previously, is to be used with the Statham pressure transducer. Its schematic diagram is shown in Figure 3-5-1. This pressure transducer with the Gould signal conditioner is then calibrated by a dead-weight gage as shown in Figure 3-5-2. The

Green Wire   Red Wire

Black Wire   White Wire

Mechanical
Displacement
Probe

Pressure

Tube for
Electrical Wires
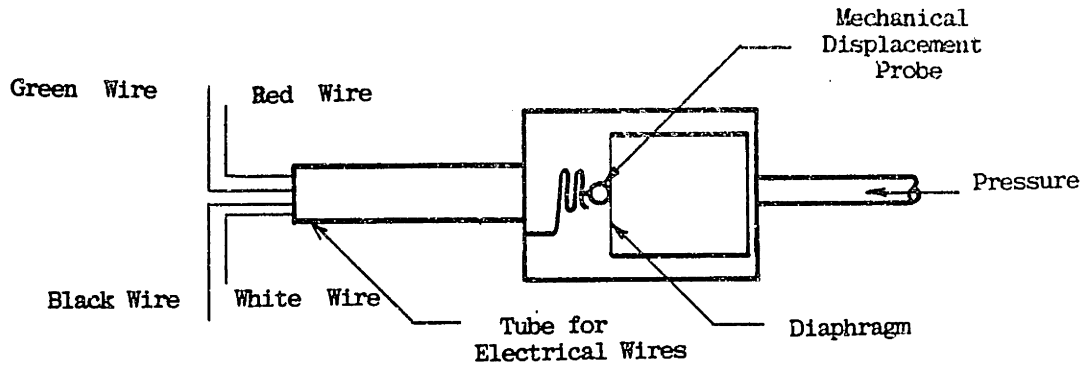
Diaphragm

Figure 3-5-1   The Schematic Diagram of the Statham Pressure
which is a Diaphragm-type Strain-gage Pressure
Transducer

adjustable dead weight

oil film

fluid buoyance on

piston

elevation
difference

D.V.M.

signal
conditioner
pressure transducer

Digital
Voltage
Meter
(D.V.M.)

Reference Point of Dead-Weight Gage

fluid (oil)
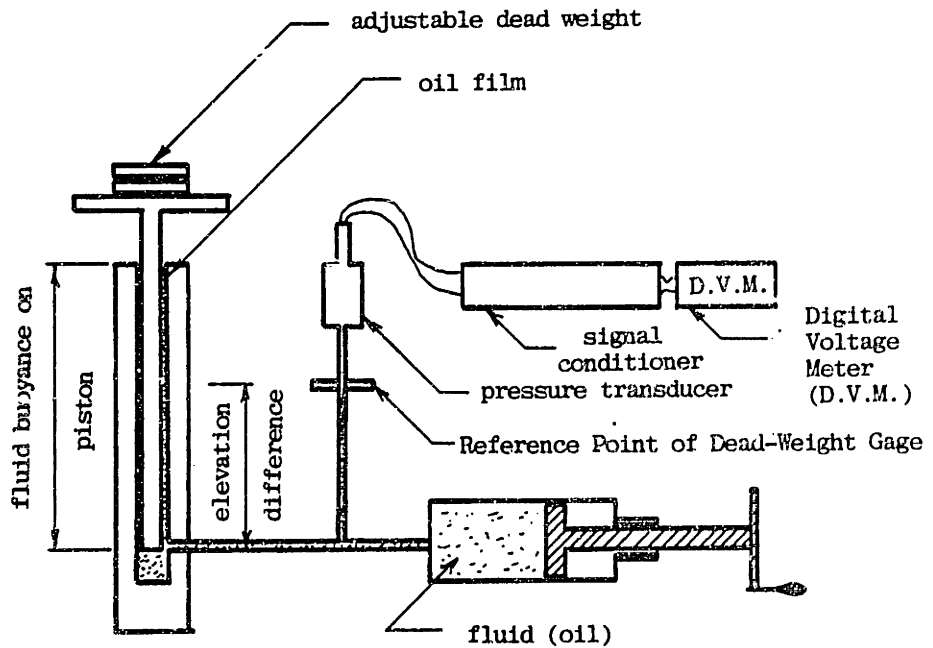
Figure 3-5-2   Calibrating the Pressure Transducer with a Gould
Signal Conditioner by using a Dead-Weight Gage

dead-weight gage is also called the piston gage and is a product of
Maxwell & Moore, Inc. The Statham transducer is connected to the chamber
filled with fluid. This chamber connects to a piston to which various
standard weights are applied. The pressure inside the steel diaphragm is
slowly built up until the piston and the standard weights are seen to
float freely. At this moment, the pressure of the transducer to be
calibrated must be equal to the dead-weight force applied, divided by the
piston area. The results are shown in Table 3-5-1 and Figure 3-5-3 where
the theoretical, calibrated sensitivity is set to be 0.05 V. D.C./psi with
the calibration knob of the Gould signal transducer be set on 3.48. For
accuracy reasons, the calibration process is repeated, and the average
values of the results are recorded in the last column of the table. In
the last row of Table 3-4-1, the final value of the electrical signal is
0.0 volts (corresponding to the case when all the weights are moved out of
the piston). However, a transient value of 0.30 volts was recorded due to
the long time constant of the transducer when the dead weight is set to be
zero.

3.6 Electrically Actuated Values

3.6.1 Introduction

Whenever an electrical and electronic signal is available, solenoid
valves can be used. Unless the solenoid valves are equipped with
explosion-proof solenoids of the appropriate type, the valves should not
be used in areas where explosion hazards exist. Since the LASC controller
is to be mounted on the Budd's Pioneer III passenger rail vehicle which
may travel through some kinds of hazardous areas of mining, paint manu-
facturing, and food processing, the solenoid valves used in the LASC
controller will be explosion-proof.

No.	Pressure (gage,psi)	Voltage (1 V.D.C.) #1	Voltage (1 V.D.C.) #2	Voltage (1 V.D.C.) Average
1	0.0	0.0	0.0	0.0
2	200.0	10.0	10.0	10.0
3	150.0	7.25	7.34	7.30
4	130.0	6.21	6.32	6.27
5	100.0	4.56	4.58	4.57
6	80.0	3.58	3.58	3.58
7	60.0	2.55	2.54	2.55
8	50.0	2.69	2.14	2.42
9	30.0	1.18	1.08	1.13
10	10.0	0.76	0.69	0.72
11	0.0	0.3	0.3	0.3

Table 3-5-1   Calibration results of the Diaphragm-type Strain-gage Pressure Transducer

VOLTAGE(UNIT / V.D.C.)

Linearized pressure curve

PRESSURE (UNIT PSI)
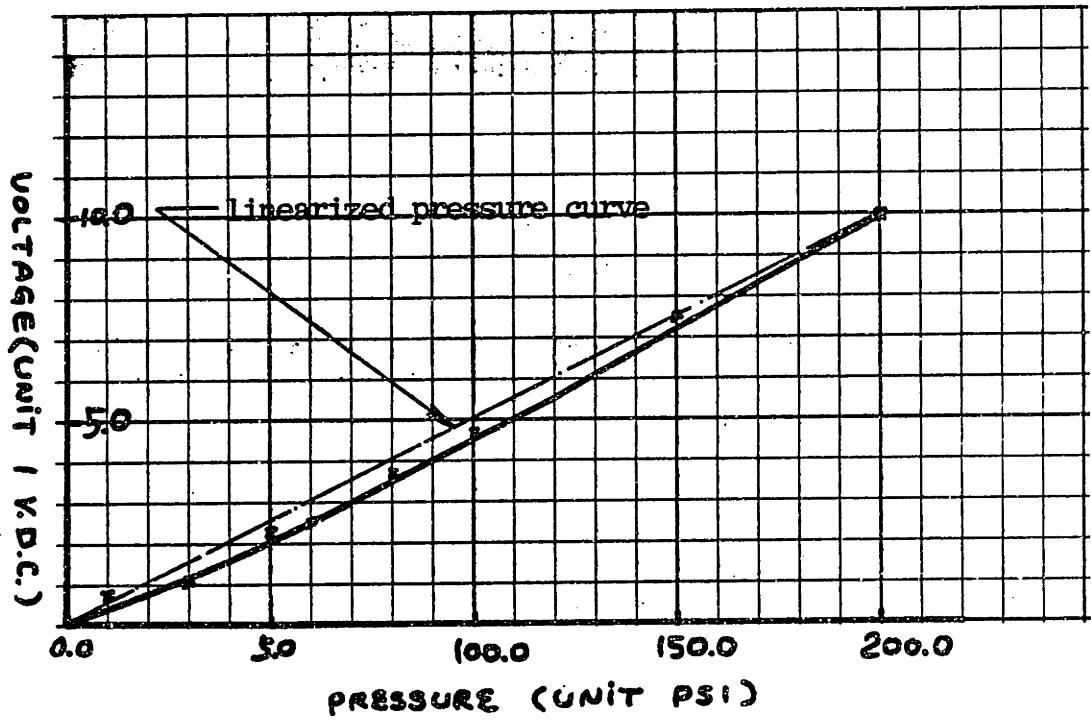
Figure 3-5-3   The Characteristic Curve of the Pressure
Transducer (Based on the Data in Table 3-5-1)

There are two kinds of valves, directly-actuated solenoid valves and indirectly-actuated solenoid valves, according to the number of stages to be actuated. The flow of compressed air is reversed directly by the solenoid for directly-controlled valves which need less actuating force than that of indirectly-controlled valves. The nominal size of the directly actuated valve is usually smaller. The actuating force of the indirectly-actuated valve (with pilot valve) is usually large to control the main valve with the solenoid via an additional pilot valve which is also called a servo-valve.

3.6.2 FESTO 4-position, 5-way Solenoid Valve

A FESTO 4-position, 5-way Solenoid valve, which is an indirectly-actuated valve, is used in this project as shown in the following Figures.

(1) Figure 3-6-1: Two Photographs of the FESTO $4861M_c$-5/4-1/2 valve (4-position, 5-way)

(2) Figure 3-6-2: Dimensions of the FESTO $4861M_c$-5/4-1/2 valve

The mechanism for controlling the main valve via an additional second-stage valve is shown in Figure 3-6-3. This control valve is a poppet valve which is indirectly actuated on both sides and with spring centering.

The air supply to the valve is denoted by a line, with an open arrowhead, entering the valve. There are four cylinder lines which can be connected to two cylinders with two provisions for exhausting air through silencers. With the two solenoids energized in a combined way, the flow is ported to the cylinder line or the exhaust as shown in Table 3-6-4. There are 4 positions corresponding to the different inputs explained in the Table.

It is possible to stop the piston rod in any desired position. With both Solenoids deenergized, the centering springs provide the 2nd porting
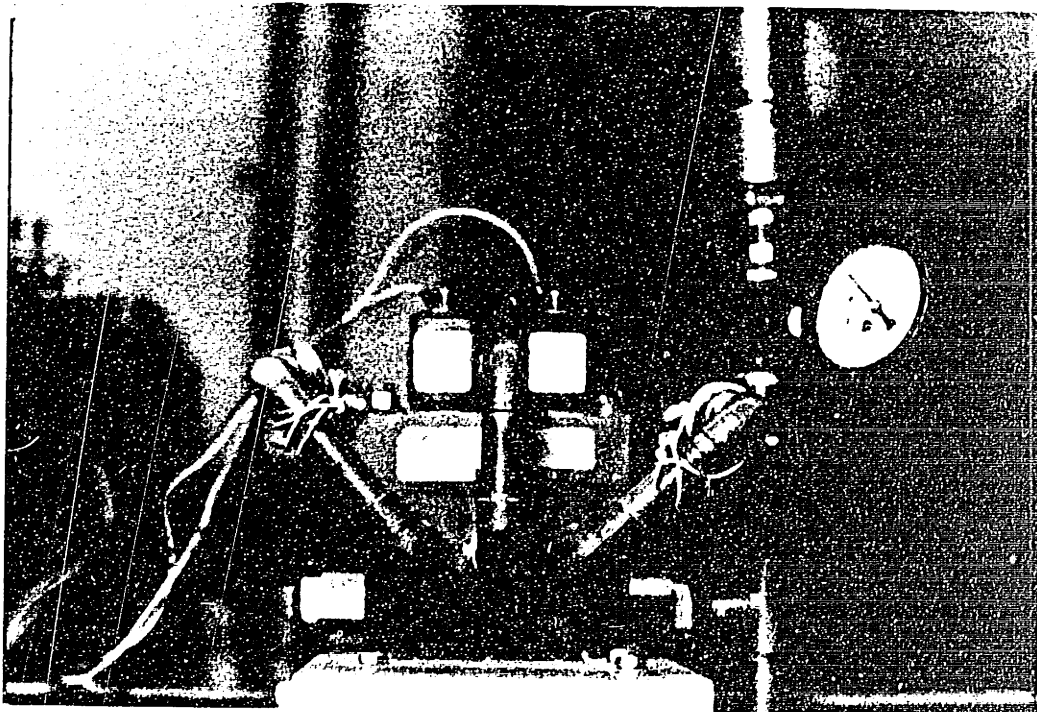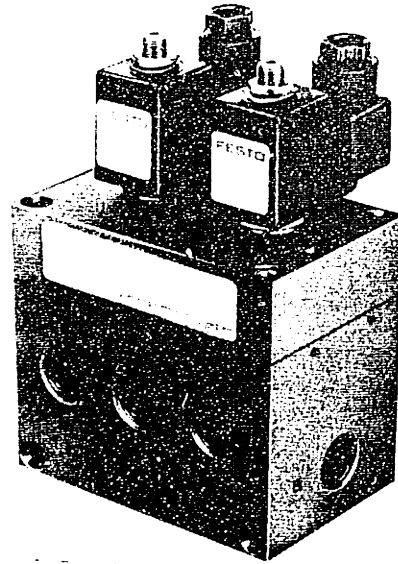
Figure 3-6-1   Two Photographs of the FESTO 4861 Mc-5/4-1/2
Valve (4-Position, 5-Way)
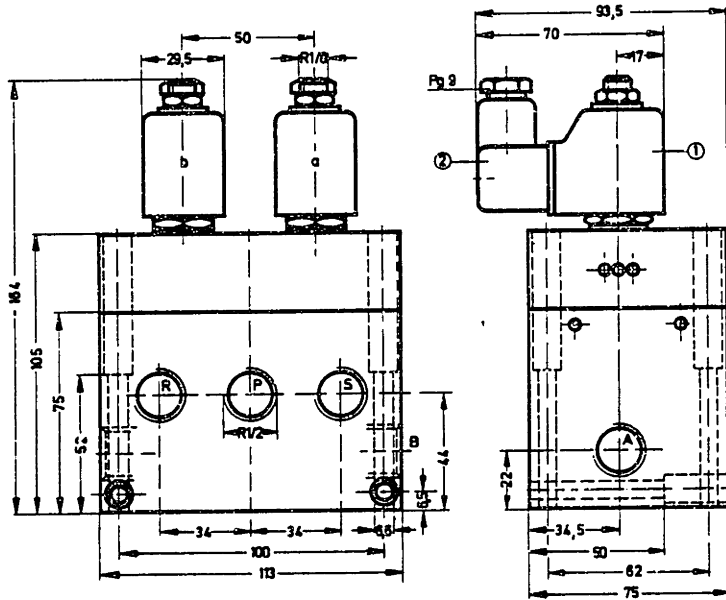
Figure 3-6-2   Dimensions of the FESTO   4861 Mc-5/4-1/2 Valve   [32]
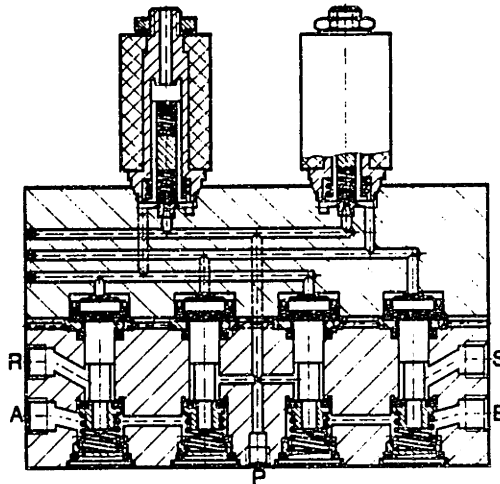
Figure 3-6-3   The Two-Stage, Indirectly-Actuated Mechanism of
the FESTO 4861 Mc-5/4-1/2 Valve   [32]

To the Actuator A ← → To the Actuator B

Valve
Positions = 1   2   3   4

A   A   O   AB   B   B

Solenoid, A   R   S   Solenoid B

Exhaust R   Exhaust S

P

Power Supply, P
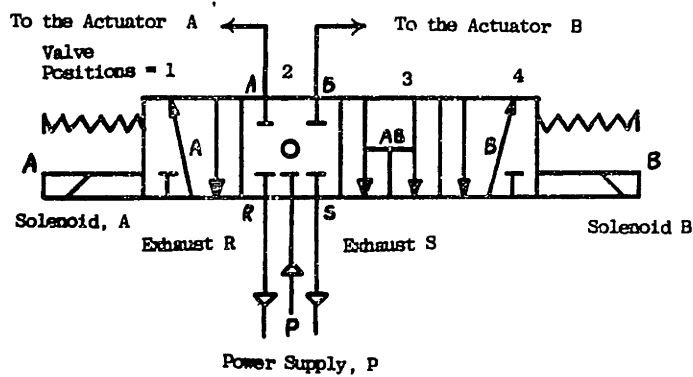
Solenoid Position	Actuator A		Actuator B		Air Flow	Comments
	E	DE	E	DE		
1	x			x	p ⟶ A B ⟶ R,S	force generated by expanding chamber A of the Actuator
2		x		x	supply, actuators, and exhausts are blocked off	Active controller acts as a very stiff spring
3	x		x		supply, actuators, and exhausts are connected internally	Fail-safe mode, Active Controller acts as a very soft spring
4		x	x		p ⟶ B A ⟶ R,S	Force generated by expanding chamber B of the actuator

E = Energized
DE = De-energized

Figure 3-6-4   The Operational Diagram and Characteristics List
of the FESTO 4861 Mc-5/4 - 1/2 Valve

	Type	FESTO 4861 MC-5/4 - ½ Valve + Voltage
1	Connection	R½
2	Nominal Size	12 mm
3	Medium	Filtered, lubricated or filtered, non-lubricated compressed air
4	Design	Poppet valve, indirectly actuated on both sides, with spring centering
5	Standard Nominal Flow Rate (P→A)	2700 1/min (or 95.4 SCFM)
6	Pressure Range	2 to 10 bar (or 29.0 to 145 psi)
7	Switching time at 6 bar	On: 28 ms, off: 33 ms
8	Ambient temperature	-5 to +40° C
9	Temperature of Medium	-10 to +60° C
10	Percentage duty cycle	100%
11	Weight	2.680 kg
12	DC voltage	24 V.D.C.
13	Power consumption DC voltage	12 to 15 W
14	Materials	Valve body: blue anodized aluminum, Seals: perbunan
15	Degree of Protection	JP 65 (DIN 40 050)
16	Notes	1. Solenoid turns 2. Connector can be shifted 90° 3. P = Compressed air port 4. A.B. = Working or outlet lines 5. R, S = Exhaust

Table 3-6-2 Valve Specifications of the FESTO 486 1 Mc-5/4 - ½ Pneumatic valve

configuration at the 2nd valve position, (i.e. the neutral position where
the ports P,A,B,R, and S are all blocked). With both solenoids energized,
the valve will operate at the 3rd porting configuration. The valve
behaves as a soft-air-spring where P,A,B,R, and S are all connected.
Energization of Solenoid A only causes the porting configuration in the
adjacent square to be in effect, and makes port A pressurized, whereas
port B is exhausted. On the contrary, energization of Solenoid B only
causes port A to be exhausted and port B to be pressurized, (i.e., the
valve reverses the flow through the cylinder lines as that of energization
of the solenoid A only).

As a practical matter, either solenoid can be energized or de-
energized at the same time, and no damage on the electrical circuit will
result. Owing to this special arrangement, these valves are especially
suitable for positioning, and for stopping double-acting cylinders at any
desired position. Besides, this valve can be energized to make the
cylinder set behave as a soft-air-spring for maintenance and safety
reasons.

The specifications of this valve are shown in Table 3-6-2. For its
electrical requirement, 24 V. D.C. voltage is needed to actuate either of
the solenoids at about 12 watts of power consumption.

3.7 Actuators

Three kinds of actuators, i.e., the air spring, the cylinder, and the
double-rod cylinder, are to be mounted on the LASC tester for experimental
investigation. In the previous chapter, these acuators were modelled and
analyzed based on the actuator's characteristic equation (which stated the
force created was equal to the effective area times the pressure
difference). The scaled carbody mass should include the mass of the

actuator and of the valve for accuracy. In this section, the method to mount the actuator on the carbody of the LASC tester is illustrated.

3.7.1 Mounting the Actuators on the LASC Tester

(1) For air springs:

Hollow column spacers are manufactured to mount a vertical plate where the air spring is supported at a distance of 3 inches from the carbody, and allows room for copper tubes. These tubes are used to connect the valve to the air spring and are placed inside the spacer. The other end of the air spring is mounted on a connection block on which a load cell is screwed.

(2) For PARKER cylinders: During the static testing of the PARKER cylinder, the cylinder was placed on the base, and the tubes were extended to connect to the cylinder. The load cell, and the connecting block, are moved downward to fit the new height of the drive rod of the cylinder, as shown in Figure 3-7-1. The method, mentioned in the following section, can be well implemented to dynamically test the performance of the PARKER cylinder. Otherwise the LASC tester is not long enough to hold two opposing PARKER cylinders for studying the dynamical response.

(3) For ANA double-rod cylinder

The application area on either side of an ANA double-rod cylinder will always be the same, hence it can be replaced by two single rod cylinders and have the same function. Its disadvantage is that the dummy rod (the idle rod at the other end of the drive rod) needs extra room to move along the cylinder. This problem can be solved by using a thick flange block which has a hole in the center for the dummy (idle) rod. The mounting method for the double-rod cylinder is illustrated in Figure 3-7-2 where the dimensions are calculated as follows:
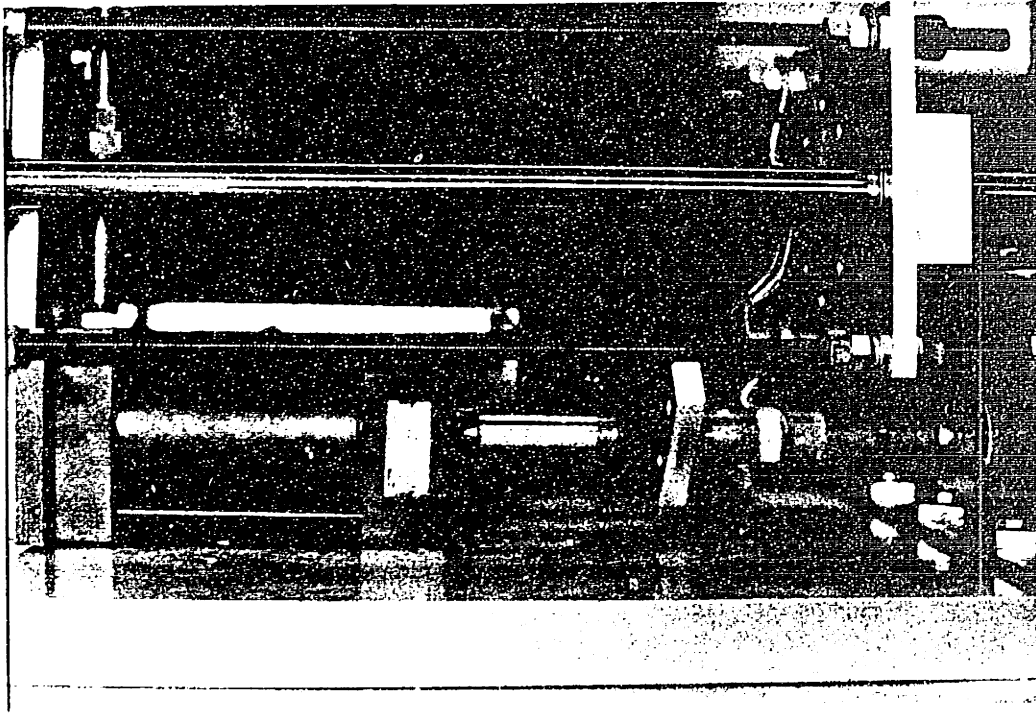
Figure 3-7-1   Mounting the PARK Cylinder on the Testing Machine,
The LASC Tester

Figure 3-7-2 Mounting the ANA Double-End Cylinder on the
Testing Machine, the LASC Tester

NOMENCLATURES:

(1)   B   length of the dummy (idle) rod

(2)   D   piston thickness

(3)   E   thickness of the side wall of the cylinder

(4)   A   height of the flange block (thickness of the block)

(5)   F   allowance for vibration input

(6)   G   thickness of. the flange base

(7)   H   length of the drive rod

(8)   I   the threaded length of H

(9)   M   the maximum length of the actuator

(10)   N   the load cell length, 8 1/2"

(11)   Q   thickness of the truck

(12)   P   thickness of the carbody

(13)   W   total length required

(14)   R   available length of the LASC tester

The following calculations are based on Figure 3-7-2.

Given: $F = 2"$, $C = 4"$, $D = 1/4"$, $E = 1/4"$, $G = 1/4"$, $H = 5"$,

$Z = 2\ 1/4"$, $I = 1"$, $Q = 1"$, $P = 6"$

Required: to find the total length occupied all the components for the

testing, w,

Solution: The geometric equations are:

$B = C - D + 1/8"$ (1)

$a - G = B - E + 1/8"$ (2)

$B = 4 - 1/4 + 1/8 = 3\ 7/8"$ (3)

$A = 3\ 7/8" - 1/4" + 1/8" = 3\ 3/4"$ (4)

$M = g + E + E + c + 5 + A - G$ (5)

$M = 13\ 1/2"$ (6)

$M + N = 22"$ (7)

Answer: Total length required,w, $= 2$ x F + N + M + P + 2Q

$$W = 33 \ 1/2" \tag{8}$$

Since the total space available of the LASC tester, R, is 37" which is greater than the value of W, we may have the following positive conclusion.

Conclusion: The current LASC tester has room enough to run the dynamical testing of the ANA double-rod cylinder.

3.8 Accelerometer

The resulting motion of the carbody was measured by transducing the motion into voltage signals through an accelerometer. The accelerometer used in this project, which is manufactured by the Columbia Research Laboratories, Inc., has the following specifications:

Range: $\pm$ g

Sensitivity : -1V./gravity

input: Port (a) $= + 15$ V.D.C.,

         Port (b) $=$ ground,

         Port (c) $= -15$ V.D.C.,

output: Port (d)

weight: 0.2 lbs

A picture of it is shown in Figure 3-8-1. This accelerometer is mounted on the top of the carbody to pick up the dynamic response of the carbody and give the value of the acceleration $\ddot{y}_c(t)$, which is integrated into $\dot{y}_c$ by an integrator later. Signals of $\ddot{y}_c(t)$ and $\dot{y}_c(t)$ are the major inputs into the control of the LASC controller law as shown in equation (1) of Chapter I.

3.9 The Compressed Air Supply

This section discusses the supply lines of the compressed air, which
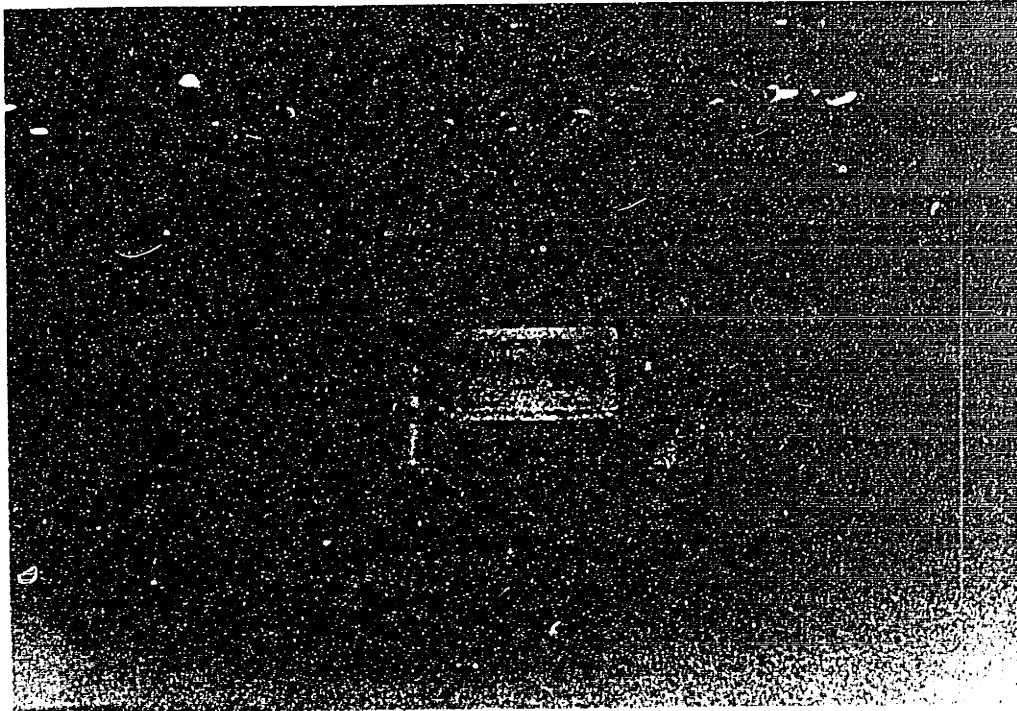
Figure 3-8-1   The Columbia Accelerometer Used in the
Lateral Active Suspension Controller

is the working medium, from its source to exhaust. An air compressor of Hp, which is capable of supplying compressed air of 200 psi with maximum speed of 585 RPM, manufactured by the Joy Manufacturing Co., Ind., is the power source of the actuators to be tested. Pipe lines are illustrated in Figure 3.9.1. A flow regulator was mounted at the end of the iron pipe to vary the pressure input from zero psi to 200 psi. Care was taken when installing the regulator because it is unidirectional. The regulator will be damaged once the flow direction is reversed. Two bypasses, p and Q, were set up for safety. Receiving the input source at Port P, the valve then controls the flow to actuator A or actuator B by internal piping as shown in Figure 3.9.2. The exhaust ports for both actuators are Ports R and S on the valve. In order to reduce the flow friction and the piping capacitance effect, the length of the LASC internal piping was minimized. Three union joints which can be de-assembled and assembled easily were installed at points adequate for maintenance reasons.

3.10 Safety Equipments

Three items of safety equipment, and safety procedures are discussed in the following:

(1) A U-shaped plastic safety shield, which was made of fiberglass, was placed in front of the LASC tester.

(2) The control circuit was placed on another bench, so that the operator would not be close to the LASC tester.

(3) Two silencers (which were also called mufflers) were screwed into exhaust Ports A and B to decrease the noise.

(4) Pipe lines and LASC internal pipings were checked to make sure that the joints were securely coupled.

From
Compressor

Safety
Valve

Main
Valve

Bypass P

Bypass, Q

Hand
Valve

Supply
Pressure
Regulator

To Valve
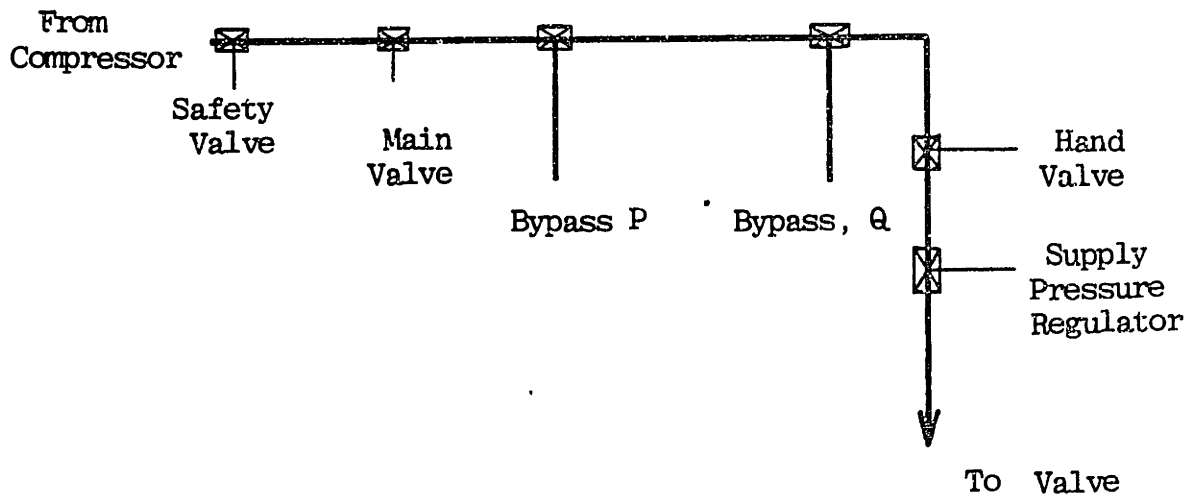
Figure 3-9-1 The Compressed Air Supply

Pressure Gage
(or Pressure Transducer)

Valve W

Union Joint

Valve

Union Joint

Cylinder A
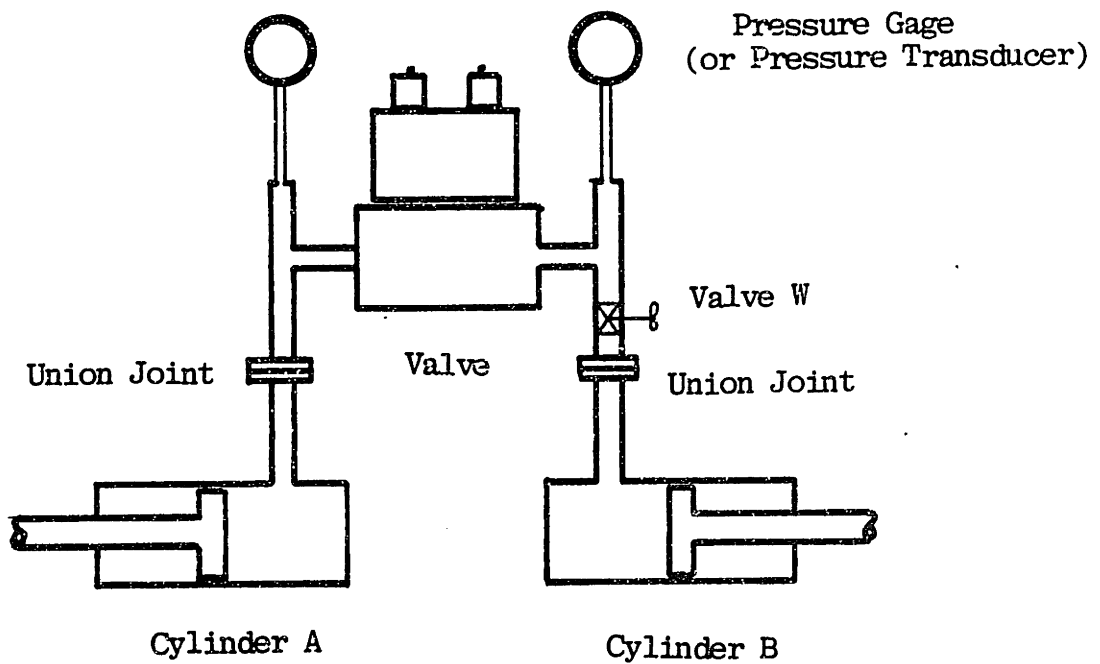
Cylinder B

Figure 3-9-2 The Tubing Diagram of the Valve, Cylinders, Pressure Gages,
Union Joints, and the Pressure Transducer

(5) A warning was provided, to always start with low pressure and
and listen carefully for any unusual noise. Input pressure should
be increased only when the test at the lower pressure are
positive.

3.11 Vibration Generators

3-11-1 Introduction

This section describes two basic types of vibration generators, i.e.
the mechanical direct-drive type and the hydraulic actuator type.
Vibration generators are used to supply the disturbance input to the plant
to be tested. For example, a vibration generator is required when the
dynamical response of the carbody, which is subject to disturbance input,
is under study.

The vibration generator, which is also called a vibration exciter, is
a device suitable for transmitting a vibratory force to the testing
structure. The vibration generator is complete with a mounting rod which
includes provisions for bolting the test article directly to it. The load
of the vibration generator includes the structure under test, and the
friction which is between the structure and the supporting horizontal
parallel shafts. For practical reasons, the later component load can be
eliminated under the assumption of the high efficiency rate of the bearings
used. Generally, the test load refers specifically to the structure under
test only. For the active suspension controller, the actuator force of it
is a function of the control law, and the effective loads for different
frequencies should be used. The static load and dynamic load are
calculated in the following:

3.11.2 Direct-Drive Mechanical Vibration Generator

The direct-drive vibration generator is sometimes referred to as a brute-force vibration generator. It consists of a rotating eccentric driving a positive linkage connection which creates a displacement between the base and the structure as shown in Figure 3-11-1. There are several other kinds of mechanisms for producing drive-vibration such as the cam and follower type, the scotch yoke type, and the eccentric and connecting link type. The last one is used in this project. Since the base is held in a fixed position, the vibration generator tends to generate a vibratory displacement of constant amplitude, which is adjusted beforehand, independent of the operating fequency and existing force.

The generator is driven by an adjustable-speed motor in conjunction with a speed-changer and a frequency-indicating tachometer. The speed-changer may be a belt-driven type or a gear-box type. Structure displacement is set during shutoff by the method discussed later and is designed to hold during operation. The above mentioned method of providing adjustability of crank offset between zero and full displacement is shown in Figure 3-11-2. The displacement adjustment is made by placing the eccentric plate to the adequate pins on the rotating disc. The distance from the center of the rotating disc to the bearing on the eccentric plate, d, is half of the total ampltitude which can be generated between the base and the structure. A non-parallel-four-bar-linkage mechanism to adjust the stroke is illustrated in Figure 3-11-3.

3.11-3. Hydraulic Vibration Generator

A block diagram of a typical hydraulic vibration generator is shown in Figure 3-11-4. It is a device which transforms fluid power from a pump to

Structure to be
Vibrated

Bearings, 4

Guide for
Drive-Rod

Base Line

Eccentric Distance
= ½ Amplitude of
Vibration
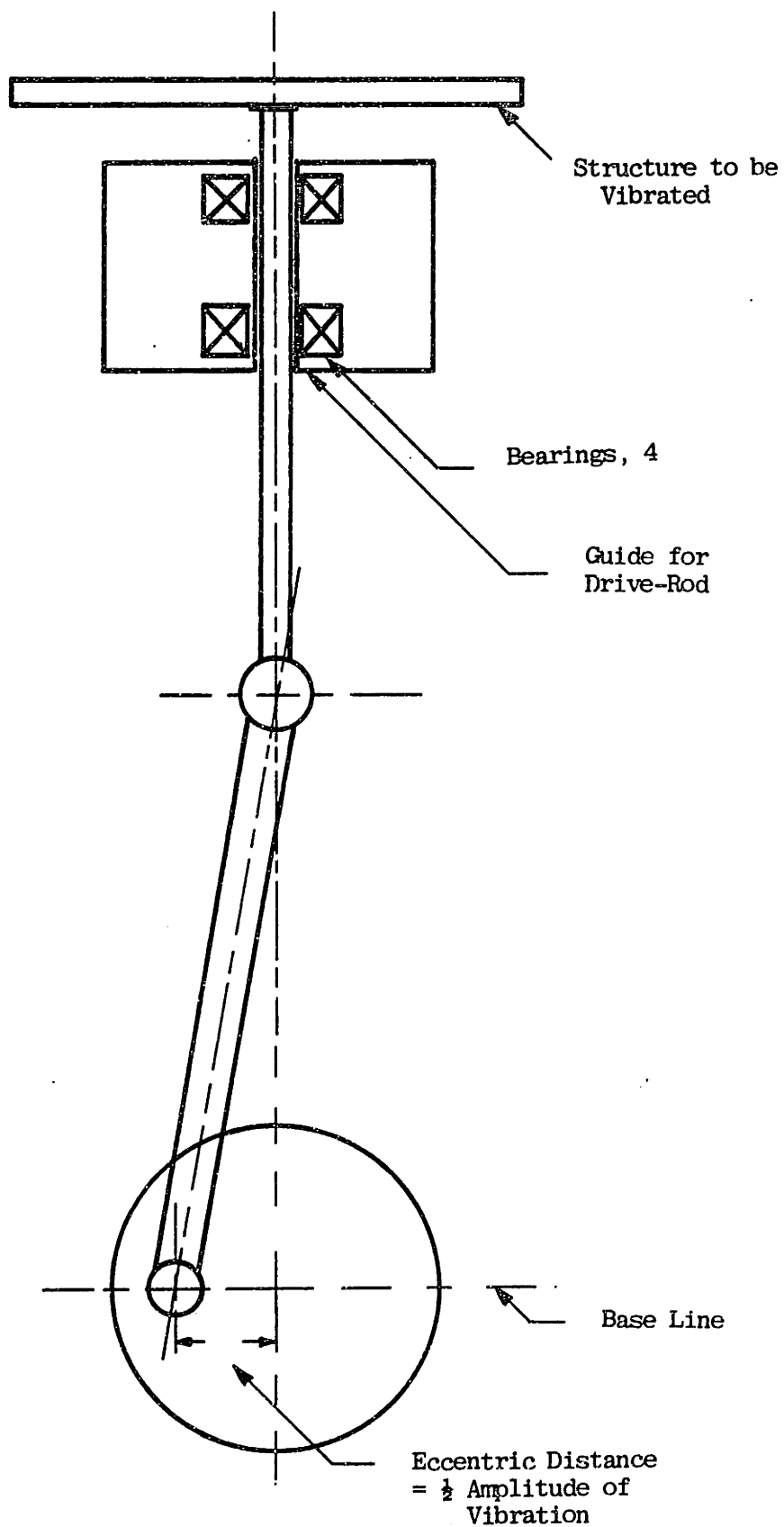
Figure 3-11-1   A Direct Drive Vibration Generator
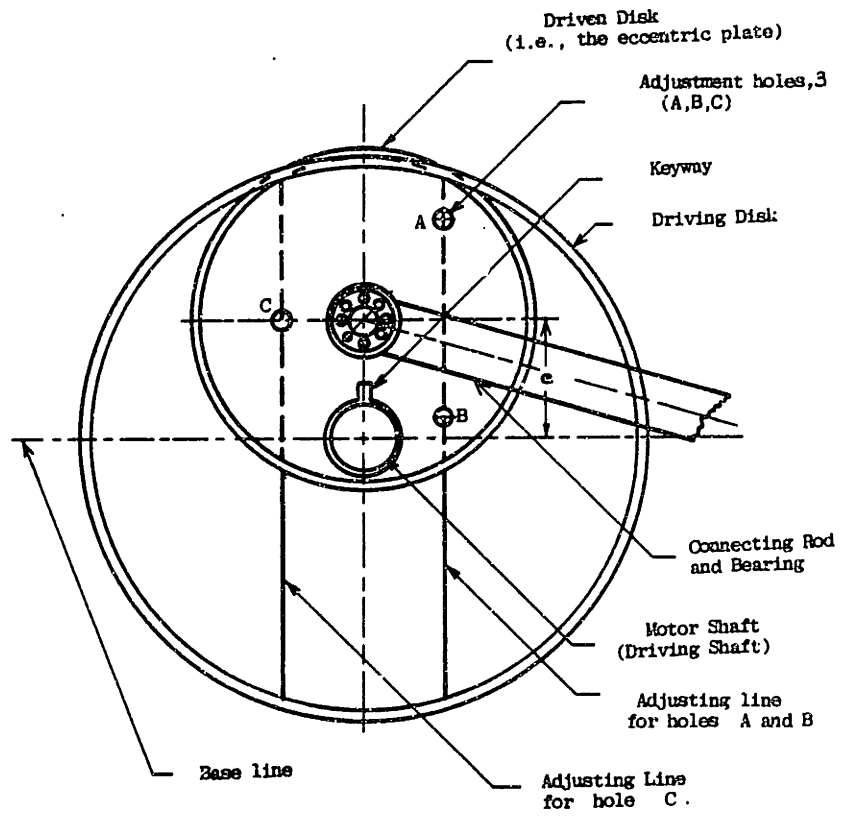
Figure 3-11-2   Adjusting the Output Amplitude of a Direct-Drive
Eccentric-Linkage Type Vibration Generator

a reciprocating motion of the piston rod of the cylinder. A valve is used to deliver fluid to or from the opposite sides of the piston forcing the hydraulic actuator to have a reciprocating motion. In order to minimize the effects of the fluid compliance and the flow friction, close proximity of the valve and cylinder is desirable. In Figure 3-11-5 the power spools of the hydraulic vibration generator are shown in the balance position, blocking both the inlet pressure flow P and the outlet return flow R. Under this condition, the piston of the hydraulic actuator is stationary since there is no fluid flow either to or from the cylinder. Due to a given displacement of the spool to the right, the valve causes a flow of high-pressure fluid from the pump to the left side of the piston, allowing it to move to the right, and forcing the trapped fluid to be expelled to return to the chamber R. The transducers on the spool and the drive rod are used to provide electrical control in the feedback circuit. The pump is capable of variable flow while maintaining a fixed pressure of up to 3,000 lb/in^2, and is a product of the ABCD Company.

The advantage of the hydraulic vibration generator is that large forces or large strokes can be provided relatively easily. The power can even be increased by the installation of several valves on a single actuator such as the combination of a pilot-stage valve with a power-stage valve. Figure 3-11-6. The main advantage of the hydraulic actuator is that it consists of shaft, piston, and cylinder which are simple in construction and the forces are generated without using bearings. However, the waveform of table motion is not as good as that of the electrodynamic type, since the actuator friction and the valve distortion are not negligible, especially at low drive levels.

Axis, fixed

Secondary Rotating Disk

Bearings, 2

A

Adjustment
holes

B

Structure
Tested

e

Adjustment Line

Motor Shaft
(driving shaft)

Base line
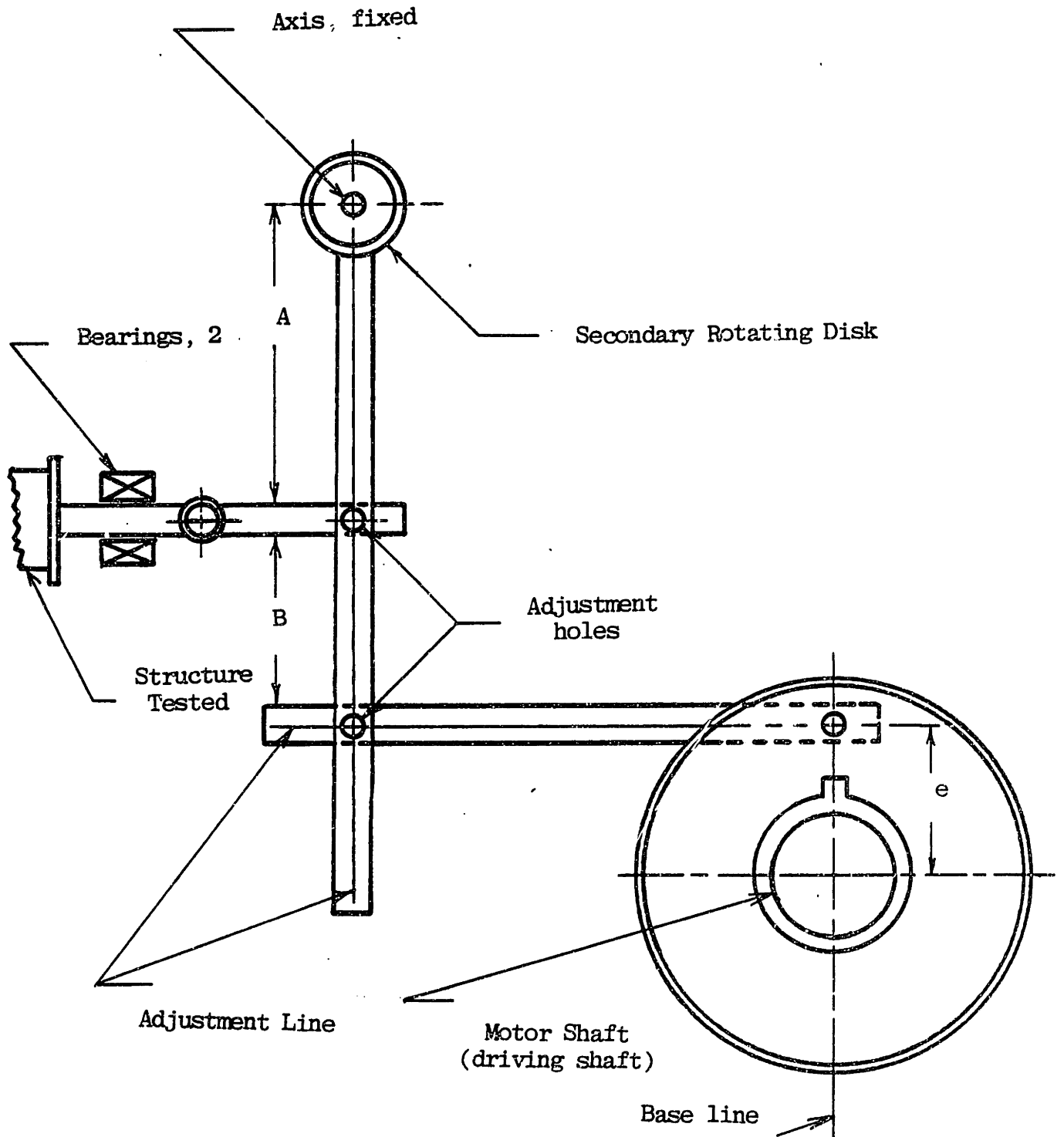
Figure 3-11-3   A Non-Parallel-Four-Bar-Linkage Mechanism Used
in Generating Sinusoidal Vibration Input
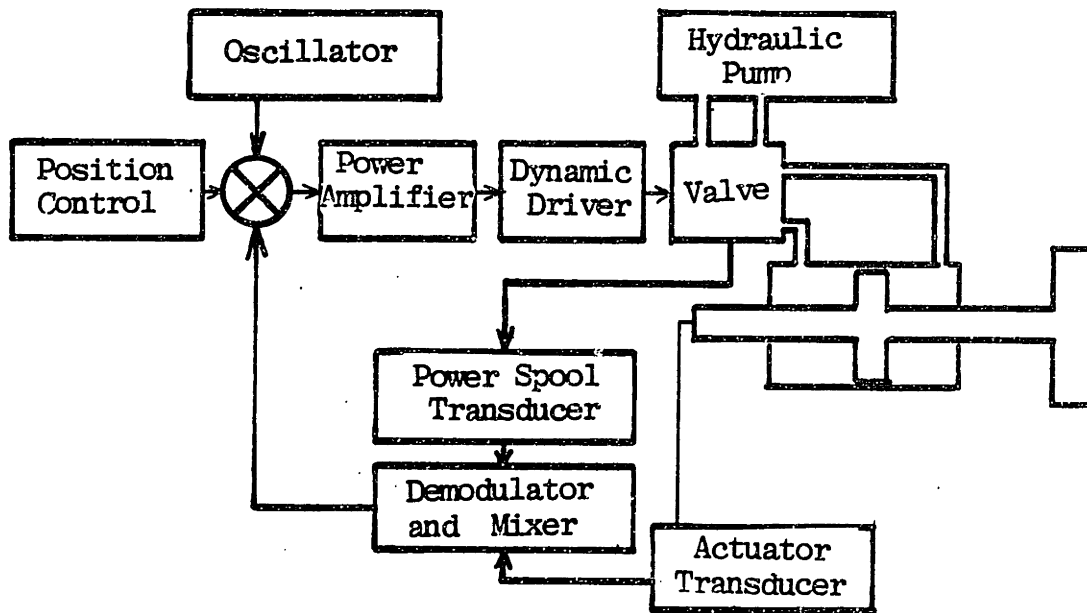
Figure 3-11-4   Block Diagram of the Hydraulic Vibration
Generator System
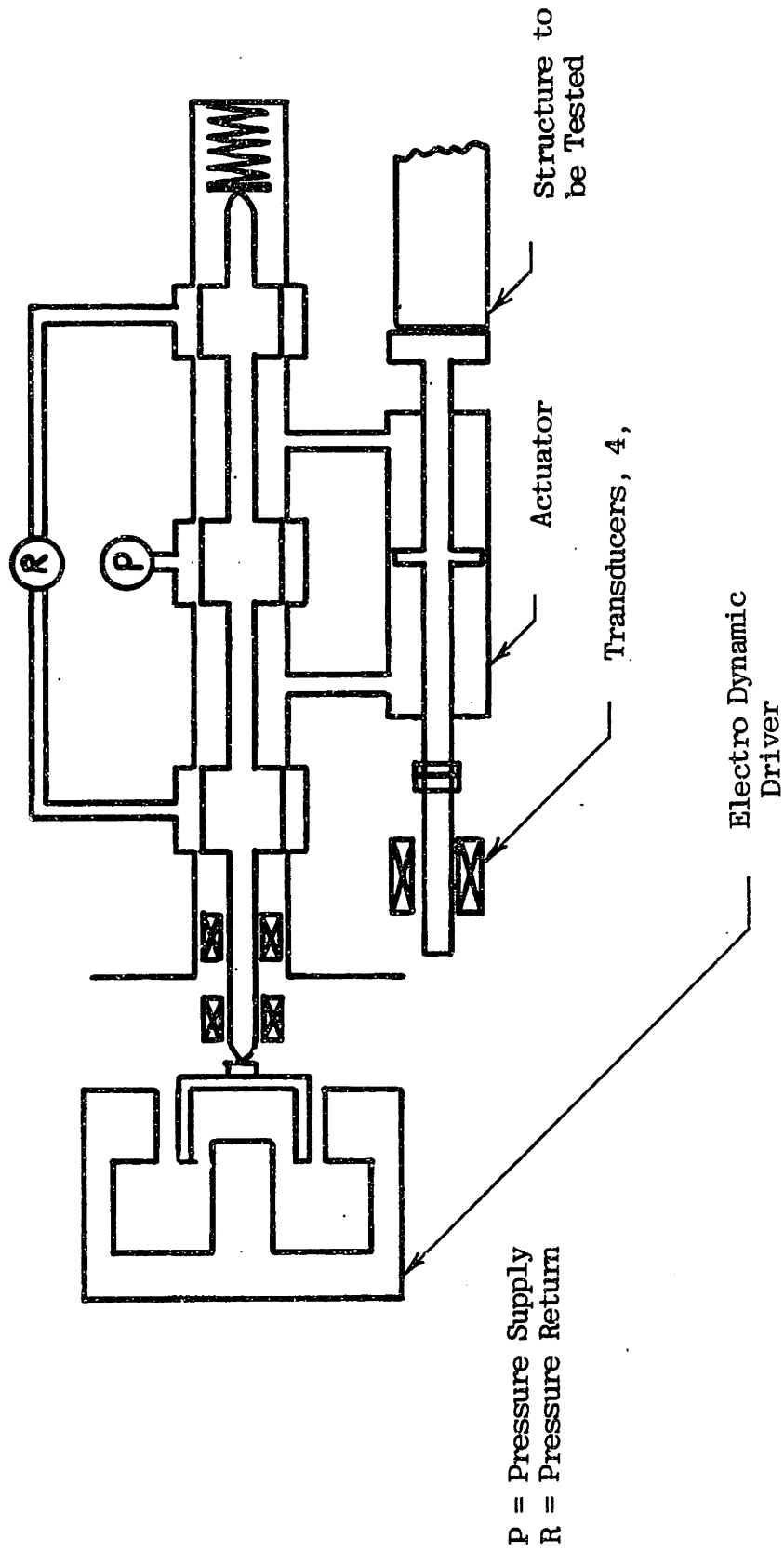
Figure 3-11-5   Schematic Diagram of the Hydraulic Vibration
Generator System

P = Pressure Supply
R = Pressure Return

3.12 <u>Designing a control circuit for the lateral active suspension contoller</u>

3.12.1 <u>Introduction</u>

In order to study the over-all system response and to analyze the individual system element, a circuit named the MCC circuit is assigned to operate the active suspension controller. The MCC circuit integrates the power supplies, the system input, the system output, the control law circuit, the switching circuit, and the display circuit together, and forms a complete control circuitry. All quantities of it are represented by voltages for signal conditioning. The MCC circuit includes the following major parts:

1. power supplies: (1) 24V. D.C. Voltage for solenoids

    (2) ±15V. D.C. Voltage for IC's

    (3) ± 6V. D.C. Voltage for artificial error input

    (4) 220V. A.C. Voltage for: (a) the Gould Signal Conditioner,
    (b) the Oscilloscope which is capable of storage and equipped with dual beams,
    (c) the Digital Voltage Meter, (DVM)
    (d) the signal generator.

    Notes: The Gould signal conditioner will furnish the +10V. D.C. bridge exitation voltage for the load cell and the pressure gages.

2. load cells: input = 10V. D.C. Voltage for bridge excitation

    output = 0-15 V. D.C. Voltage at the sensitivity of 0.05 V./psi

3. pressure gages = input = 10 V. D.C. Voltage for bridge excitation

    output = 0-15 V. D.C. Voltage at the sensitivity of 0.05 V./psi

4. accelerometer: input = port A - 15 V. D.C., port C + 15 V. D.C.,
                            B: ground

                    output = port D: $\pm$ 1.V.D.C. at sensitivity of -1 V./g.

                    range = $\pm$ 1 g

5. solenoids: + 24 V. D.C. Voltage for energization

6. reference signal to identify the valve position: 2 V., 4 V., 6 V., D.C.
                                                              Voltage

7. switching & referencing circuit: it is based on a 2-pole, 5-position
                                            rotary switch

8. control law circuit: (1) pwm circuit;
                         (2) bang-bang with lead compensation circuit

    Note: Only one of the switching and referencing circuit, and the
           control law circuit is implemented at one time.

9. signal generator: it is capable of producing standard waveforms at
                      various frequencies and amplitudes. It is also a
                      good tool for adjusting the other electrical
                      instruments.

The schematic diagram of the MCC circuitry is shown in Figure 3-12-1,

whereas photographs of the control circuits are shown in Figure 3-12-2.

3.12.2 The Switching and Referencing Circuit

The design of the switching and referencing circuit is based on a 2-

pole, 5-position switch, which is manufactured by the Switch Rotary Centro

Lab., to distribute the appropriate voltages to the solenoids of the valve.

The control law for the valve is sketched in Figure 3-6-4 of Section 3.6,

where four sets of voltage A and voltage B are formed to position the

control valve according to the desired motions of the cylinder. This

control law is further illustrated, based on the switch knob positions and

the reference signals as shown in Table 3-12-1 and Figure 3-12-3.

Input and Power Supply	Control Circuit	Control Valve and Display Instrument

+ 24 V.D.V.
± 15 V.D.V.
± 6 V.D.V.
signal generator

#1 load cell
signal

#2 load cell
signal

Multiple
Plexer

Swithching
and
Referencing
Circuit

V_A

V_B

Ref.
Signal

Control
Valve

D.V.M.
Digital
Voltage
Meter

Control
Circuit

V_A

V_B

Ref.
Signal

Oscillo-
scope

X-Y
Plotter
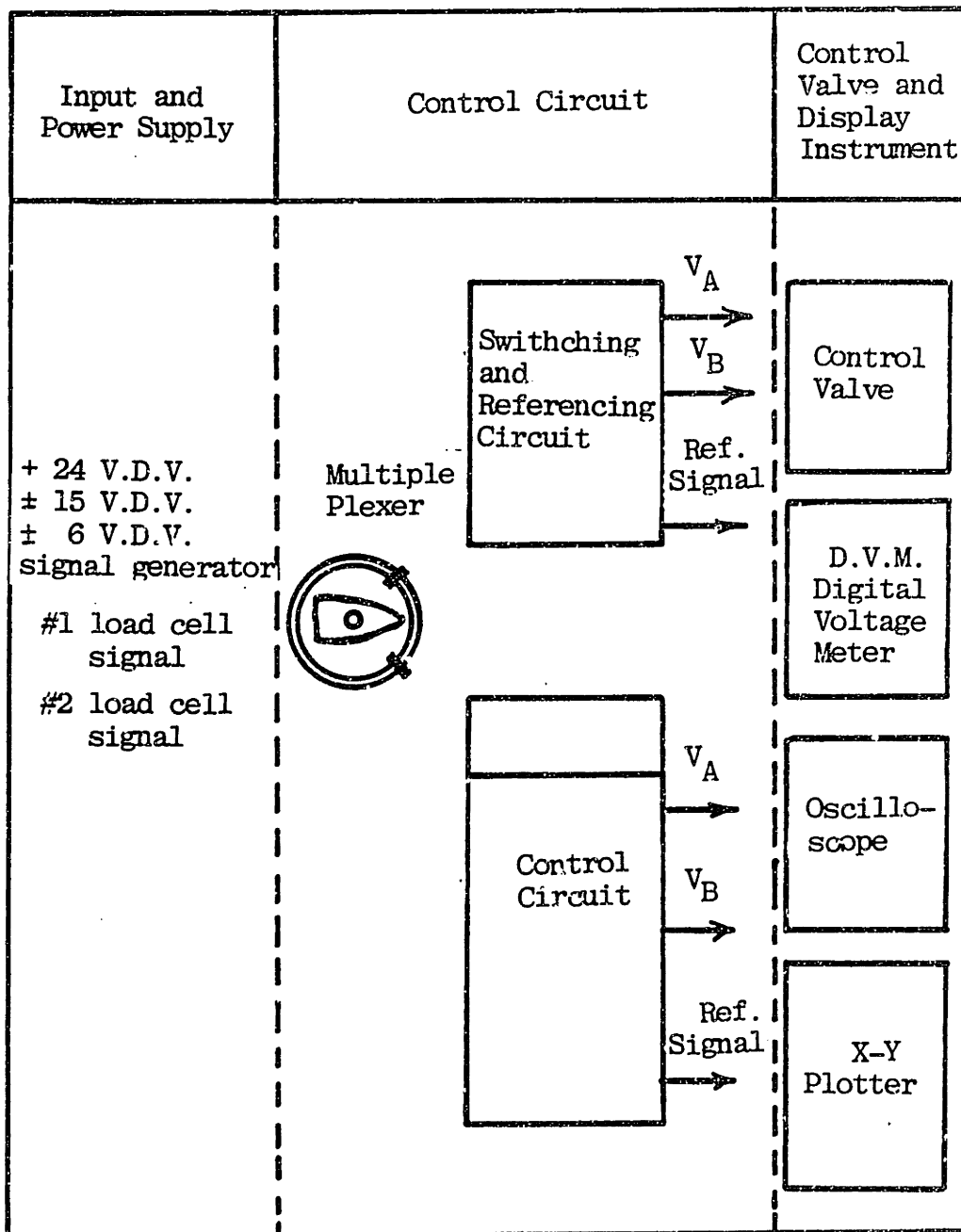
Figure 3-12-1 The Schematic Diagram of the MCC Circuitry

- 141 -
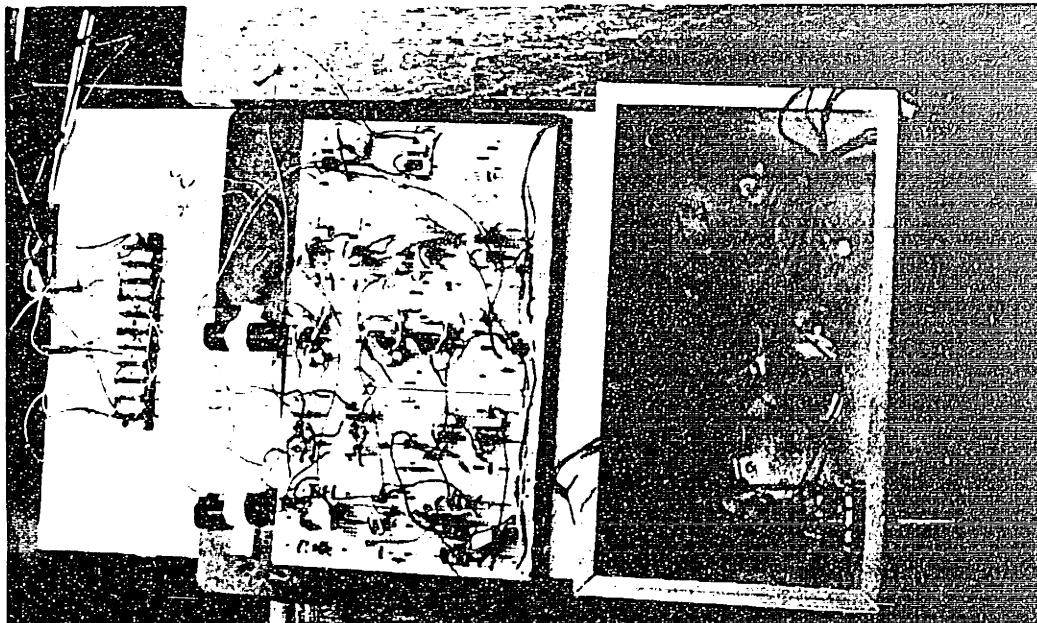
(a) The MCC Circuitry (on the right) with the Pulse Width
     Modulation (PWM) Control Circuit
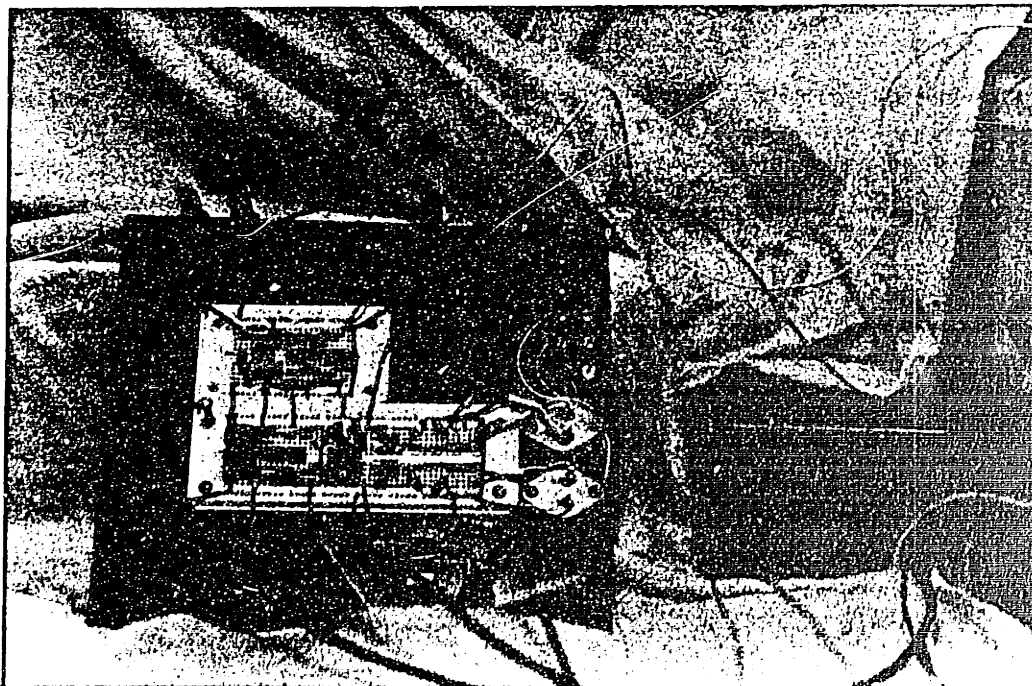
(b) The Bang-Bang with Compensation Circuit

Figure 3-12-2   Photographs of Control Circuit

The first ring
(a) for controlling
the Solenoid A

The second ring
(b) for controlling
the Solenoid B
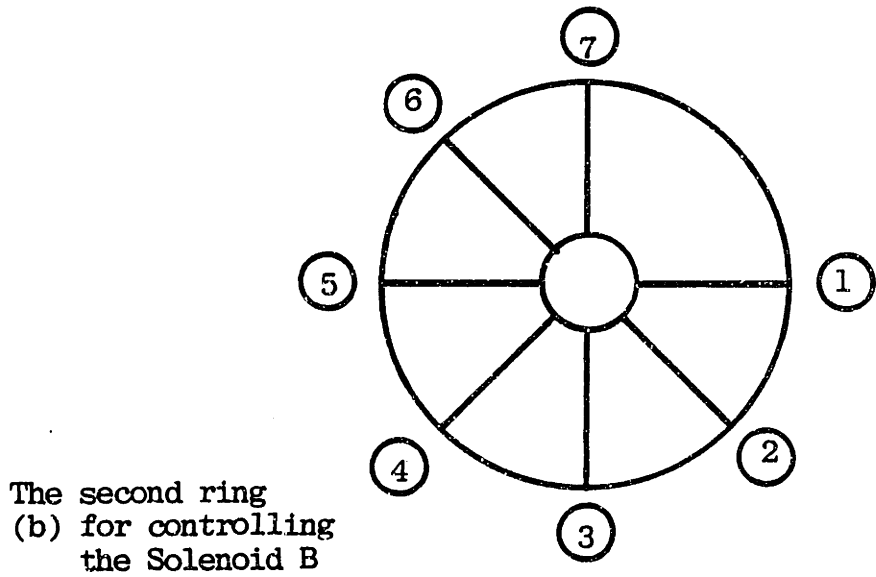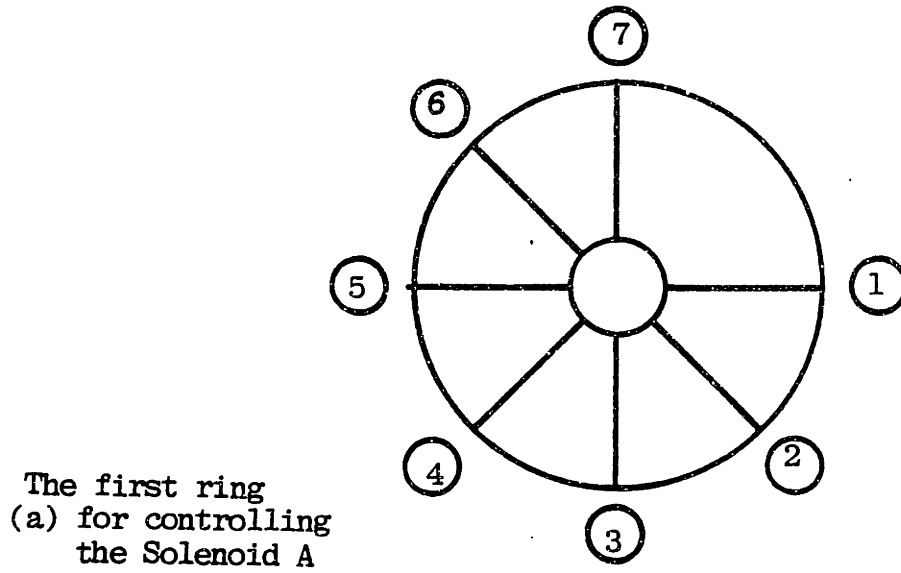
Figure 3-12-3   The Knob Positions for the Two Co-Axial Rings of the
Two-Pole, Five Position Switch

- 143 -

| Actuating Signals | | Parallel Reference Signals (V.D.C.) | Switch Knob Position |
Solenoid A (V.D.C.)	Solenoid B (V.D.C.)		
0.0	0.0	0.0	1
24.0	0.0	6.0	2
0.0	24.0	18.0	3
0.0	0.0	0.0	4
24.0	24.0	12.0	5
0.0	0.0	0.0	6

Table 3-12-1 Relations Between the Switch Knob Positions, Parallel Reference Signals, and the Actuating Signals

The first ring of the switch is to control solenoid A whereas the second
ring is to control solenoid B. It is important to note that these two
rings are co-axial, and a single turn of the shaft will position both rings
simultaneously. At each knob position, a reference signal voltage is
formed by a parallel resistor. For example, a resistor of 12 ohms of
resistance is used parallel to output 2 V. when the switch knob is at the
6th position. The status of the valve position can be monitored by the
reference voltage signal. Another important function of the reference
signal is to trigger the (time) sweeping beam of the oscilloscope.

3.13   The Flexibility of the Testing Facility

3.13.1   Introduction

In order to test a new product of several different designs, it is
better to use a tester which can allow some changes and modifications.
Research time and cost can definitely be reduced when a flexible tester is
available. This section investigates the flexibility of the LASC tester
which was designed previously to perform the testings for the LASC
controller. In case there is a need for testing a higher-degree-of-freedom
system, a higher-order-system, and a system which is subjected to multiple
disturbance inputs (or the system uses a modified actuator),this tester can
be arranged to meet the different requirements by the techniques described
below.

3.13.2   Flexibility for Installing Multiple Inputs

Two sets of disturbance inputs can be quite easily implemented by
mounting two vibration generators on both sides of the LASC tester, which
is expandable to house two external generators. The drive rod of vibration

generator A is connected to the left bolster plate and at the same time the output of the vibration generator B is transmitted to the system through the right bolster plate. The carbody's response to these two independent vibration generators can be studied by this set-up as shown in Fig. 3-13-1.

3.13.3 Flexibility for Higher-Order Systems

The equation of motion for the two-degree-of-freedom system in Fig. 3-13-2 can be derived by applying Newton's second law to each of the masses, as shown in the following:

$$m_u \ddot{y}_1 = k_1 y_1 - k(y_1-y_2) - b_1 \dot{y}_1 - b(\dot{y}_1-\dot{y}_2) + F_u(t)$$

$$m_d \ddot{y}_2 = k_2 y_2 - k(y_2-y_1) - b_2 x_2 - b(\dot{y}_2-\dot{y}_1) + F_d(t)$$

which can be arranged to

$$m_u \ddot{y}_1 + (b-b_1)\dot{y}_1 + (k+k_1)y_1 - b\dot{y}_2 - ky_2 = F_u(t)$$

$$-b\dot{y}_1 - k\dot{y}_1 + m_d \ddot{y}_2 + (b+b_2) + (k+k_2)\,\dot{y}_2 = F_d(t)$$

where the $F_u(t)$ and $F_d(t)$ are the hydraulic actuator forces applied to the respective masses m_u, m_d. The experimental investigation of this two-degree-of-freedom, which is subjected to two independent disturbance inputs, can be implemented by the arrangement of the LASC tester as shown in Fig. 3.13.3. An arrangement for an n-th order system, where n = 14, is sketched in Fig. 3-13-4.

3.13.4 Flexibility for Higher-Degree-of-Freedom Systems

As pointed out previously in Chapter 1, the carbody can be allowed to have six-degrees-of-freedom in space. For example, a schematic diagram of the carbody's plane motion is sketched in Fig. 3-13-5. Since the LASC
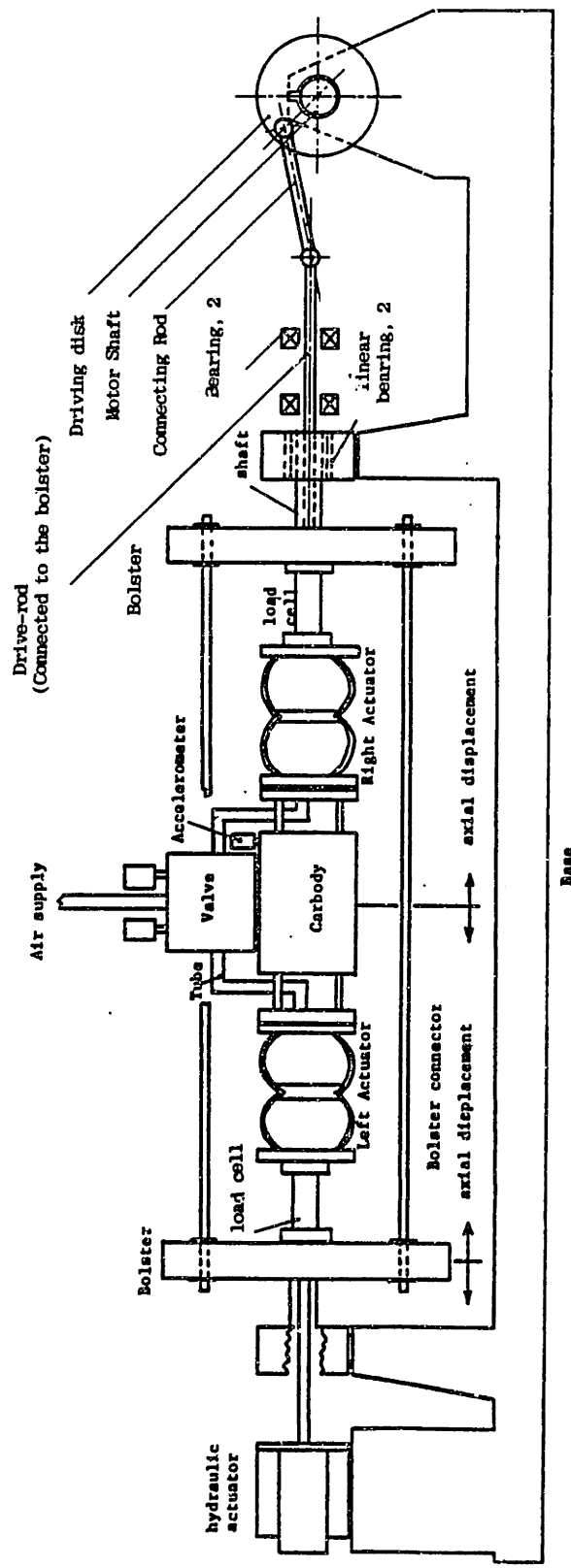
Figure 3-13-1 Mounting Two Independent Vibration Generators in the Testing Facility, the LASC Tester
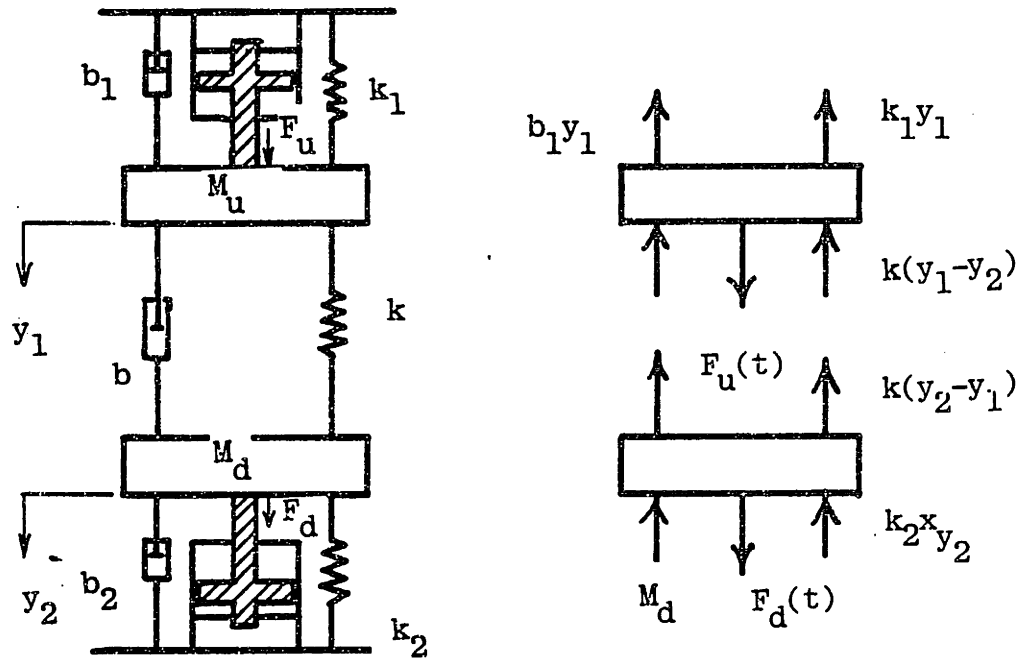
Figure 3-13-2   A Fourth Order One-Degree-of-Freedom System which is
Subjected to Two Independent Distance Inputs from
Hydraulic Actuators
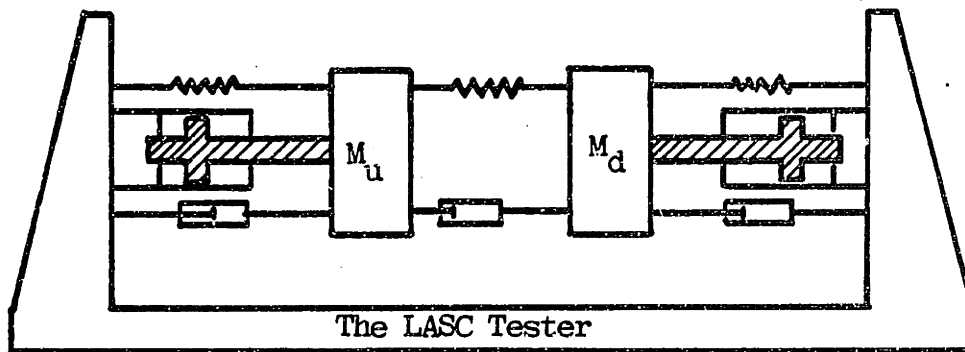
Figure 3-13-3   Mounting a Fourth Order One-Degree-of-Freedom
System on the LASC Testing Facility

c.g. = center of
gravity
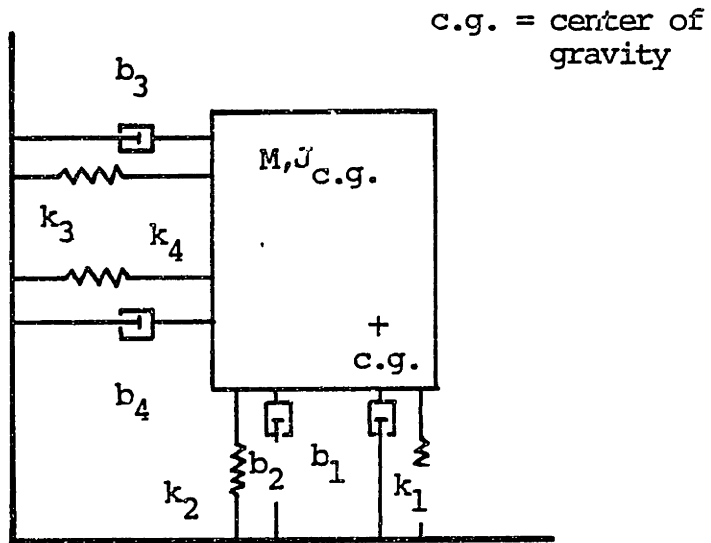
Figure   3-13-5   Carbody's Plane Motion

Two parallel shafts

16 springs

16 dampers
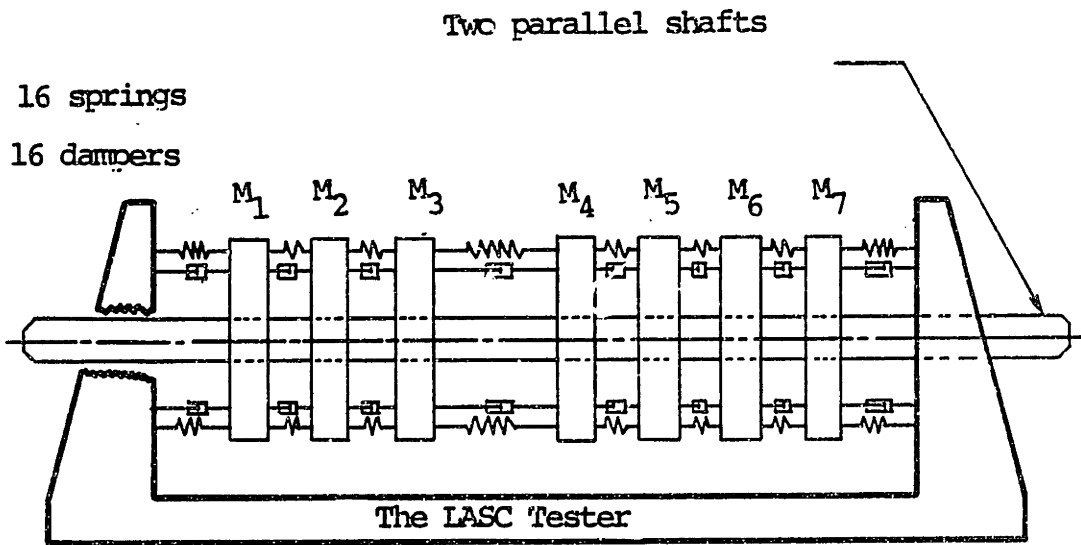
The LASC Tester

Figure 3-13-4   Arranging the LASC Tester to Perform
Testings for a 14th Order, One-Degree-
of-Freedom System

tester is designed only for testing a single-degree-of-freedom system, two

LASC testers are mounted together to give the carbody an extra degree-of-

freedom. The upper LASC tester is mounted to a LASC tester which is at a

lower position. The study of the carbody's plane motion, which can be

subjected to up to four independent disturbance inputs, can be achieved by

this arrangement. Similarly, by placing three LASC testers in the three

orthogonal axes, (i.e. the x,y,z axes), the three-degrees-of-freedom motion

of the carbody can be studied. However, the carbody's rotational movement,

(i.e. the pitching, rolling, and yawing) , is hard to investigate by

combining the LASC testers, because the nature of the tester design is for

linear motion only.

3.13.5 Flexibility of Installing the Double-rod Actuators

A double-rod actuator is designed to replace two single-rod actuators,

as discussed in the previous chapter. Only a modified foot flange block,

which has a hole of 1/2 in. in its center, is needed to place a double-

rod actuator on the LASC tester as shown in Fig. 2. By this arrangement,

the number of load cells, springs, and dampers can be cut off by the factor

of two, hence there is more room available in the tester to perform various

investigations.

3.14 Conclusion

This chapter mainly presented the design and fabrication of the LASC

tester. The selection, fabrication and calibration of its components were

well discussed. Most of the machining jobs were completed by the author

himself at the machine shop in the Mechanical Engineering Department.

Figures 3-14-1, 3-14-2, and 3-14-3 show photographs of the LASC tester

which is currently placed at the Vehicle Dynamics Laboratory of this
Institute.
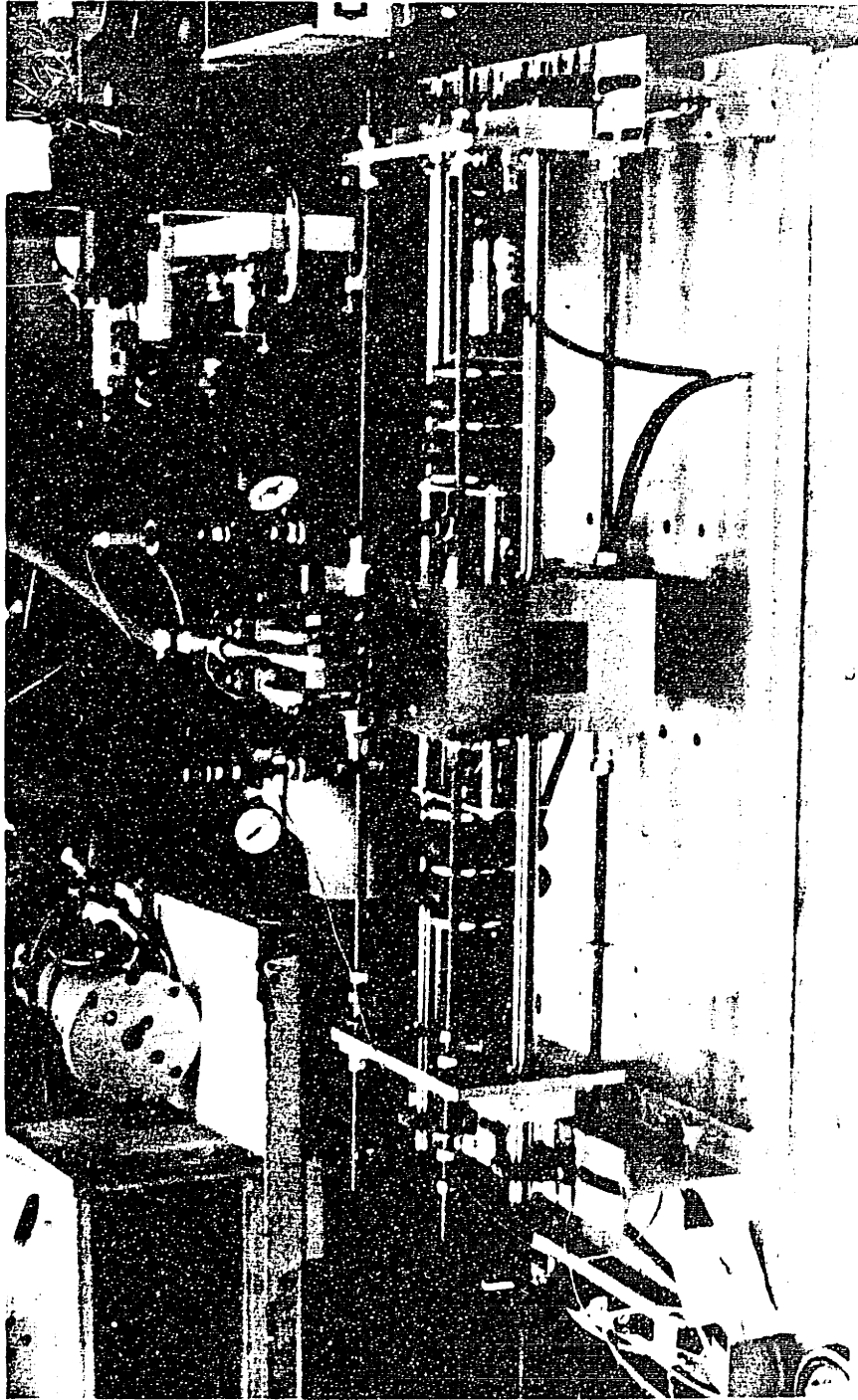
Figure 3-14-1   Photograph of the Lateral Active Suspension Controller
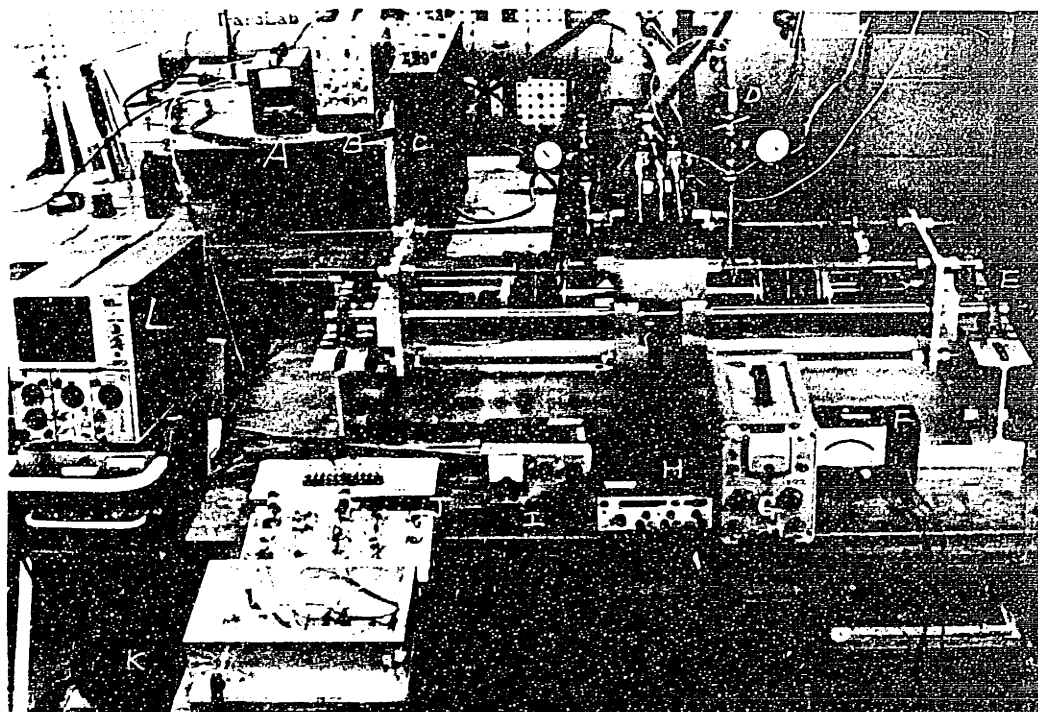
```
A  = power supply (+ 30V.)      G = signal conditioner
B  = signal conditioner         H = signal generator
C  = power supply               I = power supply (±15V.)
D  = pressure transducer        J = the MCC control circuit
E  = the mechanical assembly        (with the pwm circuit)
F  = voltage meter              K = D.V.M.

       L  =  oscilloscope
```

Figure 3-14-2 The LASC Tester with Some Supporting Equipment
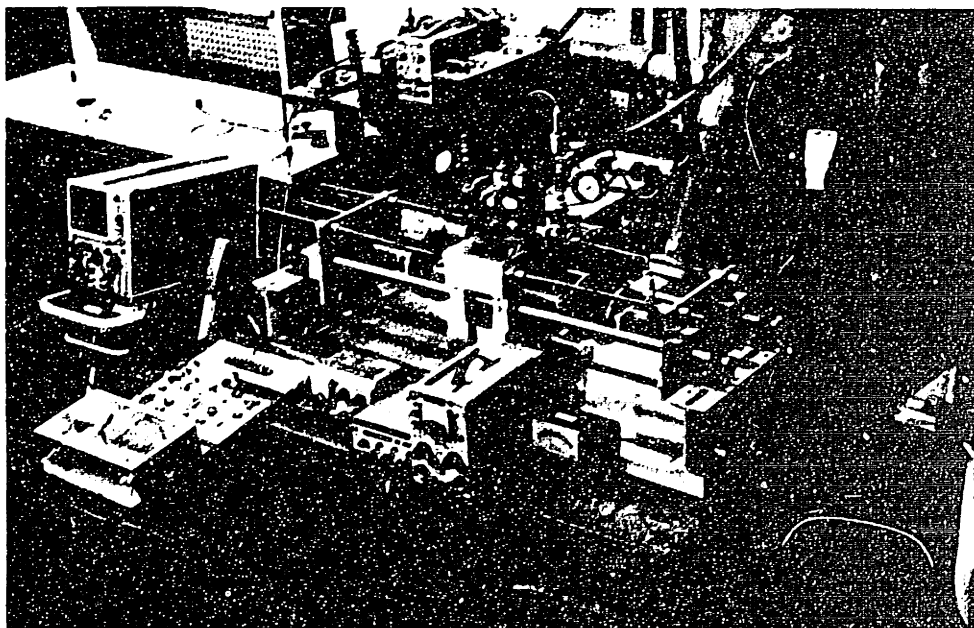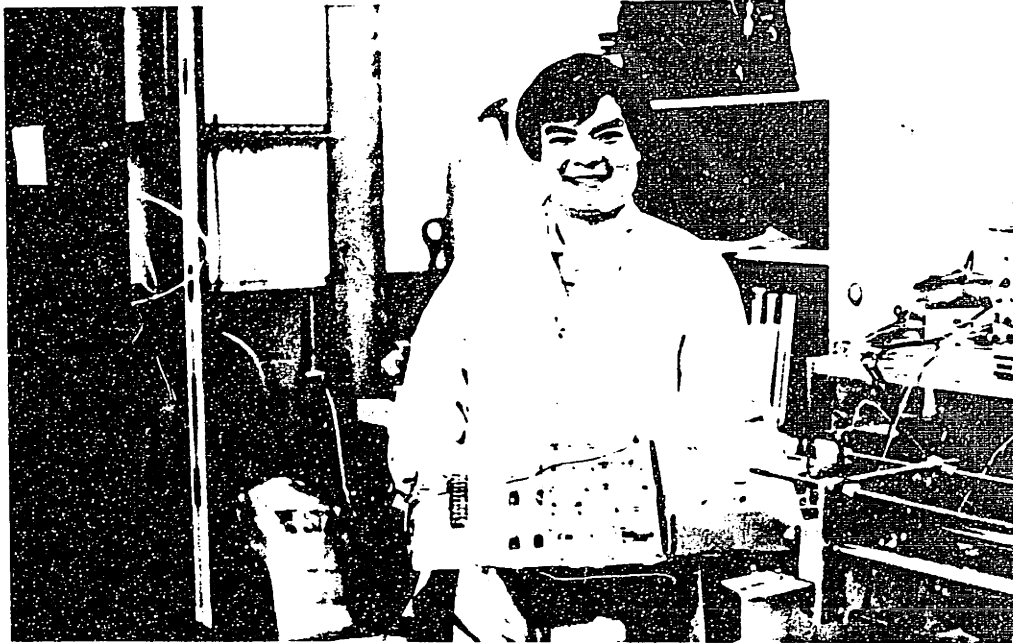
Figure 3.14.3 Photographs of the MCC Control Circuit
(with the PWM) and the LASC tester

CHAPTER IV

EXPERIMENTAL VERIFICATION OF THE CONTROLLER

4.1 Introduction

The Lateral Active Suspension Controller, the LASC controller, was designed in Chapter 2, whereas the laboratory test set-up, which is also called the LASC tester, was implemented with adequate equipment as described in Chapter 3. The LASC tester consists of the following components: the vibration generator, the LASC controller, the mechanical set up assembly, the control circuitry, the display equipment, and the compressed air supply, and is shown in Fig. 3.3.1. This chapter discusses the experimental results and compares the results to those calculated from computer simulations based on the models developed in Chapter 2. This comparison is further discussed to explain the difference between the two results.

The testing is divided into two major parts - static testing and dynamic testing. Static testing consists of testing the characteristics of the valve alone, such as the response curve and the time constant when turning the actuating signals on/off, and testing force generated by the actuator on the bolster at different heights (and at different supply pressures). However, the dynamic testing is more complex and is further divided into three ordered parts as follows:

(1) With both the carbody and the bolster locked to the ground, the force response of the actuator to a step input of the desired force is calculated.

(2) With the carbody locked to the ground, the frequency response of

the actuator to a sinusoidal-displacement input to the bolster

through the vibration generator is studied.

(3) With both the carbody and the bolster free to slide on the parallel

shafts, the carbody's response to a modified random input through

a vibration generator is studied.

In the first two cases where the carbody (or the bolster) is

required to be grounded, a practical method is proposed by Chen [24],

which is to use the nuts on the threaded rods to tighten the carbody to

the threaded rods of the bolster assembly. Later, in the following

case, (Case 3), the tightened nuts are removed in order to study the

dynamic response of the carbody to the external disturbance input.

The experimental set-up, procedures to obtain the experimental

data, and calculations of major parameters were presented in the first

part of the chapter. The results of computer simulation were analized

to select controller components in the second part of the chapter, i.e.

Section 4.8.

4.2 Preliminary Testing

The laboratory apparatus for testing the lateral active suspension

controller was designed and fabricated as shown in Figure 3.3.1.

Preliminary tests were performed to demonstrate the fundamental

operations of the testing facility. Two airsprings were mounted on the

apparatus in the first trial. The compressed air was routed to

different paths when the circuit switch was turned from one position to

another. For example, turning the knob from position 1 to position 2

parallel
reference
signal
(to indicate the
 switch's position)

history curve
of force
performance
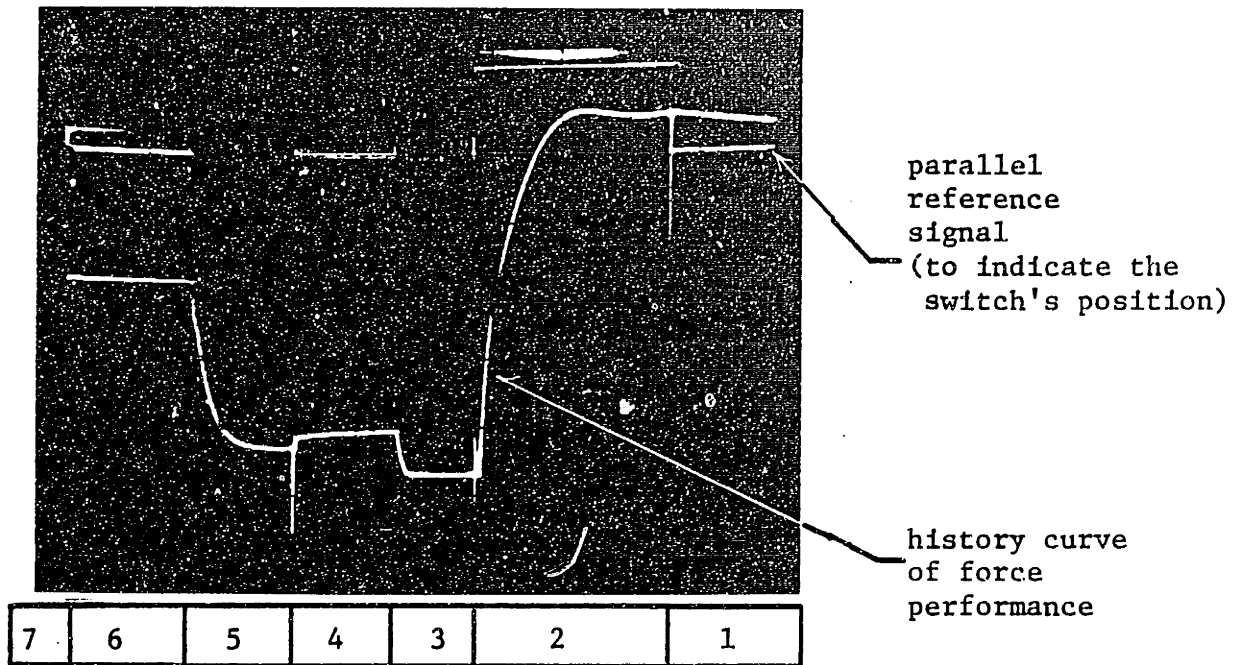
Figure 4-2-1   The Force Performance of Actuator A

Knob Position	Control				Ref. Signal	Notes
7	Preparation Position					ready to go
	Actuator A		Actuator B		Note: E = Energization	
	Sol.	Force	Sol.	Force	DE = De-energization	
6	DE	No	DE	No	0.0v.	hard spring
5	DE	Yes	E	Yes	12.0v.	fail-safe mode
4	DE	No	DE	No	0.0v.	hard spring
3	DE	No	E	Yes	13.0v.	actuator
2	E	Yes	DE	No	6.0v.	actuator
1	DE	No	DE	No	0.0v.	hard spring

Table 4-2-1   The Performance Vs. the Energization Status of
the Valve (from left to right in Figure 4-2-1)

would make actuator A filled and actuator B exhausted according to the controlling laws for solenoid A and solenoid B, which were stated in Table 3-12-1. The force performance curve of actuator A was stored on the oscilloscope screen and was photographed by a Polaroid camera with #667 film as shown in Figure 4.2.1 and Table 4.2.1.

The time intervals between two steps were very limited because the performance curve of actuator A was expected to be displayed on the narrow screen for a total of 6 continuous steps. This Figure was for reference only since time was not allowed for the actuator to reach its steady state. A three-channel chart recorder, i.e. one for actuator A, another for actuator B, and the third for the reference signal, would be needed when detailed response curves were required.

4.3 Testing the Valve Alone

In Figure 4-3-1, the set-up to test the performance of the valve alone is illustrated to show the pressure supply, the pressure gage with its signal conditioner, and the oscilloscope. The line valve (w) in between the FESTO value port B and actuator B is closed so that the pressure on the outlet port B of the FESTO valve can be sensed, and thus have it recorded on the oscilloscope. The FESTO valve was supplied with compressed air of 130 psi, and is energized by the actuating signal of 24 V.D.C., 0.48 A. from the MCC circuit.

(1) <u>Turning on the valve</u> (as shown in Fig. 4-3-2)

pressure supply 130 psi = 6.21 V. D.C.

vertical axis   = 1.0 V./Div.

horizontal axis   = 10 ms./Div.

sensitivity   = 0.048 v./psi

Δv.   = O.V.D.C to 6.42 V.D.C.

Δp = 0.0 V.D.C. to 6.42 V.D.C.

<u>Calculating the valve bandwidth</u>

Since the V(t) will be 95% of the final value of $V(\infty)$, (which is 6.42 V. D.C.), at $T = 3\ \tau$, where τ is the time constant, we can calculate the bandwidth of the valve as follows:

$V(3\tau) = 6.42$ V. x 0.95 = 6.099 V.

                         = 6.099 Vertical Divisions,

      3τ = 43 ms (4.3 horizontal divisions)

        τ = 14.2 ms

     $2\pi f$ = $1/\tau$

        f = 11.12 Hz.

bandwidth, w = 11.12 Hz. = the valve bandwidth of turning it on.

(2) <u>Turning off the valve</u> (as shown in Figure 4-3-3)

pressure supply 130 psi = 6.21 V. D.C.

vertical axis   = 1 V./Div.

horizontal axis   = 20 ms./Div.

sensitivity   = 0.048 v./psi.

Δv = from 6.43 V. D.C. to 0 V. D.C.

Δp = from 130 psi to 0.0 psi

Valve,W closed

Oscilloscope

The Gould Signal Conditioner

pressure transducer
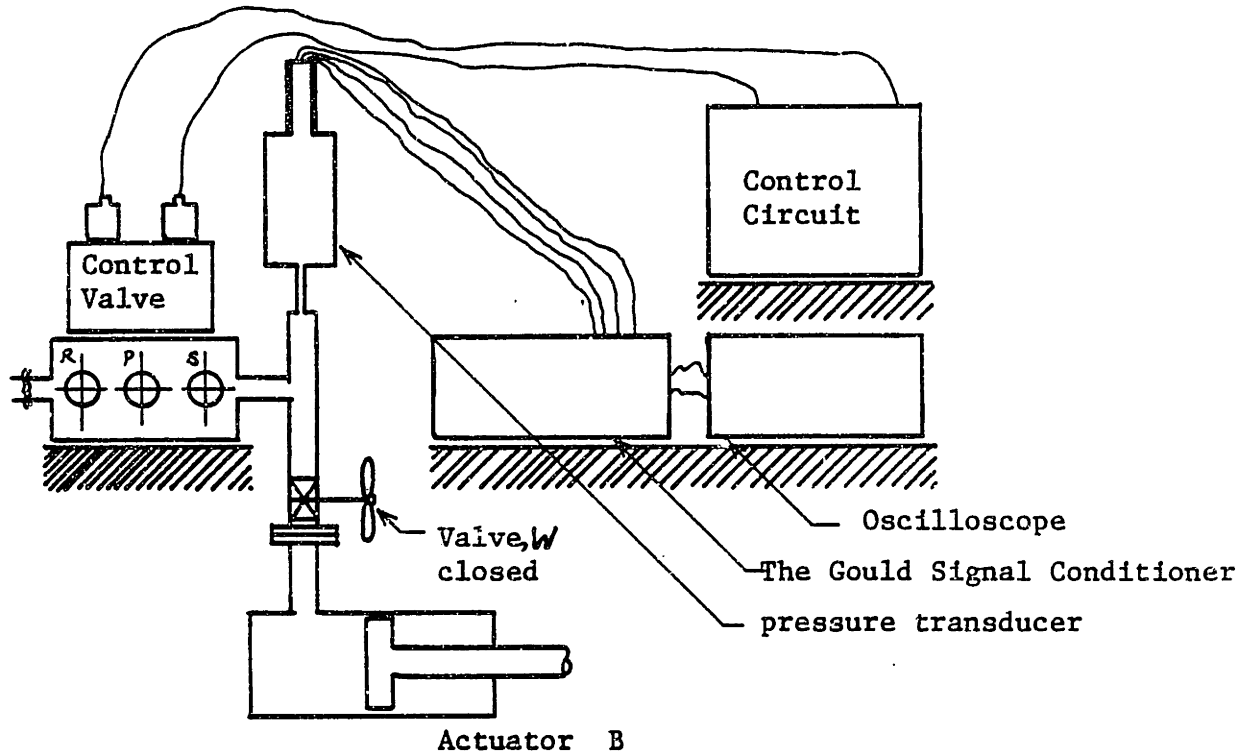
Actuator B

p: pressure supply
R.S.:   exhaust

The valve w, which is between the control valve and the B actuator is closed.

Figure 4-3-1   The Experimental Set-Up for Testing the Performance of the Control Valve Only
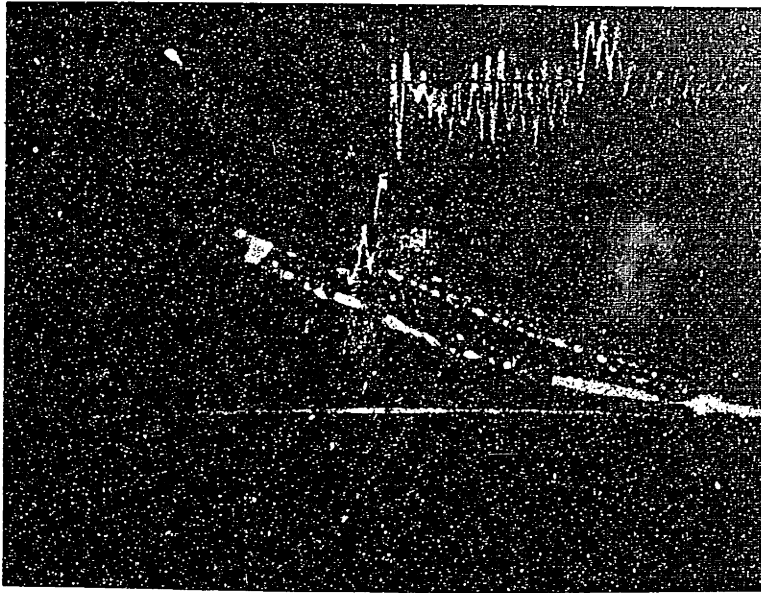
```
supply pressure = 130 psi
V. Axis   = 1 v./div.
H. Axis   = 10 ms./div.
sensitivity = 0.048 v./psi

Δv   = 0.0 v. to 0.42 v.
Δp   = 0.0 psi to 130 psi
```

Figure 4-3-2   The Performance Curve of Control Valve only when it is
Turned On
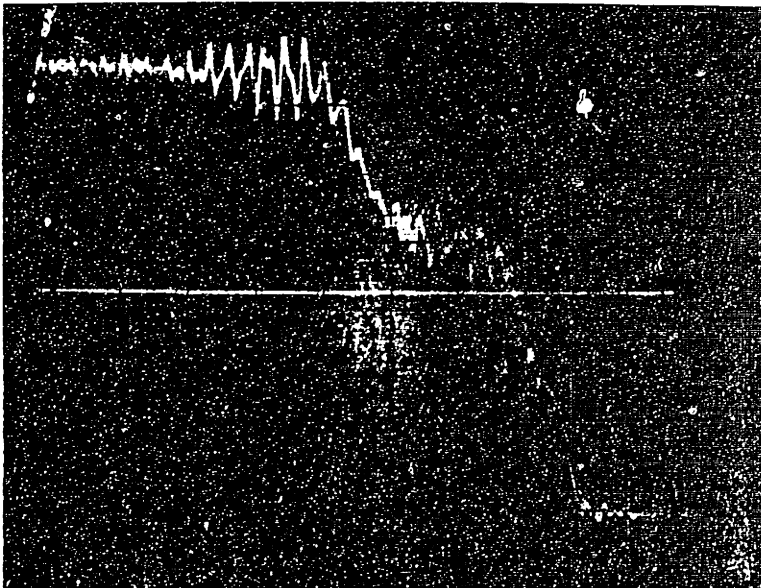

```
supply pressure  = 130 psi
V. Axis   = 1.0 v./div.
H. Axis   = 10 ms./div.
sensitivity  = 0.048 v./psi
Δv   =  6.43 v. to 0.0 v.

Δp   =  130 to 0.0 (psi)
```

Figure 4-3-3   The Performance Curve of Control Valve only when it is
Turned Off

Calculating the valve bandwidth

$V(3\tau)$ = 6.43V. x 0.95 = 6.1085 V.

= 6.11 vertical divisions

3τ = 51 ms (5.1 horizontal divisions)

τ = 17

$2\pi f$ = $1/\tau$

f = 9.36 Hz.

bandwidth, w = 9.36 Hz. = the value bandwidth of turning it off.

4.4 Testing the Actuator (Airspring)

4.4.1 Introduction

An actuator may be tested to find out its response curve to a step input by the following steps:

(1) Turning on the line valve (W) which is mounted between the FESTO valve port B and the actuator B, and then applying the known pressure on the control valve.

(2) Having the carbody and the B bolster locked to the ground at the fixed height by the method explained in section 4.1.

(3) Energizing the solenoid A and B according to the Solenoid Function Table of 3.12.1 to fill the actuator B.

(4) Transducing the force to an electrical signal by the load cell, and recording the transient response curve on the oscilloscope.

(5) Recording the oscillograph by a Polaroid camera with #667 film.

(6) Energizing solenoids A, B according to the Solenoid Function
    Table of 3.12.1 to empty the actuator B.

(7) Calculating the equivalent area A_{eq}.

(8) Adjusting the pressure supply to another desired value, and
    repeating step (1) to step (7) again.

(9) Having the carbody and the B bolster locked to the ground, and
    fixing the actuator to the desired height, then repeating steps (1)
    through (8) again.

4.4.2 Testing the airspring with the valve

Following the procedures described in the previous section, the
open-loop step response of the airspring (FIRESTONE # 25) and the valve
(FESTO 4861 MC-5/4-1/2) was studied by using the experimental apparatus,
i.e. the LASC tester, as shown in Figure 4-4-1. Photographs of the
performance traces were taken and included in the following:

   (1) Figure 4-4-2: Inflating the airspring through the valve from
                      the hard spring mode to the full force output
                      mode.

   (2) Figure 4-4-3: Deflating the airspring through the valve from
                      the full force output mode to the fail-safe
                      mode.
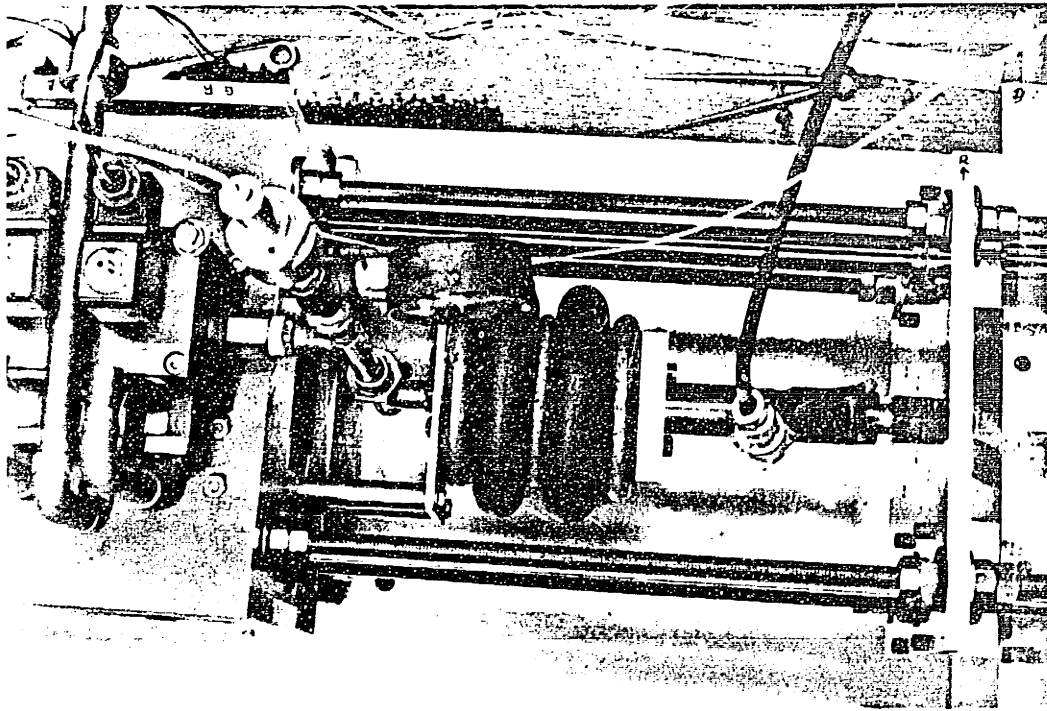
(a)   Top View
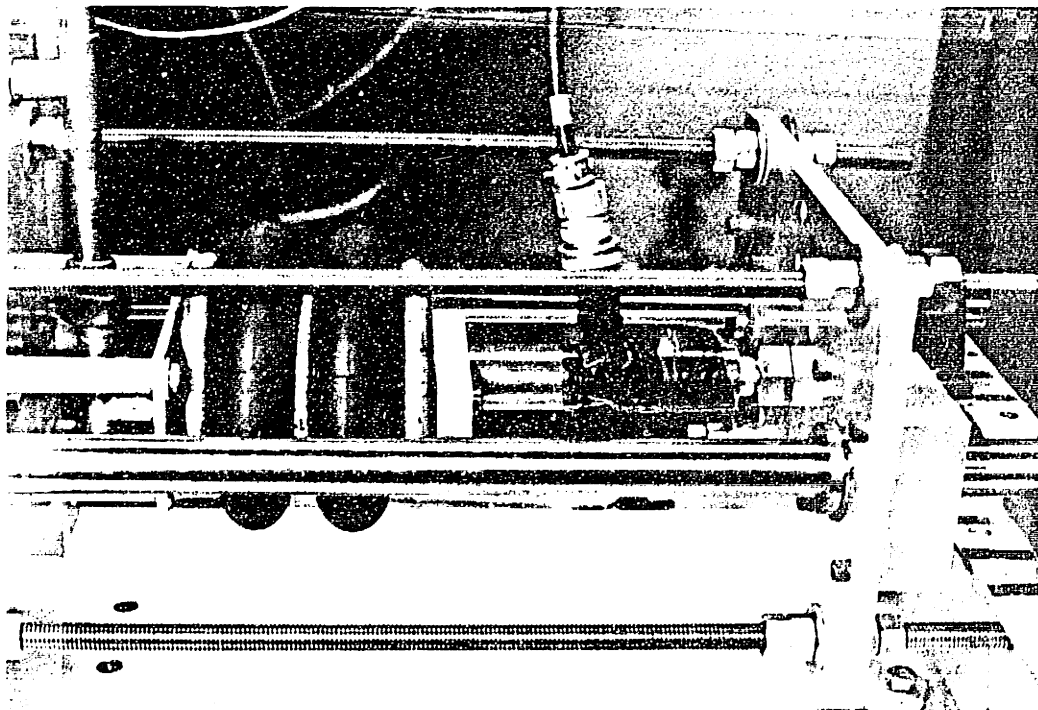
(b)   Front View

Figure 4-4-1   Testing of the FIRESTONE Ⓡ Airspring with the
FESTO Valve

- 164 -
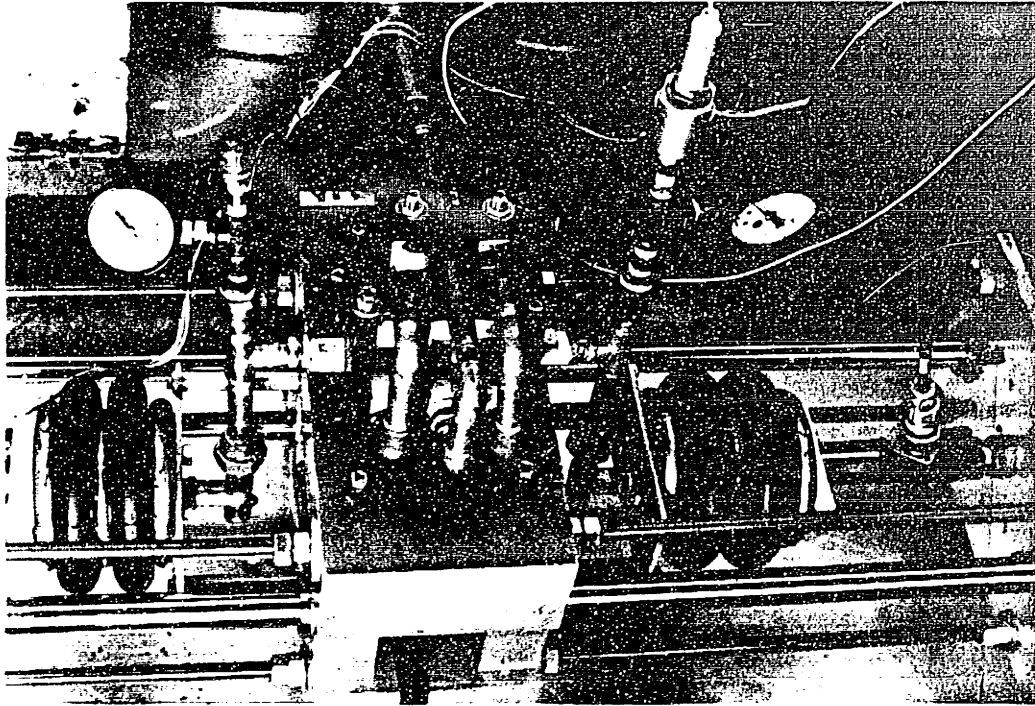
(c) Top View (The Two Opposing Airsprings Can Be Seen)
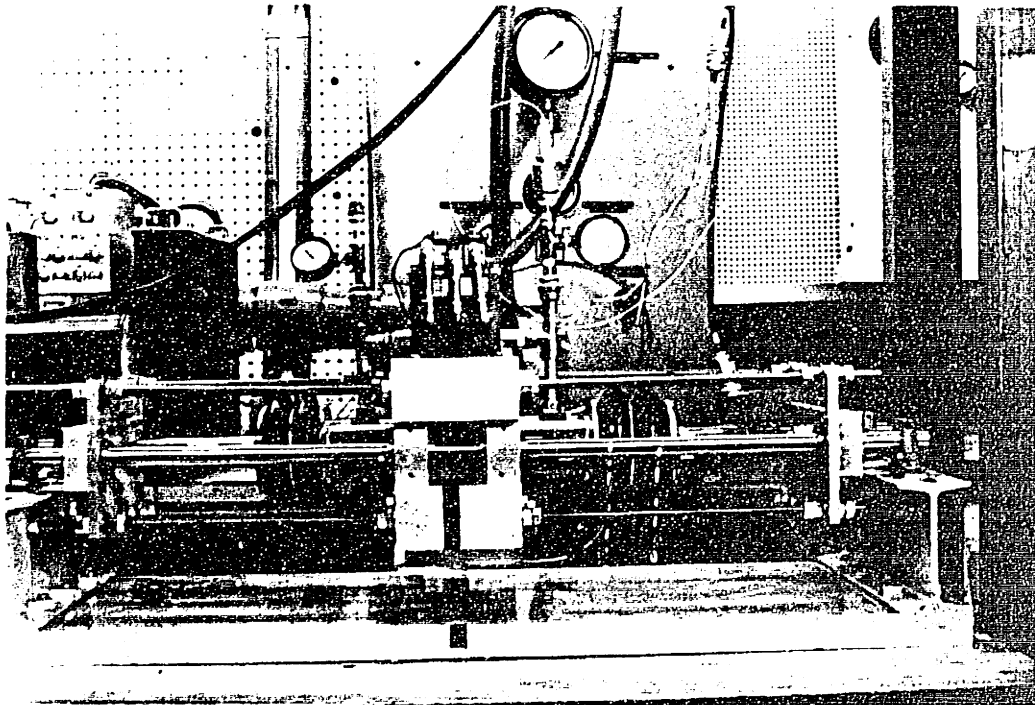
(d) Front View (The Two Opposing Airsprings Can Be Seen)

Figure 4-4-1 Testing the FIRESTONE ® Airspring with the FESTO Valve
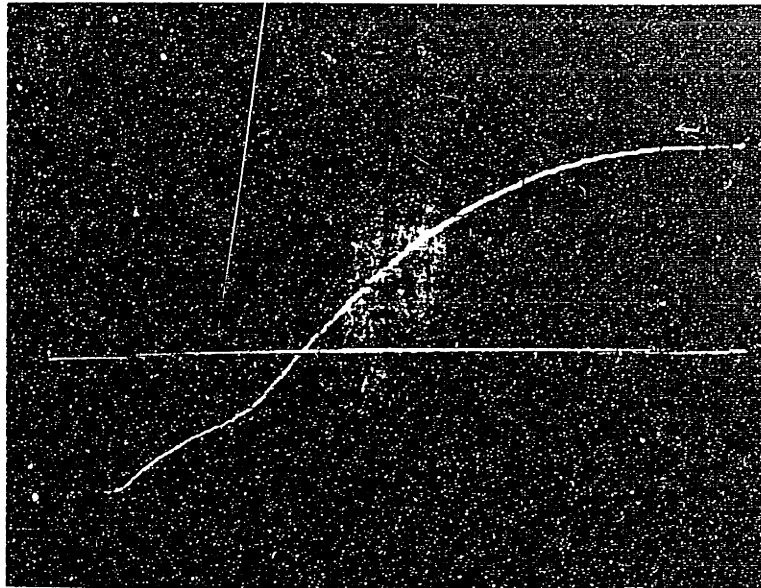
t_{A1} = 21 ms.

t_B = 22 ms.

at 3" height
V. Axis = 0.4 v./div.
H. Axis = 20 ms./div.

Figure 4-4-2   Inflating the Airspring through the Valve from the Hard
Spring Mode to the Full Force Output Mode
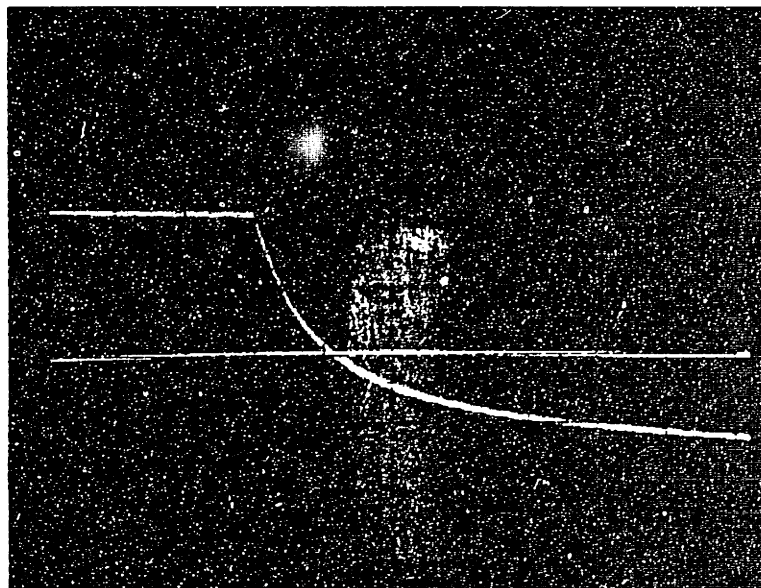
at 3" height
V. Axis   = 0.5 v./div.
H. Axis   = 50 ms./div.

t_{A2} = 150 ms.

Figure 4-4-3   Deflating the Airspring through the Valve from the
Full Force Output Mode to the Fail-Safe Mode

$F_{s.s.}$

95% ΔF ΔF

$F(0)$

$\Delta F = 0$ to $1,96$ lb_f

t_A t_B 3τ

pressure supply = 127 psi
at 5" height
V. Axis = .5 V./div.
H. Axis = 50 ms./div.
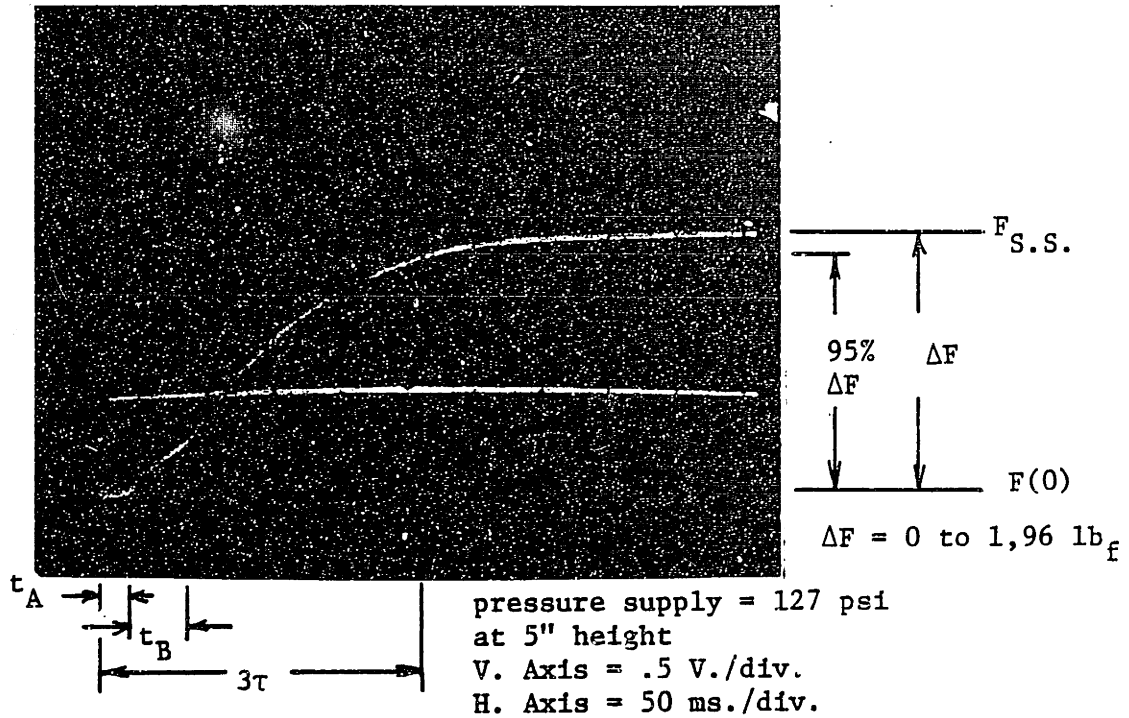
Figure 4-4-4 Filling of the FIRESTONE Airspring through the
FESTO Valve
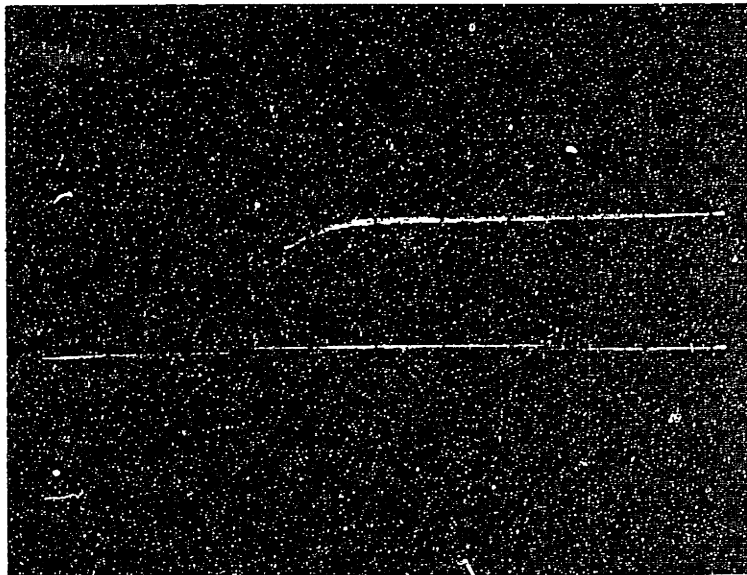
Figure 4-4-8* Filling of the FIRESTONE Airspring through the FESTO Valve

*The Figure number is not continuous here: Figures A-4-4-5 and A-4-4-6 are
included in Appendix A, and Figure 4-4-7 is included in a later part of
this section for convenience.

The airspring with the valve assembly is a cascaded system of two first-order systems as shown in the above figures. Since an airspring alone (without a control valve) can not function as an actuator independently, the bandwidth discussed below is based on the cascaded performance. The bandwidth for the actuator alone is higher than the bandwidth of the assembly because the actuating time for the solenoid valve is not included in the calculation for the actuator only . The time constant, τ, for the first order system and is defined as $f(t)$ and is within 5% (i.e. the value of e^{-3}) of the steady state value as defined by Ogata in [36].

Part (I). <u>Fill the airspring which is fixed at 5" height.</u>

    (1) General information (as shown in Figure 4.4.4):

          pressure supply   = 127 psi

          vertical axis   = 0.5 V./div.

          horizontal axis   = 50 ms./div.

          sensitivity   = 1 mv./lb_f

          Δv = 0.0 V.D.C. to 1.863 V.D.C.

          ΔF = 0.0 lb_f to 1,863 lb_f (1)

    (2) Calculating the bandwidth, w

          $F_{s.s.}$ = 1,863 lb_f

          $F(3\tau)$ = 95% of $F_{s.s.}$ = 1,769 lb_f

          $V(3\tau)$ = 1.769 V.D.C. = 3.54 divisions

Corresponds to = 4.8 horizontal divisions

$$4.8 \text{ div.} \quad = 240 \text{ ms.} = 3\tau$$

$$\tau \quad = 80 \text{ ms.} \tag{2}$$

$$f \quad = 1/2\pi\tau = 1/2\pi 80 = 1.99 \text{ Hz.}$$

$$\text{bandwidth, } w \quad = 1.99 \tag{3}$$

(3) Calculating the equivalent area and diameter

$$A_{eq} = \frac{F}{P} = \frac{1,863}{127 + 14.7} = 13.2 \text{ in}^2 \tag{4}$$

$$D_{eq} = \sqrt{\frac{4A}{\pi}} = 4.09 \text{ in.} \tag{5}$$

(4) Repeating the above procedures while regulating the supply pressure at different values such as 55 psi, 75 psi, 95 psi, and 120 psi, and calculating the ΔF, τ, w, A_{eq}, D_{eq} respectively.

Some of the photographs taken at this stage are shown in Figures A.4.4.5 and A.4.4.6.* Table 4.4.1 and Figure 4.4.7 show the results.

(5) Repeating the above processes while switching the control valve to different positions such as from the hard-spring mode to the fail-safe mode.

---

*

The figures whose numbers are initialized with A are included in Appendix A.

Part (II). <u>Fill the airspring which is fixed at 4" height.</u>

    (1) General information (as shown in Figure 4.4.8):

           pressure supply   = 123 psi

           vertical axis   = 0.5 V./div.

           horizontal axis   = 50 ms./div.

           sensitivity   = 1 mv./lb_f

           ΔF = 0.0 lb_f to 1,960 lb_f (1)

    (2) Calculating the bandwidth, w,

           $F_{s.s.}$ = 1,960 lb_f

           $F(3\tau)$ = 95% of $F_{s.s.}$ = 1,866 lb_f

           τ = 63.3 ms.   (2)

           f   = $1/2\pi\tau$ = 2.51 Hz

           bandwidth, w   = 2.51 Hz   (3)

    (3) Calculating the equivalent area A_{eq}, and equivalent diameter, D_{eq}

$$A_{eq} = \frac{1,960}{123 + 14.7} = 14.2 \text{ in}^2 \tag{4}$$

$$D_{eq} = \sqrt{\frac{4A}{\pi}} = 4.25 \text{ in.} \tag{6}$$

    (4) Similarly, repeat the procedures (4) and (6) of Part (I).

Supply Pressure psig	Steady State Force $f(\infty)$, lb_f	τ sec.	Bandwidth, ω Hz	Equivalent Area, A_{eq} in^2	Figure No.	Unit/Div. Vertical V.D.C.	Unit/Div. Horizontal ms.
127	1,863	80	1.99	13.2	4-4-1	0.5	50
120	1,821	76.7	2.07	13.5	A-4-4-5	0.5	50
95	1,370	49	2.78	12.5	A-4-4-6	0.2	20
75	1,087	46	2.96	12.1	*	*	*
55	788	41.3	3.19	11.3	*	*	*

* Not Included

Table 4-4-1   Results of Testing the FIRESTONE Ⓡ #25 Airspring Through the FESTO Valve at Different Supply Pressures

- 171 -
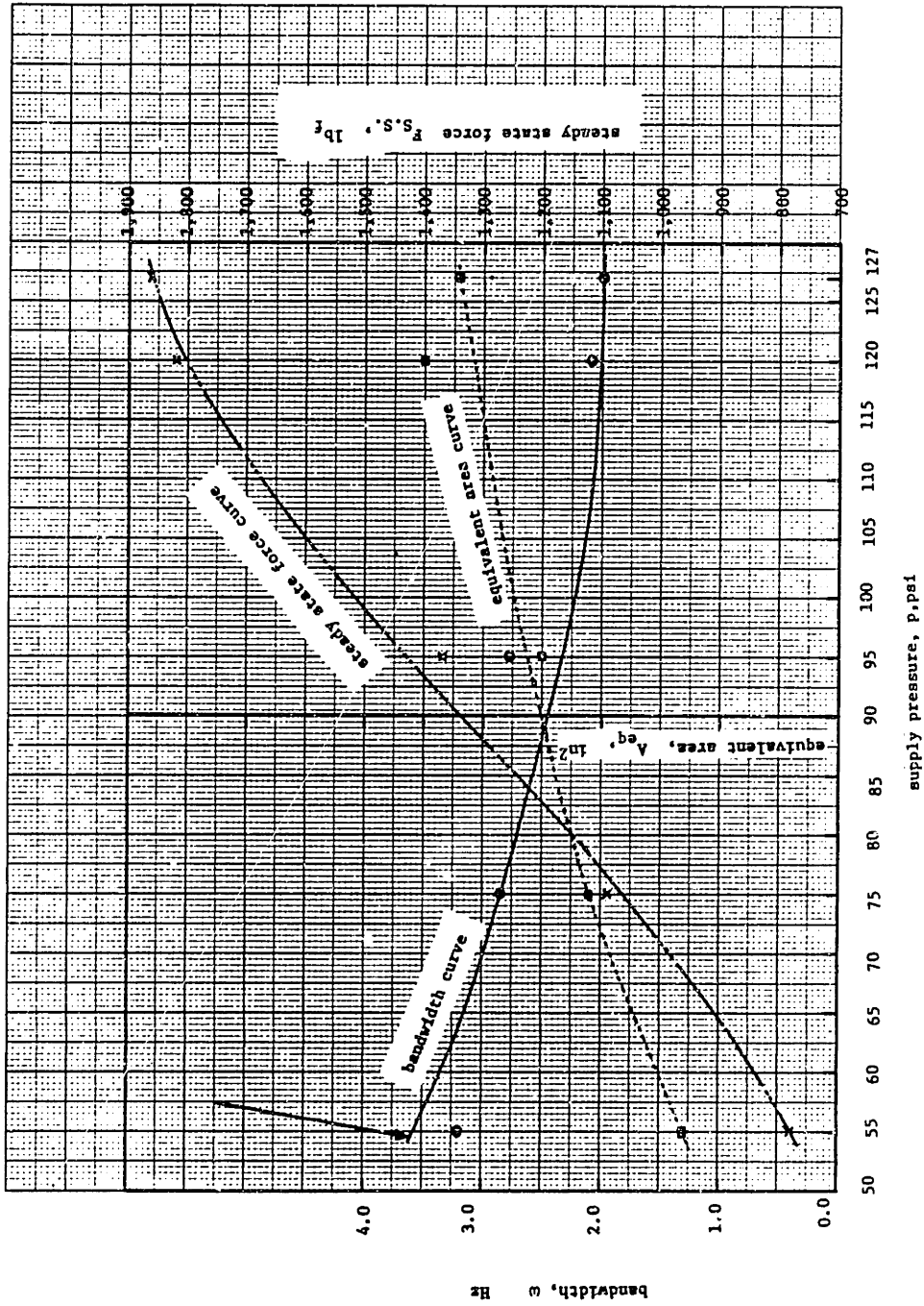
Figure 4-4-7   Results of Testing the Airspring at 5" Operating Height
   O = bandwidth
   X = steady state force
   □ = equivalent area

Part (III). **Fill the airspring which is fixed at 3" height.**

(1) General information (as shown in Figure 4.4.8):

pressure supply = 123 psi

vertical axis = 0.5V./div.

horizontal axis = 50 ms./div.

sensitivity = 1 mv./lb_f

Δ_F = 0.0 lb_f to 2,430 lb_f (1)

(2) Calculating the bandwidth, w

$F_{s.s.}$ = 2,430 lb_f

$F(3\tau)$ = 95% of $F_{s.s.}$ = 2,308

τ = 50 ms. (2)

f = $1/2\pi\tau$ = 3.18 Hz

bandwidth, w = 3.18 Hz (3)

(3) Calculating the equivalent area and equivalent diameter

$$A_{eg} = \frac{2,430}{123 + 14.7} = 17.6 \text{ in.}$$ (4)

D_{eq} = 4.73 in. (5)

Part (IV). Discussions on the air leakage problem of the valve.

The valve used in this project (FESTO 4861 MC-5/4 -1/2) is a high quality valve; however, air leakage still exists in FESTO valves. In Figure 4.4.2, the performance curve of the valve with the airspring was divided into three time intervals, t_{A1}, t_B, and t_C, where

t_{A1} = the actuating time needed by the solenoid valve

    = 20 ms.

t_B = the first stage of inflating air into the actuator, where air leakage exists

    = 38 ms.

t_C = the second stage of inflating air into the actuator, where no air leakage exists.

The rate of filling the actuator in the second stage is about 1.7 times faster than that of the first stage since no air leakage existed in the second stage. Air leakage phenomena were further proved by observing the pressure force out of the leakage ports.

The actuating time needed to turn the valve on is different from that needed to turn the valve off. It takes about 22 ms. to turn the valve on and 28 ms. to turn the valve off. However, actuating time of the valve from the full force mode to the fail-safe mode may take as much as 150 ms. as shown in Figures 4.4.2 and 4.4.3, where

t_{A1} = turning the valve on, 22 ms.

t_{A2} = turning the valve from the full force mode to the fail-safe mode, 150 ms.

PART (V). <u>Computer Simulation</u>.

Three original FORTRAN code computer programs, VALVE.FOR, STROKE.FOR, and AIRMASS.FOR were developed by Buzan [23] to simulate the lateral active suspension control system by using the software DYSYS [37] at the Joint Computer Facility Center at MIT. A fourth order Runge-Kutta routine was used in DYSYS to perform the numerical integration of the differential equation (linear or nonlinear). One of the advantages of using DYSYS software is that much supporting software has already been developed to make DYSYS more useful and powerful. The Buzan's original programs were slightly modified by Cho and De Los Reyes to suit their own purposes. Three programs (STEP, RANDRESP, and SYS) are included in Appendices D, E and F respectively. More software is expected to be developed for optimal control and adaptive control for non-linear suspension problems.

PART (VI). <u>Conclusion</u>.

From the test results shown in Figure 4.4.10 and Table 4.4.2, the following conclusions can be made:

(1) The steady state force, $F_{s.s.}$ increases with the increment of the supply pressure because the constitutive law of force is that:

$$F = (P_{applied})(A_{applied})$$

(2) The equivalent area, A_{eq}, of the airspring increases with the decreasing of the operating height of the airspring. Since the sidewall of the airspring is flexible, the decrement of the operating height would automatically push the equivalent area to a bigger value.
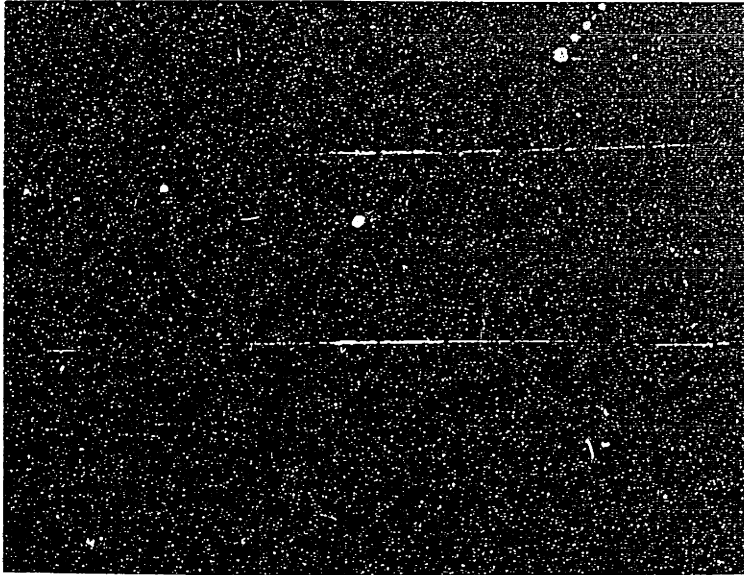
at 3" height

v. axis = 0.5 v./div

H. axis = 50 ms/div

sensitivity = 1 mv./lbf

ΔF = 2,430 lbf

Figure 4-4-9 Filling of the FIRESTONE Airspring through the
FESTO valve

Operating Height of the Air Spring in.	Corresponding Bandwidth Hz.	Equivalent Area in^2	Supply Pressure (at 125 ±2 psi)
5.0	1.989	13.2	123
4.0	2.51	14.2	123
3.0	3.18	17.6	123

Table 4-4-2   The Results of Testing FIRESTONE #25 ® Airspring at Different Operating Heights
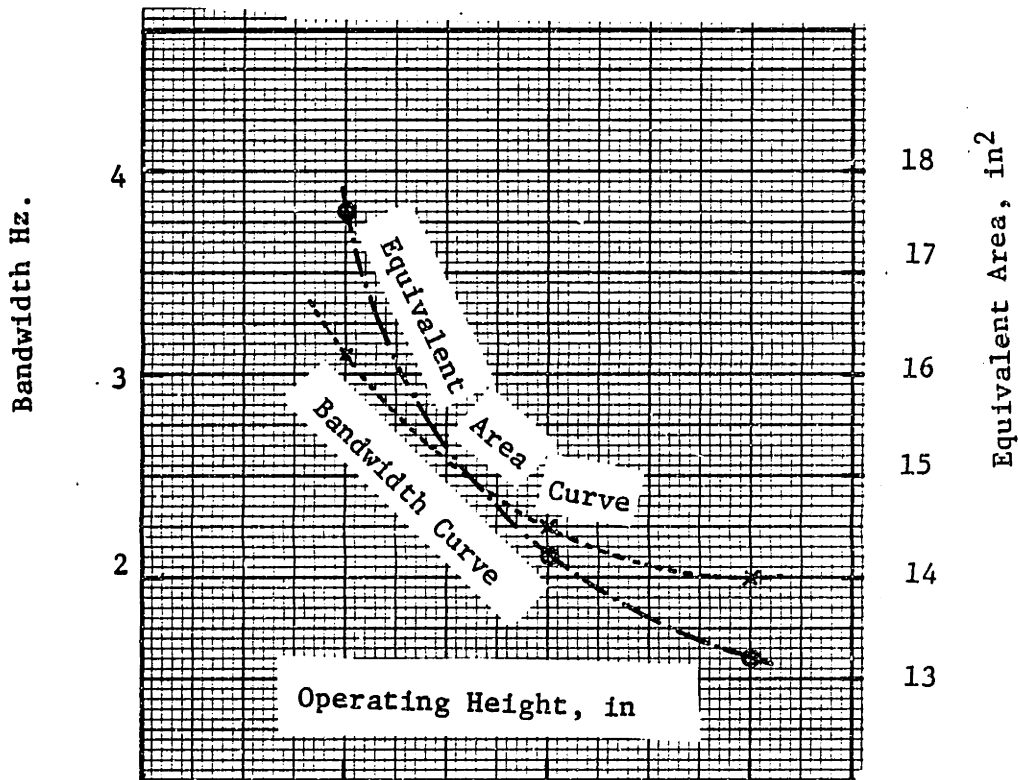
Figure 4-4-10   The Results of Testing Airspring at Different Heights (Refer to Table 4-4-2)

actuator height H,inch	magni-tude p, psig	experimental bandwidth w Hz.	theoretical bandwidth w (simulation)	0/0 deviation from theoreti-cal value
3"	0 to 125	3.18 *	** 3.30 to3.96	*** 3.6%to19%

* This value was calculated previously in this section

** lower bound corresponds to isothermal process and upper bound to adiabatic process

***small deviation from the value of simulation resul-ted

Table   4.4.3 Theoretical and Experimental bandwidth of the FIRESTONE # 25 airspring

(3) The bandwidth, w, of the airspring is reduced when the

operating height is increased. This is due to the following

reasons:

(a) The dead volume inside the airspring is reduced when it

is squeezed to a shorter operating height.

(b) The mechanical capacitance of the airspring is increased

when it is enlarged to a higher operating height.

(4) Table 4.4.3 shows the experimental and theoretical bandwidth

of the FIRESTONE® #25 airspring. It is found that the

theoretical results agreed well with the experimental

discovery.

4.5 Testing Cylindrical Actuators

As discussed in Section 3.13, the LASC tester has significant

flexibilities of testing different actuators. Figure 4.5.1 shows the

experimental set-up for testing the PARKER cylinder with the FESTO 4861

MC-5/4 -1/2 valve at different supply pressures and different heights.

The procedures presented in Section 4.1 were the guidelines for testing.

The equations for calculating the bandwidths and time constants of the

actuators, which were used in the previous section.

It is important to note that the valve air leakage problem still

existed in testing the cylindrical actuator. The air leakage problem

had nothing to do with the actuator; it is a problem which comes with

the valve. Figure 4.5.2 shows the air leakage phenomena while turning

the valve on/off. The leakage of the air slows down the rate of force

generated by the tester, the experimental and theoretical bandwidth of
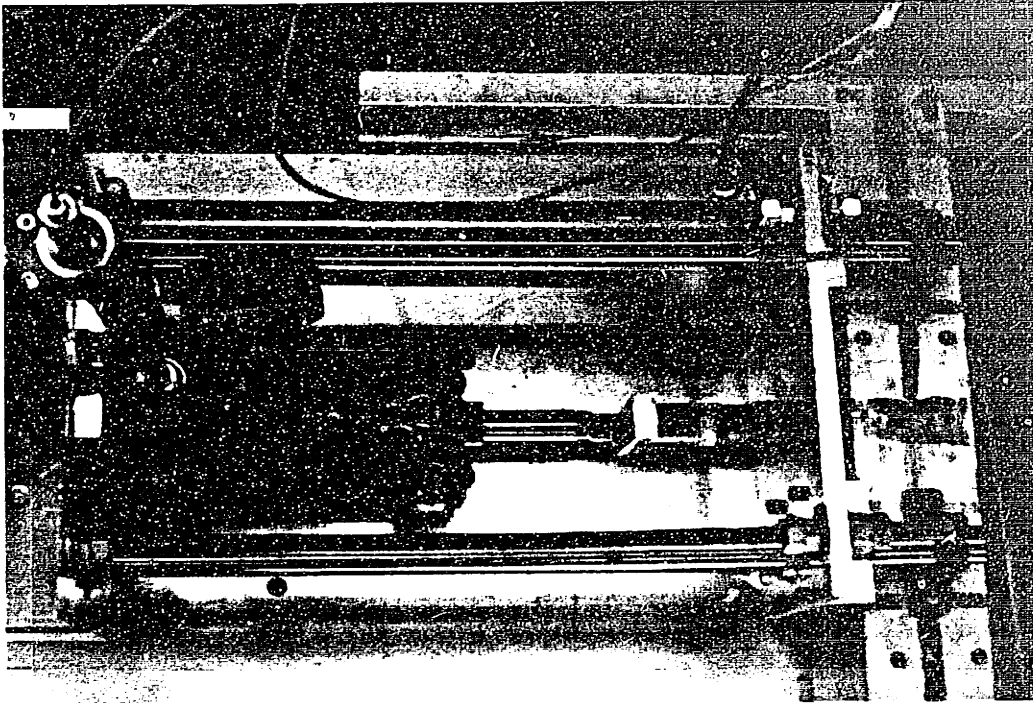
(a) Top View
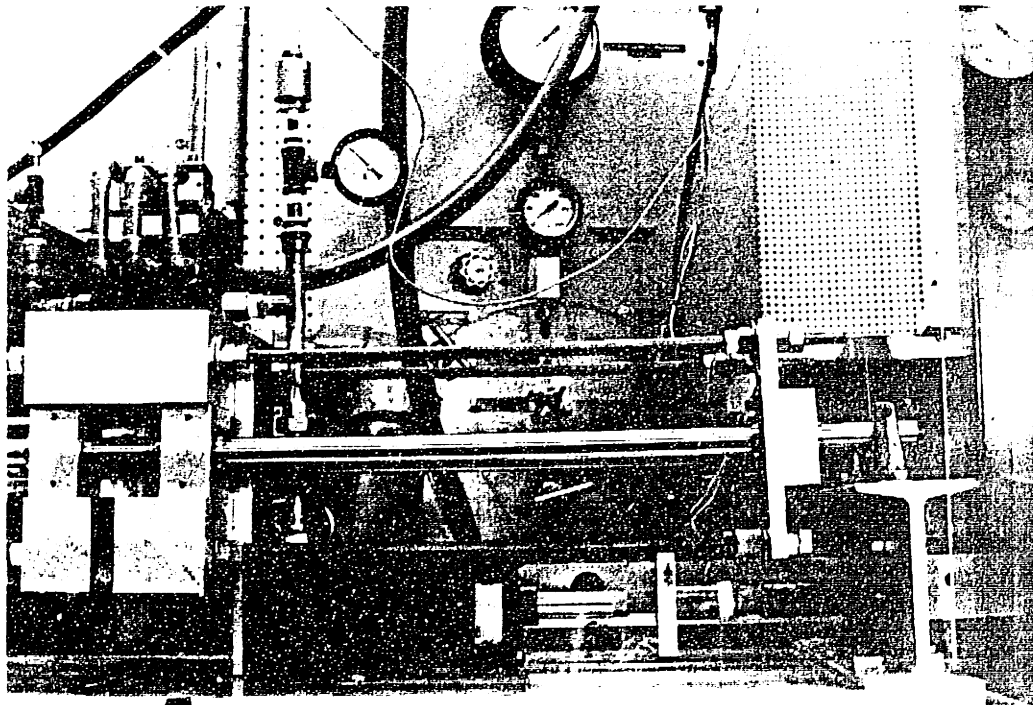
(b) Front

Figure 4-5-1   Testing the PARKER Cylinder with the FESTO 4861 valve
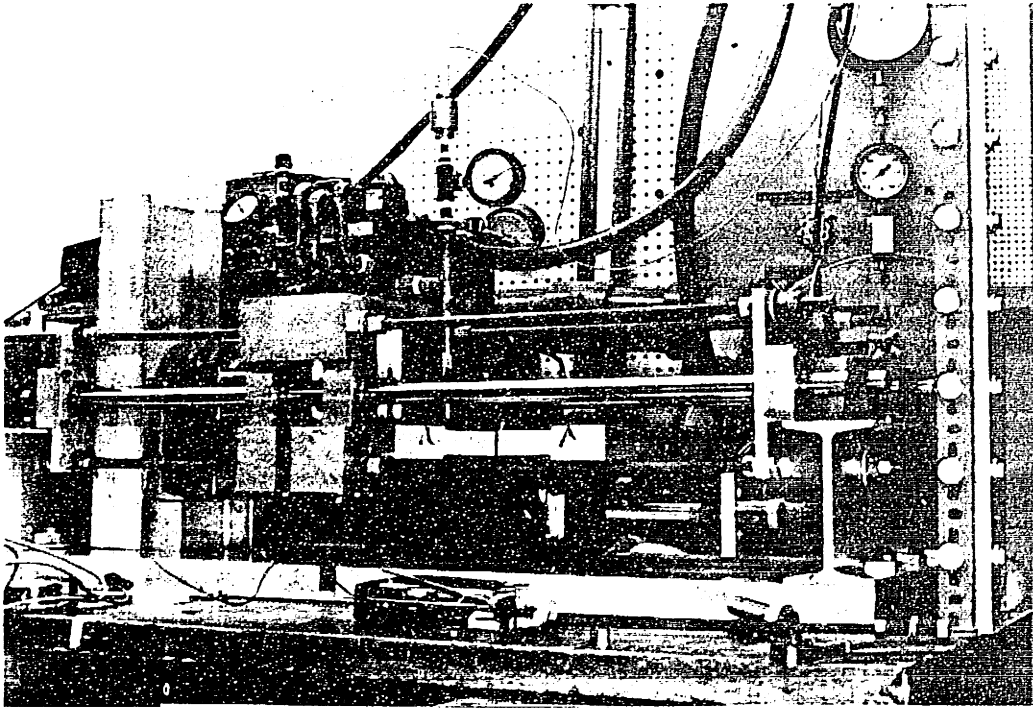
(c) Side-View from an Angle of 45°
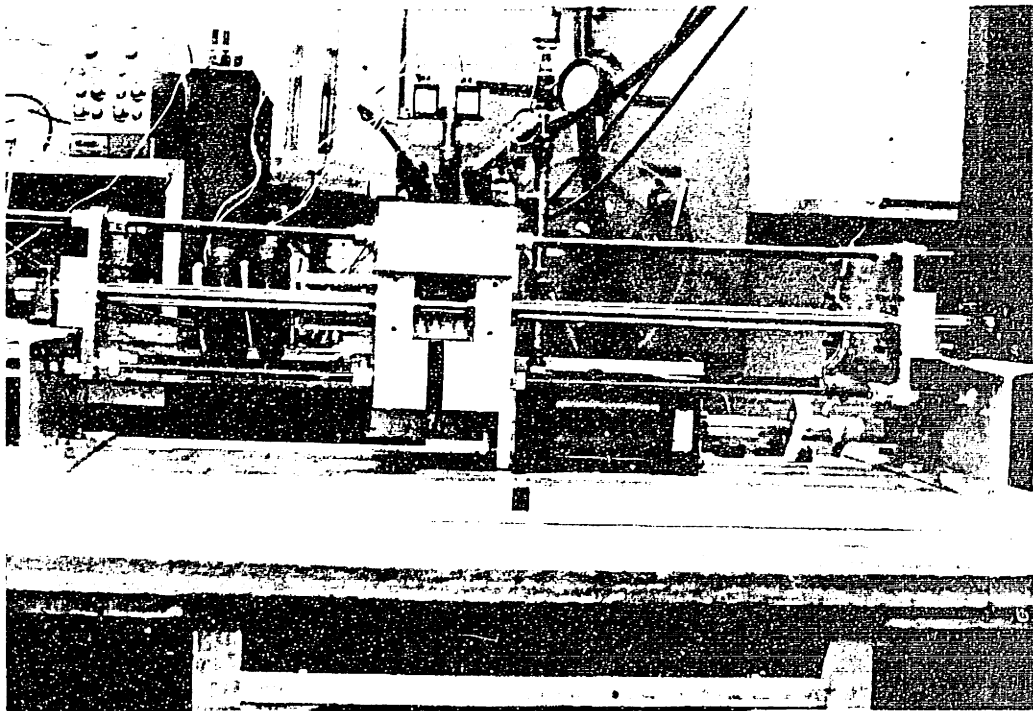
(d) Front View (Two different actuators are shown in this picture)

Figure 4-5-1 Testing the PARKER Cylinder with the FESTO Valve.

Actuator Height (Inch)	Step Size (psig)	Experimental Bandwidth (Hz)	Theoretical Bandwidth* (Hz)	% Deviation
1.16	0 → 75	8.09	7.59 - 8.18	√
1.16	0 → 125	7.34	7.38 - 7.85	0.5%
1.56	0 → 75	7.23	6.70 - 7.27	√
1.56	0 → 125	6.82	6.49 - 6.94	√
2.06	0 → 75	6.82	5.87 - 6.42	-0.6%
2.06	0 → 125	6.08	5.67 - 6.10	√
2.50	0 → 75	6.12	5.30 - 5.82	-4.9%
2.50	0 → 125	5.82	5.10 - 5.52	-5.2%
2.97	0 → 75	5.31	4.79 - 5.29	-0.4%
2.97	0 → 125	4.22	4.61 - 5.00	9.2%
3.50	0 → 75	4.77	4.32 - 4.80	√
3.50	0 → 125	4.19	4.16 - 4.53	√

*lower and upper bounds of theoretical bandwidth correspond to isothermal and adiabatic assumptions

√ indicates that experimental bandwidth lies within theoretical bounds.

Table 4-5-1   Experimental and Theoretical Bandwidth of the PARKER HMA 14, 4" Bore Cylinder [27]
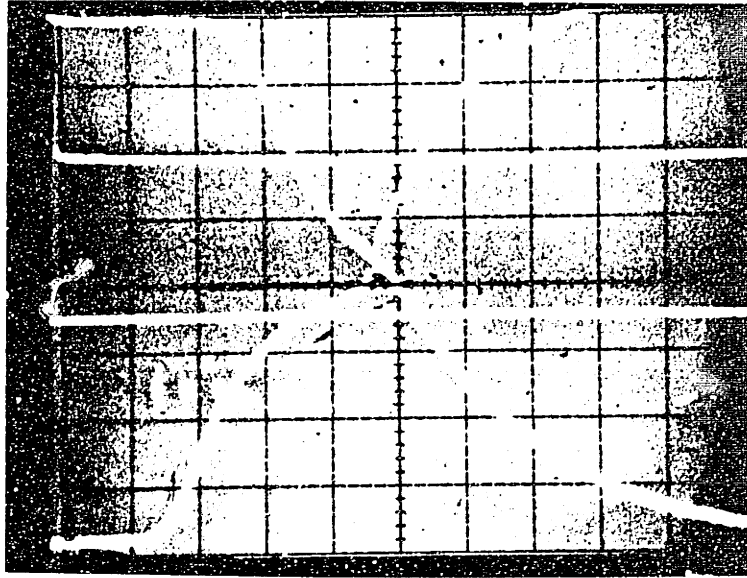
Figure 4.5.2   The Valve Air Leakage
Problem in Testing the
PARKER cylinder

the PARKER FMA 14, 4" bore cylinder were prepared by Cho in [27] as shown in Table 4.5.1. The open loop step response was experimentally studied at six different actuator heights for two different supply pressures. It was found that:

(1) The bandwidth of using a smaller supply pressure, 75 psi, is always larger than that of using a higher supply presure, 125 psi.

(2) Under the same following conditions

   (a) the supply air is at 124 $\pm$ 1 psi

   (b) the actuator height is set at 2.98 $\pm$ 0.02 in.

   it is noted that the bandwidth of the cylinder is R times larger, than that of the airspring where R = 4.22/3.18 = 1.33, after comparing the results of Table 4.5.1 and Table 4.4.1. This is because the capacitance of the airspring is considerably greater than that of the cylinder due to the mechanical capacitance term which comes from the flexible (elastic) side wall of the airspring.

(3) The theoretical bandwidth of the PARKER cylinder with FESTO valve agrees with its computer simulation very well.

4.6 Testing the Actuator/Valve with the PWM Control Circuit

As discussed in Section 2.3.7, there were two control circuits, the PWM control circuit and the BBLC control circuit, to drive the solenoid on/off valve. The FIRESTONE® #25 airspring with the FESTO 4861-MC - 5/4 - 1/2 valve was further tested by using a PWM circuit made by De Los

Reyes [28].

<u>Static Testing:</u> open loop response of the system to a step input.

(1) Have the truck and carbody grounded by the method mentioned in Section 4.3.

(2) Set the pressure regulator at 125 psi of supply pressure.

(3) Fix the airspring at 3" operating height.

(4) Input an error signal, which was generated by a D.C. power supply, to the 3rd pin of the PWM chip.

(5) Connect the solenoid coil (valve) to the power transistor switch of the PWM control circuit.

(6) From the load cell, obtain the actual actuator force, F_A.

(7) Use the PWM control circuit to turn the valve on by making the voltage at the collector of the power transistor as low as zero volts, and calculate the actuating time, t_{A1}, and the time constant of the control system.

(8) Use the PWM control circuit to turn the valve off by making the voltage at the collector of the power transistor higher than 24 V.D.C., and calculate the actuating time, T_{A1}, and the time constant of the control system.

<u>Dynamic Testing:</u> closed loop response of the system to a sinusoidal random input.

(9) Input the sinusoidal input of the desired forces, F_{AD}, to the zero summer.

(10) The signal outputs from two separate load cells were summed at the inverting summer.

Conclusion: In static testing,

(1) Both of the actuating times of turning valve on, t_{A1}, and that of turning valve off, t_{A3}, are about the same value (or a little less than) the values stated on the FESTO catalog. The value of T_{A1} is 18 ms. and that of t_{A3} is 24 ms. as shown in Figure B1 and B2 in Appendix B.

(2) Commands to turn on/off the valve should last longer than 18 ms./24 ms. to be effective, otherwise the commands can not work.

(3) The time delay of the control system response to the PWM control circuit is composed of several time intervals, as shown in Figure B.3, which significantly slows down the system response.

(4) A large phase difference between the desired force, F_{AD}, and the actual actuator force, F_A, results even at desired force frequencies of 1 Hz and 2 Hz.

(5) In order to make the valve oscillate at 10 Hz, it is necessary to oscillate the PWM modulator at a frequency of 1000 to 5000 Hz. This phenomena was explained by De Los Reyes [28].

(6) The system of the actuator/valve driven by the PWM control circuit does not perform at an acceptable level in closed loop requirement.

4.7 Testing the Actuator/Valve with the BBLC Control Circuit

A PARKER HMA 14, 4" bore cylinder with the 4-FESTO-MX-2 - 1/4 valve set was further tested by using the BBLC control circuit made by Barletta [29]. The procedures are stated as follows:

Static Testing: open loop response of the system to a step input.

(1) Set the pressure regulator at 120 psi of supply pressure.

(2) Fix the actuator at 4" operating height.

(3) Check the actuating time, $t_{A1,c}$, to turn the valve on from the catalog. $t_{A1,c}$ is 34 ms.

(4) Check the actuating time, $t_{A3,c}$, to turn the valve off from the catalog. $t_{A3,c}$ is 26ms.

(5) Using a signal generator (not from equation of 2.3.7), obtain the desired force, F_{AD}

(6) From the load cell, obtain the actual actuator force, F_A.

(7) Use the BBLC control circuit to turn the valve on and calculate the experimental actuating time, $t_{A1,E}$, and the time constant of the system, τ, of turning on the valve.

(8) Use the BBLC control circuit to turn the valve off and calculate the experimental actuating time, $t_{A3,E}$, and the time constant of the system, τ, of turning off the valve.

<u>Testing at Different Pressures</u>:

    (9)   Set the pressure regulator at 100 psi (and later 80 psi), and repeat procedures (2) through (8).

<u>Dynamic Testing</u>:

    (10)   Generate a sinusoidal signal at a fixed frequency (which ranges from 0.1 Hz to 5 Hz).

    (11)   Repeat procedures from (1) to (9).

<u>Comparing the Results</u>:

    (12)   Compare the experimental results to that from the computer simulation.

<u>Conclusion</u>:

    (1)   The experimental actuating time of turning on the valve is almost the same as that on the catalog. However, this is not true for the case of turning off the valve.

    Results: $t_{A1,C} = 34$ ms. $> t_{A1,E} = 22$ ms.

                 $t_{A3,C} = 26$ ms. $< t_{A1,E} = 60$ ms.

                 $t_{A1,E} = 2.3 \times t_{A1,C}$

    (2)   The valve air leakage problem still exists in this valve, the 4-FESTO-MX -2 - 1/4 valve set. The attenuation of the performance curve at high frequencies is larger than that of expectation.

(3)   Due to the assumption that the inflating process of one actuator can be helped by the other, the response time of the control system is expected to be faster when two actuators are implemented.

(4)   For low frequencies from 0.1 to 1.0 Hz, the simulation represents the real controller very well. However, discrepancy becomes more significant when increasing the frequency. The real controller has a significant phase lag when the frequency is above the level of 3 Hz. Instability may result when operating the BBLC control circuit beyond this value of 3 Hz; hence, a low pass filter should be implemented.

4.8   Evaluation of Results of Computer Simulation

Selecting the right kind of actuators, valves, and control circuits to meset the requirements specified by the lateral active suspension controller was not easy. The active suspension must be able to provide a sufficient improvement in acceleration below two Hz. because a human being is most sensitive to low frequencies as shown in Figure 1-2-4. Five indices were used as guidelines for selection. They are the bandwidth, w, the r.m.s. value of acceleration, the r.m.s. value of stroke travelled, the average flow rate per truck, and the horsepower required per car. In the previous sections of this chapter, experimental results were obtained and compared with theoretical values. Since the experimental results up to this stage can not provide all the index values of interest to make the selection of controller components, the results of computer simulation were used in this section to further investigate the problem of components selection.

Cho [27] and Barletta [29] used their computer program to simulate the performances of various actuators and valves. The results of the computer simulation to select the actuator and the valve to meet the performance requirements specified were discussed here (as shown in Table 4.8.1).

bandwidth, w	3-5 Hz	Actuators with a bandwidth as low as 3 Hz. was acceptable
nominal force	1,000 lb$_f$	This is the r.m.s. value calculated
peak force required, F_{peak}	3,000 lb$_f$	The peak force was defined as 3 times the nominal force. However, 1.6 times the nominal force was acceptable.
stroke	$\pm$ 1.5"	It had 3 inches of stroke in total.

Table 4-8-1   Specification List of the Desired Valve

The trade-off problem (of the actuator's performance capability/ compressor power required) was examined carefully in Table 4-8-2.   The actuators simulated are listed as follows:

(1)   FIRESTONE® #224 airspring

(2)   FIRESTONE® #25 airspring

(3)   FIRESTONE® #25M airspring which is modified with adding a plastic insert inside the FIRESTONE® #25 airspring

(4)   PARKER 5" bore cylinder

(5)   PARKER HMA 14 4" bore cylinder

(6)   PARKER 3" bore cylinder

Five kinds of valves are simulated and listed in the following:

(1) FESTO MC-5/4-1/2 valve with peak flow rate of 195 SCFM at

supply pressure of 130 psi (NOTE: SCFM stands for Standard

Cubic Feet per Minute);
  orifice area A_o = 0.175 in^2

  discharge coefficient C_d = 0.41

  peak flow rate = 195 SCFM at 130 psi

(2) FESTO valve with peak flow rate of 80 SCFM at supply pressure

of 130 psi.

(3) FESTO valve with peak flow rate of 40 SCFM at supply pressure

of 130 psi.

(4) FESTO valve with peak flow rate of 20 SCFM at supply pressure

of 130 psi.

(5) The 4-FESTO – MX – 2 – 1/4 valve set with peak flow rate of

143 SCFM and nominal flow rate of 54 SCFM.

The open loop simulation, i.e. the airspring was subjected to a
step disturbance input, was simulated by using the program STEP to
determine the bandwidth of the actuator. The idea of the 95% rise time
at three time constants for a step command was used to calculate the
bandwidth as before. The closed loop simulation, i.e. the airspring
was subjected to a random disturbance input, was simulated by using the
program RANDRESP to calculate the r.m.s. values of acceleration and
stroke, the flow rate, and the horsepower of the air compressor
required. The simulation results vs. various actuators and valves were
listed in Table 4-8-2. The parameter values for simulating the
particular actuator with valves were also listed in the above table.
The entries from row (1) to (8) simulated the FESTO MC-5/4-1/2 valve
whereas the entries from (9) to (11) simulated the same cylinder, the
PARKER 4" bore cylinder, but with different and smaller valves.

Based on the simulation results shown in Table 4-8-2, the
conclusion for selecting controller components was made as follows:

(1)   The FIRESTONE® #25 M airspring with internal plastic insert
      provided an improvement in r.m.s. acceleration of 51%
      reduction from that of passive suspension even though this
      actuator had a considerably low bandwidth.

(2)   However, the horsepower required by this actuator was still
      higher than what could be provided by the existing
      compressors.

(3)   The PARKER 4" bore cylinder was found to demonstrate
      desirable performance characteristics.

(4) If the actuator was designed to perform at 3 Hz., then the FESTO 4861-MC1-1/2 valve with a peak flow rate of 195 SCFM gave a faster response than necessary.

(5) A smaller valve which could give a slower response would reduce the average flow rate largely, hence, it was favorable to select a smaller one.

(5) When the valve's peak flow rate was less than 40 SCFM, the performance degraded. The valve with a peak flow capability of 80 SCFM was the smallest valve that was able to provide an acceptable improvement as the large valve.

(6) Due to the large reduction in power consumption, the valve with 40 SCFM flow rate had good characteristics and was able to use the existing compressor on board.

(7) Using the PARKER 4" bore cylinder with the 4-FESTO-MX-2-1/4 valve set of a nominal air flow capability of 50 SCFM, a 49% reduction in the r.m.s. stroke can be achieved by using 9.3 to 13.7 horsepower per car.

(8) This simple, economical and reliable nonlinear lateral active suspension system will improve the ride quality performance of railroad vehicles greatly..

I	II	III	IV			V			VI		VII		VIII	IX	X
Number	Actuators	$w.$ hz.	r.m.s. value of Acceleration, g			r.m.s. value of D, in			Average flow rate per truck Q, SCFM		Power Needed per car HP./car		Ef-fect. Area A, in^2	Parameter Values Used in Simulation	Comments
			Value g	% red. from pas.		Value	% red. from pas.		SCFM	%	HP.	%			
1	No.	,	0.0706	0		0.644	0							C_A, C_V, S_o, A_o, and d_S, d_V, d_A, were set to be zero	
2	Ideal	8	0.0295	58		0.443	31							F_{AD} and F_A were set to be equal; 2C_A = 400, C_V = 9,000 [A]	[1] The ideal one [2] Shift the peaks in the PSD curve of the accel. [3] Lower the freq. content of the acceleration [4] The value of C_A lowers the system's w_n.

No	Type	Bandwidth w	A g	A %	d in	d %	Flow Q, SCFM	HP HP	HP %	A, in²	Parameter Values	Comments
3	FIRST ONE #224	$W_{iso}=0.69$ $W_{aida}=0.96$ [B] [C]	0.047	33	0.307	52	126	37 to 52	0	25.7	$h_0 = 5.5$ $V_0 = 150$ in³ $dV = 27.3$ $A_0 = 25.7$ $dA = 3.9$ $k_{w0} = 7000$ $dk_w = 170$ $S_0 = 144.2$ $dS = 0.532$ $dx = 0.0032$ [D]	1 had the largest volume effective piston area, & peak force. 2 low bandwidth 3 large time lag, 50% of F_A was opposite to F_{AD} in direction. 4 The accelerations above 2 hz. were worsened. 5 power needed is too high for the existing compressor [E]

No	Type	Bandwidth w	%	Acceleration g	%	Stroke in	%	Flow SCFM	%	Power HP	%	A in²	Parameter values used in simulation	Comments
4	FIRESTONE #25	W_{iso} = 3.20 W_{aida} = 3.95		0.035	50	0.465	28	57	55	17 to 24		16.46	h_C = 4.75 V_0 = 71.0 dV = 17.75 A_0 = 16.46 dA = 2.85 kw_0 = 7000. dk_w = 170. S_0 = 51.5 dS = 0.19 dx = 0.0032	1 The smallest airspring of 3" stroke 2 dead volume = 33.5 in³ at its lowest height [F] 3 Enable to produce the peak force required. 4 Foresee power needed for compressor was still high.
5	FIRESTONE #25M	W_{iso} = 3.68 W_{aida} = 4.6	58 FROM #224	0.035	51	0.466	28	51	60	15 to 21		16.46	V_0 = 51.	! 60% of dead volume was eliminated by insert.

No	w		A		d		Q		P		A	Parameter Values	Comments
	0 hz	%	q	%	in	%	SCFM	%	HP	%	in²		
6	Parker 5" bore cylinder W_{iso} =7.11 W_{adia} =7.96		0.0291	58	0.492	24	66		19. to 27		19.6	h_0 = 19.6 stroke= 0.5"	1 Very little dead volume. 2 Can only meet 85% of peak force requested, f=2548 lb_f. 3 It performed nearly ideally when the control system was subjected to random vibration. 4 The power requirement is still too high for the existing compressors.

No	Type			A			d			d			P			A		Parameter Values	Comments
		hz	%	g	%		in	%		SCFM	%		HP	%		in²			
7	Parker 4" bore cylinder	W_{iso} = 11.0 W_{aida} = 12.3		0.036	49		0.497	23		40			12 to 17			12.6			1 Can only provide 54% of the peak force, at 130psi psi, f=1634 lb$_f$. 2 The actual actuator force F$_A$ followed the desired force without any significant lag. 3 F$_A$ was clipped at 1634 lb$_f$. 4 Significant acceleration reduction. 5 Power is still too high.

- 197 -

No	Type	w, hz	%	A		d		d		p		A in^2	Parameter Values	Comments
				g	%	in	%	SCFM	%	HP	%			
8	Parker 3" bore cylinder	W_{iso} = 18.1 W_{aida} = 20.3		0.466	34	0.504	22	19		5.5-7.7		7.07		1 Can only produce 919 lb_f peak force which is 30% of the specification. 2 It has negligible phase lag between F_A and F_{AD}.
9 [G]	Parker 4" bore cylinder with value of 80 SCFM	W_{iso} = 4.52 W_{aida} = 5.09		0.036	49	0.488	24	22		6.5-9.2		12.6	A_{max} = 0.0294 in^2	1 The average flow rate has 40% reduction of the largest valve. 2 The reduction in r.m.s. acceleration and r.m.s. stroke were as much as that achieved with the largest valve.

− 198 −

No	hz.	A g	A %	d in	d %	d SCFM	d %	P HP.	P %	A in^2	Parameter Values	Comments
10	Parker 4" bore cylinder with valve of 40 SCFM $W_{iso} = 2.26$ $W_{aida} = 2.55$	0.0372	46	0.428	34	18.5		5.4-7.6		12.6	$A_{max} = 0.0147$	Provided a barely acceptable performance with a much smaller average flow requirement (Figure 4.8.1).
11	Parker 4" bore cylinder with valve of 20 SCFM $W_{iso} = 1.13$ $W_{aida} = 1.27$	0.045	36	0.358	44	14		4.0-5.6		12.6		Performance was degraded undesirably.

— 199 —

No.	Description	W (hz)	A (g)	A (%)	d (in)	d (%)	d (SCFM)	d (%)	P (HP)	P (%)	A (in²)	Parameter Valves	Comments
12 [H] [1]	Parker 4" bore cylinder with the 4-FESTO Valve Set		0.035	49	0.45	30	32.85		9.5–13.3		12.56	$C_A = 15$ $C_V = 2400$ $\tau = 0.014$ $F_R = 300$ $C_A = K_1$ $C_V = K_2$	1 Peak force = 1634 lb$_f$ at 130 psi. 2 This power requirement, could be supplied by the existing compressor (Figure 4-8-12).

- 200 -

[A] These values of C_A C_V and K_f were used for all simulation except for the entry of row 12 (the values of $C_A = 400$ $lb_f/ft/sec^2$, $C_V=9000$ $lb_f/ft/sec$ and $K_f = 0.0003$ in^2/lb_f). Once a suitable valve controller is designed for the use with the particular actuator, the feedback gains, C_A and C_V can be determined experimentally to optimize the performance.

[B] W_{iso} = the bandwidth which was calculated on the assumption that the process was isothermal.
W_{aida} = the bandwidth which was calculated on the assumption that the process was adiabatic.

[C] The bandwidth, w, was determined by using the STEP program, and $T_{on}=0$, $T_{an}=0.00001$ k_0 minimize the dynamics of the solenoid valve.

[D] V_0 = nomial volume
dV = linearized volume constant
A_0 = nominal area
dA = linearized area constant
dh = changes in actuator height, in.
h_0 = nominal height, in.

[E] Existing air compressors on board: 75 Hp (electrical), 130 Hp. (diesel).

[F] The dead volume resulted from hollow housing inside the airspring which could be deleted to some degree by installing plastic inserts.

[G] The FESTO 4861 MC - 5/4 - 1/2 valve which has the largest one in this research was used for the simulation from row 1 to row 8.

[H] This actuator was simulated with the 4-FESTO MX-2 - 1/4 valve set which was divided into two sets, and each of the two sets controlled one actuator.

[I] This simulation was done by Barletta(.) using the modified program SYS) The controller parameters were listed below.

Acceleration feedback gain $C_A = 15$ lb_f - sec^2/in

Velocity feedback gain $C_V = 2,400$ lb_f - sec/in

Lead time $\tau = 0.014$

Dead zone width $F_r = 300$ lb_f

Table 4-8-2 Simulation results of various actuators and valves.
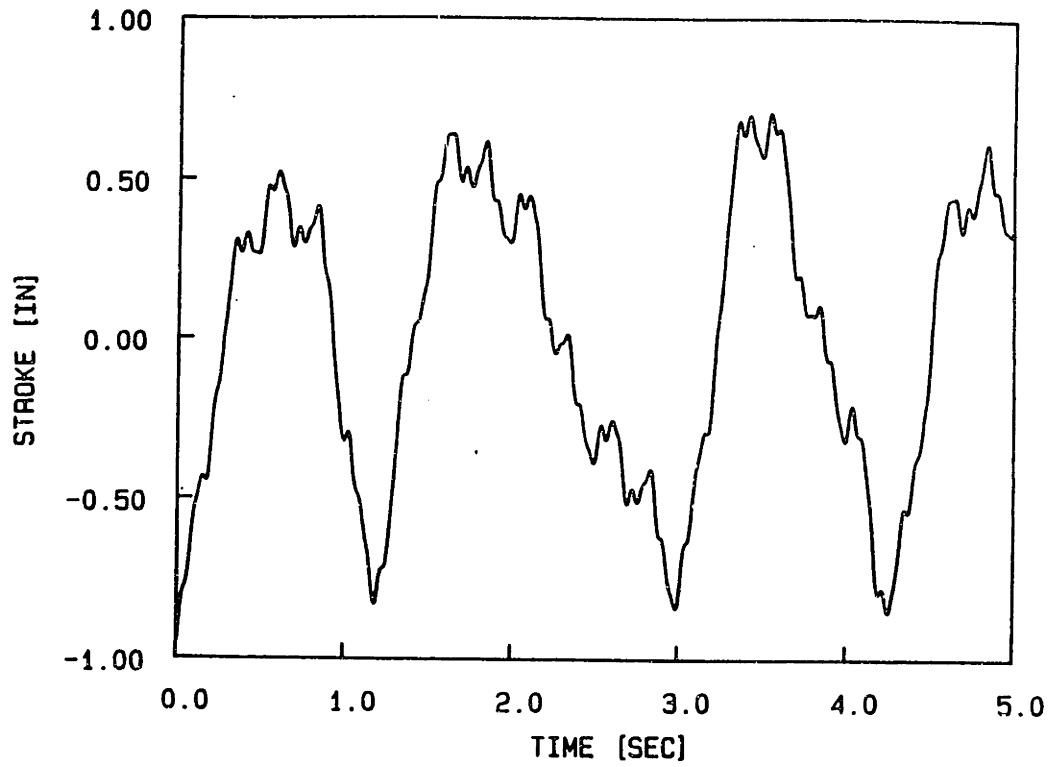
FIGURE 4.2.3 ACTIVE SYSTEM SUSPENSION STROKE.
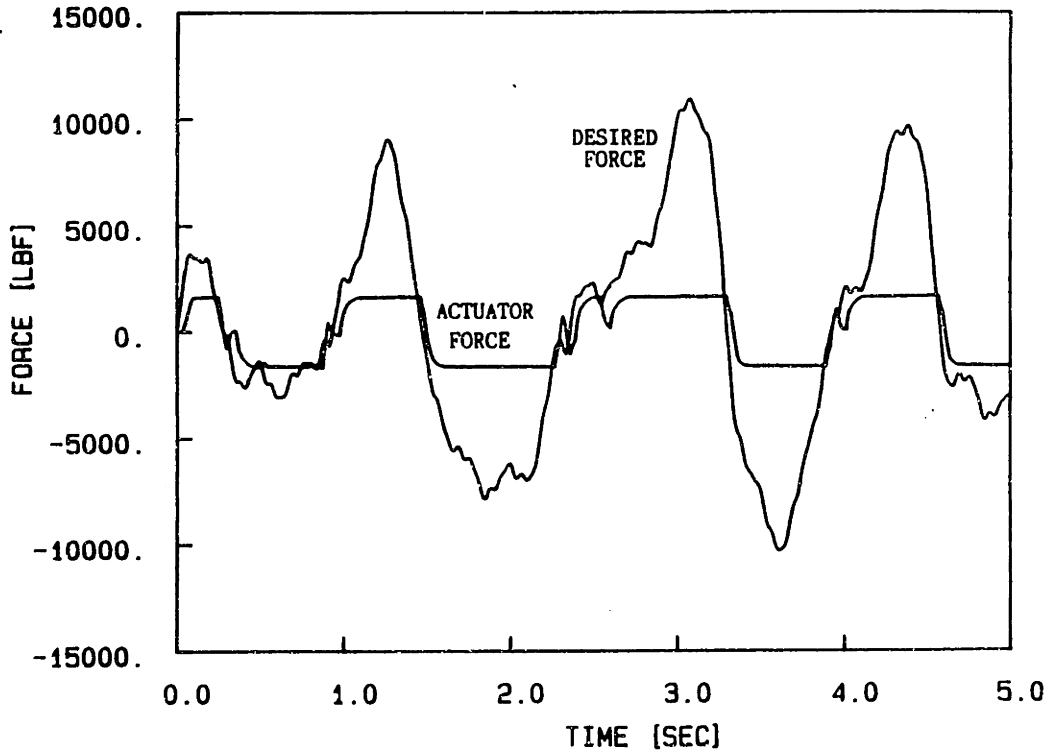
FIGURE 4.8.1 ACTIVE SYSTEM DESIRED AND ACTUAL
ACTUATOR FORCE (27)

(a)

(b)

(c)
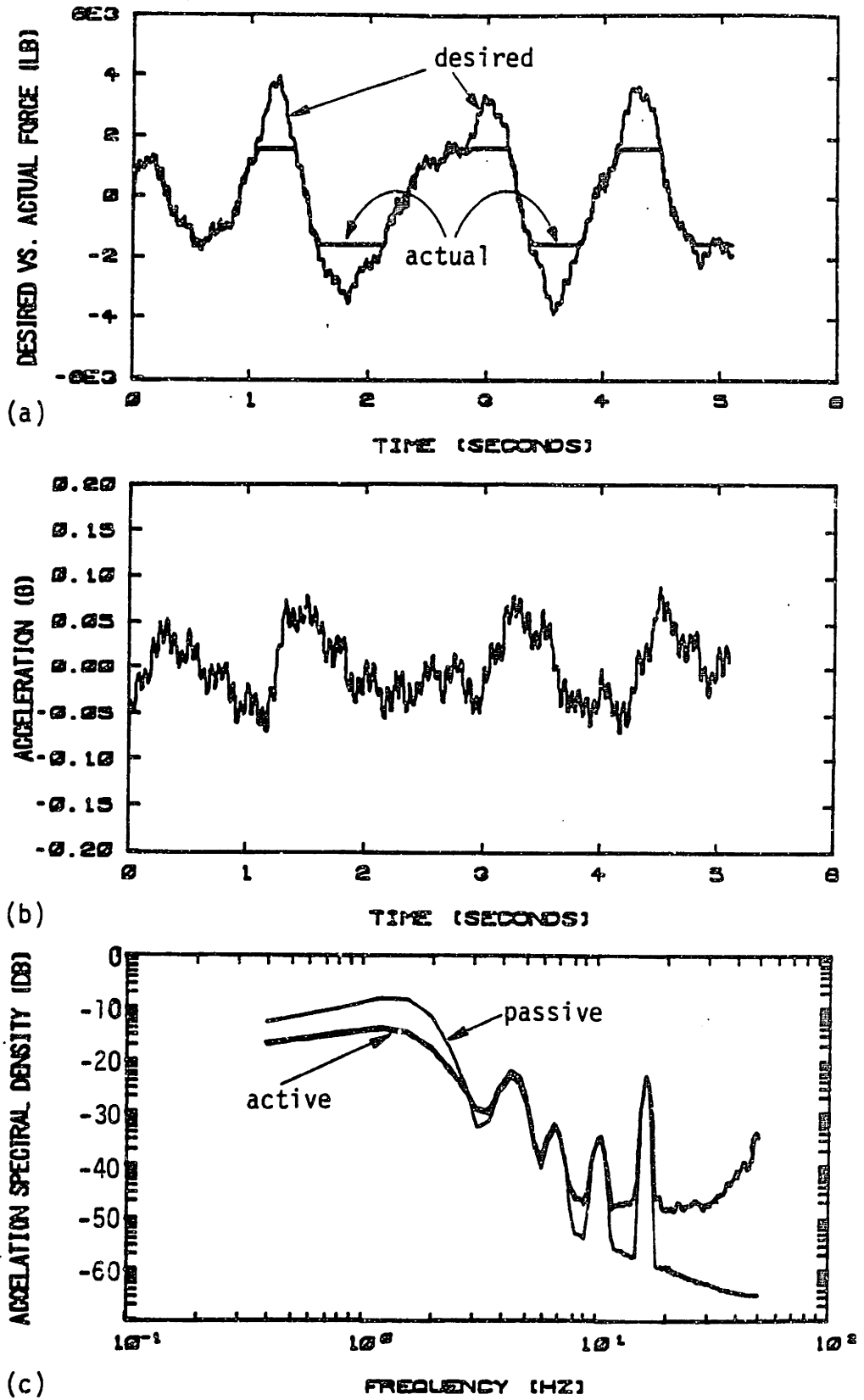
FIGURE 4.8.2   PERFORMANCE OF 4 INCH
                BORE PNEUMATIC CYLINDER(29)

CHAPTER 5

CONCLUSIONS AND RECOMMENDATIONS

An active controller was proposed to overcome the trade-off problem of the ride quality/suspension stroke for passenger rail vehicles. Active suspensions had the capacity to input energy from external power sources to the control system, rather than simply store (or dissipate) energy. Furthermore, they can be driven by signals measured from states (or combinations of states) to generate force beyond the restrictions imposed on the passive suspensions. Due to the present practice of the rail industry, a pneumatic actuator could be the most satisfying selection from the viewpoints of implementation, maintenance, and failure prevention. The physical considerations of the Budd Pioneer III truck were modelled and analyzed to understand the plant well, which is to be controlled. A Lateral Active Suspension Controller (the LASC controller) was designed and proposed to meet the requirements specified for the current AMTRAK passenger rail vehicle. This controller was an actively-controlled, band-limited actuation system with 3 Hz. bandwidth and can reduce r.m.s. carbody acceleration and r.m.s. suspension stroke significantly. In addition, it was economical and could be mounted on the current plant without much modification.

After deriving constitutive relations of each of the major components, a 5th order state equation was derived to represent the secondary lateral active suspension system. Using the Dynamic Similitude Method, a laboratory apparatus for testing the pneumatic active controller (the LASC tester) was designed and fabricated to perform experimental testing. The components of the LASC tester were discussed, modelled, and analyzed separately. It was finally completed with the

MCC control circuit, and was able to perform the testing successfully. Two control circuits, the PWM control circuit and the BBLC control circuit, which was designed to drive the solenoid valve fast enough to approximate the proportional valve, were discussed and judged critically. Components such as the valve alone, the control circuit alone, the actuator with the valve, and the actuator/valve with the control circuit were tested separately to determine their characteristics and their potentials.

Experimental results of various actuators, valves, and control circuits were further studied and compared with that of computer simulation. Adequate selections were achieved based on both the controller capability and the plant requirements. The similarity between the experimental and the computer simulational results was very promising. The PARKER HMA 14 4" bore cylinder, the 4-FESTO-MX-2-1/4 valve set, and the BBLC control circuits were selected because they performed as well as an ideal actuator (with infinite bandwidth) with a proportional valve, but at lower cost. There was a 49% reduction in the r.m.s. carbody lateral acceleration. A 22% reduction in the r.m.s. lateral suspension stroke could be achieved at a power consumption of 9.3-13.7 horsepower per car.

Recommendations for further work are as follows:

- The full dynamic testing, which requires the carbody acceleration signal measured, should be performed by implementing vibration generators on the LASC tester as described in chapter 3. These experimental results should also be compared with those of a computer simulation.

- A full scale prototype of the LASC controller should be built and

tested on the Northeast Corridor to determine the actual ride quality improvements achieved.

● Applications of the LASC controller on other control plants should be investigated as explained below.

Since vehicles other than passenger rail vehicles can also be studied by using a simple 1 DOF model similar to that used in this project, the application of the LASC controller to other plants is very plausible. The acceleration vibrations of automobiles, tractors, tanks, and motorcycles have a similar content to that of a passenger rail vehicle [34], hence the modelling, designing, and analyzing of the LASC controller and the LASC tester can be well extended to other road vehicles as well.

Furthermore, the actuator (and the power) required for those applications would be considerably below that of the LASC controller because the carbody masses of those applications are much less than that of railroad vehicle. In conclusion, the LASC controller has its own various applications to achieve the goal of advancing the ride quality control. The LASC controller does contain various applications to achieve the goal of ride quality control.

REFERENCES

1. Sussman, D. and Wormley, D.N., "Measurement and Evaluation of Ride Quality in Advanced Ground Transportation Systems."

2. Law, E.H. and Cooperrider, N.K., "A Survey of Railway Vehicle Dynamics Research," ASME Transactions, Vol. 98, Series G, No. 2, June 1974, pp. 132-146.

3. Nathanson, W., "Parametric Study Bibliography: Literature Survey for Rail System Dynamics Parametric Study," TSC RFP No. TSC/612-0368-GF, July 1976.

4. Wickens, A.H., "Vehicle Dynamics and Wheel-Rail Interface Problems," Proceedings of the Carnegie-Mellon Conference on High-Speed Ground Transportation, Pittsburgh, PA, 1969, pp. 157-171.

5. Sayers, M.W., "Analytical Methods to Reduce the Combined Track/ Vehicle Suspension Costs of Rail Systems," M.S. Thesis, Department of Mechanical Engineering, M.I.T., 1976.

6. Newland, D.E., "Steering a Flexible Railway Truck on Curved Track," Journal of Engineering for Industry, Trans. ASME, Series B, Vol. 91, No. 3, August 1969, pp. 908-918.

7. Scales, B.T., "Steering and Dynamic Stability of Railway Vehicles," Vehicle System Dynamics, Vol. 5, 1975/1976, p. 15.

8. Hedrick, J.K., et al., "Performance Limits of Rail Passenger Vehicles: Conventional, Radial, and Innovative Trucks," Final Report, U.S. DOT Contract DOT-OS-70052, September 1980.

9. Hedrick, J.K., et al., "Performance Limits of Rail Passenger Vehicles: Evaluation and Optimization," Final Report, U.S. DOT Contract DOT-OS-70052, December 1979.

10. Hedrick, J.K. and Wormley, D.N., "Active Control for Ground Transportation Vehicles: A State of the Art Review," ASME, AMD Monograph, AMD-Vol. 15, 1975.

11. Wormley, D.N., et al., "Rail Passenger Vehicle Truck Design Methodology," U.S. DOT Final Report, Report No. FRA/ORD-81/11, January 1981.

12. Scheffel, H., "A New Design Approach for Railway Vehicle Suspension," Rail International, October 1974, p. 638.

13. Klinger, D.L., "A Pneumatic On-Off Vehicle Suspension System," Journal of Dynamics Systems and Control, Trans. ASME, June 1977.

14. Goodall, R.M., Williams, R.A., and Lawton, A., "Practical Applications of Actively-Controlled Suspensions to Railway Vehicles," paper presented at the ASME Winter Annual Meeting, New York, N.Y., 1979.

15. Shapiro, S.M., "Engineering Data on Selected High Speed Passenger Trucks," Final Technical Report, Report No. 0391, The Budd Technical Center, Fort Washington, PA., May 1977.

16. International Organization for Standardization Standard No. 2631, "Guide for the Evaluation of Human Exposure to Whole-Body Vibration."

17. Society of Automotive Engineers Standard No. J1013 "Measurement of Whole-Body Vibration of the Seated Operator of Off-Highway Work Machines."

18. Sussman, D. and Wormley, D.N., "Measurement and Evaluation of Ride Quality in Advanced Ground Transportation Systems."

19. Partridge, M.A., "The Effects of Suspension System Passive Modification on Rail Vehicle Lateral Dynamics," S.M. Thesis, Department of mechanical Engineering, M.I.T., March 1982.

20. Celniker, G.W., "The Application of Active Control to Rail Vehicles," S.M. Thesis, Department of Mechanical Engineering, M.I.T., January 1981.

21. Celniker, G.W. and Hedrick, J.K., "Rail Vehicle Active Suspensions for Lateral Ride and Stability Improvement," presented at the 1981 ASME Winter Annual Meeting, Washington, D.C., 1981.

22. Hedrick, J.K., et al., "The Application of Active and Passive Suspension Techniques to Improve High Speed Ground Vehicle Performance," Final Report, U.S. DOT Contract DTRS5680-C-00018, March 1983.

23. Buzan, F.T., "The Influence of Finite Bandwidth Actuators on Rail Vehicle Active Suspensions," S.M. Thesis, Department of Mechanical Engineering, M.I.T., July 1982.

24. de los Reyes, G., Chen, L.C. and Hedrick, J.K., "Controller Implementation for a Pneumatic Active Suspension," ASME Winter Annual Meeting, November, 1983, Boston, MA.

25. Thomson Industries, Inc., "Linear Motion Designer's Guide," Catalog #FORM9900, 0482-50.

26. Blackburn, et al., Fluid Power Control, M.I.T. Press, Cambridge, MA, 1960. (Chapter 9, by Ezekiel).

27. Cho, D., Performance of Pneumatic-Powered, Vehicle Active Suspension Subject to Impulsive and Random Disturbances," S.M. Thesis, Department of Mechanical Engineering, M.I.T., August 1983.

28. de los Reyes, G., "A Pulse-Width-Modulated Controller for a Rail Vehicle, Pneumatic Active Suspension," S.M. Thesis, Department of Mechanical Engineering, M.I.T., August 1983.

29. Barletta, R., "Nonlinear Control of Active Pneumatic Suspensions," S.M. Thesis, Department of Mechanical Engineering, M.I.T., May 1984.

30. Jindzi, K., Kenjiro, K., Katsyuki, T., Yutaka, K., Fumio, I., "Fundamental Study on Semi-Actively Controlled Pneumatic Servo Suspensions for Railcars," Japanese National Railways-Hitachi Report, 1980.

31. Mauer, L., "Improvement of Rail Car Vehicle Performance, State of the Art Report," U.S.-German cooperative project MAN New Technologies, Munich, EDS-022, October, 1979.

32. FESTO pneumatic, "Electrically Actuated Valves," Catalog #806101MA.

33. FIRESTONE Industrial Product Company, IND., "Airstroke® Actuators Airmount® isolators," Catalog #1DM480.

34. Jolly, A., "Study of Ride Comfort Using a Nonlinear Mathematical Model of a Vehicle Suspension", International Journal of Vehicle Design, Vol. 4, No. 3, May 1983.

35. Takahashi, Y., et al., Control and Dynamic Systems, Addison-Wesley Publishing Co., Reading, Massachusetts, 1972.

36. Ogata, K., Modern Control Engineering, Prentice-Hall, Inc., Englewood Cliffs, New Jersey, 1970.

37. "DYSYS" M.I.T. Joint Computer Facility Library, 1980.

APPENDIX A

Oscilloscope Photographs (I)

(Experimental Results of FIRESTONE® #25 Airspring)
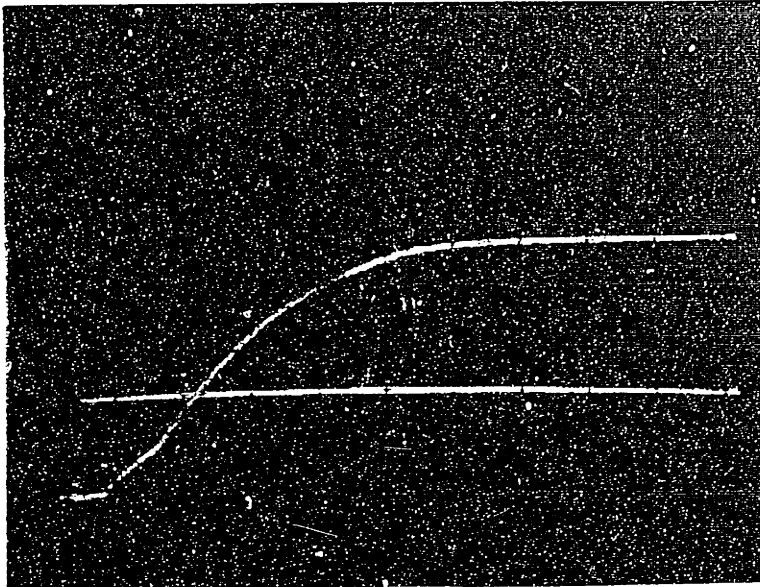
Figure A-4-4-5   (Refer to Table 4-4-1)
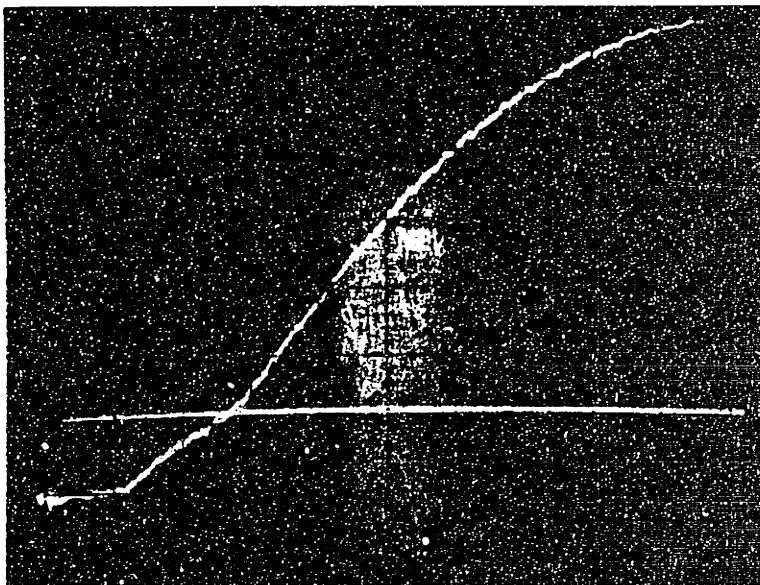
Figure A-4-4-6   (Refer to Table 4-4-1)

APPENDIX B

Oscilloscope Photographs (II)

(Experimental Results with PWM Control Circuit)

20 ms/div
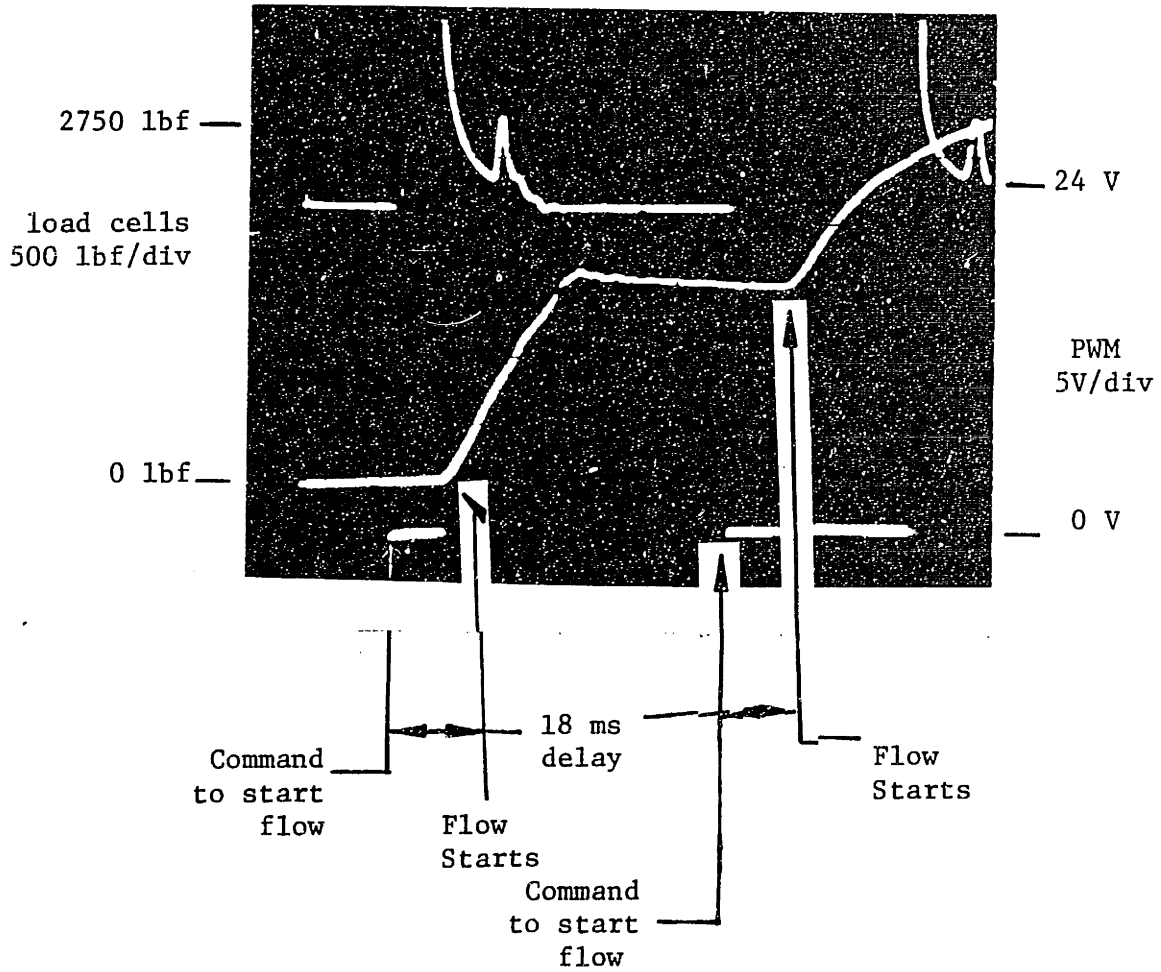
Figure b.1 Solenoid Valve/airspring No-Flow
Delay (28)

Command
to exhaust

Flow starts
to exhaust

95% exhausted
(140 lbf)

24
ms

134 ms

2750 lbf —

load cell
500 lbf/div

24 V

PWM
5V/div

0 lbf —

0 V

20 ms/div
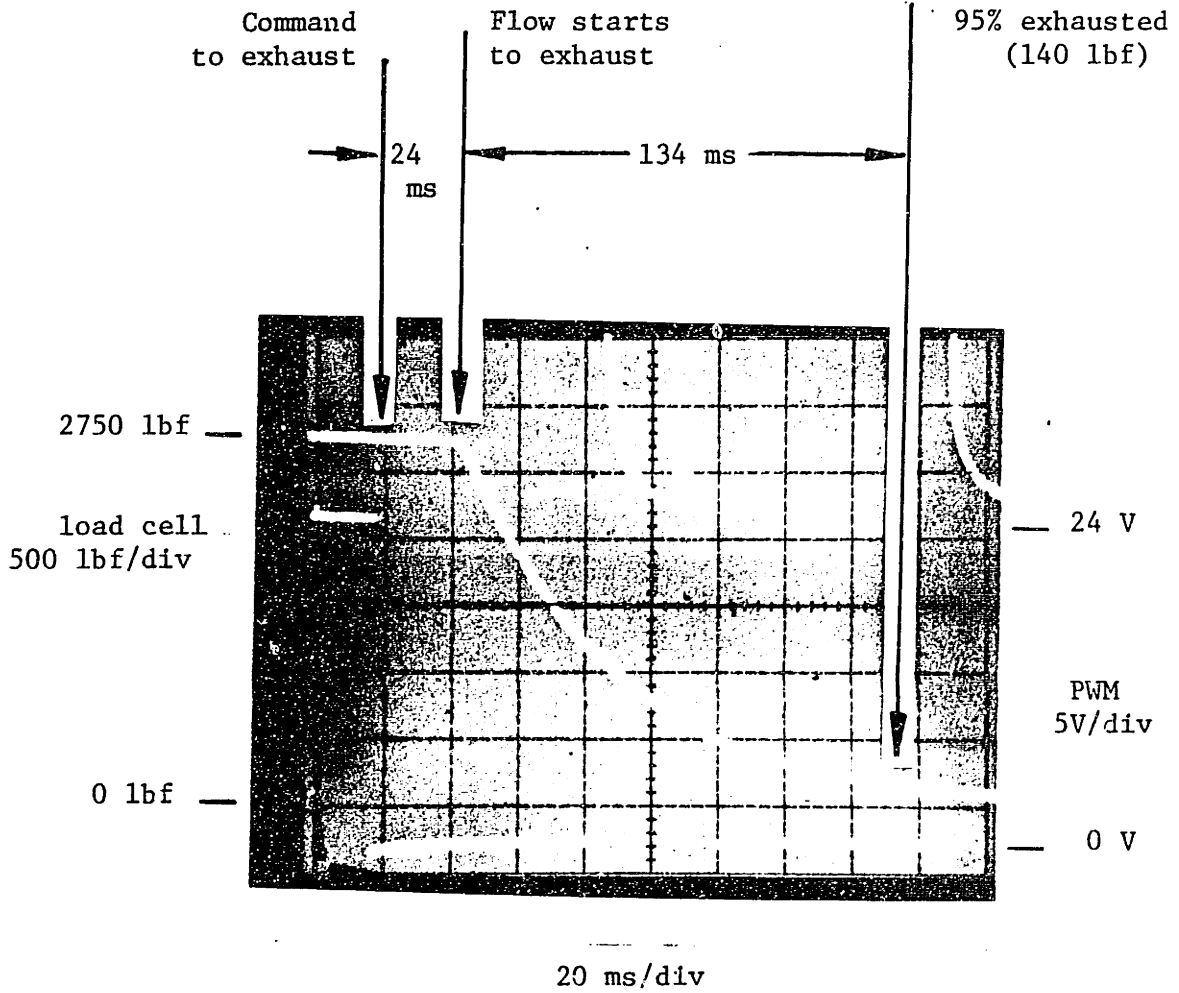
Figure B.2   Solenoid Valve/ Airspring
             Exhausting Step Response [28]
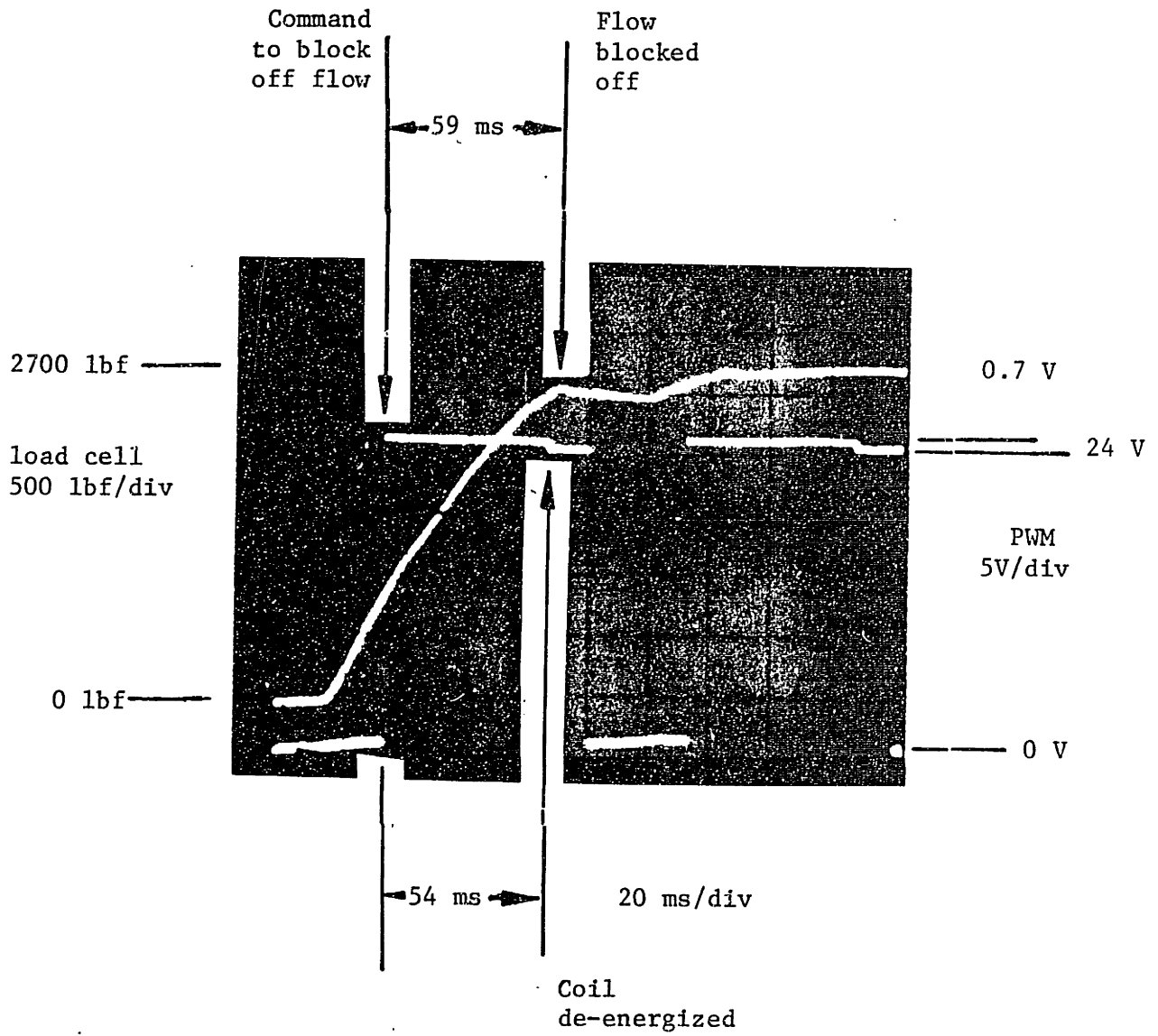
Figure B.3 Step Response of Pulse-Width-Modulated System with Diode Across Coil (28)

APPENDIX C

Oscilloscope Photographs (IV)

Experimental and Simulation Results with BBLC Control Circuit
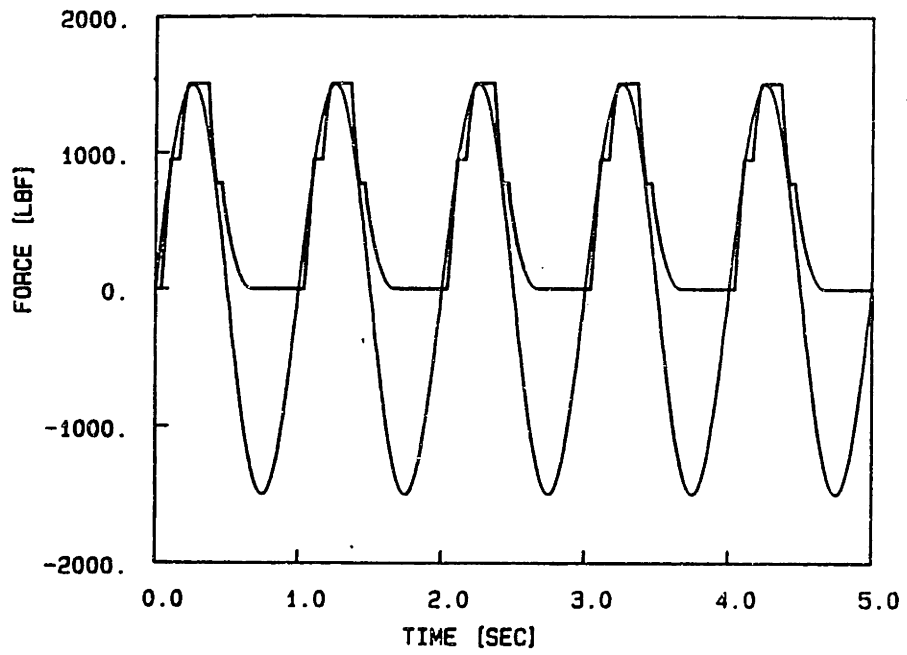
Model response
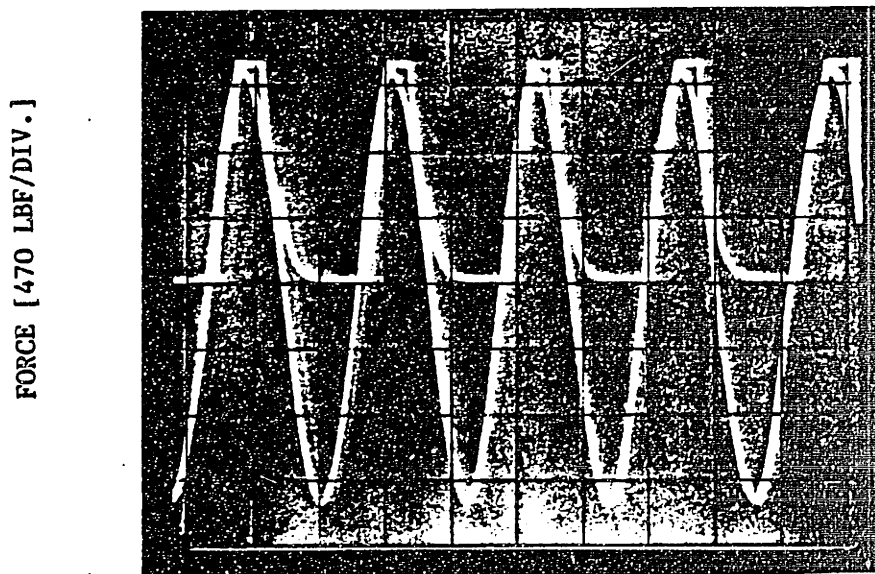
TIME [0.5 SEC/DIV.]

Experimental result

FIGURE   C.1   CLOSED LOOP FREQUENCY RESPONSE

W = 1.0 HZ. (29)
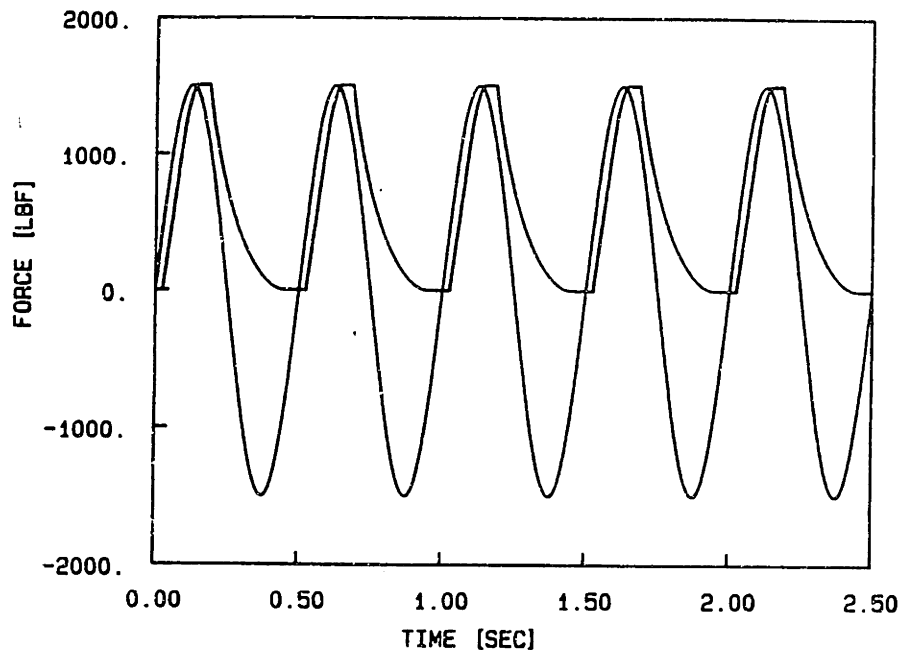
Model response
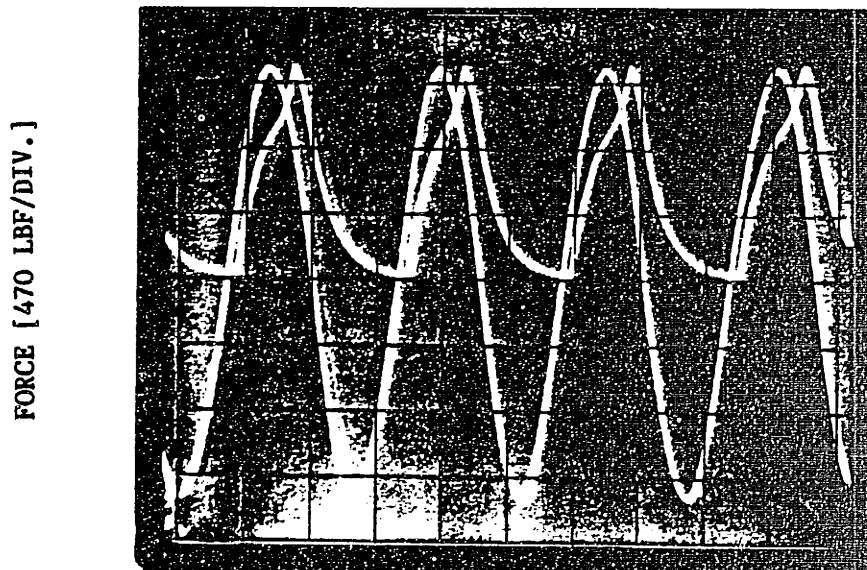
TIME [0.2 SEC/DIV.]

Experimental result

FIGURE C.2 CLOSED LOOP FREQUENCY RESPONSE

W = 2.0 HZ. (29)

APPENDIX D

FORTRAN Code of Computer Program: STEP

APPENDIX   D

STEP.FOR

```
C                              .    .
C*************************************************************
C
C This subroutine is run with DYSYS and shows the response of a
C pneumatic actuator/solenoid valve assembly to a step command.
C
C*************************************************************
C
      SUBROUTINE EQSIM
      COMMON T,DT,Y(30),F(30),STIME,FTIME,NEWDT,NEWRUN,N,
     1        IPR,ICK,ICN,TBREAK,PNEXT,TBACK
      REAL MC,KSY
      REAL kf,k,kwo,kwa,kwb
      REAL KD(3)
      EQUIVALENCE (Y(1),Pa),     (Y(2),Pb),      (Y(3),Aeff),
     1            (Y(4),Wa),     (Y(5),Wb),      (Y(6),Force),
     1            (Y(7),Wa1),    (Y(8),Wb1),     (Y(9),Ba),
     1            (Y(10),Xa),    (Y(11),kwa),    (Y(12),Sa),
     1            (Y(13),Cwa),   (Y(14),Cva)
C
C "NEWDT" is set as follows:
C         NEWDT = -1 on first call to EQSIM
C                  0 at intermediate steps
C                  1 at beginning of an integration step
C
      IF (NEWDT .EQ.  0)GOTO 35
      IF (NEWDT .NE. -1)GOTO 20
C
C*************************************************************
C
C This section is processed only once in the program. (i.e. NEWDT=-1)
C
C*************************************************************
C
C Reading in the suspension and disturbance parameters
C
                READ(8,100)NDUM
```

```
            READ(8,2020) MC
C
            READ(8,100)NDUM
            READ(8,2020)KSY,Csy
C
            READ(8,100)NDUM
            READ(8,2020)So,dS,kwo,dkw,xo,dx
C
            READ(8,100)NDUM
            READ(8,2020)KD(1),KD(2),KD(3)
C
            READ(8,100)NDUM   .
            READ(8,2020)kf
C
            READ(8,100)NDUM
            READ(8,2020)k,R,Ts,g,Vo,dV,Apo,dAp
C
            READ(8,100)NDUM
            READ(8,2020)Pe,Ps,Pai,Pbi,Amax,Fp,Freq,Ton,Tau
C
C Echo-printing the input parameters
C
            WRITE(5,105)Mc,Ksy,Csy
            WRITE(5,105)So,dS,kwo,dkw,xo,dx
            WRITE(5,105)KD(1),KD(2),KD(3)
            WRITE(5,105)kf
            WRITE(5,105)k,R,Ts,g,Vo,dV,Apo,dAp
            WRITE(5,105)Pe,Ps,Pai,Pbi,Amax,Fp,Freq,Tau
C
 100    FORMAT(9I4)
2020    FORMAT(9G15.5)
 105    FORMAT(1X,/,1X,9G10.2)
C
C Initializing variables
C
        C       =       Ps**(1.-1./k) / (R*Ts)
        Pa      =       Pai
        Pb      =       Pbi
C
C
C*****************************************************************
C*****************************************************************
C
C This section is processed only once at the beginning  of a
C Runge-Kutta Integration step. (i.e. NEWDT=1)
C
C*****************************************************************
C
```

```
 20      CONTINUE
C
C Determining the actuator areas
C
         Apa     =       Apo
         Apb     =       Apo
C
C Step-input command
C
         Force   =       Pa*Apa - Pb*Apb
         Fi      =       Fp * cos (WF * T)
         Aeff    =       kf * Fi
C
C Computing the flow through the valve for a given set
C of upstream and down stream conditions
C   Since a solenoid valve takes "Ton" (milisecond) to energize
C   the coil, if T is less than Ton skip to line 33.
C
 30      IF(T.LT.Ton) GOTO 33
C
         Teff    =       T - Ton
C
         IF(Aeff .GE. 0.0)then
            If(Aeff .GT. Amax)Aeff = Amax
            Wa2 = 0.0
            Wb1 = 0.0
            Call Flow(Pa,Ps,Aeff,Ts,Wal,Teff,Tau)
            Call Flow(Pe,Pb,Aeff,Ts,Wb2,Teff,Tau)
         ENDIF
C
         IF(Aeff .LT. 0.0) THEN
            If(Aeff .LT. -Amax)Aeff = -Amax
            Aeffn = - Aeff
            Wal = 0.0
            Wb2 = 0.0
            Call Flow(Pe,Pa,Aeffn,Ts,Wa2,Teff,Tau)
            Call Flow(Pb,Ps,Aeffn,Ts,Wb1,Teff,Tau)
         ENDIF
C
         Wa      =       Wal - Wa2
         Wb      =       Wb1 - Wb2
C
C
 33      CONTINUE
C
C Computing the adiabatic temperatures
C
C
```

-222 -

```
        Ta      =       (Ps/Pa)**(1.-1./k) * Ts
        Tb      =       (Ps/Pb)**(1.-1./k) * Ts
C
C Computing the mechanical and fluid capacitances of actuators
C
        Pga     =       Pa - Pe
        Sa      =       So + dS * Pga
        kwa     =       kwo + dkw * Pga
        xa      =       xo + dx * Pga
        Ba      =       (Pa+Pga)*Sa - Pa*dkw*xa + Pa*Pga*dS
C
        Pgb     =       Pb - Pe
        Sb      =       So + dS * Pgb
        kwb     =       kwo + dkw * Pgb
        xb      =       xo + dx*Pgb
        Bb      =       (Pb+Pgb)*Sb - Pb*dkw*xb + Pb*Pgb*dS
C
        Cwa     =       Sa * Ba * g / ( k * kwa * R * Ta )
        Cwb     =       Sb * Bb * g / ( k * kwb * R * Tb )
C
        Va      =       Vo
        Vb      =       Vo
C
        Cva     =       (Ps/Pa)**(1.-1./k) * Va * g / ( k * R * Ts )
        Cvb     =       (Ps/Pb)**(1.-1./k) * Vb * g / ( k * R * Ts )
C
C*********************************************************************
C*********************************************************************
C
C This section contains the diffrential equations and is processed
C for every step of the Runge-Kutta integration routine (i.e. NEWDT=0)
C
C*********************************************************************
C
  35    F(1)    =       Wa / ( Cva + Cwa )
        F(2)    =       Wb / ( Cvb + Cwb )
C
C*********************************************************************
C
        RETURN
        END
```

```fortran
        SUBROUTINE FLOW(Pd,Pu,Aeff,Ts,W,Teff,Tau)
        REAL k
C
C*************************************************************************
C
C       This subroutine calculates the compressible flow through a valve.
C
C*************************************************************************
C
C       Pu                              !       psia
C       Aeff                            !       in**2
C       Ts                              !       R
C       W                               !       lbf/sec
        C1 = 2.06                       !       sqrt(R)/sec
        C2 = 0.532                      !       sqrt(R)/sec
        k = 1.4
C
        If (Pd/Pu .LE. 0.528) GOTO 10
C
        If (Pd .GT. Pu) GOTO 5
C
        W       =        Aeff * C1 * Pu / Ts**0.5  *
     1                   (Pd/Pu)**(1./k) *
     1                   ( 1. - (Pd/Pu)**((k-1)/k) )**0.5
        W       =        W * (1.- exp(-Teff/Tau))
        RETURN
C
 5      Pu5 = Pd
        Pd5 = Pu
        W       =      - Aeff * C1 * Pu5 / Ts**0.5  *
     1                   (Pd5/Pu5)**(1./k) *
     1                   ( 1. - (Pd5/Pu5)**((k-1)/k) )**0.5
        W       =        W * (1.- exp(-Teff/Tau))
        RETURN
C
 10     W       =        Aeff * C2 * Pu / Ts**0.5
        W       =        W * (1.- exp(-Teff/Tau))
C
C*************************************************************************
C
        RETURN
        END
```

APPENDIX E

FORTRAN Code of Computer Program: RANDRESP

APPPENDIX   E

RANDRESP.FOR


```
C
C********************************************************************
C
C This program is run with DYSYS and evaluates the performance of
C active suspensions subject to random disturbances.
C
C********************************************************************
C
      SUBROUTINE EQSIM
      PARAMETER (NPTS=32768)
      COMMON T,DT,Y(30),F(30),STIME,FTIME,NEWDT,NEWRUN,N,
     1        IPR,ICK,ICN,TBREAK,PNEXT,TBACK
      REAL    Mc,Ksy,Kbump
      REAL    kf,k,kwo,kwa,kwb
      REAL    KD(3),VAL1(NPTS),VAL2(NPTS),VAL3(NPTS),VAL4(NPTS)
      EQUIVALENCE (Y(1),Yc),     (Y(2),Vc),     (Y(3),Pa),
     1            (Y(4),Pb),     (Y(5),Yt),     (Y(6),Vt),
     1            (Y(7),Aeff),   (Y(8),Wa),     (Y(9),Wb),
     1            (Y(10),Force), (Y(11),Apa),   (Y(12),Apb),
     1            (Y(13),Stroke),(Y(14),Accelg),(Y(15),Fi),
     1            (Y(16),Ta),    (Y(17),Tb),    (Y(18),Cwa),
     1            (Y(19),Cwb),   (Y(20),Cva),   (Y(21),Cvb),
     1            (Y(22),Keff),  (Y(23),Fvel),  (Y(24),Faccel)
C
C "NEWDT" is set as follows:
C         NEWDT  =  -1 on first call to EQSIM
C                    0 at intermediate steps
C                    1 at beginning of an integration step
C
      IF (NEWDT .EQ.  0)GOTO 35
      IF (NEWDT .NE. -1)GOTO 20
C
C********************************************************************
C
C This section is processed only once in the program. (i.e. NEWDT=-1)
C
C********************************************************************
C
```

```
C Reading in the suspension and disturbance parameters
C
              READ(8,100)NDUM
              READ(8,2020) Mc,Ksy,Kbump,Csy
C
              READ(8,100)NDUM
              READ(8,2020)So,dS,kwo,dkw,dx
C
              READ(8,100)NDUM
              READ(8,2020)Vo,dV,Apo,dAp
C
              READ(8,100)NDUM
              READ(8,2020)KD(1),KD(2),KD(3)
C
              READ(8,100)NDUM
              READ(8,2020)kf
C
              READ(8,100)NDUM
              READ(8,2020)k,R,Ts,g
C
              READ(8,100)NDUM
              READ(8,2020)Pe,Ps,Pai,Pbi,Amax
C
              READ(8,100)NDUM
              READ(8,2020)Yt1,Yt2,Yt3,Yt4,Yt5,Yt6,Yt7,Yt8,Yt9
C
              READ(8,100)NDUM
              READ(8,2020)Freq1,Freq2,Freq3,Freq4,Freq5,Freq6,
      1            Freq7,Freq8,Freq9
C
              READ(8,100)NDUM
              READ(8,2020)Phs1,Phs2,Phs3,Phs4,Phs5,Phs6,Phs7,Phs8,Phs9
C
C
C Echo-printing the input parameters
C
              WRITE(5,105)Mc,Ksy,Kbump,Csy
              WRITE(5,105)So,dS,kwo,dkw,dx
              WRITE(5,105)Vo,dV,Apo,dAp
              WRITE(5,105)KD(1),KD(2),KD(3)
              WRITE(5,105)kf
              WRITE(5,105)k,R,Ts,g
              WRITE(5,105)Pe,Ps,Pai,Pbi,Amax
              WRITE(5,105)Yt1,Yt2,Yt3,Yt4,Yt5,Yt6,Yt7,Yt8,Yt9
              WRITE(5,105)Freq1,Freq2,Freq3,Freq4,Freq5,Freq6,
      1               Freq7,Freq8,Freq9
              WRITE(5,105)Phs1,Phs2,Phs3,Phs4,Phs5,Phs6,Phs7,Phs8,Phs9
C
```

```
  100     FORMAT(15I4)
 2020     FORMAT(15G15.5)
  105     FORMAT(1X,/,1X,15G10.2)
C
C Initializing variables and setting parameters
C

          Yc      =       0.
          Yt      =       0.
          Vc      =       0.
          Vt      =       0.
          Pa      =       Pai
          Pb      =       Pbi
          WF1     =       2.*3.14*Freq1
          WF2     =       2.*3.14*Freq2
          WF3     =       2.*3.14*Freq3
          WF4     =       2.*3.14*Freq4
          WF5     =       2.*3.14*Freq5
          WF6     =       2.*3.14*Freq6
          WF7     =       2.*3.14*Freq7
          WF8     =       2.*3.14*Freq8
          WF9     =       2.*3.14*Freq9
C
C Initializing variables used in computing
C averages and variances
C
          Ncount    =     0.0
          SumYc     =     0.0
          SumYc2    =     0.0
          SumVact   =     0.0
          SumVact2  =     0.0
          SumYt     =     0.0
          SumYt2    =     0.0
          SumAeff   =     0.0
          SumAeff2  =     0.0
          SumFrc    =     0.0
          SumFrc2   =     0.0
          SumAc     =     0.0
          SumAc2    =     0.0
          SumStr    =     0.0
          SumStr2   =     0.0
          SumW      =     0.0
          SumW2     =     0.0
C
C
C********************************************************************
C********************************************************************
C
C This section is processed only once at the beginning of a
```

```
C Runge-Kutta integration step. (i.e. NEWDT=1)
C
C***************************************************************************
C
 20      CONTINUE
C
C Yt and Vt are the truck disturbances
C
         Yt      = - (  Yt1 * sin (WF1*T+Phs1)  +
     1                  Yt2 * sin (WF2*T+Phs2)  +
     1                  Yt3 * sin (WF3*T+Phs3)  +
     1                  Yt4 * sin (WF4*T+Phs4)  +
     1                  Yt5 * sin (WF5*T+Phs5)  +
     1                  Yt6 * sin (WF6*T+Phs6)  +
     1                  Yt7 * sin (WF7*T+Phs7)  +
     1                  Yt8 * sin (WF8*T+Phs8)  +
     1                  YT9 * sin (WF9*T+Phs9)  )
C
         Vt      = - (  WF1 * Yt1 * cos (WF1*T+Phs1)    +
     1                  WF2 * Yt2 * cos (WF2*T+Phs2)    +
     1                  WF3 * Yt3 * cos (WF3*T+Phs3)    +
     1                  WF4 * Yt4 * cos (WF4*T+Phs4)    +
     1                  WF5 * Yt5 * cos (WF5*T+Phs5)    +
     1                  WF6 * Yt6 * cos (WF6*T+Phs6)    +
     1                  WF7 * Yt7 * cos (WF7*T+Phs7)    +
     1                  WF8 * Yt8 * cos (WF8*T+Phs8)    +
     1                  WF9 * Yt9 * cos (WF9*T+Phs9)    )
C
C Computaion of system dynamics
C
         If (Pa.ge.Ps) Pa=Ps
         If (Pa.le.Pe) Pa=Pe
         If (Pb.ge.Ps) Pb=Ps
         If (Pb.le.Pe) Pb=Pe
C
         Apa     =      Apo    +        dAp*(Yc-Yt)
         Apb     =      Apo    -        dAp*(Yc-Yt)
C
         Force   =      Pa*Apa -        Pb*Apb
         Stroke  =      Yt     -        Yc
         Vact    =      Vc     -        Vt
C
         If (Stroke.LT.-1.5) Then
                 Fbump = Kbump * (Yt-Yc+1.5)
         Elseif (Stroke.GT.1.5) Then
                 Fbump = Kbump * (Yt-Yc-1.5)
         Else
                 Fbump = 0.
```

```
      Endif
C
      Accel    =         ( Ksy*(Yt-Yc) + Fbump + Csy*(Vt-Vc) +
   1                      Force ) / Mc
C
      Accelg   =         Accel / 386.
C
      Fi       =         KD(2) * Vc   +   KD(3) * Accel
      Faccel   =         KD(3) * Accel
      Fvel     =         KD(2) * Vc
C
C Computing the flow through a valve for a given set
C of upstream and downstream conditions
C
   30 Aeff     =         kf * (Fi - Force)
C
      If (Aeff .GE. 0.0) Then
          If (Aeff .GT. Amax) Aeff=Amax
          Wa2 = 0.0
          Wb1 = 0.0
          Call Flow(Pa,Ps,Aeff,Ts,Wa1)
          Call Flow(Pe,Pb,Aeff,Ts,Wb2)
      Endif
C
      If (Aeff .LT. 0.0) Then
          If (Aeff .lt. -Amax) Aeff = -Amax
          Aeffn = - Aeff
          Wa1 = 0.0
          Wb2 = 0.0
          Call Flow(Pe,Pa,Aeffn,Ts,Wa2)
          Call Flow(Pb,Ps,Aeffn,Ts,Wb1)
      Endif
C
      Wa       =         Wa1 - Wa2
      Wb       =         Wb1 - Wb2
C
C Computing the adiabatic temperatures
C
      Ta       =         (Pa/Ps)**(1.-1./k) * Ts
      Tb       =         (Pb/Ps)**(1.-1./k) * Ts
C
C Computing the mechanical and fluid capacitances of actuators
C
      Pga      =         Pa - Pe
      Sa       =         So + dS * Pga
      kwa      =         kwo + dkw * Pga
      xa       =         dx * Pga
      Ba       =         (Pa+Pga)*Sa - Pa*dkw*xa + Pa*Pga*dS
```

```
C
        Pgb     =       Pb - Pe
        Sb      =       So + dS * Pgb
        kwb     =       kwo + dkw * Pgb
        xb      =       dx * Pgb
        Bb      =       (Pb+Pgb)*Sb - Pb*dkw*xb + Pb*Pgb*dS
C
C
        Cwa     =       Ba * Sa * g / ( k * kwa * R * Ta )
        Cwb     =       Bb * Sb * g / ( k * kwb * R * Tb )
C
C
        Va      =       Vo + (Yc-Yt) * dV
        Vb      =       Vo - (Yc-Yt) * dV
C
C
        Cva     =       Va * g / ( k * R * Ta )
        Cvb     =       Vb * g / ( k * R * Tb )
C
C -----------------------------------------------------------
C
C The following section marked with --------'s are used for
C computation of averages and variances.
C
C -----------------------------------------------------------
C
C
        Ncount          =       Ncount          +       1
C
        VAL1(Ncount)    =       Accel / g
        VAL2(Ncount)    =       Fi
        VAL3(Ncount)    =       Force
        VAL4(Ncount)    =       Stroke
C
        SumYc           =       SumYc           +       Yc
        SumYc2          =       SumYc2          +       Yc**2
C
        SumYt           =       SumYt           +       Yt
        SumYt2          =       SumYt2          +       Yt**2
C
        SumVact         =       SumVact         +       Vact
        SumVact2        =       SumVact2        +       Vact**2
C
        SumAeff         =       SumAeff         +       Aeff
        SumAeff2        =       SumAeff2        +       Aeff**2
C
        SumFrc          =       SumFrc          +       Force
        SumFrc2         =       SumFrc2         +       Force**2
```

```
C
          SumAc        =        SumAc        +        Accel
          SumAc2       =        SumAc2       +        Accel**2
C
          SumStr       =        SumStr       +        Stroke
          SumStr2      =        SumStr2      +        Stroke**2
C
          SumW         =        SumW         +        Wa1
     1                                       +        Wb1
          SumW2        =        SumW2        +        Wa1**2
     1                                       +        Wb1**2
C
          If (T.GE.FTIME) Then
C
          AYc     =        SumYc   / Ncount
          VYc     =        ((SumYc2-SumYc**2/Ncount) / (Ncount-1))
C
          AYt     =        SumYt   / Ncount
          VYt     =        ((SumYt2-SumYt**2/Ncount) / (Ncount-1))
C
          AVact   =        SumVact / Ncount
          VVact   =        ((SumVact2-SumVact**2/Ncount) / (Ncount-1))
C
          AAeff   =        SumAeff / Ncount
          VAeff   =        ((SumAeff2-SumAeff**2/Ncount) / (Ncount-1))
C
          AFrc    =        SumFrc  / Ncount
          VFrc    =        ((SumFrc2-SumFrc**2/Ncount) / (Ncount-1))
C
          AAc     =        SumAc   / Ncount
          VAc     =        ((SumAc2-SumAc**2/Ncount) / (Ncount-1))
C
          AStr    =        SumStr  / Ncount
          VStr    =        ((SumStr2-SumStr**2/Ncount) / (Ncount-1))
C
          AW      =        SumW    / Ncount
          VW      =        ((SumW2-SumW**2/Ncount) / (Ncount-1))
C
       Write(5,301)
 301   FORMAT(//22X,'Mean',19X,'Variance'//)
C
C Writing the computed averages and variances to an external file
C
       Write(5,302)AYc,VYc
       Write(5,303)AYt,VYt
       Write(5,309)AVact,VVact
       Write(5,304)AAeff,VAeff
```

```fortran
      Write(5,305)AFrc,VFrc
      Write(5,306)AAc,VAc
      Write(5,307)AStr,VStr
      Write(5,308)AW,VW
C
 302  FORMAT(1X,'Yc',15X,E10.3,11X,E10.3/)
 303  FORMAT(1X,'Yt',15X,E10.3,11X,E10.3/)
 304  FORMAT(1X,'Aeff',13X,E10.3,11X,E10.3/)
 305  FORMAT(1X,'Force',12X,E10.3,11X,E10.3/)
 306  FORMAT(1X,'Accel',12X,E10.3,11X,E10.3/)
 307  FORMAT(1X,'Stroke',11X,E10.3,11X,E10.3/)
 308  FORMAT(1X,'Flow',13X,E10.3,11X,E10.3/)
 309  FORMAT(1x,'Vact',13X,E10.3,11X,E10.3/)
C
C
C ----------------------------------------------------------------
C
C Writing acceleration, stroke and forces to an external
C file in a format compatible with PMPSE program
C
      OPEN (UNIT=37,ACCESS='SEQUENTIAL',TYPE='NEW',
     1      NAME='ACCELG.DAT',FORM='UNFORMATTED')
C
      WRITE(37) (VAL1(I),I=1,NPTS)
C
      CLOSE (unit=37)
C
      OPEN (UNIT=35,ACCESS='SEQUENTIAL',TYPE='NEW',
     1      NAME='FDES.DAT',FORM='UNFORMATTED')
C
      WRITE(35) (VAL2(I),I=1,NPTS)
C
      CLOSE (UNIT=35)
C
      OPEN (UNIT=36,ACCESS='SEQUENTIAL',TYPE='NEW',
     1      NAME='FACT.DAT',FORM='UNFORMATTED')
C
      WRITE(36) (VAL3(I),I=1,NPTS)
C
      CLOSE(UNIT=36)
C
      OPEN (UNIT=34,ACCESS='SEQUENTIAL',TYPE='NEW',
     1      NAME='STROKE.DAT',FORM='UNFORMATTED')
C
      WRITE(34) (VAL4(I),I=1,NPTS)
C
      CLOSE(UNIT=34)
C
```

```
          Endif
C
C*******************************************************************
C*******************************************************************
C
C This section contains the differential equations and is processed
C for every step of the Runge-Kutta integration routine. (i.e. NEWDT=0)
C
C*******************************************************************
C
 35            F(1)    =         Vc
C
               If (Stroke.LT.-1.5) Then
                        Fbump = (Yt-Yc+1.5)
               Elseif (Stroke.GT.1.5) Then
                        Fbump = (Yt-Yc-1.5)
               Else
                        Fbump = 0.
               Endif
C
               F(2)    =         ( Ksy*(Yt-Yc) + Fbump + Csy*(Vt-Vc) +
     1    .                       (Pa*Apa - Pb*Apb) ) / Mc
C
               F(3)    =         Wa/(Cva+Cwa) - k*Pa*dV*(Vc-Vt)/Va
C
               F(4)    =         Wb/(Cvb+Cwb) + k*Pb*dV*(Vc-Vt)/Va
C
C
C*******************************************************************
C
          RETURN
          END
```

```
      SUBROUTINE FLOW(Pd,Pu,Aeff,Ts,W)
      REAL k
C
C*********************************************************************
C
C This subroutine calculates the compressible flow through a valve
C
C*********************************************************************
C     Pu                                  !     psia
C     Aeff                                !     in**2
C     Ts                        .         !     R
C     W                                   !     lbf/sec
      C1 = 2.06                           !     sqrt(R)/sec
      C2 = 0.532                          !     sqrt(R)/sec
      k = 1.4
C
      If (Pd/Pu .LE. 0.528) GOTO 10
C
      If (Pd .GT. Pu)GOTO 5
      W  =  Aeff * C1 * Pu / Ts**0.5  * (Pd/Pu)**(1./k)
    1        *( 1. - (Pd/Pu)**((k-1)/k) )**0.5
      RETURN
C
  5   Pu5 = Pd
      Pd5 = Pu
      W  = - Aeff * C1 * Pu5 / Ts**0.5  * (Pd5/Pu5)**(1./k)
    1        *( 1. - (Pd5/Pu5)**((k-1)/k) )**0.5
      RETURN
C
 10   W  =  Aeff * C2 * Pu / Ts**0.5
C
C*********************************************************************
C
      RETURN
      END
```

APPENDIX F

FORTRAN Code of Computer Program: SYS

Page 1 of program SYS

```
C                         SUBROUTINE SYS.
C
C       This subroutine is run with a fourth order Runge-Kutta
C       routine and evaluates the performace of active pneumatic
C       suspensions subject to a random disturbance.
C
C
        SUBROUTINE DIFEQ
        COMMON  T,DT,Y(30),F(30),STIME,FTIME,DTNEW,N
        REAL    Mc,Ksy,Kbump
        REAL    k
        REAL    kd(2),Yti(9),Freq(9),Phs(9),Wf(9)
        EQUIVALENCE (Y(1),Yc),(Y(2),Vc),(Y(3),Pa),(Y(4),Pb)
C
C       DTNEW is set as follows:
C           DTNEW =  0, on first call of DIFEQ,
C           DTNEW =  1, at intermediate integration steps,
C           DTNEW = -1, at the begining of an integration step.
C
        IF (DTNEW .NE. 0.) GO TO 20
C
C       Reading of system parameters.
C
        OPEN(10,FILE='OUT')
       •OPEN(8,FILE='DAT')

        READ(8,*) NDUM
        READ(8,*) Mc,Ksy,Kbump,Csy

        READ(8,*) NDUM
        READ(8,*) Vo,Apo

        READ(8,*) NDUM
        READ(8,*) Kd(1),Kd(2)

        READ(8,*) NDUM
        READ(8,*) k,R,Ts,g,Ro

        READ(8,*) NDUM
        READ(8,*) Pe,Ps,Amax,On,Off,Err,Dlead

        READ(8,*) NDUM
        READ(8,*) (Yti(I),I=1,9)

        READ(8,*) NDUM
        READ(8,*) (Freq(I),I=1,9)

        READ(8,*) NDUM
        READ(8,*) (Phs(I),I=1,9)
```

Page 2 of program SYS

```
        CLOSE(8)
C
C       Variable initialization.
C
        Yc    =    0.0
        Vc    =    0.0
        Pa    =    Pe
        Pb    =    Pe

        DO 15 I=1,9
15          Wf(I)    =    2.*3.14*Freq(I)

        Count     =    0.0
        SumYc     =    0.0
        SumYc2    =    0.0
        SumVact   =    0.0
        SumVact2=       0.0
        SumYt     =    0.0
        SumYt2    =    0.0
       ,SumFrc    =    0.0
        SumFrc2   =    0.0
        SumAc     =    0.0
        SumAc2    =    0.0
        SumStr    =    0.0
        SumStr2   =    0.0
        SumW      =    0.0
        SumW2     =    0.0
C
C       This section is executed only at each new time step.
C
20      IF (DTNEW .EQ. 1) GO TO 10
C
C       Calculation of carbody acceleration.
C
        Stroke   =    Yt -Yc
        Vact     =    Vt -Vc

        Fbump    =    0.0
        IF (Stroke .GT. 1.5) Fbump = Kbump*(Stroke-1.5)
        IF (Stroke .LT.-1.5) Fbump = Kbump*(Stroke+1.5)
        Accel    =    (Ksy*Stroke+Fbump+Csy*Vact+Force)/Mc
        Acc      =    Accel/g
C
C       Calculation of actual actuator force.
C
        Force0   =    Force
        Force    =    Pa*Apo - Pb*Apo
C
C       Calculation of desired force.
C
```

Page 3 of program SYS

```
        Fvel     =    Kd(1) * Vc
        Faccel   =    Kd(2) *Accel
        Fi0      =    Fi
        Fi       =    Fvel + Faccel
C
C    Lead compensation of the error.
C
        Ferror   =    (Fi-Force)+Dlead*((Fi-Fi0)/DT
        1             -(Force-Force0/DT)
C
C    Calculation of controller voltage output.
C
        IF (ABS(Ferror) .LE. Err) THEN
             V1   =    0.0
             V2   =    0.0
             V3   =    0.0
             V4   =    0.0
             GO TO 60
        ENDIF
        IF (Ferror .GT. 0.0) THEN
             V1   =    24.0
             V2   =    0.0
             V3   =    24.0
             V4   =    0.0
             GO TO 60
        ELSE
             V1   =    0.0
             V2   =    24.0
             V3   =    0.0
             V4   =    24.0
             GO TO 60
        ENDIF
C
C    Computation of valve dynamics.
C
60      CALL VALVE(V1,V10,D1,Ae1,Tf1,DT,On,Off,T,Amax,F31)
        CALL VALVE(V2,V20,D2,Ae2,Tf2,DT,On,Off,T,Amax,F32)
        CALL VALVE(V3,V30,D3,Ae3,Tf3,DT,On,Off,T,Amax,F33)
        CALL VALVE(V4,V40,D4,Ae4,Tf4,DT,On,Off,T,Amax,F34)
C
C    Computation of averages and variances.
C
        W1c          =    W1*60./Ro
        W4c          =    W4*60./Ro

        Count        =    Count    +    1
        SumYc        =    SumYc    +    Yc
        SumYc2       =    SumYc2   +    Yc**2
        SumYt        =    SumYt    +    Yt
        SumYt2       =    SumYt2   +    Yt**2
```

Page 4 of program SYS

```
        SumVact     =    SumVact +    Vact
        SumVact2    =    SumVact2+    Vact**2
        SumFrc      =    SumFrc   +   Force
        SumFrc2     =    SumFrc2  +   Force**2
        SumAc       =    SumAc    +   Acc
        SumAc2      =    SumAc2   +   Acc**2
        SumStr      =    SumStr   +   Stroke
        SumStr2     =    SumStr2  +   Stroke**2
        SumW        =    SumW     +   W1c+W4c
        SumW2       =    SumW2    +   (W1c+W4c)**2


        IF (T .GE. FTIME) THEN

            AYc     =    SumYc/Count
            VYc     =    ((SumYc2-SumYc**2/Count)/(Count-1))
            SVYc    =    SQRT(VYc)
            AYt     =    SumYt/Count
            VYt     =    ((SumYt2-SumYt**2/Count)/(Count-1))
            SVYt    =    SQRT(VYt)
            AVact   =    SumVact/Count
            VVact   =    ((SumVact2-SumVact**2/Count)/(Count-1))
            SVVact  =    SQRT(VVact)
            AFrc    =    SumFrc/Count
            VFrc    =    ((SumFrc2-SumFrc**2/Count)/(Count-1))
            SVFrc   =    SQRT(VFrc)
            AAc     =    SumAc/Count
            VAc     =    ((SumAc2-SumAc**2/Count)/(Count-1))
            SVAc    =    SQRT(VAc)
            AStr    =    SumStr/Count
            VStr    =    ((SumStr2-SumStr**2/Count)/(Count-1))
            SVStr   =    SQRT(VStr)
            AW      =    SumW/Count
            VW      =    ((SumW2-SumW**2/Count)/(Count-1))
            SVW     =    SQRT(VW)
C
C   Writing  of  the  computed  averages  and variances to an
C   external file and console.
C
            WRITE(1,70)
            WRITE(10,70)
            WRITE(1,71) AYc,SVYc
            WRITE(10,71) AYc,SVYc
            WRITE(1,72) AYt,SVYt
            WRITE(10,72) AYt,SVYt
            WRITE(1,73) AVact,SVVact
            WRITE(10,73) AVact,SVVact
            WRITE(1,74) AFrc,SVFrc
            WRITE(10,74) AFrc,SVFrc
            WRITE(1,75) AAc,SVAc
            WRITE(10,75) AAc,SVAc
```

Page 5 of program SYS

```
          WRITE(1,76) AStr,SVStr
          WRITE(10,76) AStr,SVStr
          WRITE(1,77) AW,SVW
          WRITE(10,77) AW,SVW

          CLOSE(10)

70        FORMAT(//25X,'Mean',14X,'Desviation'//)
71        FORMAT(1X,'Yc',15X,F10.4,11X,F10.4/)
72        FORMAT(1X,'Yt',15X,F10.4,11X,F10.4/)
73        FORMAT(1X,'Vact',13X,F10.4,11X,F10.4/)
74        FORMAT(1X,'Force',12X,F10.2,11X,F10.2/)
75        FORMAT(1X,'Accel',12X,F10.4,11X,F10.4/)
76        FORMAT(1X,'Stroke',11X,F10.4,11X,F10.4/)
77        FORMAT(1X,'Flow',13X,F10.4,11X,F10.4/)


      ENDIF
C
C     This section is run four times for each time step.
C
C     Computation of disturbance input.
C
10    Yt  =    0.0
      Vt  =    0.0
      DO 25 I=1,9
          Yt  =    Yt - ( Yti(I) * SIN (Wf(I)*T+Phs(I)))
25        Vt  =    Vt - ( Wf(I) * Yti(I) * COS (Wf(I)*T+Phs(I)))
C
C     Calculation of adiabatic temperatures.
C
      Ta  =    (Pa/Ps)**(1.-1./k)*Ts
      Tb  =    (Pb/Ps)**(1.-1./k)*Ts

      CALL FLOW (Pa,Ps,Ae1,Ts,W1)
      CALL FLOW (Pe,Pa,Ae2,Ta,W2)
      CALL FLOW (Pe,Pb,Ae3,Tb,W3)
      CALL FLOW (Pb,Ps,Ae4,Ts,W4)
C
C     Calculation of actuator capacitance.
C
      Wa  =    W1 - W2
      Wb  =    W4 - W3

      Va  =    Vo - (YT-YC)*Apo
      Vb  =    Vo + (YT-YC)*Apo

      Cva =    Va*g/(k*R*Ta)
      Cvb =    Vb*g/(k*R*Tb)
```

Page 6 of program SYS

```
C
C     System's differential equations.
C
      F(1)     =    Vc

      Fbump    =    0.0
      IF ((Yt-Yc) .GT. 1.5) Fbump = (Yt-Yc+1.5)*Kbump
      IF ((Yt-Yc) .LT.-1.5) Fbump = (Yt-Yc-1.5)*Kbump
      F(2)     =    (Ksy*(Yt-Yc)+Fbump+Csy*(Vt-Vc)
     1              +(Pa*Apo-Pb*Apo))/Mc

      F(3)     =    Wa/Cva-k*Pa*Apo*(Vc-Vt)/Va

      F(4)     =    Wb/Cvb+k*Pb*Apo*(Vc-Vt)/Vb

      RETURN
      END
```

Page 1   of program VALVE

```
C
C                         SUBROUTINE VALVE
C
C     This subroutine  calculates the dynamics  of the valve by
C     the simulation of the opening and closing time delays.
C
      SUBROUTINE VALVE(V,V0,Dp,Ae,Tf,DT,On,Off,T,Amax,F3)
      IF (V .EQ. V0) GO TO 20
      Dp  =    0.0
      F3  =    0.0
20    V0  =    V
      IF (V.EQ. 24.) THEN
          Tdp =    On/DT
          Dp  =    Dp + 1.
          IF (Dp .LT. Tdp) RETURN
          IF (F3 .EQ. 0.0) Tf=T
          F3  =    1.
          Ae  =    Amax
          RETURN
        ELSE
          Tdp =    Off/DT
          Dp  =    Dp + 1.
          IF (Dp .LT. Tdp) RETURN
          IF (F3 .EQ. 0.0) Tf=T
          F3  =    1.
          Ae  =    0.0
          RETURN
      ENDIF
      END
```

Page 1 of program FLOW

```
C                    SUBROUTINE FLOW
C
C     This subroutine calculates  the compressible  flow through
C     a valve.
C
      SUBROUTINE FLOW(Pd,Pu,Aeff,Ts,W)
      REAL K
      C1  =    2.06
      C2  =    0.532
      k   =    1.4

      IF (Pd/Pu .LE. 0.528) GO TO 10
      IF (Pd .GT. Pu) GO TO 15

      W   =    Aeff*C1*Pu/Ts**0.5*(Pd/Pu)**(1./k)*(1.-(Pd/Pu)**
     1         ((k-1.)/k))**0.5
      RETURN

15    Pue =    Pd
      Pde =    Pu
      W   =    -Aeff*C1*Pue/Ts**0.5*(Pde/Pue)**(1./k)
     1          *(1.-(Pde/Pue)**((k-1.)/k))**0.5
      RETURN

10    W   =    Aeff*C2*Pu/Ts**0.5
      RETURN
      END
```